博士論文

Theoretical Studies on New Physics behind the Higgs Sector

Naoki Machida

Department of Physics, University of Toyama,
3190 Gofuku, Toyama 930-8555, Japan

March 2016

富山大学大学院 理工学教育部 新エネルギー科学専攻
理論物理学研究室

ACKNOWLEDGMENTS

I would particularly like to thank my supervisor, Prof. Shinya Kanemura for giving me insightful comments and considerable instructions in particle physics. I am deeply grateful to Prof. Tetsuo Shindou, Dr. Kunio Kaneta, and Dr. Toshifumi Yamada for their fruitful collaborations and discussions. I want to thank Prof. Takeshi Kurimoto and Prof. Mitsuru Kakizaki for many academic advices. I would like to express my gratitude to Prof. Satoshi Iida, Prof. Kaori Kobayashi, and Prof. Fusakazu Matsushima for careful reading of the thesis. I would also like to thank to other members of Theoretical Physics Group, University of Toyama, Dr. Hiroaki Sugiyama, Dr. Hiroshi Yokoya, Dr. Kei Yagyu, Dr. Takehiro Nabeshima, Dr. Hiroyuki Taniguchi, Dr. Makoto Nakamura, Ms. Mariko Kikuchi, Mr. Toshinori Matsui, Mr. Akiteru Santa, Mr. Ryo Amai, Mr. Katsuya Hashino, Mr. Shota Nakatani, Mr Shinya Odori, Mr. Kodai Sakurai, Mr. Yoshiaki Ishigure, and Mr. Koichi Ishida for their hospitality. Thanks to secretary of our group, Ms. Asami Takagi.

Abstract

In July 2012, a new boson has been discovered at Large Hadron Collider (LHC) in CERN. The mass and spin turned out to be 126 GeV and 0. Therefore, the new boson must be the scalar boson. Moreover, its couplings to the Standard Model (SM) particles are in good agreement with the SM predictions of the Higgs boson. These results indicate that the property of this scalar boson is very close to that of the Higgs boson in the SM. Thereby the SM has been confirmed its correctness within the uncertainty of the current data. There is no signal for the new particle until now.

On the other hand, it is also well known that several phenomenological problems remain in the SM. For example, the existence of dark matter, the tiny mass of the neutrinos and the baryon number assymetry of the Universe (BAU). These problems cannot be explained in the framework of the SM. Therefore, the SM must be extended to solve these problems.

Moreover, the hierarchy problem is known as the theoretical problem of the SM. The quadratic divergence in the radiative correction to the Higgs boson mass appears because the Higgs boson is the scalar particle. Supersymmertic extended models are considered as the attractive candidate which can solve the hierarchy problem. In these class of models, the scalar particles are naturally justified by the supersymmetry. In additions to this, the quadratic divergence from supersymmetric particles cancel the that of the SM particle when the supersymmetry doesn't break, so that the hirarchy problem can be solved. As an alternative solution, there is a new paradigm which can solve the hierarchy problem, such as technicolour models and composite Higgs models. In these scenarios, the Higgs boson is not the elementary particle rather than the composite particle. At the high energy scale, the hierarchy problem disappears because there is no scalar boson.

In this thesis, we make a study on the ideas based on the Higgs boson as the composite particle. One is the supersymmetric QCD scenario and one is the composite Higgs scenario.

First, we report our study [1] based on the supersymmetric QCD theory. In this model, thanks to a new supersymmetric gauge symmetry which exists higer than the electroweak scale, the extended Higgs sector appears as the composite state of the fundamental fields in the new gauge symmetry at the low-energy effective theory. Interestingly, three phenomenological problems mentioned above can be solved at the TeV scale new physics in this model, simultaneously. The existence of the extra scalar bosons which strongky couple to the SM-like Higgs boson enhances the first order electroweak phase transition. This is the neccesary condition for realizing the BAU. Moreover, thanks to the unbroken Z_2 symmetry, the dark matter and neutrino mass problems can be explained, simultaneously, in the framework of the radiative seesaw scenario. We have also discussed the testability of this model at future collider experiments.

Second, we report our study [2] based on the composite Higgs theory. In these models, the Higgs bosons appear as the Nambu-Goldstone bosons (NBGs) which are originated from the breakdown of the global symmetry $\mathcal{G}$ at a higher scale than the electroweak scale. The *exact* NGBs cannot have the mass by the shift symmetry. However, these NGBs must get the mass because the observed Higgs boson has the mass. By the Coleman-Weinberg mechanism, these particles obtain the mass so that they are called the *pseudo* Nambu-Goldsotne bosons (pNBGs). In the composite Higgs models, the breaking pattern of the global symmetly $\mathcal{G}$ leads various models with extended Higgs sectors to the low-energy effective theory. The simplest model is the minimal composite Higgs models (MCHMs). In the MCHMs, the global symmetry $\mathcal{G} = SO(5)$

breaks into $\mathcal{H} = SO(4)$ by a certain strong dynamics at the scale f. The breaking scale f is highter than the electroweak scale ~ 100 GeV. The number of the NGBs is 4 corresponding to the degrees of freedom of the SM Higgs doublet. The gauge boson and Higgs boson coupling deviation only depends on $\mathcal{G}/\mathcal{H}$. On the other hand, the deviation patterns of the Higgs boson couplings to charged fermions and Higgs boson itself depends on representation of the matter field in $SO(5)$. These deiviations areo parametrized by one parameter, so-called the compositeness parameter ξ. We list the deviation patterns of the variation models of the MCHM.

We investigate the single and double Higgs boson production of the MCHM and constraints on the model parameter. The production cross sections and the signal strengths significantly differ from the SM predictions due to the diviations of the Higgs boson coupling constants. We discuss the possibility to distinguish the MCHMs from other new physics models.

In addtion to the MCHMs, we investigate a next-to-minimal composite Higgs model with composite doublet and composite singlet scalar. We also discuss the collider phenomenology of this model.

The composite Higgs model is an analogy of the quantum chromodynamics (QCD). The realistic pNGB is pions in the QCD. The chiral symmetry $SU(2)_L \times SU(2)_R$ is broken into the vectorial $SU(2)$. After that, three pions appear as the pNGBs, π^+, π^0, π^-. The source of the small pion masses are the explicit breaking of the chiral symmetry. When we calculate pion scattering process $\pi\pi \to \pi\pi$, this amplitude would diverge at high enegies. However, the measured observable did not diverge because a new particle contribution unitalizes the scattering amplitude at high energy, which is known as the rho meson. In the MCHMs, the logitudinal modes of the weak gauge bosons W_L, Z_L can be identified as pions. The weak gauge boson scattering amplitude in the MCHMs also diverges due to the non-vanishing compositeness parameter ξ, which differs from the SM prediction. We here assume that this process should be stabilized by the new introduced particle like the rho meson in the QCD. We can estimate its mass scale by extracting phase shift imformation.

As a phenomenological application of the framework of the composite Higgs models, we investigate the diphoton excess at 750 GeV at the LHC. At the end of 2015, the diphoton singnal around 750 GeV has been found at the LHC experiments. We consider that this anomaly would be the new particle. The composite Higgs models with extended Higgs sectors could contain such particle and explain this phenomena [3].

As a result, we study two scenarios whose Higgs sectors are composed of the fundamental particles at high energy with/without supersymmetry (SUSY). In the model based on specific choice of SUSY QCD gauge symmetry, the gauge coupling of the new symmetry behaves asymptotic free like that of realistic QCD, $SU(3)_C$. The extended Higgs sector appears at the low energy effective theory. We propose new model with an additional discrete symmetry. In this model, the dark matter, the neutrino mass, and the baryon number asymmetry problems can be solved, simultaneously. We also investigate non-SUSY model. In this model, the Higgs boson appears as a pNGB which is accompanied by the global symmetry breakdown at high energy. The MCHM and its several variation models contain a minimal Higgs sector corresponding to the SM Higgs sector. The deviation pattern of the Higgs boson couplings in the MCHMs can be distinguished each other at future collider experiments. They also affect the Higgs pair production processes. This would be utilized to test the models. As an analogy of QCD dynamics, weak gauge boson scattering amplitude in the MCHMs should be stabilized

by the new particle. We can estimate its mass scale by using phase shift beyond the reach of current experiments. The diphoton excess at 750 GeV could be explained by the extended composite Higgs models

Contents

Chapter 1

Introduction

The SM is the most successful model in describing the high energy collider experiments below the electroweak scale ~ 100 GeV. The SM is based on the gauge principle and the spontaneous symmetry breaking. The gauge principle defines the interactions among the elemenrary particles and forbid the masses of fermions and gauge bosons. The SM gauge symmetry is $SU(3)_C \times SU(2)_L \times U(1)_Y$. However, we already know that these particles have non-zero mass. In order to obtain the particle masses, the spontaneous symmetry breaking is required. The electroweak symmetry $SU(2)_L \times U(1)_Y$ is broken into the electromagnetic symmetry $U(1)_{\rm EM}$ by the vacuum expectation value (VEV), denoted by v, of the SM Higgs doublet. After that, charged fermions, weak gauge bosons, and the Higgs boson masses are proportional to the VEV v. The Higgs boson mass was strongly constrained by several experiments [4], but it not have been discovered for a long time. At long last, in July 2012, a new boson has been discovered at a mass of 126 GeV at LHC [5]. Its spin and parity is also measured and turned out to be 0^+ [6]. The coupling of the new scalar boson to the SM paricles is comfirmed to the SM Higgs boson predictions within the error. Therefore, the new scalar boson is identified to the SM-like Higgs boson. The SM is very successful until now.

However, there are many room and hints to consider the new physics beyond the SM. For example, the existence of dark matter, tiny masses of the neutrinos and the BAU as phenomenological problems. These problems cannot be solved in the SM. There is no dark matter candidate, the neutrino mass is exactly zero because there is no right-handed neutrinos, baryon asymmetry of the Universe cannot be generated. Therefore, the SM must be extended to solve these problems.

On the other hand, as the theoretical problem, the hierarchy problem is well-known one. If the SM is valid at very high-energy scale (e.g. Planck scale $\sim 10^{19}$GeV), a very large difference in the radiative corrections to the Higgs boson masss appears in order to obtain the appropriate physical Higgs boson mass as $\mathcal{O}(10^{38}\text{GeV}^2) - \mathcal{O}(10^{38}\text{GeV}^2) \simeq (100\text{GeV})^2$. The supersymmetric extension is a promissing candidate which can solve the hierarchy problem. New particles whose spin differs 1/2 from SM particles appear and these effects cancel the SM contributions, exactly. In addition to this, models based on SUSY usually contain extended Higgs sectors. For example, the minimal supersymmetric standard model (MSSM) contains two Higgs doublets with opposite hypercharge, $Y = \pm 1/2$. Therefore, the Higgs sector of the MSSM is the two Higgs doublet model. The SM Higgs sector is extended by the requirement of SUSY. The another solution of the hierarchy problem is the Higgs boson as the composite particle. In these class of scenarios, the Higgs bosons are not elementary particles. At the

high-energy scale, the Higgs bosons are deomposed into the fundamental elementary particle and there is no scalar particle. Therefore, the hierarchy problem disappears.

Throughout this thesis, we consider two paradigm whose Higgs bosons appears as the composite particle. One is based on a model with the supersymmetric QCD theory. One is based on a model with the composite Higgs scenario.

First, we study the supersymmetric QCD model which could explain the hierarchy model [1]. In the realistic QCD, $SU(3)_C$, its gauge coupling constant behaves asymptotically free and would become strong around the QCD scale $\sim$ 200 MeV. Naively speaking, below the QCD scale, quarks are cofined each other by the strong QCD dynamics. The typical these bound state is the pion, π^+, π^0, π^-. We propose a new model which contains the supersymmetric QCD-like gauge symmetry. Its gauge coupling also behaves asymptotically free and would become strong around the TeV scale. The new fundamental fields of the new gauge symmetry are confined, like pions. The model based on the supersymmetric $SU(2)_H$ gauge theory leads an extended Higgs sector as a low-energy effective theory. In this model, three phenomenenological problems can be explained, simultaneously. The first order electroweak phase transition, the necessary condition for the baryon number asymmetry of the Universe, can be realized by the existence of many extra scalar bosons. By introducing an additional unboken discrete Z_2 symmetry, there are some DM candidates, the tiny neutrino masses are generated by the loop-induces diagrams. Interestingly, these problems are realized by the TeV scale physics. Therefore, the model would be tested by future high energy experiments.

As an alternative scenario to solve or avoid the hierarchy problem, the Higgs boson is considered as a composite particle which consist of elementary particle in very high-energy scale. There are several scenarios along this line, thecnicolour models [7], little Higgs models [8], and composite Higgs models [9]. In this thesis, we focus on the composite HIggs models with the minimal and extended Higgs sectors [2]. Such class of models, the Higgs boson appears as the NGB which is originated from the breaking of the global symmetry $\mathcal{G}$ to its subgroup $\mathcal{H}$. This subgroup $\mathcal{H}$ is larger than the SM gauge group at least $SU(2)_L \times U(1)_Y$ because the portion of the subgroup is gauged and becomes the SM gauge group. We here omit the remnant part of $\mathcal{H}$. We demand two conditions to set of $\mathcal{G}/\mathcal{H}$, the subgroup $\mathcal{H}$ should have the custodial symmetry in order to satisfy electroweak precision data and the Higgs sector after breakdown of the global symmetry $\mathcal{G}$ should contains one doublet at least. The minimal model is the minimal composite Higgs model (MCHM). In this model, the global symmetry is $SO(5)$ and it breaks into $SO(4)$ at the scale f which is higer than the SM VEV. The breaking scale f is an analogy of f_π in the QCD. The number of the broken generator is $\dim(SO(5)/SO(4)) = 4$ correspoding to the degrees of freedom of the SM Higgs doublet. Therefore, this model contains only one composite Higgs doublet. In this sense, the MCHM is called minimal model. We assume that the particle content is exactly equal to that of the SM, all fermions and gauge bosons. The scalar potential is generated by the Coleman-Weinberg mechanism through the contrinbutions of the $SU(2)_L$ gauge bosons and the top quark, dominantly. The coupling constants of the composite Higgs boson to the SM particles deviate from the SM prediction. Especially, the Higgs-gauge boson coupling uniquely deviates if we choose $SO(5)/SO(4)$ as $\mathcal{G}/\mathcal{H}$. These deviations are parametrised by one characteristic parameter, the compositeness parameter $\xi = v^2/f^2$. This parameter is always smaller than 1. If we take the SM limit as $\xi \to 0$ ($= f \to \infty$), all Higgs boson couplings in the MCHM become the SM values. Then, the coupling constants of the Higgs boson to the fermions and itself depend on the representation of the SM matter field

in $SO(5)$. Therefore, there are several variation models. We classify these MCHM variation models, list the MCHMs Higgs coupling constants, and discuss how to distinguish models at the international linear collider (ILC).

In addition to this, we study how to extract the higher resonance scale at the LHC. In the SM, thanks to the existence of the SM Higgs boson, the perturbative unitarity of the vector boson scattering process $W^+W^- \to W^+W^-$ is conserved. However, as we mentioned, the gauge-Higgs coupling constant deviates from the SM value and it violates unitarity. A similar phenomena is likely to occur in the $\pi\pi$ scattering because we identify the logitudinal mode of the weak gauge bosons as pion. Practically, the unitarity is maintained by a new vector particle, the rho meson. Hence, we introduce such new particle to the MCHM and estimate this energy scale by extracting the phase shift imformation.

We study the double Higgs production via gluon and vector boson fusion process at the LHC and the ILC. The double Higgs boson production process is very important to test the new physics models. We investigate three typical cases, the gluon fusion, the vector boson fusion, and the Z strahlung process. The gluon fusion process is a dominant contribution at hadron colliders. As mentioned above, in the MCHMs, the Higgs boson coupling constants deviates from the SM predictions. Therefore, the production cross section should be changed by these effects. In addition to this, in the MCHMs, higher dimensional operators appear, which absent in the SM. This effect plays an important role in the gluon fusion process. The vector boson fusion (VBF) and the Z strahlung process contribute in the LHC and the ILC. Due to deviations of the Higgs boson couplings, these two process show the charactaristic energy dependence. Its interesting energy dependence could be distinguished at future lepton collider exoeriments.

We also investigate a non-minimal model, composite singlet model. In this model, the global $SO(6)$ symmetry is broken into $SO(5)$ and one Higgs doublet and one singlet field appear. We discuss the collider phenomenology of this mode along the discussion fof the MCHMs.

Finally, we discuss an application of the framework of the extended composite Higgs models to the diphoton excess at the LHC. At the end of 2015, the signal of the diphoton excess at 750 GeV had found. This signal may come from a new particle with the mass 750 GeV. We want to explain this phenomena by relatively simple way. We introduce a neautral singlet and (multiply) charged scalar particles. By this simple setup, diphoton excess could be explained [3].

Chapter 2

The standard model (Review)

We briefly review the SM. The SM Lagrangian is invariant under $SU(3)_C \times SU(2)_L \times U(1)_Y$. The portion of the gauge symmetry $SU(2)_L \times U(1)_Y$ is broken into $U(1)_{\rm EM}$ by the VEV of the Higgs doublet, this is called the electroweak symmetry breaking (EWSB). In the SM, there is only one Higgs doublet. After the EWSB, the masses of quarks, charged leptons, weak gauge bosons, and the Higgs boson are proportional to the SM Higgs VEV v.

2.1 The Lagragian of the standard model

The particle content of the SM is shown in Table 2.1.

	$SU(3)_C$	$SU(2)_L$	$U(1)_Y$
Q_L^i	**3**	**2**	$+1/6$
u_R^i	**3**	**1**	$+2/3$
d_R^i	**3**	**1**	$-1/3$
L_L^i	**1**	**2**	$-1/2$
e_L^i	**1**	**1**	-1
G^λ	**8**	**1**	0
W^α	**1**	**3**	0
B	**1**	**1**	0
Φ	**1**	**2**	$+1/2$

Table 2.1: SM particle content.

where we define the electric charge Q as $Q = T_3 + Y$ and superscript i = 1-3 means family indices.

The SM gauge invariant Lagrangian can be expressed as

$$\mathcal{L}_{\rm SM} = \mathcal{L}_{\rm kin} + \mathcal{L}_{\rm Yukawa} - V_{\rm Higgs} \ . \tag{2.1}$$

$\mathcal{L}_{\rm kin}$ means the kinetic terms of the SM particles, $\mathcal{L}_{\rm Yukawa}$ means the Yukawa interactions between the Higgs doublet and fermions, and $V_{\rm Higgs}$ is the Higgs potential.

2.2 Fermion and Gauge boson masses

As mentioned above, charged fermions and weak gauge bosons obtain their masses after the spontaneous symmetry breakdown by the Higgs doublet VEV. We can parametrize the VEV v as

$$\Phi = \begin{pmatrix} \omega^+ \\ \frac{1}{\sqrt{2}}(v + h + iz) \end{pmatrix} . \tag{2.2}$$

Fermion masses come from $\mathcal{L}_{\text{Yukawa}}$;

$$\mathcal{L}_{\text{Yukawa}} = -\left[\overline{Q}_L^i Y_u^{ij} \widetilde{\Phi} u_R^j + \overline{Q}_L^i Y_d^{ij} \Phi d_R^j + \overline{L}_L^i Y_e^{ij} \Phi e_R^j + \text{h.c.}\right] \tag{2.3}$$

where $\widetilde{\Phi}$ is a charge conjugation of the SM doublet, $\widetilde{\Phi} = i\sigma_2\Phi$, and Y's are Yukawa matrices. In general, the Yukawa matrices are not diagonal one. Fortunately, we can always rotate these three matirces in the family index space, independently. Therefore, the Yukawa matrices are always diagonalized without loss of generality;

$$Y_u^{ij} = \text{diag}(Y_u^1, Y_u^2, Y_u^3), \quad Y_d^{ij} = \text{diag}(Y_d^1, Y_d^2, Y_d^3), \quad Y_e^{ij} = \text{diag}(Y_e^1, Y_e^2, Y_e^3). \tag{2.4}$$

By expanding the component field, the fermion mass is given by

$$m_f = \frac{Y_f}{\sqrt{2}} v. \tag{2.5}$$

Gauge boson masses are obtained by the kinetic term. The relevant terms are

$$\mathcal{L}_{\text{kin}}^{\text{gauge mass}} = |D_\mu \Phi|^2 \ . \tag{2.6}$$

D_μ is convariant derivative for the Higgs doublet;

$$D_\mu = \partial_\mu - ig\frac{1}{2}\vec{\tau}\cdot\vec{W}_\mu - ig'\frac{1}{2}B_\mu \ , \tag{2.7}$$

where g (g') is the gauge coupling of the $SU(2)_L$ ($U(1)_Y$), and $\tau_{1,2,3}$ is the Pauli Matrices.

The mass basis gauge boson eigenstates are written in the linear combination of the gauge basis;

$$\begin{aligned} W^\pm &= \frac{1}{\sqrt{2}}\left(W^1 \mp iW^2\right) \ , \\ \begin{pmatrix} Z \\ A \end{pmatrix} &= \begin{pmatrix} \cos\theta_W & -\sin\theta_W \\ \sin\theta_W & \cos\theta_W \end{pmatrix} \begin{pmatrix} W^3 \\ B \end{pmatrix} \ . \end{aligned} \tag{2.8}$$

where θ_W is the Weinberg (or Weak) angle, $\tan\theta_W = g'/g$. Then we get the gauge boson masses as

$$\begin{aligned} m_W &= \frac{1}{2}gv, \\ m_Z &= \frac{1}{2}\sqrt{g^2 + g'^2}\ v, \\ m_A &= 0 \ . \end{aligned} \tag{2.9}$$

The phoron mass m_A is forbidden by the $U(1)_{EM}$ symmetry. As we can see, fermions and gauge boson masses are proportional to the VEV v.

2.3 The standard model Higgs sector

The Higgs potential of the SM takes very simple form

$$V_{\rm SM} = -\mu_0^2|\Phi|^2 + \lambda\left(|\Phi|^2\right)^2 \ . \tag{2.10}$$

We here assume that $-\mu_0^2$ is negative. After using the stationary condition,

$$\left.\frac{\partial V_{\rm SM}}{\partial h}\right|_{h=0} = 0 \quad \rightarrow \quad \mu_0^2 = \lambda v^2 \ , \tag{2.11}$$

the SM Higgs boson mass around the VEV is

$$m_h^2 = 2\lambda v^2 \ . \tag{2.12}$$

The Higgs boson mass is also proportional to v.

2.4 Decay of the standard model Higgs boson

The SM Higgs boson branching ration is the function of the Higgs boson mass, Figure 2.1.

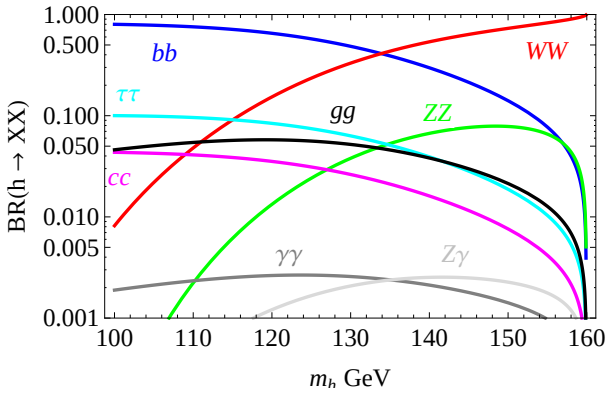

Figure 2.1: The SM Higgs boson braching ratio.

We already know the Higgs boson mass is 126 GeV. Therefore, the dominant channel is $h \rightarrow b\bar{b}$. The numerical calculation beyond leading order contributions is shown in Appendix.

2.5 Beyond/Behind the Higgs sector

The SM Higgs sector with only one doublet is the minimal one for providing particle masses. However, there is no principle to forbid the extended Higgs sectors containing more than two doublets and/or more larger representation (triplet, fiveplet, septet, $\cdots$). The SM Higgs sector is just an assumption. For example, two Higgs doublet model (2HDM) is one of the promissing candidate describing New physics. Moreover, as we glance, the mass term $-\mu^2$ in the Higgs sector is negative. This is also just an assumption. In addition to this, we do not know the origin of the Higgs force λ. We do not understand the essence of the Higgs sector at all. We consider two case to make clear the mystery of the Higgs sector.

2.5.1 The hierarchy problem and its solutions

The most well-known theoretical problem in the SM is the hierarchy problem. The Planck scale is a typical energy scale of the garavitatinal interaction.

$$M_P = G_N^{-1/2} \sim 10^{19} \text{ GeV}. \tag{2.13}$$

where G_N is the gravitational constant. From this viewpoint, the mass parameter μ_0^2, the only dimensionful parameter in the SM, should be of order $\mathcal{O}(10^{19})$ GeV. At this time, if the planck scale is the cutoff scale in a theory, the radiative corrections to the SM Higgs boson mass is also of order $\mathcal{O}(10^{19})$ GeV.

On the other hand, from the gauge boson and the SM Higgs boson masses, the renormalized parameter μ^2 in the SM Higgs potential should be of order $\mathcal{O}(100^2)$ GeV^2;

$$\mu^2 \sim \mu_0^2 - \Lambda^2 = \left[\mathcal{O}(10^{38}) - \mathcal{O}(10^{38})\right] \text{ GeV}^2 \sim \mathcal{O}(100^2)\text{GeV}^2 \tag{2.14}$$

There is a dramatic cancellation. This is so-called *gauge hierarchy prpblem*.

There are several mechanism which can solve or avoid this problem. One is supersymmetry (SUSY). This is the symmetry between fermion and boson. Such class of the models, new particles appear with 1/2 from the SM particle. If SUSY is conserved, the SM particle and its partner have the same mass. Thanks to the existence of supersymmetric particle, the quadratic divergence disappear.

One is the Higgs boson as composite particle. The quadratic divergence to the scalar boson does not appear when we compute radiative corrections to fermion and gauge boson masses by chiral symmetry and gauge symmetry. Throughout this thesis, we consider these two cases.

2.5.2 Origin of the Higgs sector : Supersymmetry strong dynamics

First, we consider the supersymmetric strong dynamics with confinment. This scenario is based on the supersymmetric QCD theory. Previous work is called minimal supersymmetric fat Higgs model. "Fat Higgs" means that the lightesr Higgs boson mass (the SM-like Higgs boson mass m_h at that time) is heavy $m_h \geq 200$ GeV. The Higgs potential is generated by the composite statesof the fundamental field in supersymmetric QCD. The Higgs sector of this model is nMSSM. However, the discovered Higgs boson mass is 126 GeV. Then, original motivation of this model is already excluded. We use this idea. By introducing the discrete symmetry, the lightest Higgs boson mass can be 126 gev and solve phenomenological problem which we mentioned.

2.5.3 Origin of the Higgs sector : non-Supersymmetry strong dynamics

Second, we consider the composite higgs scenario . In such class of scenario, we assume that there is a QCD-ike strong dynamics at higher energy scale. This dynamics is not supersymmetric one. The Higgs boson appears as the Nambu-Goldstone boson (NGB) after the global symmetry breaking. These boson are not exact NGB since the discovered Higgs boson has mass. Therefore, they are called pseudo NGB (pNGB). In the nature, the pion in QCD is the well-known pNGB. The global symmetry $SU(2)_L \times SU(2)_R$ is broken into the vectrial $SU(2)$ and three NGBs will appear, $\pi^{\pm}, \pi^0$ at the low energy scale. Then, we consider that if we investigate the property of

the low energy effective theory such class of scenarios, we can unveil the mystery behind/beyond the Higgs sector.

Chapter 3

The Higgs boson as a Composite state with supersymmetry

We want to explain three phenomenological problems in the SM, the dark matter, the tiny neutrino masses, and the baryon number asymmetry of the Universe. Especially, we expect that these phenomena are related to the Higgs physics because such new physics are described at TeV scale and possibly tested at future collider experiments. For exmaple, we consider a neutrino mass generation scenario by the loop quantum effects [10, 11, 12, 13, 14, 15], called the radiative seesaw scenarios. There is a class of models with an additional Z_2 symmetry [12, 13, 14, 15]. Thanks to the Z_2 symmetry, the tree-level diagrams are forbidden and the neutrino masses are generated by loop-level diagrams. Therefore, the neutrino masses could naturally small by the loop suppression factor. In addition to this, the lightest Z_2-odd particle can be a dark matter candidate because the discrete Z_2 symmetry ensures the stability of the dark matter. The simplest example along this line is the Ma model. In this model, the Z_2-odd scalar doublet (inert doublet) and the Z_2-odd right-handed neutrinos. The lightest Z_2-odd particle, a neutral component of the inert doublet or the right-handed neutrino can be the dark matter candidate. The neutrino masses are generated by one-loop diagram. On the other hand, the Aoki-Kanemura-Seto model contains two Z_2-even doublets, one Z_2-odd neutral singlet and one Z_2-odd charged singlet, and the Z_2-odd right-handed neutrinos. In this model, the neutrino masses are generated by three-loop diagrams and the lightest Z_2-odd particle can be the dark matter. Moreover, the electroweak phase transition can be realized, simultaneously due to the contributions from extra scalars.

These radiative seesaw scenarios seem to be an artificial model. In order to realize the electroweak phase transition, some of the introduced couplings should be of order one. Such large couplings leads the Landau pole below the Planck scale or the GUT scale, and the model is only valid below the Landau pole. This indicates that there is a more fundamental theory above the Landau pole, which leads the low-energy effective theory. We propose a simple model which can explain the DM, the tiny neutrino masses, and the BAU in the low-energy effective theory (BAU).

In this chapter, we discuss the supersymmetric QCD theory. In this class of models, the new gauge coupling constant diverges at the low-energy scale and the low-energy effective theory is described by the composite states of the fundamental fields on the new gauge symmetry. The

simplest model is based on the colour number $N_c = 2$ and the flavour number $N_f = 3$. The minimal supersymmetric fat Higgs model [16] is an application of this setup. We impose an additional discrete Z_2 symmetry. We propose a new model which can explain dark matter, tiny neutrino massse, and the baryon asymmetry of the Universe, simultaneously. This chapter is based on [1].

3.1 The supersymmetric $SU(2)_H$ gauge theory with the discrete symmetry

3.1.1 The Higgs potential

At high energy scale, there are six fundamental doublet fields ($N_f = 3$) under new $SU(2)_H$ gauge symmetry. Below the scale Λ_H, the Higgs potential appears as the composite state of

	$SU(3)_C$	$SU(2)_L$	$U(1)_Y$	Z_2
$\begin{pmatrix} T_1 \\ T_2 \end{pmatrix}$	**1**	**2**	0	$+1$
T_3	**1**	**1**	$+1/2$	$+1$
T_4	**1**	**1**	$-1/2$	$+1$
T_5	**1**	**1**	$+1/2$	-1
T_6	**1**	**1**	$-1/2$	-1
N_R	**1**	**1**	0	-1

Table 3.1: The SM charges and Z_2 parity assignment on the fundamental fields, T's.

T's. As we discuss below, the unbroken Z_2 symmetry is introduced to explain tiny neutrino mass and dark matter problems and we also introduce the Z_2-odd right-handed neutrino superfield to explain the neutrino masses.

The tree-level superpotential, invariant under all gauge symmetry and Z_2 parity, is written as

$$W_{\rm tree} = m_1 T_1 T_2 + m_3 T_3 T_4 + m_5 T_5 T_6 \ . \tag{3.1}$$

At the very high energy scale, the $SU(2)_H$ gauge coupling behaves asymptotic free, like realistic QCD gauge coupling constant. Below the confinement scale, denoted by Λ_H, the gauge coupling becomes strong. The composite chiral superfields are discribed in such low-energy theory as

$$H'_{ij} = T_i T_j \ . \tag{3.2}$$

We can write the dynamically generated superpotential by these chiral superfields as

$$W_{\rm dyn} = -\frac{1}{\Lambda^3}\epsilon^{ijk\ell mn} H'_{ij} H'_{k\ell} H'_{mn} \tag{3.3}$$

where Λ is a dynamical scale [17]. Therefore, the effective superpotential is

$$\begin{aligned} W_{\rm eff} &= W_{\rm tree} + W_{\rm dyn} \\ &= W_{\rm dyn} + 4\pi\Lambda_H (m_1 H_{ij} + m_3 H_{k\ell} + m_5 H_{mn}) \end{aligned} \tag{3.4}$$

with

$$H_{ij} \simeq \frac{1}{4\pi\Lambda_H} T_i T_j \ . \tag{3.5}$$

We cannot determine the dynamically generated scale Λ. However, by using the naive dimensional analysis [18], the effective superpotential can be written as

$$W_{\text{eff}} \simeq 4\pi H_{ij} H_{k\ell} H_{mn} + 4\pi\Lambda_H (m_1 H_{ij} + m_3 H_{k\ell} + m_5 H_{mn}) \ . \tag{3.6}$$

The basic concept is the same as the minimal SUSY fat Higgs model [16]. In general, there are fifteen composite fields at the low-energy theory in this model setup. However, in the minimal SUSY fat Higgs model, the authors introduce additional superfields and symmetries in order to limit the low-energy Higgs sector to the nMSSM one. In our model, all fifteen composite chiral superfields contribute to the theory because we do not impose such restrictions.

The composite Higgs fields are identified as shown in Table 3.2. The superfields H_u, H_d are the MSSM Higgs doublets and others are the exotic superfields.

	$SU(3)_L$	$SU(2)_L$	$U(1)_Y$	Z_2
$H_d = \begin{pmatrix} H_{14} \\ H_{24} \end{pmatrix}$	1	**2**	$-1/2$	$+1$
$H_u = \begin{pmatrix} H_{13} \\ H_{23} \end{pmatrix}$	1	**2**	$+1/2$	$+1$
$\Phi_d = \begin{pmatrix} H_{15} \\ H_{25} \end{pmatrix}$	1	**2**	$-1/2$	-1
$\Phi_u = \begin{pmatrix} H_{16} \\ H_{26} \end{pmatrix}$	1	**2**	$+1/2$	-1
$\Omega_- = H_{46}$	1	1	-1	-1
$\Omega_+ = H_{35}$	1	1	$+1$	-1
$N = H_{56}, N_\Phi = H_{34}, N_\Omega = H_{12}$	1	1	0	$+1$
$\zeta = H_{36}, \eta = H_{45}$	1	1	0	-1

Table 3.2: The composite Higgs sector

The low energy effective superpotential in the Higgs sector is

$$\begin{aligned} W_{\text{eff}} = {} & \lambda N \left(H_u \cdot H_d + v_0^2 \right) + \lambda N_\Phi \left(\Phi_u \cdot \Phi_d + v_\Phi^2 \right) + \lambda N_\Omega \left(\Omega_+ \Omega_- + v_\Omega^2 \right) \\ & + \lambda \left(\zeta H_d \cdot \Phi_u + \eta H_u \cdot \Phi_d - \Omega_+ H_d \cdot \Phi_d - \Omega_- H_u \cdot \Phi_u - N N_\Phi N_\Omega \right) \ , \end{aligned} \tag{3.7}$$

and the relevant part of the soft SUSY breaking Lagrangin is

$$
\begin{aligned}
-\mathcal{L}_{\rm soft} &= m_{H_u}^2 H_u^\dagger H_u + m_{H_d}^2 H_d^\dagger H_d + m_{\Phi_u}^2 \Phi_u^\dagger \Phi_u + m_{\Phi_d}^2 \Phi_d^\dagger \Phi_d \\
&+ m_N^2 N^* N + m_{N_\Phi}^2 N_\Phi^* N_\Phi + m_{N_\Omega}^2 N_\Omega^* N_\Omega \\
&+ m_{\Omega_+}^2 \Omega_+^* \Omega_+ + m_{\Omega_-}^2 \Omega_-^* \Omega_- + m_\zeta^2 \zeta^* \zeta + m_\eta^2 \eta^* \eta \\
&+ \lambda \left\{ C v_0^2 N + C_\Phi v_\Phi^2 N_\Phi + C_\Omega v_\Omega^2 N_\Omega + \text{h.c.} \right\} \\
&+ \left\{ B\mu H_u \cdot H_d + B_\Phi \mu_\Phi \Phi_u \cdot \Phi_d + B_\Omega \mu_\Omega \left(\Omega_+ \Omega_- + \zeta \eta \right) + \text{h.c.} \right\} \\
&+ \lambda \Big\{ A_N H_u \cdot H_d N + A_{N_\Phi} \Phi_u \cdot \Phi_d N_\Phi + A_{N_\Omega} \left(\Omega_+ \Omega_- - \zeta \eta \right) N_\Omega \\
&\quad + A_\zeta H_d \cdot \Phi_u \zeta + A_\eta H_u \cdot \phi_d \eta + A_{\Omega_-} H_u \cdot \Phi_u \Omega_- + A_{\Omega_+} H_d \cdot \Phi_d \Omega_+ + \text{h.c.} \Big\} \\
&+ \left\{ m_{\zeta\eta}^2 \eta^* \zeta + \frac{B_\zeta^2}{2} \zeta^2 + \frac{B_\eta^2}{2} \eta^2 + \text{h.c.} \right\}
\end{aligned}
\tag{3.8}
$$

where the dimensionless coupling λ becomes 4π at the confinement scale. The mass paramers of $\mu, \mu_\Phi, \mu_\Omega$ are described by

$$
\mu \equiv \lambda \langle N \rangle, \quad \mu_\Phi \equiv \lambda \langle N_\Phi \rangle, \quad \mu_\Omega \equiv \lambda \langle N_\Omega \rangle. \tag{3.9}
$$

In our model, Z_2-even neutral superfields N_Ω and N_Φ are irrelevant to discussion. Then, we omit. After that, the effective Z_2-even Higgs sector is identical with that of the nearly-minimal supersymmetric standard model (nMSSM) [19].

In order to explain the tiny neutrino mass and the dark matter problem in the framework of the radiative seesaw scenario, we introduce following terms to the effective superpotential

$$
W_N = y_N^i N_R^c L_i \Phi_u + h_N^i N_R^c E_i^c \Omega_- + \frac{M_R}{2} N_R^c N_R^c + \frac{\kappa}{2} N N_R^c N_R^c \ . \tag{3.10}
$$

where L_i and E_i^c are the left-handed lepton doublets and the right-handed lepton singlet, repectively.

3.1.2 The lightest Higgs boson mass

The lightest Higgs boson (= the SM-like Higgs boson) mass is estimated as

$$
m_h^2 \simeq m_Z^2 \cos^2 2\beta + \frac{\lambda^2 v^2}{2} \sin^2 2\beta + \delta m_h \tag{3.11}
$$

where δm_h comes from loop corrections. In order to realize the first order phase transition, λ should be large. Therefore, we need large $\tan\beta$ value.

3.1.3 Neutrino mass : Hybrid radiative seesaw scenario

In our scenario, the neutrino masses are generated by one-loop nad three-loop diagrams shown in Figure 3.1 and Figure 3.2. These types of diagrams are shown in [12] and [14].

The neutrino masses in the flavour basis ($i, j = e, \mu, \tau$) is represented as

$$
(m_\nu)_{ij} = m_{ij}^{(\rm one)} + m_{ij}^{(\rm three)} \ . \tag{3.12}
$$

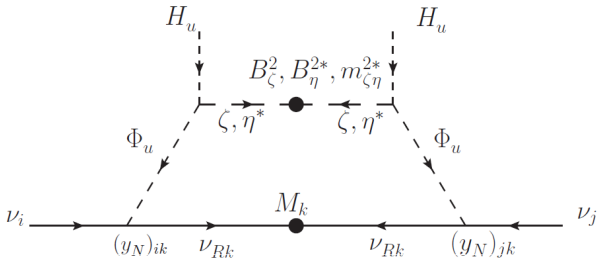

Figure 3.1: One-loop diagram

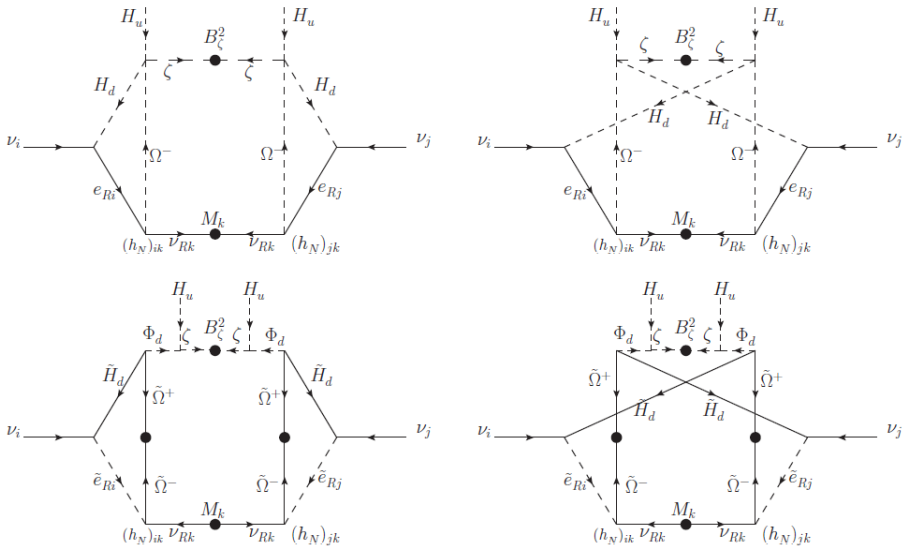

Figure 3.2: Three-loop diagrams

One-loop diagram contribution is evaluated as

$$m_{ij}^{(\mathrm{one})} = \frac{y_N^i y_N^j}{(4\pi)^2} \left\{ (O_0)^{1\alpha} (O_0)^{1\alpha} m_{\nu_R} - (O_0)^{5\alpha} (O_0)^{5\alpha} m_{\nu_R} \right\} \overline{B}_0(m^2_{\Phi_\alpha}, m^2_{\nu_R}) \tag{3.13}$$

and three-loop diagram contribution is evaluated as

$$\begin{aligned}
m_{ij}^{(\text{three})} =& \frac{\lambda^4 v_u^2 y_E^i y_E^j h_N^i h_N^j m_{\nu_R}}{(4\pi)^6} \sin^4\beta \\
& \times \left(U_+^*\right)_{4\gamma} (U_+)_{4\gamma} \left(U_+^*\right)_{4\delta} (U_+)_{4\delta} \left\{ (O_0)_{2\rho} (O_0)_{2\rho} - (O_0)_{6\rho} (O_0)_{6\rho} \right\} \\
& \times F(m_{\nu_R}^2, m_{\Phi_\rho}^2; m_{e_i}^2, m_{\Phi_\gamma^\pm}^2; m_{e_j}^2, m_{H^\pm}^2, m_{\Phi_\delta^\pm}^2) \\
& + 2 \frac{\lambda^2 y_E^i y_E^j h_N^i h_N^j m_{\nu_R} m_{\Phi_\gamma}^\pm m_{\Phi_\delta}^\pm}{(4\pi)^6} \\
& \times (V_L^*)_{2\alpha} (V_L)_{2\alpha} (V_L^*)_{2\beta} (V_L)_{2\beta} (U_L^*)_{2\gamma} (U_L)_{2\gamma} (U_L^*)_{2\delta} (U_L)_{2\delta} \\
& \times \left\{ (O_0)_{3\rho} (O_0)_{3\rho} - (O_0)_{7\rho} (O_0)_{7\rho} \right\} F(m_{\nu_R}^2, m_{\Phi_\rho}^2; m_{\tilde{\chi}_\pm}^2, m_{\tilde{e}_{R_i}}^2, m_{\tilde{\Phi}_\gamma}^2; m_{\tilde{\chi}^\pm}^2, m_{\tilde{e}_{R_j}}^2, m_{\tilde{\Phi}_\delta^\pm}^2)
\end{aligned} \tag{3.14}$$

where $\overline{B}_0$ is finite part of the one-loop scalar B_0 function with external momentum square $p^2 = 0$

$$\overline{B}_0(m_1^2, m_2^2) = -\frac{m_1^2 \log m_1^2 - m_2^2 \log m_2^2}{m_1^2 - m_2^2} \ , \tag{3.15}$$

the loop function F is

$$\begin{aligned}
& F(M^2, m_\Phi^2; m_{\phi 1}^2, m_{\Omega 1}^2; m_{\chi 2}^2, m_{\phi 2}^2, m_{\Omega 2}^2) \\
=& \frac{(4\pi)^6}{i} \int \frac{d^D k}{(2\pi)^D} \frac{1}{k^2 - M^2} \frac{1}{k^2 - m_\Phi^2} \int \frac{d^D p}{(2\pi)^D} \frac{\not{p}}{p^2 - m_{\chi 1}^2} \frac{1}{p^2 - m_{\phi 1}^2} \frac{1}{(k+p)^2 - m_{\Omega 1}^2} \\
& \times \int \frac{d^D q}{(2\pi)^D} \frac{-\not{q}}{(-q)^2 - m_{\chi 2}^2} \frac{1}{(-q)^2 - m_{\phi 2}^2} \frac{1}{(k + (-q))^2 - m_{\Omega 2}^2}
\end{aligned} \tag{3.16}$$

The mixing matrices O_0, U_+, U_L, U_R, and V_L are defined as

$$\begin{pmatrix} \Phi_u^{\text{even}} \\ \zeta^{\text{even}} \\ \Phi_d^{\text{even}} \\ \eta^{\text{even}} \\ \Phi_u^{\text{odd}} \\ \zeta^{\text{odd}} \\ \Phi_d^{\text{odd}} \\ \eta^{\text{odd}} \end{pmatrix} = O_0 \begin{pmatrix} \Phi_1 \\ \Phi_2 \\ \Phi_3 \\ \Phi_4 \\ \Phi_5 \\ \Phi_6 \\ \Phi_7 \\ \Phi_8 \end{pmatrix} \ , \qquad \begin{pmatrix} \Phi_u^+ \\ \Omega_+ \\ \left(\Phi_d^-\right)^* \\ \left(\Omega_d^-\right)^* \end{pmatrix} = U_+ \begin{pmatrix} \Phi_1^+ \\ \Phi_2^+ \\ \Phi_3^+ \\ \Phi_4^+ \end{pmatrix} \ ,$$

$$\begin{pmatrix} \tilde{\Phi}_d^- \\ \tilde{\Omega}_- \end{pmatrix} = U_L \begin{pmatrix} \tilde{\Phi}_{1L}^- \\ \tilde{\Phi}_{2L}^- \end{pmatrix} \ , \qquad \begin{pmatrix} \left(\tilde{\Phi}_u^+\right)^* \\ \left(\tilde{\Omega}_+\right)^* \end{pmatrix} = U_R \begin{pmatrix} \tilde{\Phi}_{1R}^- \\ \tilde{\Phi}_{2R}^- \end{pmatrix} \ , \qquad \begin{pmatrix} \tilde{W} \\ \tilde{H}_d^- \end{pmatrix} = V_L \begin{pmatrix} \tilde{\chi}_{1L}^- \\ \tilde{\chi}_{2L}^- \end{pmatrix} \ , \tag{3.17}$$

where the superscript "even" ("odd") means CP-even (CP-odd) neutral scalar components, Φ_i's express the mass eigenstates of the Z_2-odd neutral scalrs, $\Phi_i^\pm, \Omega_\pm$ are charged scalar components in the Z_2-odd sector, $\tilde{\Phi}_i^\pm, \tilde{\Omega}_\pm$ are the fermionic fields of their chiral superfields and their mass eigenstates are $\tilde{\Phi}_{iL,iR}^-$, $\tilde{W}(\tilde{H}_d)$ is the wino (the Higgsino) as same as in the MSSM and $\tilde{\chi}$ are their mass eigenstates.

3.1.4 The dark matter : Multi-Component DM scenario

There are many dark matter candidate in thie model. The additional unbroken Z_2 symmetry and R-parity ensure the stability of them. Therefore, three cases are considered; $(Z_2, R_p) = (+,-), (-,+), (-,-)$. In our model, we can idetify these cadidates as the lightest neutralino, the right-handed neutrino and the right-handed sneutrino. For simplicity, the dark matter candidate with $(Z_2, R_p) = (+,-)$ is much heavier in order to decay into the right-handed neutrino and the right-handed sneutrino. Then, it cannot become the dark matter candidate. We here choose the dark matter as right-handed neutrino ν_R and sneutrino $\tilde{\nu}_R$. The relic abundance is expressed by

$$\Omega_{\rm DM} = \Omega_{\nu_R} + \Omega_{\tilde{\nu}_R} \simeq 0.12 \ . \tag{3.18}$$

The DM annihilation processes are shown in Figure 3.3.

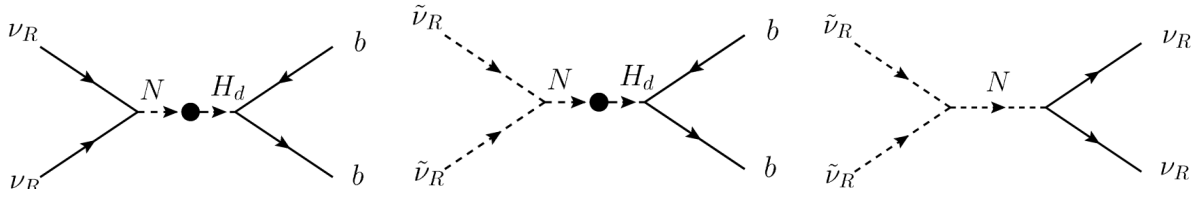

Figure 3.3: The left and center diargrams are dominant contributions to the dark matter annihilation processes. The right diagram is the dark matter number conversion process. N is the Z_2-even neutral singlet and it mix with the netral component of the neutral component of the doublet.

In order to reproduce the measured DM relic abundance $\Omega_{\rm DM} \simeq 0.12$, we set the masses of ν_R and $\tilde{\nu}_R$ as $m_{\nu_R} = m_{\tilde{\nu}_R} \simeq m_h/2$. In this case, the s-channel resoncance enhances the annihilation production cross section and thus the experimental data can be satisfied. Along this line, the relic abundance of our model is determined by the coupling constant κ and the mixing parameter among N and H_d. The DM number convesion process is also important to reproduce the observed relic abundance [20].

The numerical evaluation of the DM abundance is obtained by calculating the Boltzmann equations as

$$\begin{aligned}
\frac{dY}{dx} = 0.264 g_*^{1/2} \left(\frac{\mu_R M_P}{x^2}\right) \Bigg\{ & - \langle \sigma_\nu v \rangle \left(Y^2 - Y_{\rm eq}^2\right) \\
& - \langle \sigma_{\nu\tilde{\nu}} v \rangle \left(Y^2 - \tilde{Y}^2 \frac{Y_{\rm eq}^2}{\tilde{Y}_{\rm eq}^2}\right) + \langle \sigma_{\tilde{\nu}\nu} v \rangle \left(\tilde{Y}^2 - Y^2 \frac{\tilde{Y}_{\rm eq}^2}{Y_{\rm eq}^2}\right) \Bigg\} \\
\frac{d\tilde{Y}}{dx} = 0.264 g_*^{1/2} \left(\frac{\mu_R M_P}{x^2}\right) \Bigg\{ & - \langle \sigma_{\tilde{\nu}} v \rangle \left(\tilde{Y}^2 - \tilde{Y}_{\rm eq}^2\right) \\
& - \langle \sigma_{\tilde{\nu}\nu} v \rangle \left(\tilde{Y}^2 - Y^2 \frac{\tilde{Y}_{\rm eq}^2}{Y_{\rm eq}^2}\right) + \langle \sigma_{\nu\tilde{\nu}} v \rangle \left(Y^2 - \tilde{Y}^2 \frac{Y_{\rm eq}^2}{\tilde{Y}_{\rm eq}^2}\right) \Bigg\}.
\end{aligned} \tag{3.19}$$

In above equations, the raios of particle number density of ν_R and $\tilde{\nu}_R$ to the entropy density are denoted by Y and $\tilde{Y}$, g_* is the effective degrees of freedom in the thermal equilibrium, x is the dimensionless inverse temperature $x = \mu_R/T$, μ_R is the reduced mass in the two component DM system defined by $\mu_R^{-1} = m_{\nu_R}^{-1} + m_{\tilde{\nu}_R}^{-1}$, M_P is the Planck mass scale, $\langle\sigma v\rangle$ is the thermal averaged cross section, the cross sections $\sigma_\nu, \sigma_{\tilde{\nu}}, \sigma_{\tilde{\nu}\nu}, \sigma_{\nu\tilde{\nu}}$ correspond to the process of $\nu_R\nu_R \to b\bar{b}$, $\tilde{\nu}_R\tilde{\nu}_R \to b\bar{b}$, $\nu_R\nu_R \to \tilde{\nu}_R\tilde{\nu}_R$ and $\tilde{\nu}_R\tilde{\nu}_R \to \nu_R\nu_R$.

3.1.5 First order electroweak phase trasition

The first order electroweak phase transition is the necessary condition for the electroweak baryogenesis. This condition is written as

$$\frac{\varphi_C}{T_C} \gtrsim 1 \ . \tag{3.20}$$

In the SM, in order to satisfy this condition, the SM Higgs boson mass must be lighter than about 60 GeV. However, the SM Higgs boson mass is much heavier, 125 GeV. In our model, the extra scalar bosons which strongly couple to the SM-like Higgs boson enhance φ_C/T_C. Moreover, such non-decoupling effect significantly contributes to the Higgs boson triple coupling λ_{hhh} [21].

3.1.6 Falvour violating process

The right-hahded neutrino contribute to the flavour violationg process, $\mu \to e\gamma$ and $\mu \to eee$. These experimental values strongly constrain the model parameter space. The relevant diagrams are shown in Figure 3.4.

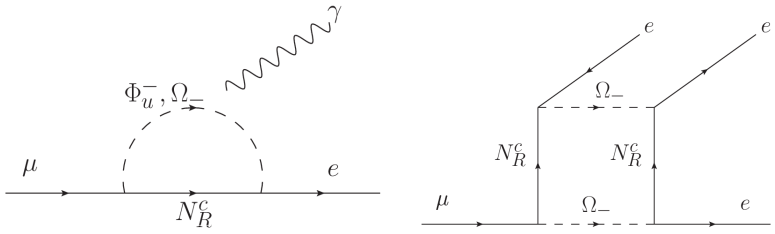

Figure 3.4: The flavour violationg processes contribute to $\mu \to e\gamma$ (left) and $\mu \to eee$ (right) from the right-handed neutrino.

The Z_2-even SUSY sector generally contribute to the LFV process. In our model, we assume that the off-diagonal components of the squarks and sleptons are zero and thus their contributions vanish.

3.1.7 Benchmark scenario

We discuss our benchmark scenario which can explain the first order electroweak phase transition, the neutrino oscillation data, and the relic abundance of the DM, simultaneously.

First, we discuss the first order electroweak phase transition. In order to satisfy $\varphi_C/T_C \gtrsim 1$ by the mechanism by [22], the coupling λ is $\lambda = 1.8$. This coupling enhances φ_C/T_C and contributes to the Higgs triple coupling and $h \to \gamma\gamma$.

Second, in our model, one-loop and three-loop diagram contribute to the neutrino oscillation. The solar and atmospheric neutrino mass differences are dominated by one-loop and three-loop

diagram, respectively. In this benchmark scenario, the neutrino mass hierarchy pattern is the normal hierarchy $m_1 < m_2 < m_3$. In the case of the inverted hierarchy $m_1 > m_2 > m_3$, the LFV experimental data is difficult to be satisfied with only one right-handed neutrino. By intorducing more than two right-handed neutrinos, this condition could be relaxed. The experimental constrains [23] are

$$\begin{aligned} 2.28 \times 10^{-3}\mathrm{eV}^2 <& |m_3^2 - m_1^2| < 2.70 \times 10^{-3}\mathrm{eV}^2 \ , \\ 7.0 \times 10^{-5}\mathrm{eV}^2 <& m_2^2 - m_1^2 < 8.1 \times 10^{-5}\mathrm{eV}^2 \ , \\ 0.27 <& \sin^2\theta_{12} < 0.34, \\ 0.34 <& \sin^2\theta_{23} < 0.67, \\ 0.016 <& \sin^2\theta_{13} < 0.030. \end{aligned} \tag{3.21}$$

Third, the DM cadidates in our model are the right-handed neutrino and sneutrino. The annihilation processes, shown in , occurs by the Z_2-even neutral scalar bosons, including the SM-like Higgs boson. Such scenario is called the Higgs portal DM scenario. A constrain from the DM direct detection experiment, the XENON100 [24] and LUX100 [25], can be satisfied because the right-handed neutrino and sneutrino are $SU(2)_L$ gauge singlets. The spin-independent cross section via the Z_2-even neutral scalar bosons N and H_d, $\sigma^{\mathrm{SI}}_{\nu_R}$ and $\sigma^{\mathrm{SI}}_{\tilde{\nu}_R}$, are evaluated as

$$\begin{aligned} \sigma^{\mathrm{SI}}_{\nu_R} &= 3.1 \times 10^{-46}\ \mathrm{cm}^3 \ , \\ \sigma^{\mathrm{SI}}_{\tilde{\nu}_R} &= 7.7 \times 10^{-47}\ \mathrm{cm}^3 \ . \end{aligned} \tag{3.22}$$

Therefore, the DM-proton spin-independent cross section si

$$\sigma_{\mathrm{DM}} = \frac{\Omega_{\nu_R}}{\Omega_{\mathrm{DM}}}\sigma^{\mathrm{SI}}_{\nu_R} + \frac{\Omega_{\tilde{\nu}_R}}{\Omega_{\mathrm{DM}}}\sigma^{\mathrm{SI}}_{\tilde{\nu}_R} = 1.1 \times 10^{-46}\ \mathrm{cm}^3 \ . \tag{3.23}$$

The input parameters for numerical calculation and output parameters (predictions) are shown in Table 3.3 and Table 3.4. The relic abundance of the DMs as a function of the right-handed neutrino mass and the relic abundance of the DMs with fixed mass as a function of $x = \mu_R/T$ are shown in Figure 3.5.

We also calculate the lepton flavour violationg processes. In order to satisfy these experimental constrainrs, we set $h^1_N = 0$.

3.2 Conclusion

We have investigated the simple model which explain the problems of the SM, the tiny neutrino masse, the existence of the DM and the baryon number asymmetry of the Universe. The model based on the supersymmetric new gauge theory $SU(2)_H$ with confinement at the low-energy scale. In addition to this symmetry, we introduce the unbroken Z_2 symmetry and Z_2-odd right-handed neutrino superfield. At the low-energy theory, the extended Higgs sector appears as a composite states of the fundamental field in $SU(2)_H$. The first order electroweak phase transition is successfully satisfied when the confinement scale is of order 10 TeV and thus the non-decoupling effect becomes large. In addition to R-parity, the unbroken Z_2 symmetry ensures the stability of the DM. The tiny neutrino masses and mixing angles are explaind by the one-loop nad three-loop quantum effect via the right-handed neutrino. We have found the benchmark scenario whicn explain these phenomenological problems which cannot solve in the framework of the SM and avoid the experimental constraints.

Table 3.3: The input parameters in our benchmaek scenario. We define $\bar{m}^2_{\Phi_i} = m^2_{\Phi_i} + |\mu_i|^2$, where $\mu_i = \mu_\Phi$ for $\Phi_i = \Phi_{u,d}$ and $\mu_i = \mu_\Omega$ for $\Phi_i = \Omega_\pm, \zeta, \eta$.

$\lambda, \tan\beta$ and μ-terms
$\lambda = 1.8, \quad \tan\beta = 15, \quad \mu = 250\text{GeV}, \quad \mu_\Phi = 250\text{GeV}, \quad \mu_\Omega = -550\text{GeV}$
Z_2-even Higgs sector
$m_h = 126\text{GeV}, \quad m_{H^\pm} = 990\text{GeV}, \quad m_N = 1050\text{GeV}, \quad A_N = 2900\text{GeV}$
Z_2-odd Higgs sector
$\bar{m}^2_{\Phi_u} = \bar{m}^2_{\Omega_-} = (175\text{GeV})^2, \quad \bar{m}^2_{\Phi_d} = \bar{m}^2_{\Omega_+} = \bar{m}^2_\zeta = (1500\text{GeV})^2, \quad \bar{m}^2_\eta = (2000\text{GeV})^2,$
$B_\Phi = B_\Omega = A_\zeta = A_\eta = A_{\Omega_+} = A_{\Omega_-} = m^2_{\zeta\eta} = 0, \quad B^2_\zeta = (1400\text{GeV})^2, \quad B^2_\eta = (700\text{GeV})^2$
Right-handed neutrino and sneutrino sector
$m_{\nu_R} = 63\text{GeV}, \quad m_{\tilde{\nu_R}} = 65\text{GeV}, \quad \kappa = 0.9,$
$y_N = (3.28i, 6.70i, 1.72i) \times 10^{-6}, \quad h_N = (0, 0.227, 0.0204)$
Other SUSY SM paramerers
$m_{\tilde{W}} = 500\text{GeV}, \quad m_{\tilde{q}} = m_{\tilde{\ell}} = 5\text{TeV}$

Table 3.4: Predictions of our benchmark scenario given from Table 3.3.

Non-decoupling effects
$\varphi_C/T_C = 1.3, \quad \lambda_{hhh}/\lambda_{hhh}\vert_{\text{SM}} = 1.2, \quad \text{BR}(h \to \gamma\gamma)/\text{BR}(h \to \gamma\gamma)_{\text{SM}} = 0.78$
Neutrino masses and mixing angles
$(m_1, m_2, m_3) = (0, 0.0084, 0.050)\text{eV}, \quad \sin^2\theta_{12} = 0.32, \quad \sin^2\theta_{23} = 0.50, \quad \vert\sin\theta_{13}\vert\ 0.14$
LFV processes
$\text{BR}(\mu \to e\gamma) = 3.6 \times 10^{-13}, \quad \text{BR}(\mu \to eee) = 5.6 \times 10^{-16}$
Relic abundance of the DMs
$\Omega_{\nu_R}h^2 = 0.055, \quad \Omega_{\tilde{\nu}_R}h^2 = 0.065, \quad \Omega_{\text{DM}}h^2 = \Omega_{\nu_R}h^2 + \Omega_{\tilde{\nu}_R}h^2 = 0.12$
Spin-independent DM-proton scattering cross sections
$\sigma^{\text{SI}}_{\nu_R} = 3.1 \times 10^{-46}\ \text{cm}^3, \quad \sigma^{\text{SI}}_{\tilde{\nu}_R} = 7.7 \times 10^{-47}\ \text{cm}^3, \quad \sigma_{\text{DM}} = 1.1 \times 10^{-46}\ \text{cm}^3$

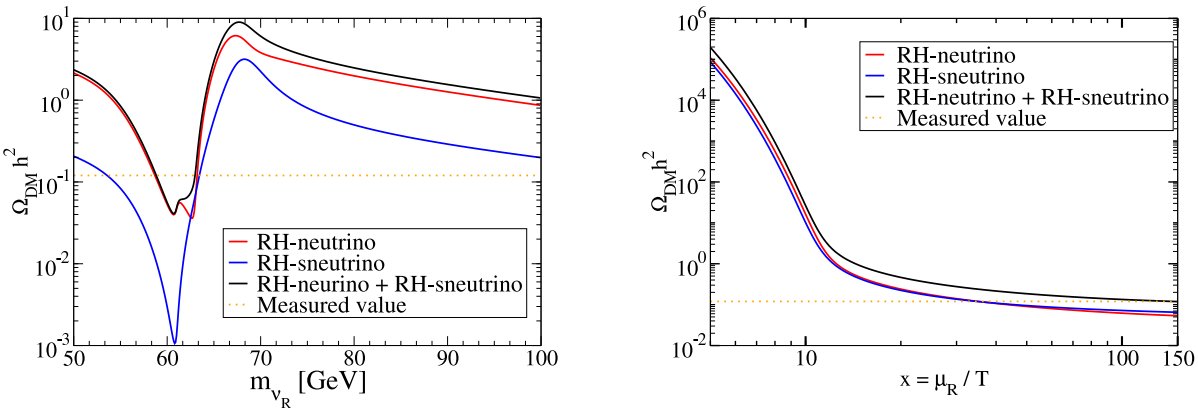

Figure 3.5: (Left) The predictions of the thermal relic abundance of the right-handed neutrino and senutrino as a function of the mass of the right-handed neutrino m_{ν_R}. The right-handed sneutrino mass is taken to be $m_{\tilde{\nu}_R} = m_{\nu_R} + 2$ GeV for all parameter region. (Right) The thermal relic abundence in the benchmark scenario with $m_{\nu_R} = 63$ GeV.

Chapter 4

The Higgs boson as a pseudo Nambu-Goldstone boson

4.1 Introduction

The basic idea of composite Higgs models is originally proposed by Georgi and Kaplan [9]. In this class of models, there is no scalar boson at the very high-energy scale, so that the gauge hierarchy problem disappears. The Higgs boson appears as a Nambu-Goldstone boson (NGB) associated with the breakdown of the global symmetry $\mathcal{G}$ to its subgroup $\mathcal{H}$. The subgroup $\mathcal{H}$ must contain the SM gauge group, at least $SU(2)_L \times U(1)_Y$. We here consider that the global symmetry $\mathcal{G}$ is just an approximate symmetry at the high energy scale. We already know that the $SU(3)_C$ gauge symmetry behaves asymptotically free. By the explicit breaking effect of the shift symmetry, the Higgs boson obtains the mass by one-loop quantum effects via the gauge bosons and fermions. Therefore, these are called pseudo-NGBs (pNGBs). Thanks to this dynamics, we could explain the light Higgs boson mass 125 GeV, naturally. The breaking scale of global symmetry f, which is alologue of the pion decay constant f_π in the QCD, is much higher than the vacuum expectation value of the SM Higgs field v.

The composite Higgs scenario is an analogue of the QCD and we already know the existence of the pNGB, pion. The pions are the NGBs originated from the chiral symmetry breaking, $SU(2)_L \times SU(2)_R \to SU(2)$. They obtain masses from the explicit breaking effect of the chiral symmetry. The theory, describing the pion physics, are well-known one as the chiral perturbation theory [26]. In the pion scattering process, it is well-known that the perturbative unitarity will be violated at a certain scale. However, it's recoverd by an existence of a new particle, called the rho meson. In this case, the phase shift occurs around the rho meson mass scale. We expect that there is a new particle whose properties are almost as same as the rho meson in the QCD and also the phase shift will occurs.

In this thesis, we have investigated the minimal composite Higgs model. This chapter is based on [2], [3] and some recent development.

4.2 The Minimal Composite Higgs models

The minimal composite Higgs model is the minimal model with one composite Higgs doublet [27]. In this model, the global symmetry is $SO(5)$ and it breaks into $SO(4)$. The number of NGB is 4(=dim$(SO(5)/SO(4))$). It corresponds to the degrees of freedom of the SM Higgs

doublet. The subgroup $SO(4)(\simeq SU(2)_L \times SU(2)_R)$ contains the custodial symmetry. Thanks to the custodial symmetry, the T-parameter does not recieve any large effect. Moreover, the extra $U(1)_X$ symmetry is introduced to reproduce $U(1)_Y$ symmetry. The hypercharge Y is generated by the third component of $SU(2)_R$ and $U(1)_X$, $Y = T_3^R + X$.

4.2.1 Lagrangian

In order to obtain the interacting Lagrangian, we follow the method of [27]. The non-linear realized Higgs field is expressed as

$$\Sigma = \Sigma_0 e^{\Pi/f} \ , \quad \Sigma_0 = (0,0,0,0,1) \ , \quad \Pi = -iT^{\hat{a}} h^{\hat{a}} \sqrt{2} \ , \tag{4.1}$$

where f is the breaking scale, Σ_0 is $SO(5)$ breaking vacuum and $T^{\hat{a}}$'s are the broken generators with corresponding to NGB fields $h^{\hat{a}}$. We can rewrite Σ as

$$\Sigma = \frac{\sin(h/f)}{h}(h^1, h^2, h^3, h^4, h\cot(h/f)), \tag{4.2}$$

with $h = \sqrt{h^{\hat{a}} h^{\hat{a}}}$. We here assume that h^3 is the physical Higgs field h and choose the unitary gauge; $h^{1,2,4} \to 0, \ h_3 \to h$

$$\Sigma = \frac{\sin(h/f)}{h}\,(0,0,h,0,h\cot(h/f)) \ . \tag{4.3}$$

The $SO(5) \times U(1)_X$ invariant effective Lagrangian is the momentum space is written as

$$\begin{aligned} \mathcal{L}_{\rm eff} &= \mathcal{L}_{\rm eff}^{\rm gauge} + \mathcal{L}_{\rm eff}^{\rm matter} \\ &= \frac{1}{2} P_{\mu\nu} \left[\Pi_0^X(p) X^\mu X^\nu + \Pi_0(p) {\rm Tr}[A^\mu A^\nu] + \Pi_1(p) \Sigma A^\mu A^\nu \Sigma^T \right] + \mathcal{L}_{\rm eff}^{\rm matter} \ , \end{aligned} \tag{4.4}$$

where A_μ are the $SO(5)$ gauge fields, $A_\mu = T^a A_\mu^a + T^{\hat{a}} A_\mu^{\hat{a}}$, T^a's are unbroken generators in $SO(4)$, X_μ is the $U(1)_X$ gauge field, $\Pi_{0,1}$ are the form factor and $P_{\mu\nu}$ is the projection operator, $P_{\mu\nu} = g_{\mu\nu} - p_\mu p_\nu / p^2$. The matter Lagrangian $\mathcal{L}_{\rm eff}^{\rm matter}$ depends on the representation of the matter fields. We discuss $\mathcal{L}_{\rm eff}^{\rm matter}$ and classify the variation models of the MCHMs below sections. The irrelevant part of the gauge Lagrangian is omitted and the remnant part is

$$\begin{aligned} \mathcal{L}_{\rm eff}^{\rm gauge} =& \frac{1}{2} P^{\mu\nu} \Bigg[\left(\Pi_0^X(p) + \Pi_0(p) + \frac{\sin^2(h/f)}{4} \Pi_1(p) \right) B_\mu B_\nu \\ &+ \left(\Pi_0^X(p) + \frac{\sin^2(h/f)}{4} \Pi_1(p) \right) W_\mu^{a_L} W_\nu^{a_L} \\ &+ 2\sin^2(h/f) \Pi_1(p) \hat{H}^\dagger T^{a_L} Y \hat{H} W_\mu^{a_L} B_\nu \Bigg] \ , \end{aligned} \tag{4.5}$$

where $W_\mu^{a_L}$ are the $SU(2)_L$ gauge fields, B_μ is the $U(1)_Y$ gauge field, $\hat{H}$ can be reconstructed as

$$\hat{H} = \frac{1}{h} \begin{pmatrix} h^1 - ih^2 \\ h^3 - ih^4 \end{pmatrix} \ , \tag{4.6}$$

and $T^{a_L}(Y)$ is the iegenvalue of $\hat{H}$, $T^{a_L}(Y) = 1/2$.

At the tree-level, the Higgs boson mass is exactly zero by the shift symmetry of the NGB. The Higgs potential of the effective $SU(2)_L \times U(1)_Y$ gauge theory is generated at the one-loop level as

$$V_{\rm eff} = V_{\rm eff}^{\rm gauge} + V_{\rm eff}^{\rm fermion} \ , \tag{4.7}$$

where $V_{\rm eff}^{\rm gauge}$ denotes the contributions from the $SU(2)_L$ gauge boson loops and $V_{\rm eff}^{\rm fermion}$ denotes those from the SM matter fermion loops. The gauge boson contirbution is expressed as

$$V_{\rm eff}^{\rm gauge} = \frac{9}{2}\int \frac{d^4p}{(2\pi)^4} \ln\left(\Pi_0(p) + \frac{1}{4}\Pi_1(p)\sin^2(h/f)\right) \ . \tag{4.8}$$

If we turn off the fermionic fonctribution $V_{\rm eff}^{\rm fermion}$, the electroweak symmetry $SU(2)_L \times U(1)_Y$ is not broken. The explicit form of $V_{\rm eff}^{\rm fermion}$, which depends on the matter embedding of the fermions sector $\mathcal{L}_{\rm eff}^{\rm matter}$, plays an important role for the realistic model building.

After that, the gauge symmetry $SU(2)_L \times U(1)_Y$ is broken by the Coleman-Weinberg mechanism, the one-loop quantum effects of the gauge and matter fields. The electroweak symmetry breaking vacuum is written as

$$\langle \Sigma \rangle = \left(0, 0, \sqrt{\xi}, 0, \sqrt{1-\xi}\right) \ , \tag{4.9}$$

where ξ is the compositeness parameter, defining by $\xi = \sin^2(\langle h \rangle / f)$, and $\langle h \rangle$ is the VEV of h.

By expanding h around the VEV as $h \to \langle h \rangle + \hat{h}$, the effective Lagrangian given in Eq. (4.5) leads to the interaction terms between the Higgs boson $\hat{h}$ and the weak bosons. Therefore, we ontain

$$\begin{aligned}\mathcal{L}_{\rm eff}^{\rm gauge} =& \frac{g^2v^2}{4}W_\mu^+W^{-\mu} + \frac{g^2v}{2}\sqrt{1-\xi}\hat{h}W_\mu^+W^{-\mu} + \frac{g^2(1-2\xi)}{4}\hat{h}^2W_\mu^+W^{-\mu} \\ &+ \frac{g_Z^2v^2}{4}Z_\mu Z^\mu + \frac{g_Z^2v}{2}\sqrt{1-\xi}\hat{h}Z_\mu Z^\mu + \frac{g_Z^2(1-2\xi)}{4}\hat{h}^2Z_\mu Z^\mu \ ,\end{aligned} \tag{4.10}$$

where $g_Z^2 = g^2 + g'^2$ and the VEV in the SM is defined by $v = f\sqrt{\xi}$ ($= 246$ GeV). The range of the compositeness parameter is easily understood as $0 < \xi < 1$. The coupling deviation pattern between the gauge bosons and the Higgs boson are determined by the breaking pattern of the global symmetry, $SO(5) \to SO(4)$. The scale factor is obtained by $g_{hVV} = g_{hVV}^{\rm SM}\sqrt{1-\xi}$, it is independently given by the matter sector.

4.3 Phase shift

In the MCHMs, the gauge-Higgs boson couplings deiviate from the SM predictions; i.e., $g_{hVV} = g_{hVV}^{\rm SM}\sqrt{1-\xi}$ and $g_{hhVV} = g_{hhVV}^{\rm SM}(1-2\xi)$. Interestingly, these deviations break perturbative unitarity of the scattering process $W_LW_L \to W_LW_L$, W_L denotes the logitudinal mode of the weak gauge boson. The unitarity argument gives us the constrain on partial wave amplitudes a_l in the channel of the angular momentum ℓ:

$$\mathrm{Re}[a_\ell]^2 + \left(\mathrm{Im}[a_\ell] - \frac{1}{2}\right)^2 = \left(\frac{1}{2}\right)^2 , \tag{4.11}$$

which means that a_ℓ is bound on a circle in the complex plane of the radius $1/2$ with the centre at $(0, 1/2)$. It cannot exceed $1/2$. We here consider the s-wave amplitude of $W_L W_L \to W_L W_L$,

$$a_0 = \frac{G_F \xi S}{16\sqrt{2}\pi} + \frac{G_F(m_h^2 - M_W^2)(1-\xi)}{4\sqrt{2}\pi} \qquad (\sqrt{S} \gg m_h), \tag{4.12}$$

where $\sqrt{S}$ is the centre-of-mass energy of the system. The unitarity bound is expressed as $|a_0| \leq \frac{1}{2}$. In MCHMs, the non-vanishing compositeness parameter ξ violates the perturbative unitarity. In Fig. 4.1, we show the unitarity bound on the plane of the $\sqrt{S}$–ξ, the perturbative unitarity is violated in the region above the solid curve. This limit tells us the larger non-vanishing ξ gives the smaller $\sqrt{S}$.

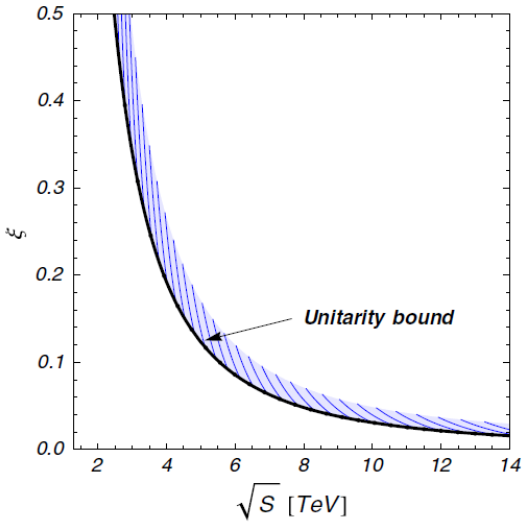

Figure 4.1: The unitarity bound as a function of ξ and $\sqrt{S}$ given in Eq.(4.12). The region above the solid curve forbidden by violating perturbative unitarity.

We obtain an important argument from the perturbative unitarity violation. If the obseved cross section of the W_L scattering process becomes larger than the SM prediction, two different possibilities are considered, (i) at high energies, the electroweak theory becomes a strongly coupled theory, where we cannot apply the perturbative calculation. (ii) the purterbative unitarity is recovered by a new resonance state with a broad width. The latter is a similar situation to the Fermi theory where the cutoff scale is the W boson mass. The case (ii) corresponds to an analogy of the contribution of the rho meson in the QCD pion effective theory. Therefore, if we could measure the phase shift imformation of the scattering amplitude of new resonance, we may extract the imformation of the new resonance.

Next, we discuss the energy scale of the new resonance and how to extract its scale from the phase shift imformation. There are previous studies [28, 29] which investigated the phase shift of the scattering process. The energy dependence of the phase shift is unknown. Fortunately,

the phase shift of the pion svcattering is measured and shown in [29],

$$\delta = \begin{cases} \tan^{-1}\left[\dfrac{\Gamma_\rho}{m_\rho}\dfrac{S}{m_\rho^2+\Gamma_\rho^2-S}\right] & \text{for} \quad \sqrt{S} < \sqrt{m_\rho^2+\Gamma_\rho^2}, \\ \tan^{-1}\left[\dfrac{\Gamma_\rho}{m_\rho}\dfrac{S}{m_\rho^2+\Gamma_\rho^2-S}\right]+\pi & \text{for} \quad \sqrt{S} \geq \sqrt{m_\rho^2+\Gamma_\rho^2}, \end{cases} \tag{4.13}$$

where m_ρ and Γ_ρ are the rho meson mass and its total decay width, respectively. By using the analogy between the pion scattering and the W_L scattering, we assume that the same fitting function (4.13) can be applied to the W_L scattering in the MCHMs as in [29].

The phase δ as a function of a_0 is defined by

$$\delta \equiv \tan^{-1}\left[\frac{\mathrm{Im}[a_0]}{\mathrm{Re}[a_0]}\right] = \tan^{-1}\left[\frac{1}{2\mathrm{Re}[a_0]} \pm \sqrt{\frac{1}{4\mathrm{Re}[a_0]^2}-1}\right], \tag{4.14}$$

The above equation is given by (4.11), by using the fact that a_0 is bound on the circle, not within the circle. Therefore, this condition is a conservative limit which gives the maximal $|a_0|$.

In Figure. 4.2, by using (4.13) and (4.14), the phase δ is obtained as functions of the new resonance mass m_ρ and the compositeness parameter ξ. This figure means that the resonance state mass m_ρ can be converted to ξ. The width-to-mass ratio Γ_ρ/m_ρ are set to be 0.1, 0.2 and 0.3 in the upper-left, upper-right and bottom-left panels, respectively. We note that the shaded regions in the figures are always on the unitarity circle, and the centre-of-mass energy $\sqrt{S}$ is just a parameter at this stage. The non-vanishing compositeness parameter ξ violates the perturbative unitarity. However, as shown in the Figures, the unitarity is recovered by the new resonance. The maximal value of $\delta = \pi/4$ in all figures corresponds to $(\mathrm{Re}[a_0], \mathrm{Im}[a_0]) = (1/2, 1/2)$ on the unitarity circle. We also show the phase δ dependence of m_ρ with fixed serveral ξ, shown in Figure 4.3.

Next, we discuss the possibility to measure the phase sfift imformation at current and future collider experiments. The direct phase extraction from the elastic scattering of W_L requrires very high energy experiments [42]. As an alternative method, we consider the production process $u\bar{d} \to WZ$ with full leptonic channel at hadron colliders. We assume that the phase shift of this process is the same that of the W_L scattering as stuidied in [29]. The phase δ is extracted by the angular correlation betweean the charged lepton from W boson decay and the production plane of WZ [29, 31, 32]. The kinematics is shown in Appendix. From the angular distribution of the charged lepton from the W boson in $\ell\ell\ell + \not{E}_T$ final states, we expecte that the phase shift imformation could be measured.

We here define the rhoduction amplitude of $u\bar{d} \to WZ$, $\mathcal{M}_{\mathrm{Prod}}(\Theta; \lambda_W, \lambda_Z)$, with $\lambda_{W,Z}$ are polarizations of W and Z bosons, respectively, with $\lambda_{W,Z} = \pm 1, 0$. The production angle Θ means the scattering angle between incoming u-quark and outgoing W^+.

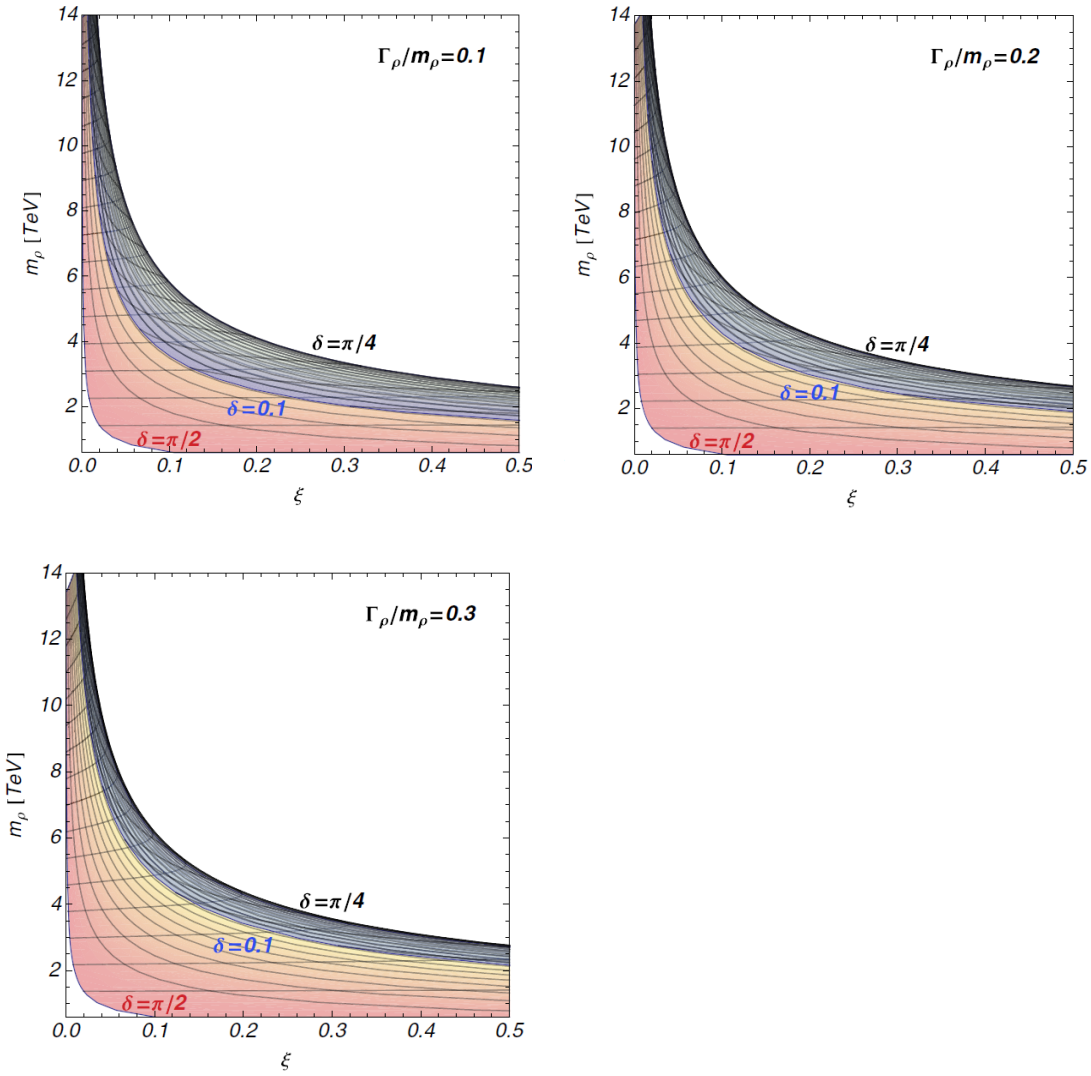

Figure 4.2: Three panels show new resonance scales predicted by perturbative unitarity, where a sizable phase shift appears. We take the width-to-mass ratio as $\Gamma_\rho/m_\rho = 0.1, 0.2$ and 0.3 in the upper-left, upper-right and bottom-left panels, respectively.

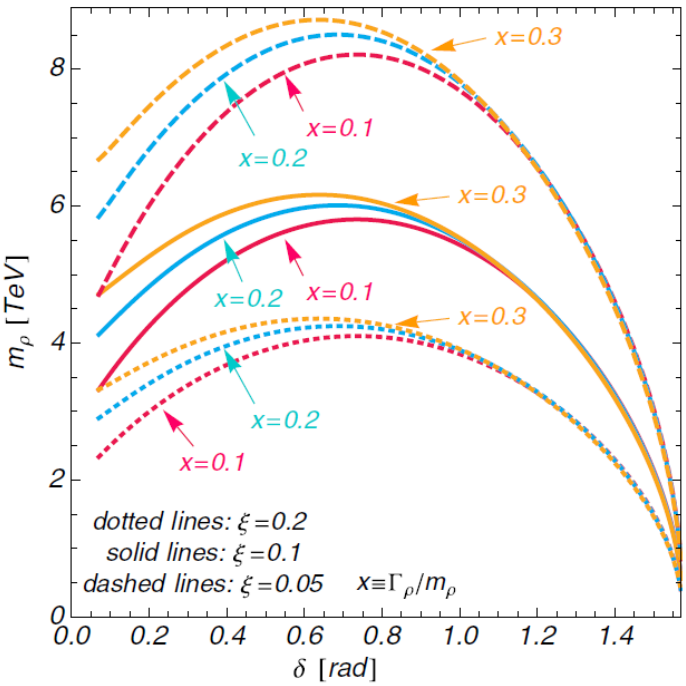

Figure 4.3: The relation between m_ρ and δ for fixed ξ and Γ_ρ/m_ρ. Each curve corresponds to the slice at $\xi = 0.05, 0.1$ or 0.2 in Fig. 4.2.

The decay amplitudes of $W^+ \to \ell^+\nu_\ell$ and $Z \to \ell^+\ell^-$ are denoted as $\mathcal{M}_W(\theta_1, \phi_1; \lambda_W)$ and $\mathcal{M}_Z(\theta_2, \phi_2; \lambda_Z)$, respectively, as functions of two polar angles (θ_1, θ_2) and two azimuthal angles (ϕ_1, ϕ_2) of the each final state leptons. The full amplitude is proportional to

$$d\sigma(u\bar{d} \to WZ \to l\nu ll) \propto \left| \sum_{\lambda_W, \lambda_Z} \mathcal{M}_{\rm Prod}(\Theta; \lambda_W, \lambda_Z) \mathcal{M}_W(\theta_1, \phi_1; \lambda_W) \mathcal{M}_Z(\theta_2, \phi_2; \lambda_Z) \right|^2 . \quad (4.15)$$

We can identify the logitudinal modes of the vector bosons W_L and Z_L to the NGBs. The phase δ would appear the scattering amplitude for W_L and Z_L. We then introduce the phase by $\mathcal{M}_{\rm Prod}(\Theta; 0, 0) \to \mathcal{M}_{\rm Prod}(\Theta; 0, 0)e^{i\delta}$, and we regard this δ as the phase shift which appears in $W_L W_L$ scattering. Therefore, we introduce the phase to $\mathcal{M}_{\rm Prod}(\Theta; 0, 0) \to \mathcal{M}_{\rm Prod}(\Theta; 0, 0)e^{i\delta}$, as mentioned above, we assume that this δ is the same one which appears in the W_L scattering. We show the result the hadronic cross section $\sigma(pp \to WZ \to l\nu ll)$ as a function of the phase δ, with $\sqrt{s}$ =14, 30, 100 TeV. For numerical computation, we utilize the parton distribution function (PDF) as MSTW 2008lo [44]. At the point of $\delta = 0$ (corresponding to the SM), the hadronic cross section is given by $\sigma(14\ \text{TeV}) \sim 0.01$ pb, $\sigma(30\ \text{TeV}) \sim 0.04$ pb and $\sigma(100\ \text{TeV}) \sim 0.1$ pb.

The polarization $\lambda_{W,Z}$ dependence of the decay ampplitudes are expressed as

$$\mathcal{M}_W(\theta_1, \phi_1; \lambda_W) \propto e^{i\lambda_W \phi_1}, \quad \mathcal{M}_Z(\theta_2, \phi_2; \lambda_Z) \propto e^{-i\lambda_Z \phi_2} . \quad (4.16)$$

Therefore, the phase δ dependence can be estimated from the squared amplitude as

$$|\text{amplitude}|^2 \supset \sin(\lambda_W \phi_1 - \lambda_Z \phi_2) \sin\delta \quad \text{for} \quad \lambda_W \neq 0, \ \lambda_Z \neq 0. \quad (4.17)$$

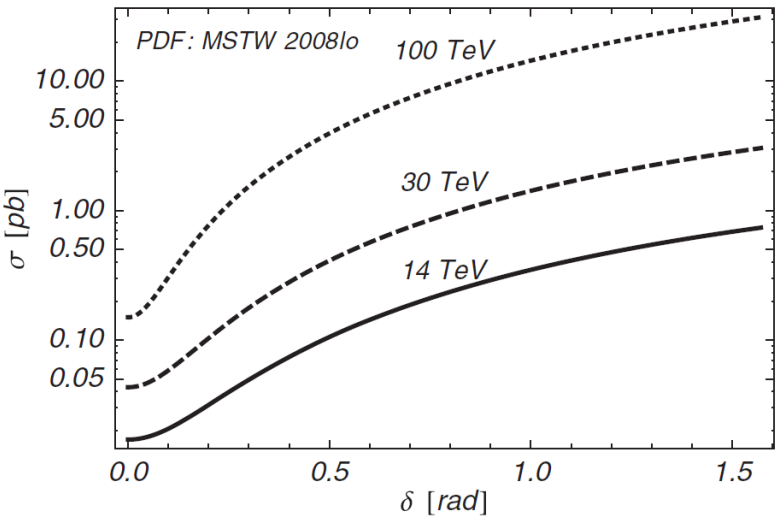

Figure 4.4: Total cross section as a function of the phase δ. Solid, dashed and dotted curves show the case that the center of mass energy is 14 TeV, 30 TeV and 100 TeV, respectively. At the point of $\delta = 0$, the cross section is given by $\sigma(14\text{ TeV}) \sim 0.01$ pb, $\sigma(30\text{ TeV}) \sim 0.04$ pb and $\sigma(100\text{ TeV}) \sim 0.1$ pb.

One can easily find that if $\delta = 0$ such correlation disappears. Therefore, we can extract the phase δ from the direction of charged lepton with ϕ_1 or ϕ_2. In the following discussion, we focus on ϕ_1, the azimutial angle of the charged lepton from the W^+ boson decay.
In order to identify the events, we discuss two ambiguity. One is the misidentification of the incoming u-quark direction, whose kinematics leads to $(\Theta, \phi_1, \phi_2) \to (\pi - \Theta, \pi + \phi_1, \pi + \phi_2)$. Therefore, we carry out the phase space integration $0 < \cos\Theta < 1$ or $-1 < \cos\Theta < 0$. In other words, we only pick up a contribution of the definite incoming direction of u-quark. Other is the neutrino missing energy. We here define the asymmetry at the hadronic level,

$$A_\pm \equiv \frac{|\sigma_+ - \sigma_-|}{\sigma_+ + \sigma_-}, \quad \sigma_\pm \equiv \sigma(\sin\phi_1 \gtrless 0), \tag{4.18}$$

where $\sigma_+(\sigma_-)$ is the cross section integrated over $0 < \phi_1 < \pi$ ($\pi < \phi_1 < 2\pi$). Consequently, the direction of the neutrino does not affect. The numerical result as a function of the phase δ for $\sqrt{s} = 14, 30, 100$ TeV is shown in Figure 4.5.

The asymmetry at the parton level is defined by

$$\hat{A}_\pm \equiv \frac{|\hat{\sigma}_+ - \hat{\sigma}_-|}{\hat{\sigma}_+ + \hat{\sigma}_-}, \quad \hat{\sigma}_\pm \equiv \hat{\sigma}(\sin\phi_1 \gtrless 0), \tag{4.19}$$

where $\hat{\sigma}_\pm$ are parton-level cross sections, which depend on the centre-of-mass energy $\sqrt{\hat{s}}$ of the subprocess. In Figure 4.6, we show the parton level asymmetry as a function of $\sqrt{\hat{s}}$ with $\delta = 0.1, 0.2, 0.3, \pi/4$ and $\pi/2$. The maximal values are shown in the figure as red points for each δ.

The maximal point becomes smaller and smaller for large pahse δ. Therefore, the maximal point could appear around lower energy. After utilizing the PDF, the asymmetry becomes

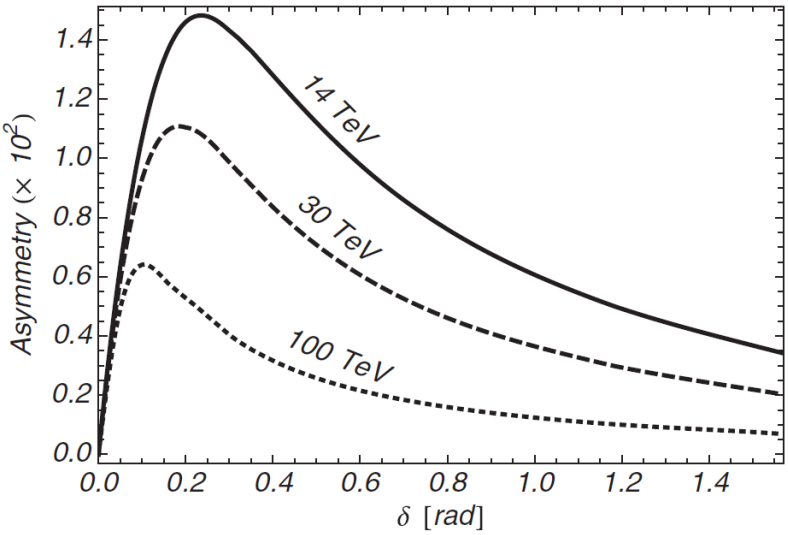

Figure 4.5: The asymmetry $A_\pm$ as a function of δ, where solid, dashed and dotted curves correspond to the case of the collision energy 14 TeV, 30 TeV and 100 TeV, respectively.

maximal around $\delta \sim 0.2$ for $\sqrt{s} = 14$ TeV, Figure 4.5. The asymmetry becomes smaller for larger phases, which can be understood by kinematics as follows. As shown in Fig. 4.6, when the phase is larger, the value of $\sqrt{\hat{s}}$ where the parton-level asymmetry becomes maximal gets smaller, and finally goes below the WZ threshold.

In Fig. 4.5, the asymmetry also becomes smaller when the phase is getting smaller. This behavior is reasonable because a smaller phase shift corresponds to a higher resonance scale so that we cannot reach such an energy scale. We find that the asymmetry is most sensitive to the case of $\delta \sim 0.2$ at LHC with the collision energy 14 TeV. When we extend the collision energy to 30 TeV and 100 TeV, the sensitivity to a smaller phase increases, as shown by the dashed and dotted curves in the figure.

Before closing this section, let us discuss the possibility to observe the phase shift in this channel at future hadron collider experiments. As shown in Fig. 4.4, the non-vanishing phase predicts larger cross section compared to the SM prediction. The asymmetry is expected to be observed at future LHC experiments. For example, $\sigma \simeq 0.037$ pb with the collision energy 14 TeV when $\delta \simeq 0.24$ (and $A_\pm \simeq 0.015$). In this case, the statistic error is comparable to the value of the asymmetry with integrated luminosity 300 fb^{-1}, and thus more statistics is required. If we accumulate 3000 fb^{-1} at the high-luminosity phase of future LHC experiment, the statistics is almost one order of magnitude improved, and thus the phase shift can be observed. Furthermore, when we consider higher-energy collider experiments such as collision energies 30 TeV and 100 TeV, the cross section get larger. In the case of the collision energy 30 TeV, the cross section becomes $\sigma \simeq 0.095$ fb at $\delta \simeq 0.018$ where the asymmetry is maximally large. Although the cross section with the collision energy 30 TeV becomes large as compared to that with 14 TeV, the maximal asymmetry decreases because $A_\pm$ is normalized by the cross section itself. Thus the higher luminosity is also required in this case. The sensitivity to the asymmetry is not improved even in the case of the collision energy 100 TeV. Therefore, in order to observe the asymmetry, the increasing luminosity might be efficient rather than the

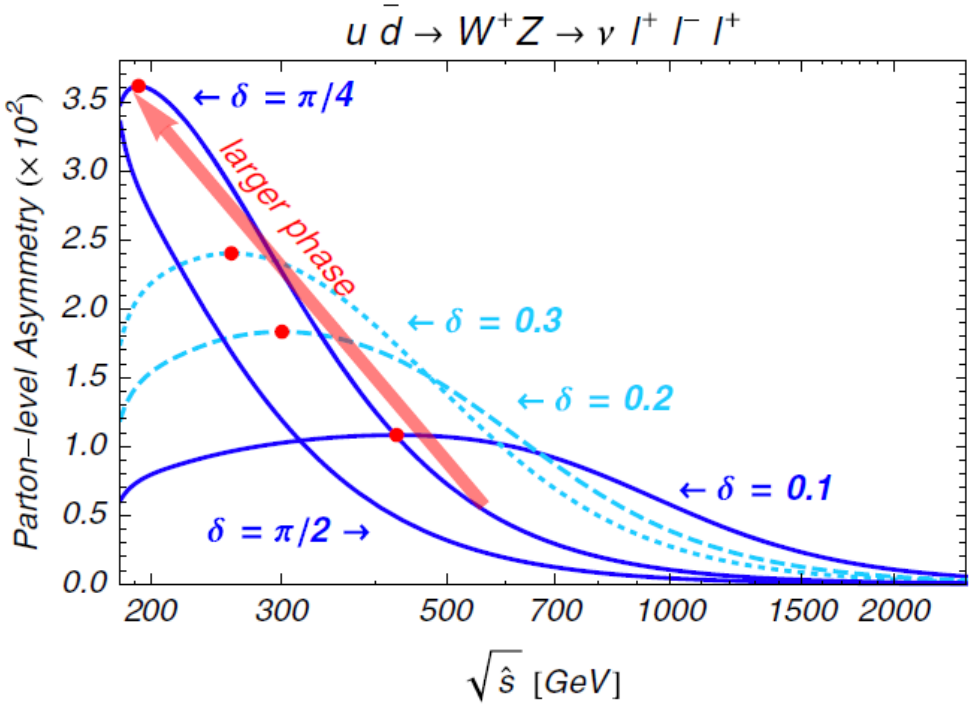

Figure 4.6: Parton-level asymmetry as a function of the center of mass energy $\sqrt{\hat{s}}$. The asymmetry is shown for the case of $\delta = 0.1, 0.2, 0.3, \pi/4$ and $\pi/2$, and the red dots represent the points at which the asymmetry becomes maximally large for each δ.

increasing collision energy.

It should be noted that for the signal event $pp \to WZ \to l\nu ll$ there are large background events. However, since we see the asymmetry, it is not necessary to suppress the SM background after extracting the events. The efficiency of the event selection for $pp \to WZ \to l\nu ll$ is about 70. Although this efficiency makes the statistic error larger, our naive estimation is not largely affected by the background. An ingenious technique is also helpful to probe the phase shift in this channel. For example, although we have studied only leptonic decay of Z, larger cross sections can be achieved by taking hadronic decay modes into account, where the asymmetry does not decrease since it is induced by the W decay.

Let us finally comment on the future e^+e^- collision experiments such as ILC in which more precise measurement can be achieved. For example, the similar procedure can be applied to $e^+e^- \to W^+W^- \to l^+\nu_l\bar{u}d$ so that information of the phase shift can be extracted from the kinematics. It might also be possible to apply the same manner to the Higgs-strahlung process. These cases will be studied elsewhere.

4.4 Fingerprint identification in the MCHMs

As discussed in the previous section, appearance of a new resonance with a relatively broad width can be the first evidence of composite Higgs scenarios. However, there exists a variety of MCHMs depending on matter representations so that as the second step we have to narrow down the MCHMs to a class of specific models by experiments. One of the promising strategies for this purpose is to fingerprint MCHMs by precisely measuring a set of the Higgs boson couplings. The precision measurements at the high-luminosity LHC as well as at future e^+e^- colliders will be able to provide a strong clue to understand the detail of the MCHMs. In this section, we demonstrate how to distinguish variations of the MCHMs by patterns of the deviations from the SM predictions. In order to investigate such deviations, we utilize scale factors defined by $\kappa_a \equiv g_a/g_a^{\rm SM}$, where g_a denote the Higgs boson couplings with the weak gauge bosons $V(V = W, Z)$, matter fermions and the Higgs boson itself such as $a = hVV$, hhh, htt and hbb. For some of them, we use simple forms as $\kappa_V \equiv \kappa_{hVV}$, $\kappa_t \equiv \kappa_{htt}$, and $\kappa_b \equiv \kappa_{hbb}$. We also discuss contact interactions such as $hhVV$, $hhhh$, $hht\bar{t}$ and $hhb\bar{b}$, where we define their couplings as g_{hhVV}, g_{hhhh}, g_{hhtt} and g_{hhbb}. For $hhVV$ and $hhhh$, we use the parameters $c_{hhVV} \equiv g_{hhVV}/g_{hhVV}^{\rm SM}$ and $c_{hhhh} \equiv g_{hhhh}/g_{hhhh}^{\rm SM}$. Each MCHM basically predicts a specific pattern of deviations in these couplings, so that we can distinguish models by detecting such a pattern by experiments.

As already shown in above section, universal predictions for the scale factors of the Higgs couplings to the gauge bosons are obtained as $\kappa_V = \sqrt{1-\xi}$ and $c_{hhVV} = 1-2\xi$ in the MCHMs. It means that the compositeness parameter ξ is determined by the measurement of κ_V. We can also test the consistency with the MCHMs by measuring the correlations among κ_V and c_{hhVV} independent of the detail in matter sector of the MCHMs. For example, in the minimal supersymmetric SM, κ_V is reduced by the mixing angle, but c_{hhVV} is always unity regardless of the mixing angle. However, it could be challenging to precisely measure c_{hhVV} even at future collider experiments and should be a task for future colliders [34].

On the other hand, the main contribution to the one-loop effective Higgs potential is driven by the Yukawa coupling of matter fermions. Therefore, self-couplings of the Higgs boson as well as the Higgs boson couplings to the matter fermions reflect the matter sector of the MCHMs

$\mathcal{L}_{\rm eff}^{\rm matter}$. The effective Lagrangian for the matter sector is determined by how the SM matter fermions are embedded into the $SO(5)$ representations. In the following, we define various MCHMs according to the matter representations in order, and discuss deviations in Higgs boson couplings.

First, we introduce the simplest model, so-called MCHM$_4$. In this model, all the matter fermions are embedded into four-dimensional representations $\Psi_r^{(4)}(r = q, u, d)$ of $SO(5)$ as

$$\Psi_q^{(4)} = \begin{pmatrix} q_L \\ Q_L \end{pmatrix} , \quad \Psi_u^{(4)} = \begin{pmatrix} q_R^u \\ \begin{pmatrix} u_R \\ d'_R \end{pmatrix} \end{pmatrix} , \quad \Psi_d^{(4)} = \begin{pmatrix} q_R^d \\ \begin{pmatrix} u'_R \\ d_R \end{pmatrix} \end{pmatrix} . \tag{4.20}$$

Here, $q_L = (u_L, d_L)^T$, u_R, and d_R are SM quark $SU(2)_L$ doublet, right-handed up-type quark and right-handed down-type quark, respectively, and the other fields as Q_L, q_R^u, q_R^d, u'_R, and d'_R are non-dynamical fields so that their contributions are negligible. The relevant matter part of the effective Lagrangian is given by

$$\mathcal{L}_{\rm eff}^{\rm matter} = \sum_{r=q,u,d} \overline{\Psi}_r^{(4)} \not{p} \left[\Pi_0^r(p) + \Pi_1^r(p) \Gamma^i \Sigma_i \right] \Psi_r^{(4)} + \sum_{r=u,d} \overline{\Psi}_q^{(4)} \left[M_0^r(p) + M_1^r(p) \Gamma^i \Sigma_i \right] \Psi_r^{(4)} , \tag{4.21}$$

where $\Gamma^i (i = 1, \cdots, 5)$ are gamma matrices in five-dimensional representation of $SO(5)$, and M's are the form factors. The loop contributions of the matter fermion to the Higgs potential is dominated by the top-quark loop, and it is evaluated in the MCHM$_4$ as

$$V_{\rm eff}^{\rm fermion} \simeq -2N_C \int \frac{d^4p}{(2\pi)^4} \left[\ln \not{p} \Pi_{b_L} + \ln(p^2 \Pi_{t_R} \Pi_{t_L} - \Pi_{t_L t_R}^2) \right] , \tag{4.22}$$

where

$$\Pi_{t_L} = \Pi_{b_L} = \Pi_0^q + \Pi_1^q \sin(h/f) , \quad \Pi_{t_R} = \Pi_0^u - \Pi_1^u \cos(h/f) , \quad \Pi_{t_L t_R} = M_1^u \sin(h/f) , \tag{4.23}$$

and $N_C = 3$ is the colour number of QCD. Notice that this contribution $V_{\rm eff}^{\rm fermion}$ depends on the representation of the quark fields. From Eqs. (4.8) and (4.22), the effective potential given in Eq. (4.7) can be rewritten as

$$V_{\rm eff} \simeq \alpha \cos(h/f) - \beta \sin^2(h/f) , \tag{4.24}$$

where

$$\begin{aligned} \alpha =& 2N_C \int \frac{d^4p}{(2\pi)^4} \left(\frac{\Pi_1^u}{\Pi_0^u} - 2\frac{\Pi_1^q}{\Pi_1^q} \right) , \\ \beta =& \int \frac{d^4p}{(2\pi)^4} \left(2N_C \frac{|M_1^u|^2}{(-p^2)(\Pi_0^q + \Pi_1^q)(\Pi_0^u - \Pi_q^u)} - \frac{9}{8}\frac{\Pi_1}{\Pi_0} \right) . \end{aligned} \tag{4.25}$$

By the contribution of $V_{\rm eff}^{\rm fermion}$, the $SU(2)_L \times U(1)_Y$ is broken at the minimum of the effective potential $V_{\rm eff}$. Actually, the vacuum conditions given by,

$$\begin{aligned} \left\langle \frac{\partial V_h}{\partial h} \right\rangle &= \frac{\sin(\langle h \rangle / f)}{f} \left(\alpha + \beta \cos(\langle h \rangle / f) \right) = 0 , \\ \left\langle \frac{\partial^2 V_h}{\partial h^2} \right\rangle &= \frac{2\beta}{f^2} \left(1 - \frac{\alpha^2}{4\beta^2} \right) = m_h^2 > 0 , \end{aligned} \tag{4.26}$$

are satisfied with $\sin(\langle h\rangle/f) = v/f \neq 0$. The coupling constant for the triple Higgs boson coupling is predicted as

$$\lambda_{hhh} \equiv \left\langle \frac{\partial^3 V_h}{\partial h^3} \right\rangle = \frac{3m_h^2}{v}\sqrt{1-\xi}\,. \tag{4.27}$$

Eq. (4.21) also leads to the mass terms of the third generation quarks and these interaction terms with the Higgs boson as

$$\begin{aligned}\mathcal{L}_{\text{eff}} =& M_1^t \sin(h/f)\bar{t}t + M_1^b \sin(h/f)\bar{b}b \\ =& M_1^t\sqrt{\xi}\left(1+\sqrt{1-\xi}\frac{\hat{h}}{v} - \frac{1}{2}\xi\frac{\hat{h}^2}{v^2}+\cdots\right)\bar{t}t + M_1^b\sqrt{\xi}\left(1+\sqrt{1-\xi}\frac{\hat{h}}{v} - \frac{1}{2}\xi\frac{\hat{h}^2}{v^2}+\cdots\right)\bar{b}b \\ =& m_t\bar{t}t + \frac{m_t}{v}\sqrt{1-\xi}\hat{h}\bar{t}t - \frac{m_t}{2v^2}\xi\hat{h}^2\bar{t}t + m_b\bar{b}b + \frac{m_b}{v}\sqrt{1-\xi}\hat{h}\bar{b}b - \frac{m_b}{2v^2}\xi\hat{h}^2\bar{b}b + \cdots\,,\end{aligned} \tag{4.28}$$

where m_t and m_b are the masses of the top quark and the bottom quark, respectively. It provides us $\kappa_t = \kappa_b = \sqrt{1-\xi}$. For the contact interactions of two Higgs bosons and two fermions, their coupling constants are given by $g_{hhtt} = -m_t\xi/(2v^2)$ and $g_{hhbb} = -m_b\xi/(2v^2)$ in the MCHM$_4$ model. We parametrize these couplings as $c_{hhtt} \equiv g_{hhtt}/(m_t/(2v^2))$ and $c_{hhbb} \equiv g_{hhbb}/(m_b/(2v^2))$ in the following discussions.

Next, we consider variations of MCHMs. There are other representations of $SO(5)$ into which we can embedd the SM quark fields, such as one-, five-, ten- and fourteen-dimensional representations and so on. In general, $q_L = (u_L, d_L)$, u_R, and d_R can be embedded into individual representations. We already discussed one of the simplest model, MCHM$_4$. Another simple model is the MCHM$_5$ in which all the quark fields, u_L, d_L, u_R and d_R, are embedded into the five-dimensional representations. The detail of the model is given in the Appendix. The factors κ_V and c_{hhVV}, in the MCHM$_5$ are the same as those in the MCHM$_4$. On the other hand, the MCHM$_5$ predicts different deviation patterns from the MCHM$_4$ predictions for the factors κ_{hhh}, c_{hhhh}, κ_t, κ_b c_{hhtt} and c_{hhbb}. The MCHM$_4$ and MCHM$_5$ predict $(\kappa_{hhh}, c_{hhhh}, \kappa_{t(b)}, c_{hhtt(hhbb)}) \simeq (1-\frac{1}{2}\xi, 1-\frac{7}{3}\xi, 1-\frac{1}{2}\xi, -\xi)$ and $(1-\frac{3}{2}\xi, 1-\frac{25}{3}\xi, 1-\frac{3}{2}\xi, -4\xi)$, respectively. If these deviations can be measured prescisely enough, we can distinguish the MCHM$_4$ and the MCHM$_5$.

Similarly, we can classify the MCHMs by the precision measurements of the deviation patterns in the Higgs boson couplings. In order to demonstrate the classification of the MCHMs, we consider several models with different representations of the quark fields. The MCHMs discussed here and the predicted deviation patterns are listed in the Table 4.1. The effective Lagrangian for the matter sector and the Higgs potential in each models are shown in the Appendix. In the model named MCHM$_{i\text{-}j\text{-}k}$, the quark fields $q_L = (u_L, d_L)$, u_R, d_R are embedded into i-, j- and k-dimensional representations, respectively. In the case of $i = j = k$, we simply write MCHM$_i$ instead of MCHM$_{i\text{-}i\text{-}i}$. Patterns of scale factors in various models are partly studied in Ref. [35]. In this thesis, we make more complete list of the models[1] and we add the predictions on the deviations for additional intereractions such as $hhVV$, $hhhh$, $hhtt$, and

[1]We cannot make a realistic model for some combinations of the matter representations. For example, in the model MCHM$_{5\text{-}1\text{-}10}$, the electroweak symmetry breaking cannot occur as shown in the Appendix. Therefore we don't consider such a model in the analysis of the scale factors.

hhbb. In the table, we use the functions defined in Ref. [35] as

$$\begin{aligned} F_3 &= \frac{1}{\sqrt{1-\xi}}\frac{3(1-2\xi)M_1^t + 2(4-23\xi+20\xi^2)M_2^t}{3M_1^t + 2(4-5\xi)M_2^t}, \\ F_4 &= \sqrt{1-\xi}\frac{M_1^t + 2(1-3\xi)M_2^t}{M_1^t + 2(1-\xi)M_2^t}, \quad F_5 = \sqrt{1-\xi}\frac{M_1^t - (4-15\xi)M_2^t}{M_1^t - (4-5\xi)M_2^t}, \end{aligned} \tag{4.29}$$

where M_1^t and M_2^t are form factors in effective theories shown in the Appendix, and they cannot be determined within the framework of the low energy theories. We here additionally introduce

$$\begin{aligned} F_6 &= -4\xi\frac{3M_1^t + (23-40\xi)M_2^t}{3M_1^t + 2(4-5\xi)M_2^t}, \quad F_7 = -\xi\frac{M_1^t + 2(7-9\xi)M_2^t}{M_1^t + 2(1-\xi)M_2^t}, \\ F_8 &= -\xi\frac{M_1^t - (34-45\xi)M_2^t}{M_1^t - (4-5\xi)M_2^t}, \\ H_1 &= 1 - \frac{3\xi}{2} - \frac{5\xi^2}{8} + \frac{\xi^3}{3m_h^2}\left[-\frac{21m_h^2}{16} + \frac{48\gamma}{v^2}\right], \\ H_2 &= 1 - \frac{25\xi}{2} + \xi^2 + \frac{\xi^3}{3m_h^2}\left[3m_h^2 + \frac{288\gamma}{v^2}\right], \end{aligned} \tag{4.30}$$

where γ is one of the form factors defined in the Appendix. In the models such that two different form factors M_1^t and M_2^t contribute to the scale factor, we examine two typical cases of $M_1^t \to 0$ or $M_2^t \to 0$ for simplicity. For the form factors H_1 and H_2, we take the terms up to $O(\xi^2)$, and thus the contribution through the γ term in the potential Eq. (C.9) can be neglected because it is proportional to ξ^3.

In Fig. 4.7, several scale factors are shown as a function of κ_V which is uniquely determined by ξ. Upper-left panel of Fig. 4.7 is also shown in Ref. [36] for MCHM$_4$ and MCHM$_5$[2], and our result is consistent with their one. As seen in the set of figures, we can basically discriminate some models from the others by the correlations among scale factors. For instance, the models {A, D, E, F, F'}, which are defined in Tab. 4.1, can be separated from the other models by κ_b. These four models are then classified into three sets as {A, E}, {D, F'} and F by measuring κ_t. The degeneracy between A and E can be solved by the measurement of $\lambda_{hhh}/\lambda_{hhh}^{\rm SM}$.

4.5 Double Higgs production at collider experiments

The double Higgs production is an important process which will give us to hint for the essence of the Higgs sector and new physics effects.

[2]They also show the case of MCHM$_{5\text{-}1\text{-}x}$ (x is arbitrary) with additional fermionic resonances [37]. Without such resonances, the model cannot maintain electroweak symmetry breaking as is the case with MCHM$_{5\text{-}1\text{-}10}$ mentioned in Appendix.

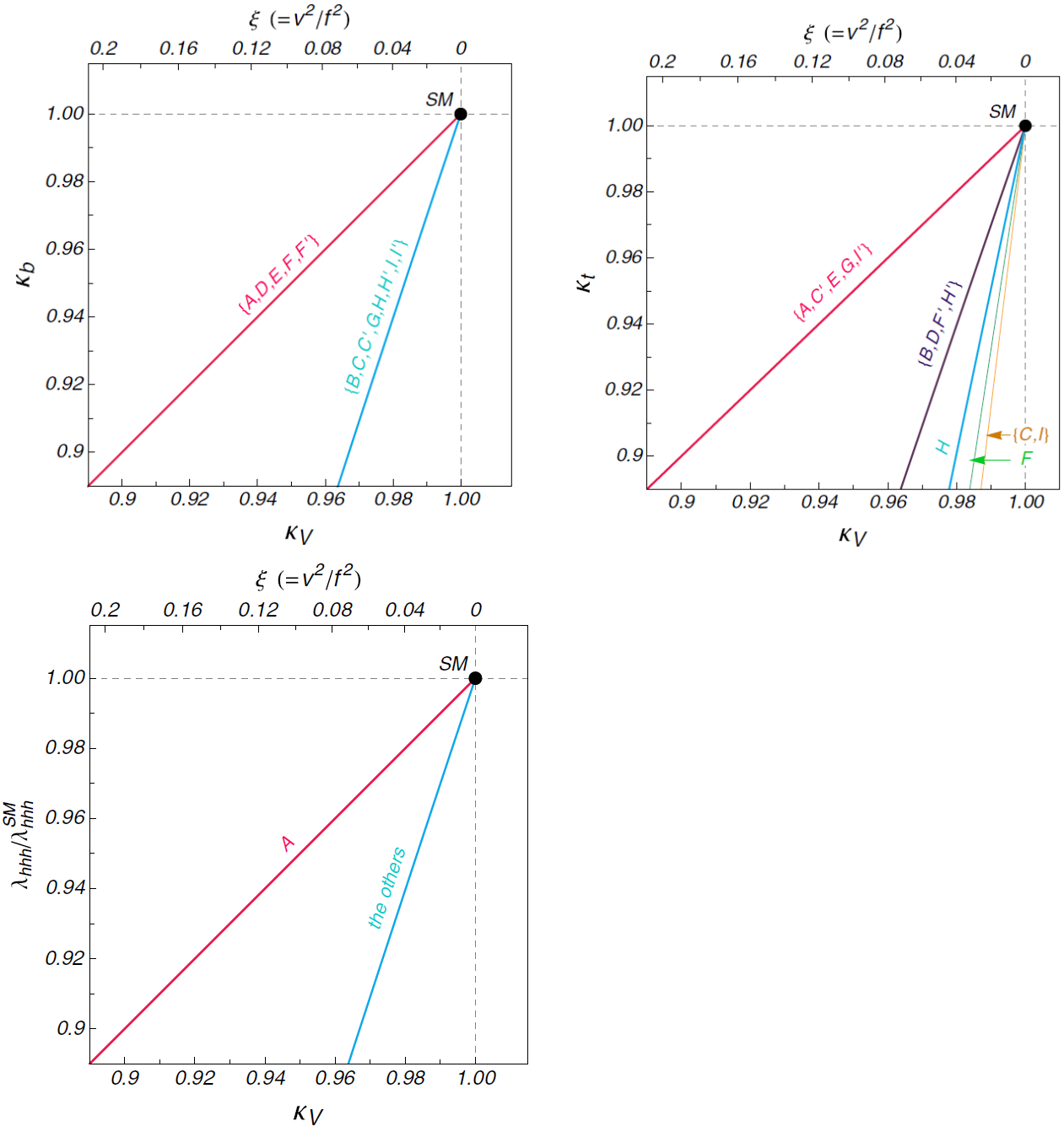

Figure 4.7: Correlations between scale factors. κ_V is universal for all MCHMs, and thus ξ-dependence is the same.

Table 4.1: Scale factors for MCHMs with various matter representations. The labels are used in Fig. 4.7, where C, H and I are the case of $M_1^t \to 0$, and C', H' and I' are the case of $M_2^t \to 0$.

Label	Model	κ_V	c_{hhVV}	κ_{hhh}	c_{hhhh}	κ_t	κ_b	c_{hhtt}	c_{hhbb}
A	MCHM_4	$\sqrt{1-\xi}$	$1-2\xi$	$\sqrt{1-\xi}$	$1-\frac{7}{3}\xi$	$\sqrt{1-\xi}$	$\sqrt{1-\xi}$	$-\xi$	$-\xi$
B	MCHM_5	$\sqrt{1-\xi}$	$1-2\xi$	$\frac{1-2\xi}{\sqrt{1-\xi}}$	$\frac{1-28\xi/3+28\xi^2/3}{1-\xi}$	$\frac{1-2\xi}{\sqrt{1-\xi}}$	$\frac{1-2\xi}{\sqrt{1-\xi}}$	-4ξ	-4ξ
B	MCHM_{10}	$\sqrt{1-\xi}$	$1-2\xi$	$\frac{1-2\xi}{\sqrt{1-\xi}}$	$\frac{1-28\xi/3+28\xi^2/3}{1-\xi}$	$\frac{1-2\xi}{\sqrt{1-\xi}}$	$\frac{1-2\xi}{\sqrt{1-\xi}}$	-4ξ	-4ξ
C, C'	MCHM_{14}	$\sqrt{1-\xi}$	$1-2\xi$	H_1	H_2	F_3	$\frac{1-2\xi}{\sqrt{1-\xi}}$	F_6	-4ξ
D	$\text{MCHM}_{5\text{-}5\text{-}10}$	$\sqrt{1-\xi}$	$1-2\xi$	$\frac{1-2\xi}{\sqrt{1-\xi}}$	$\frac{1-28\xi/3+28\xi^2/3}{1-\xi}$	$\frac{1-2\xi}{\sqrt{1-\xi}}$	$\sqrt{1-\xi}$	-4ξ	$-\xi$
E	$\text{MCHM}_{5\text{-}10\text{-}10}$	$\sqrt{1-\xi}$	$1-2\xi$	$\frac{1-2\xi}{\sqrt{1-\xi}}$	$\frac{1-28\xi/3+28\xi^2/3}{1-\xi}$	$\sqrt{1-\xi}$	$\sqrt{1-\xi}$	$-\xi$	$-\xi$
F, F'	$\text{MCHM}_{5\text{-}14\text{-}10}$	$\sqrt{1-\xi}$	$1-2\xi$	H_1	H_2	F_5	$\sqrt{1-\xi}$	F_8	$-\xi$
G	$\text{MCHM}_{10\text{-}5\text{-}10}$	$\sqrt{1-\xi}$	$1-2\xi$	$\frac{1-2\xi}{\sqrt{1-\xi}}$	$\frac{1-28\xi/3+28\xi^2/3}{1-\xi}$	$\sqrt{1-\xi}$	$\frac{1-2\xi}{\sqrt{1-\xi}}$	$-\xi$	-4ξ
B	$\text{MCHM}_{10\text{-}14\text{-}10}$	$\sqrt{1-\xi}$	$1-2\xi$	H_1	H_2	$\frac{1-2\xi}{\sqrt{1-\xi}}$	$\frac{1-2\xi}{\sqrt{1-\xi}}$	-4ξ	-4ξ
B	$\text{MCHM}_{14\text{-}1\text{-}10}$	$\sqrt{1-\xi}$	$1-2\xi$	$\frac{1-2\xi}{\sqrt{1-\xi}}$	$\frac{1-28\xi/3+28\xi^2/3}{1-\xi}$	$\frac{1-2\xi}{\sqrt{1-\xi}}$	$\frac{1-2\xi}{\sqrt{1-\xi}}$	-4ξ	-4ξ
H, H'	$\text{MCHM}_{14\text{-}5\text{-}10}$	$\sqrt{1-\xi}$	$1-2\xi$	H_1	H_2	F_4	$\frac{1-2\xi}{\sqrt{1-\xi}}$	F_7	-4ξ
B	$\text{MCHM}_{14\text{-}10\text{-}10}$	$\sqrt{1-\xi}$	$1-2\xi$	H_1	H_2	$\frac{1-2\xi}{\sqrt{1-\xi}}$	$\frac{1-2\xi}{\sqrt{1-\xi}}$	-4ξ	-4ξ
I, I'	$\text{MCHM}_{14\text{-}14\text{-}10}$	$\sqrt{1-\xi}$	$1-2\xi$	H_1	H_2	F_3	$\frac{1-2\xi}{\sqrt{1-\xi}}$	F_6	-4ξ

4.5.1 The Decay Branching Raios of the MCHMs

Before discussing the Higgs boson production processes, we calculate the Higgs boson decay width and branching ratios. The decay width of the MCHMs at the leadnig order are evaluated

$$\begin{aligned}
\Gamma^{\text{LO}}_{\text{MCHM}}(h \to f\bar{f}) &= \kappa_f^2 \cdot \Gamma^{\text{LO}}_{\text{SM}}(h \to f\bar{f}) \ , \\
\Gamma^{\text{LO}}_{\text{MCHM}}(h \to V^*V^*) &= \kappa_V^2 \cdot \Gamma^{\text{LO}}_{\text{SM}}(h \to V^*V^*) \ , \\
\Gamma^{\text{LO}}_{\text{MCHM}}(h \to gg) &= \frac{\alpha_S^2 g^2 m_h^3}{512\pi^3 m_W^2} \left| \sum_{q=t,b,c} \kappa_q \cdot F_i \right|^2 \ , \\
\Gamma^{\text{LO}}_{\text{MCHM}}(h \to \gamma\gamma) &= \frac{\alpha_{em}^2 g^2}{1024\pi^3} \frac{m_h^3}{m_W^2} \left| \kappa_V \cdot F_W + \sum_{\ell=\mu,\tau} F_\ell + \sum_{q=t,b,c} \kappa_q \cdot N_C e_q^2 F_q \right|^2 \ , \\
\Gamma^{\text{LO}}_{\text{MCHM}}(h \to Z\gamma) &= \frac{\alpha_{em}^2 g^2}{512\pi^3} \frac{m_h^3}{m_W^2} \left| \kappa_V \cdot A_W + \sum_{f=t,b,c,\tau,\mu} \kappa_f \cdot A_F \right|^2 \ ,
\end{aligned} \tag{4.31}$$

where $\Gamma^{\text{LO}}_{\text{SM}}$ is the SM decay width and loop functions $F_W, F_{f=q,\ell}, A_f$, and A_W are found in [39]. In the following , the fermions whose masses are lighter than the bottom quark are also intoduced. As mentioned above, when we take the limit $\xi \to 0$, these decay width correspond to the SM values.

In Figure 4.8, we show the ratios of the Higgs boson branching ratios of the MCHM_5 and $\text{MCHM}_{14}(M_1^t = 0)$ to that of the SM predictions. In the MCHM_4, the leading order decay

width are shifted by the same factor, $\kappa_V^2 = \kappa_f^2 = 1 - \xi$. Therefore, the branching ratios of the MCHM$_4$ are same in the SM. We note that the total Higgs boson decay width is always smaller than the SM prediction because all scale factors κ's are less than 1.

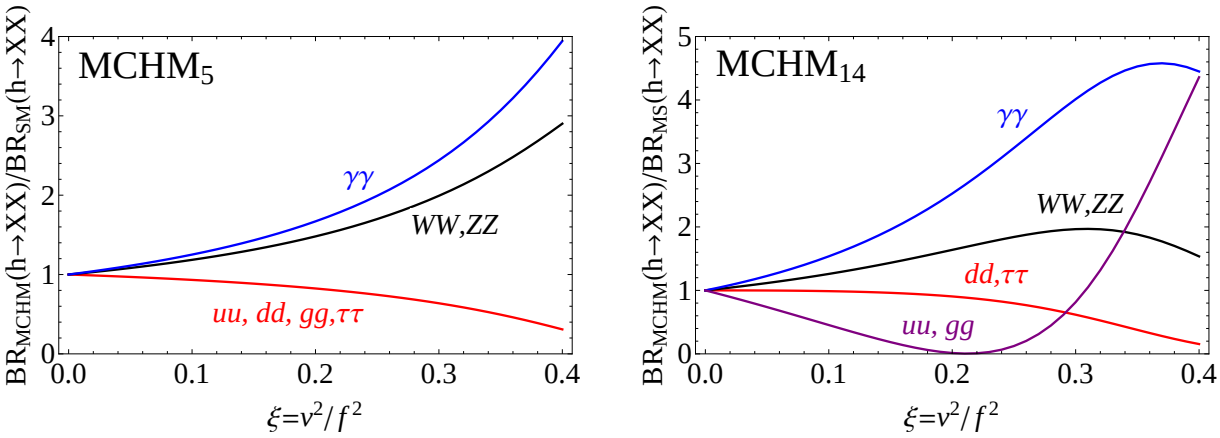

Figure 4.8: The ratios of the branching ratios in MCHM$_5$ and MCHM$_{14}$ to the SM predictions as the functions of the compositeness parameter ξ.

4.5.2 Current constraints on the compositeness parameter ξ from the single Higgs production

The Higgs boson coupling deviations are only described by the compositeness parameter ξ. We here consider constrains on ξ from current experiments.

In order to extract extract constrains from the LHC Run-I data, we utilize the signal strength, defined by

$$\mu = \frac{\sigma(\text{Prod}) \cdot \text{BR}(h \to XX)}{\sigma(\text{Prod})_{\text{SM}} \cdot \text{BR}(h \to XX)_{\text{SM}}} \ . \tag{4.32}$$

The signal strength of the single Higgs production via gluon fusion and vector boson fusion processes are obtained in [40] as shown in Table 4.2.

We here consider two single Higgs boson production processes, the gluon fusion and the vector boson fusion process as shown in Figure 4.9.

The gluon fusion cross section of the SM is evaluated as

$$\sigma_{\text{SM}}(pp \to gg \to h + X) = \int_{m_h^2/s}^1 d\tau \frac{d\mathcal{L}^{gg}}{d\tau} \hat{\sigma}(\hat{s} = \tau s) \ , \tag{4.33}$$

where $d\mathcal{L}^{gg}/d\tau$ is the luminocity function of the initial gluons, the cross section for the gluon fusion $gg \to h$ is

$$\sigma_{\text{SM}}(gg \to h) = \frac{G_F \alpha_S^2}{288\sqrt{2}\pi} \left| \frac{3}{4} F_t \left(\frac{4m_t^2}{\hat{s}} \right) \right|^2 , \tag{4.34}$$

Table 4.2: The signal strength in various decay modes measured at ATLAS an CMS with 1σ. These values are taken from Table 13 for 10-parameter fit in [40]. μ_F^{XX} is denoted as $\mu_F^{XX} = \mu_{ggF+ttH}^{XX}$ and μ_V^{XX} is denoted as $\mu_F^{XX} = \mu_{VBF+VH}^{XX}$.

	ATLAS + CMS	ATLAS	CMS
$\mu_V^{\gamma\gamma}$	$1.05^{+0.44}_{-0.41}$	$0.69^{+0.64}_{-0.58}$	$1.37^{+0.62}_{-0.56}$
μ_V^{ZZ}	$0.48^{+1.37}_{-0.91}$	$0.26^{+1.60}_{-0.91}$	$1.44^{+2.32}_{-2.30}$
μ_V^{WW}	$1.38^{+0.41}_{-0.37}$	$1.56^{+0.52}_{-0.46}$	$1.08^{+0.65}_{-0.58}$
$\mu_V^{\tau\tau}$	$1.12^{+0.37}_{-0.35}$	$1.29^{+0.58}_{-0.53}$	$0.87^{+0.49}_{-0.45}$
μ_V^{bb}	$0.65^{+0.30}_{-0.29}$	$0.50^{+0.39}_{-0.37}$	$0.85^{+0.47}_{-0.44}$
$\mu_F^{\gamma\gamma}$	$1.19^{+0.28}_{-0.25}$	$1.31^{+0.37}_{-0.34}$	$1.01^{+0.34}_{-0.31}$
μ_F^{ZZ}	$1.44^{+0.38}_{-0.34}$	$1.73^{+0.51}_{-0.45}$	$0.97^{+0.54}_{-0.42}$
μ_F^{WW}	$1.00^{+0.23}_{-0.20}$	$1.10^{+0.29}_{-0.26}$	$0.85^{+0.28}_{-0.25}$
$\mu_F^{\tau\tau}$	$1.10^{+0.61}_{-0.58}$	$1.72^{+1.24}_{-1.13}$	$0.91^{+0.69}_{-0.64}$
μ_F^{bb}	$1.09^{+0.93}_{-0.89}$	$1.51^{+1.15}_{-1.08}$	$0.10^{+1.83}_{-1.86}$

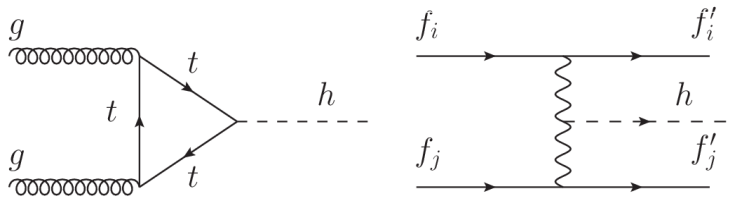

Figure 4.9: The gluon fusion process (left) an the vector boson fusion process (right). We denote that f and f' have the opposite electromagnetic charges.

with $\hat{s}$ is the centre-of-mass energy of this subprocess, and k is the k-factor for the QCD correction, $k = 3$ at the LHC 8 TeV. The gluon fusion cross section of the MCHM is simply given by

$$\sigma_{\rm MCHM}(pp \to gg \to h + X) = \kappa_t^2 \cdot \sigma_{\rm SM}(pp \to gg \to h + X), \tag{4.35}$$

because the dominant contribution is the top-loop diagram.

Therefore, the vector boson fusion cross section of the SM can be found in [41],

$$\sigma_{\rm SM}(pp \to W^+W^- \to h + X) = 1.58[\text{pb}] \ . \tag{4.36}$$

The vector boson fusion cross section of the MCHM is also given by

$$\sigma_{\rm MCHM}(pp \to W^+W^- \to h + X) = \kappa_V^2 \cdot \sigma_{\rm SM}(pp \to W^+W^- \to h + X) \ . \tag{4.37}$$

The signal strength for μ_F^{XX} is given by

$$\begin{aligned}\mu_F^{XX} &= \frac{\sigma(pp \to gg \to h) \cdot \mathrm{BR}(h \to XX)}{\sigma(pp \to gg \to h)_{\mathrm{SM}} \cdot \mathrm{BR}(h \to XX)_{\mathrm{SM}}} \\ &= \kappa_t^2 \cdot \frac{\mathrm{BR}(h \to XX)}{\mathrm{BR}(h \to XX)_{\mathrm{SM}}} \ .\end{aligned} \tag{4.38}$$

and the signal strength for μ_V^{XX} is given by

$$\begin{aligned}\mu_V^{XX} &= \frac{\sigma(pp \to W^+W^- \to h) \cdot \mathrm{BR}(h \to XX)}{\sigma(pp \to W^+W^- \to h)_{\mathrm{SM}} \cdot \mathrm{BR}(h \to XX)_{\mathrm{SM}}} \\ &= \kappa_V^2 \cdot \frac{\mathrm{BR}(h \to XX)}{\mathrm{BR}(h \to XX)_{\mathrm{SM}}} \ .\end{aligned} \tag{4.39}$$

These results for $XX = \gamma\gamma, WW, ZZ$ are shown in Figure 4.10 and Figure 4.11.

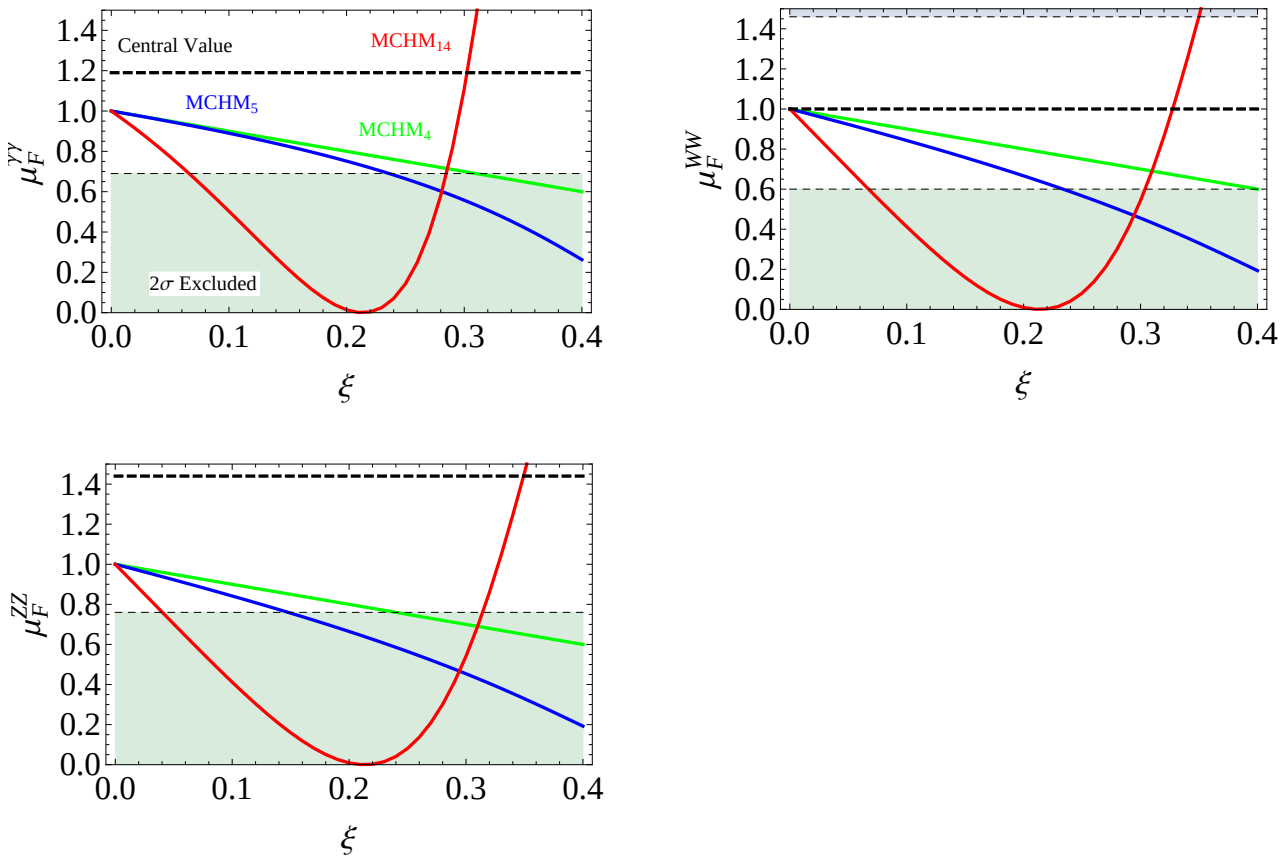

Figure 4.10: The signal strength from the gluon fusion process of $\mu_F^{\gamma\gamma}$(upper left), μ_F^{WW}(upper right), and $\mu_F^{\gamma\gamma}$(lower left). The green solid line corresponds to MCHM_4, the blue solid line corresponds to MCHM_5, and the red solid line corresponds to MCHM_{14}. The black solid line is the central value. The shaded regions are 2σ exluded regions.

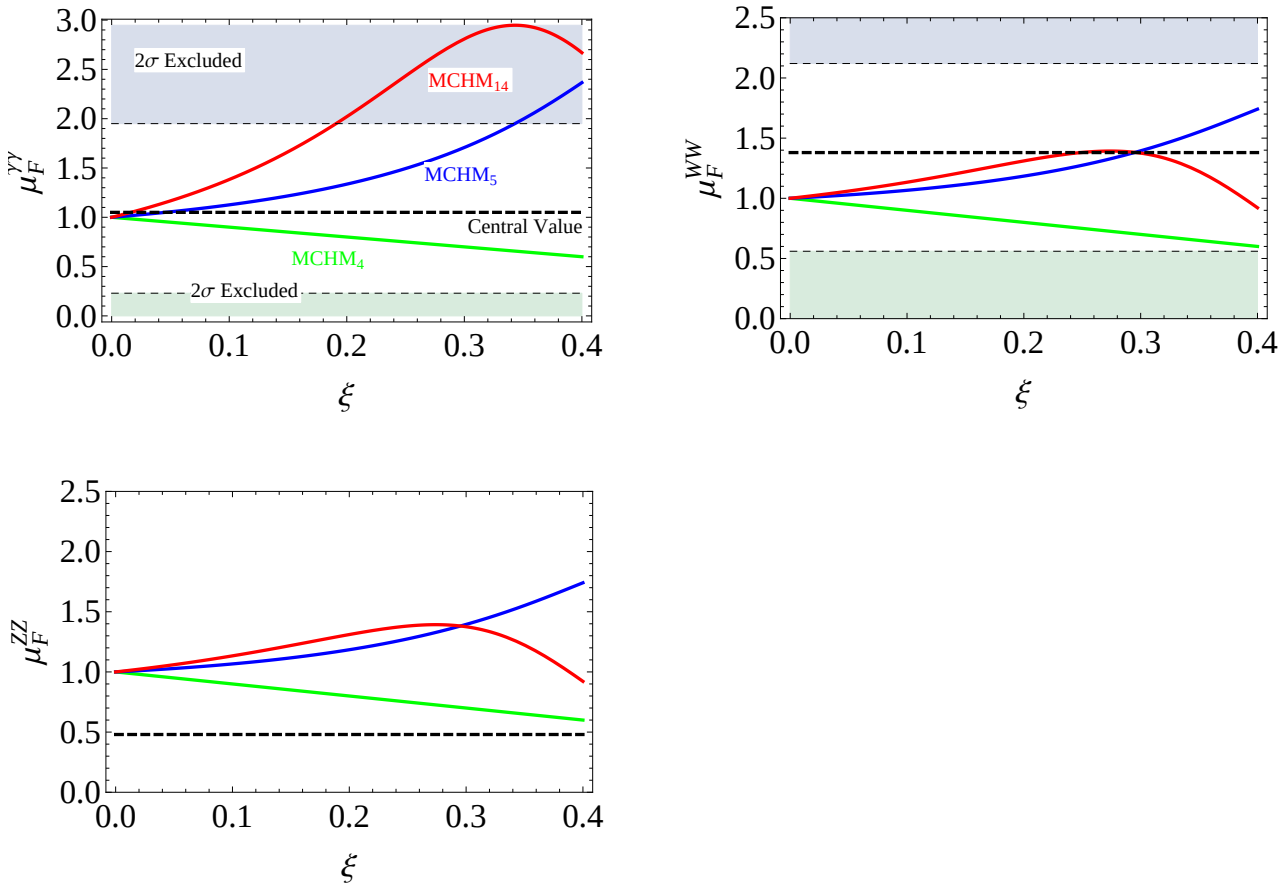

Figure 4.11: The signal strength from the gluon fusion process of $\mu_F^{\gamma\gamma}$(upper left), μ_F^{WW}(upper right), and $\mu_F^{\gamma\gamma}$(lower left). The green solid line corresponds to MCHM$_4$, the blue solid line corresponds to MCHM$_5$, and the red solid line corresponds to MCHM$_{14}$. The black solid line is the central value. The shaded regions are 2σ exluded regions.

The shaded regions are already excluded with 2σ CL. From these figures, the compositeness parameter ξ are constrained for each models as shown in Table 4.3.

4.5.3 Double Higgs procution via the gluon fusion at the LHC

Next, we discuss the double Higgs production at the LHC 14 TeV. In [42], the authos investegated that the double Higgs production at the LHC in the framework of the MCHMs. The dominant contribution to the double Higgs production at the LHC is gluon fusion process via the quark loop. The relevant diagrams are shown in Figure 4.12. As mentioned above sections, the Higgs boson coupling deviates from the SM predictions. In addition to this, in the MCHMs, there is a new contribution shown in Figure 4.12. This dimension-five operator plays an important role to the cross section.

Table 4.3: The constraints on the compositeness parameter for each models.

	$\mu_F^{\gamma\gamma}$	$\mu_F^{\gamma\gamma}$	$\mu_F^{\gamma\gamma}$
MCHM_4	$\xi < 0.31$	$\xi < 0.40$	$\xi < 0.24$
MCHM_5	$\xi < 0.23$	$\xi < 0.23$	$\xi < 0.15$
$\text{MCHM}_{14}(M_1^t = 0)$	$\xi < 0.07$	$\xi < 0.07$	$\xi < 0.04$

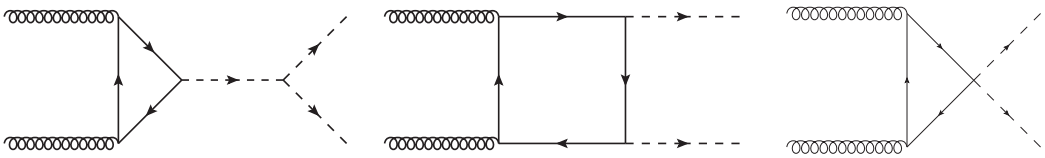

Figure 4.12: Left and center diagrams are SM contributions. Right diagram is a new contribution in the MCHMs.

The differential cross section of the SM at the parton-level is found in [43],

$$\frac{d\hat{\sigma}}{d\hat{t}} = \frac{G_F^2 \alpha_S^2}{256(2\pi)^3}\Big[\left|C_{\triangle}^{\text{SM}} F_{\triangle} + C_{\square}^{\text{SM}} F_{\square}\right|^2 + \left|C_{\square}^{\text{SM}} G_{\square}\right|^2\Big], \tag{4.40}$$

where $\hat{t}$ is the momentum transfer squared from one of the initial gluons to one of the final Higgs bosons, G_F is the Fermi constant, α_S is the strong coupling constant, the coefficients of $C_{\triangle}^{\text{SM}}, C_{\square}^{\text{SM}}$ are defined as

$$C_{\triangle}^{\text{SM}} = \frac{3m_h^2}{\hat{s} - m_h^2}, \quad C_{\square}^{\text{SM}} = 1, \tag{4.41}$$

and the definitions of form factors $F_{\triangle}, F_{\square}, G_{\square}$ can be found in [43]. In the MCHMs, these coefficients are modified as

$$C_{\triangle}^{\text{MCHM}} = \frac{3m_h^2}{\hat{s} - m_h^2}\kappa_t \kappa_{hhh} + \frac{m_t}{\sqrt{2}v} c_{hhtt}, \quad C_{\square}^{\text{MCHM}} = \kappa_t^2. \tag{4.42}$$

The form factors are the same in the SM. The second term in $C_{\triangle}^{\text{MCHM}}$ is the effect from the dimension-5 operator. We investigate MCHM_4, MCHM_5, and MCHM_{14} and these scale factors are shown in Table 4.4. For numerical calculation, we utilized the PDF as MSTW2008lo [44].

The numerical results are shown in Figure 4.13. At the leading order, the hadronic cross section is

$$\sigma(pp \to hh) = 16.3 \text{ [fb]} \tag{4.43}$$

The k-factor is taken to be abount 2.4 in [45], then

$$\sigma(pp \to hh + X) = 39.1 \text{ [fb]} \ . \tag{4.44}$$

	κ_t	κ_{hhh}	c_{hhtt}
MCHM$_4$	$1-\frac{1}{2}\xi$	$1-\frac{1}{2}\xi$	$-\xi$
MCHM$_5$	$1-\frac{3}{2}\xi$	$1-\frac{3}{2}\xi$	-4ξ
MCHM$_{14}$	$1-4\xi$	$1-\frac{3}{2}\xi$	$-\frac{23}{2}\xi$

Table 4.4: Coupling deviations in the MCHMs by expanding for small ξ.

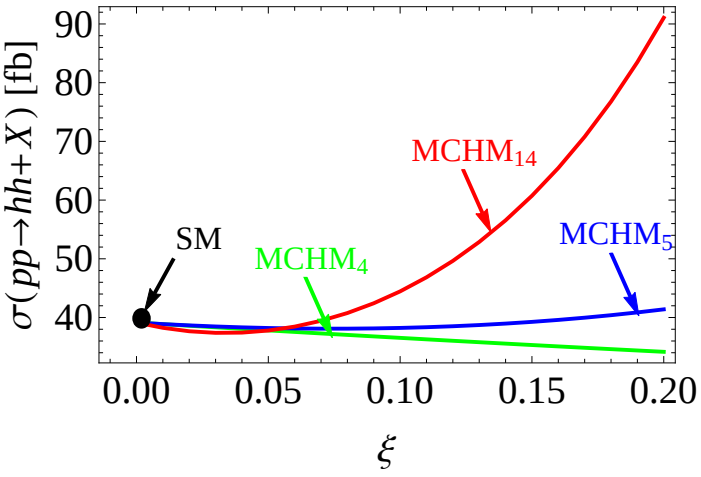

Figure 4.13: The pair Higgs production via gluon fusion in several MCHMs.

The SM value corresponds to $\xi = 0$ for each models. The large difference between around $\xi = 0.2$ comes from the dimension-five operator. As shown in Table 4.4, c_{hhtt} is significantly larger than that of the MCHM$_{4,5}$. This effect can be easily understood from the energy dependence of the parton-level cross section, shown in Figure 4.14. Therefore, the hadronic cross section of the MCHM$_{14}$ with large ξ becomes large. At $\xi = 0.2$, their ratios to the SM value is

$$\frac{\sigma_{\rm MCHM_4}}{\sigma_{\rm SM}} \simeq 0.87, \quad \frac{\sigma_{\rm MCHM_5}}{\sigma_{\rm SM}} \simeq 1.06, \quad \frac{\sigma_{\rm MCHM_{14}}}{\sigma_{\rm SM}} \simeq 2.33. \tag{4.45}$$

The most clear mode at the LHC could be the $\gamma\gamma bb$. Its cross sectino and the signal strength are shown in Figure 4.15.

4.5.4 Double Higgs procution via the vecor boson fusion at the LHC

The relevant diagrams are shown in Figure 4.16. The energy dependence of this process is very interesting. These diagrams contain the subprocess $WW \to hh$. It is well kwown that the energy dependence of $W_LW_L \to hh$ scattering amplitude in the SM disappear as same as the $W_LW_L \to W_LW_L$. However, as we mentioned, the Higgs boson couplings deviate from the SM value. These deviations violate the perturbative unitarity for each channels. In this case, the centre-of-mass energy squred dependence $\sim s$ does not disappear dut to the non-vanihsing the mocpositeness parameter ξ. The amplitude would diverge at the high nergy scale and the unitarity may be recovered by heavy resonance contribution. The porduction cross section is

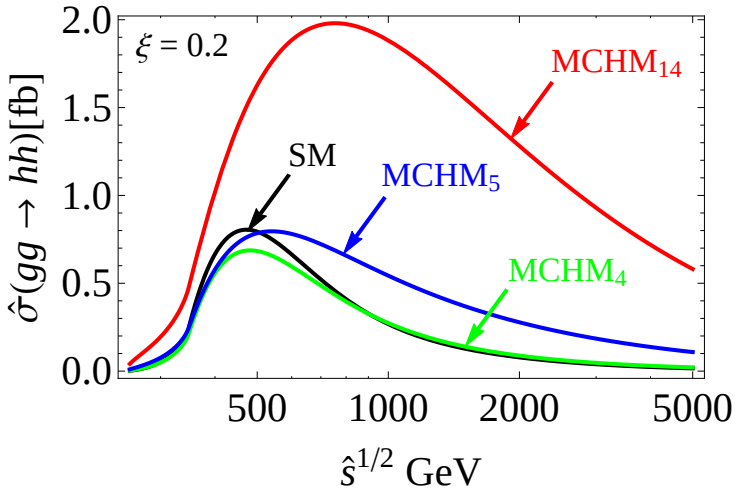

Figure 4.14: The parton-level cross section of double Higgs production as a function of $\sqrt{\hat{s}}$ of this subprocess centre-of-mass energy.

shown in Figure 4.17. At the double Higgs production cross section, the degenracy between MCHM$_5$ and MCHM$_{14}$ does no resolved. By considering the Higgs boson decay modes, we could distinguish these models. These results are shown in Figure 4.18 and Figure 4.19.

4.5.5 Double Higgs procution via the vecor boson fusion at the ILC

The ILC can measure the gauge-Higgs coupling deviation $\kappa_V = \sqrt{1-\xi}$ of the MCHMs at 0.2 % by $ee \to Zh$. In addition, the double Higgs production process is important process to explore the Higgs sector, e.g. the Higgs triple couling. Two dominant contributions are considered here, Z strahlung process and W fusion process.

Z strahlung process

The Z strahlung diagrams are shown in Figure 4.20. This process can be regarded as the heavy virtual Z boson decay whose mass corresponds to the centre-of-mass energy $\sqrt{s}$. The Higgs boson couplings are always suppressed. Therefore, the cross section also suppressed. We can not distinguish MCHM$_5$ and MCHM$_{14}$ at this level. The production cross section and their ratios to the SM values are shown in Figure 4.21. By including several decay modes of the Higgs boson, the degeneracy is resolved. The results are shown in Figure 4.22 and Figure 4.23.

$ee \to \nu\nu hh$: W fusion + Z strahlung

The double Higgs cross section from $ee \to \nu\nu hh$ has interesting energy dependence because W fusion process Z strahlung process contribute to the cross section. As we mentioned, the Z strahlung process is always suppressed and the W fusion process is enhanced by the unitarity violation. Around the centre-of-mass 600 GeV, the domninant contribution is transfered the

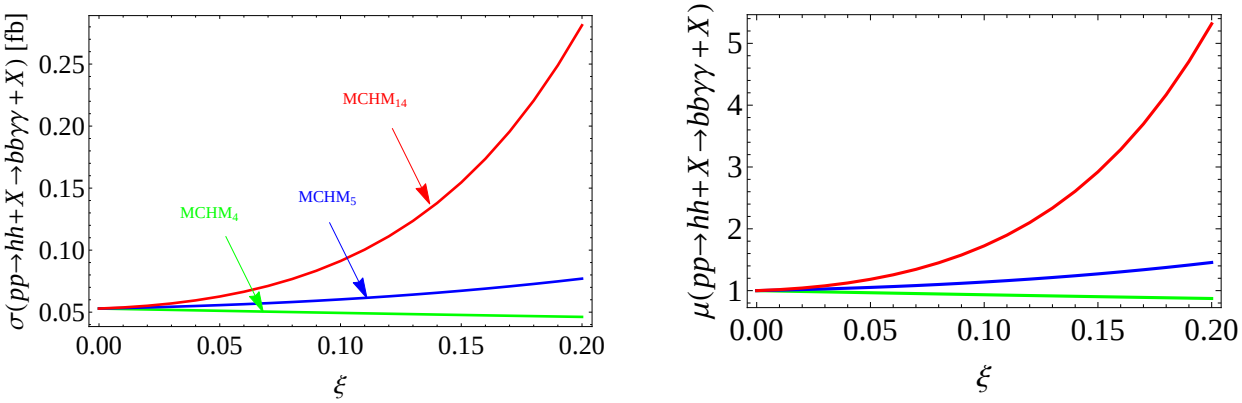

Figure 4.15: The cross section for $pp \to hh + X \to bb\gamma\gamma + X$ and its signale strength.

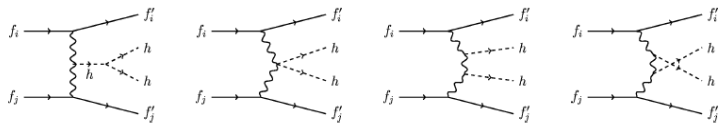

Figure 4.16: The double Higgs production via the vector boson fusion process.

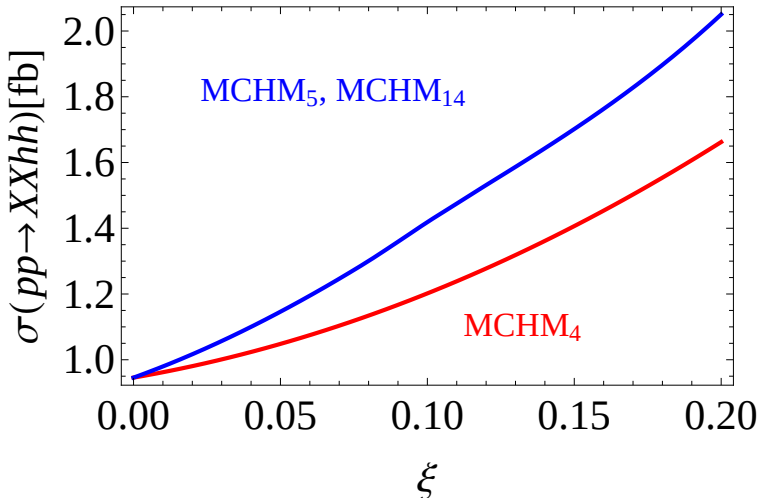

Figure 4.17: The cross section for $pp \to XXW^+W^- \to XXhh$ of MCHM$_4$ and MCHM$_{5,14}$.

Z strahlung to the W fusion. In other words, below 600 GeV, the ratios of the MCHM cross section ti the SM is less than 1 and above 600 GeV, the ratios of the MCHM cross section ti the SM is greater than 1. These results are shown in Figure 4.24. The results including the decay of the double Higgs bosons are shown in Figure 4.25. The signal strength of these modes are shown in Figure 4.26. In the MCHMs

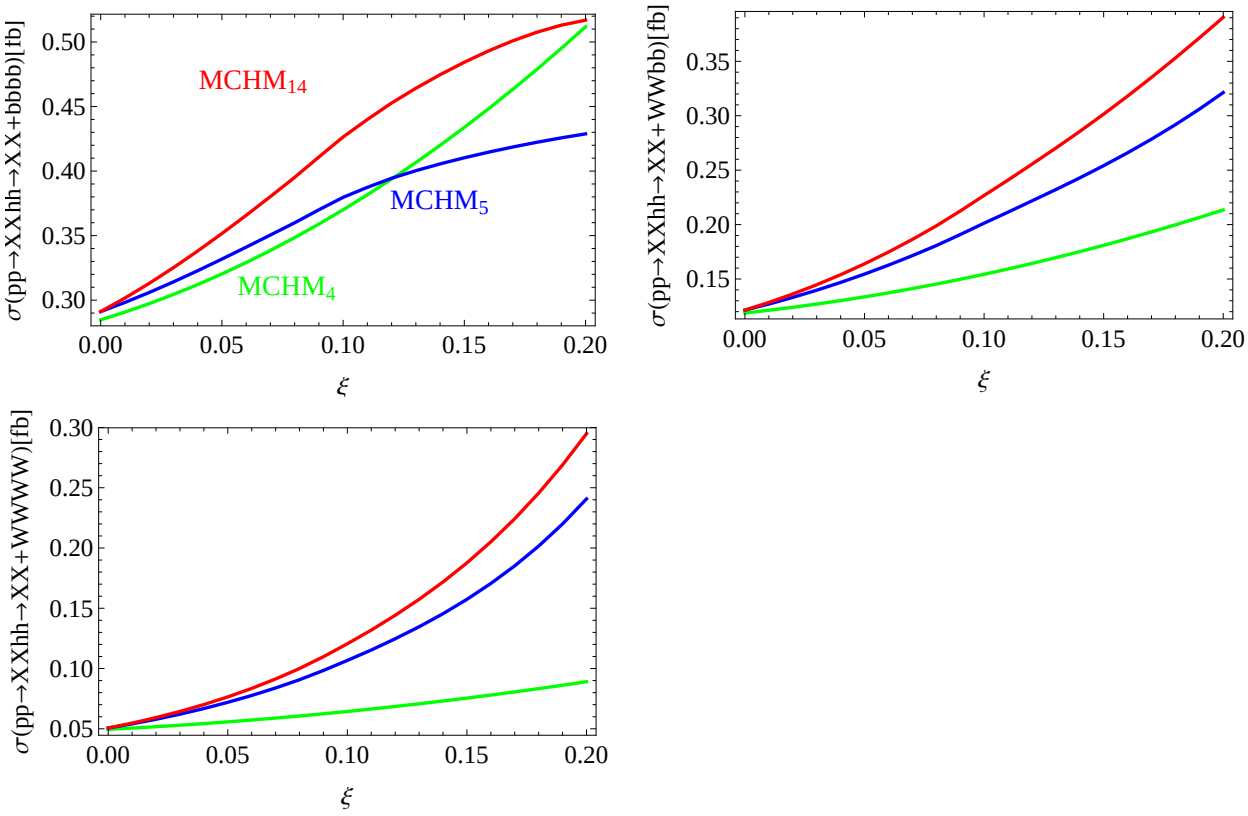

Figure 4.18: The cross sectutions for various double Higgs decay modes of MCHM_4, MCHM_5, and MCHM_{14}.

4.6 Next-to-minimal model : Composite singlet model

4.6.1 Non-linear Higgs field in $SO(6)/SO(5)$ model $(\Phi + S)$

The non-linear realized Higgs fields Σ in $SO(6)$ are parametrized as

$$\Sigma = \exp(\Pi/f)\ \Sigma_0, \quad \Sigma_0 = (0,0,0,0,0,1), \quad \Pi = -iT^{\hat{a}}h^{\hat{a}}\sqrt{2}, \tag{4.46}$$

and can be written by a unit vector of $SO(6)$

$$\Sigma = \sin\frac{\phi}{f}\left(\frac{h_1}{\phi}, \frac{h_2}{\phi}, \frac{h_3}{\phi}, \frac{h_4}{\phi}, \frac{h_5}{\phi}, \cot\frac{\phi}{f}\right), \qquad \text{with} \quad \phi = \sqrt{(h_{\hat{a}})^2}. \tag{4.47}$$

where f is a breaking scale of the global symmetry. We choose the unitary gauge, $h_1, h_2, h_4 = 0$, and indentify that $h_3 = h$ is a physical Higgs field from the doublet and $h_5 = \eta$ is a singlet field. Therefore, Σ in the *cartesian* basis becomes

$$\Sigma = \sin\frac{\phi}{f}\left(0, 0, \frac{h}{\phi}, 0, \frac{\eta}{\phi}, \cot\frac{\phi}{f}\right), \qquad \phi^2 = h^2 + \eta^2\ . \tag{4.48}$$

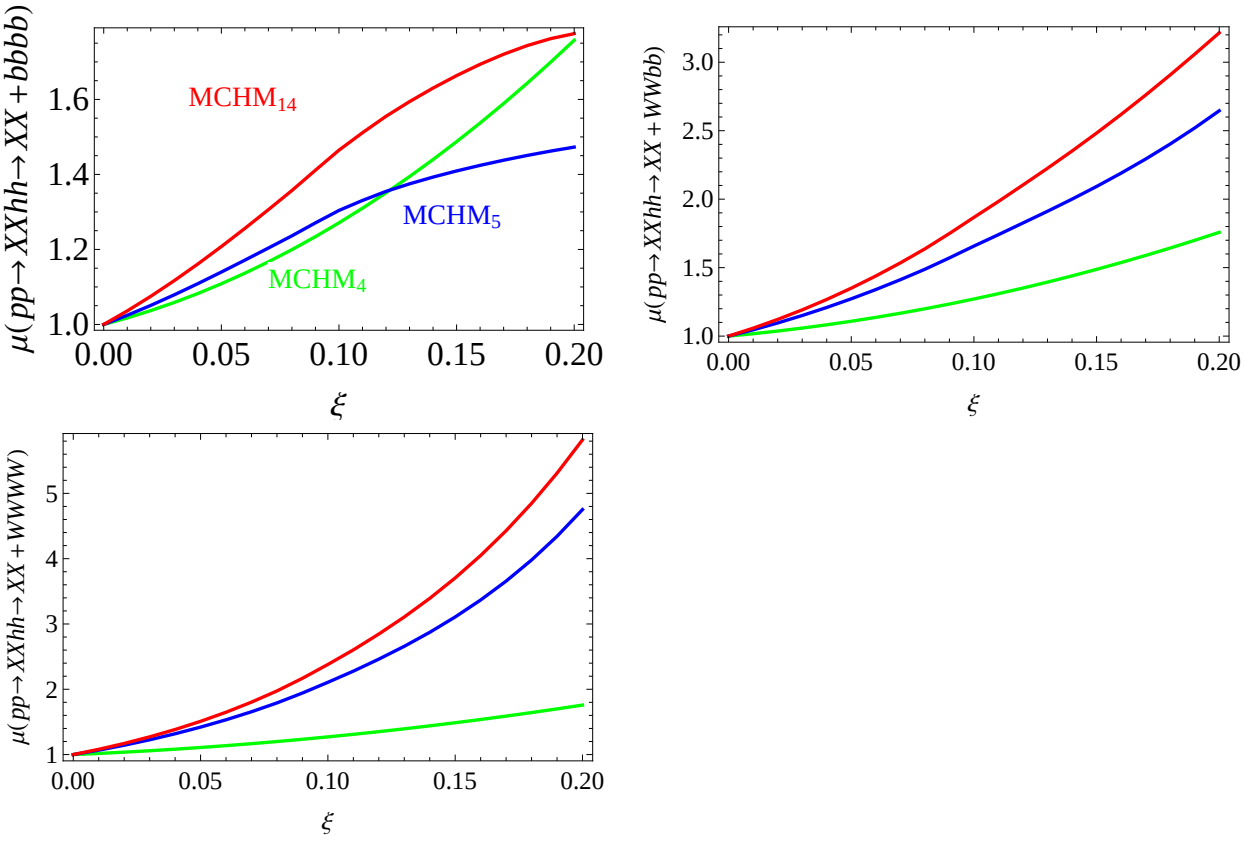

Figure 4.19: The signal strength for various double Higgs decay modes of MCHM_4, MCHM_5, and MCHM_{14}.

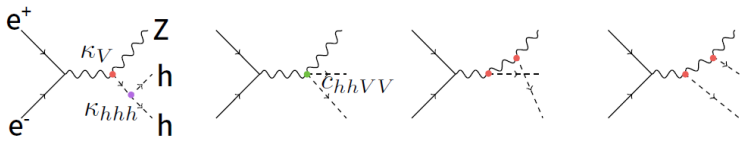

Figure 4.20: The relevant diagrams for Z strahlung processes.

Moreover, a convenient parametrization exists as

$$h = \phi \cos\frac{\psi}{f}, \quad \eta = \phi \sin\frac{\psi}{f}, \tag{4.49}$$

we obtain Σ in the *polar* basis

$$\Sigma = \sin\frac{\phi}{f}\left(0, 0, \cos\frac{\psi}{f}, 0, \sin\frac{\psi}{f}, \cot\frac{\phi}{f}\right) \tag{4.50}$$

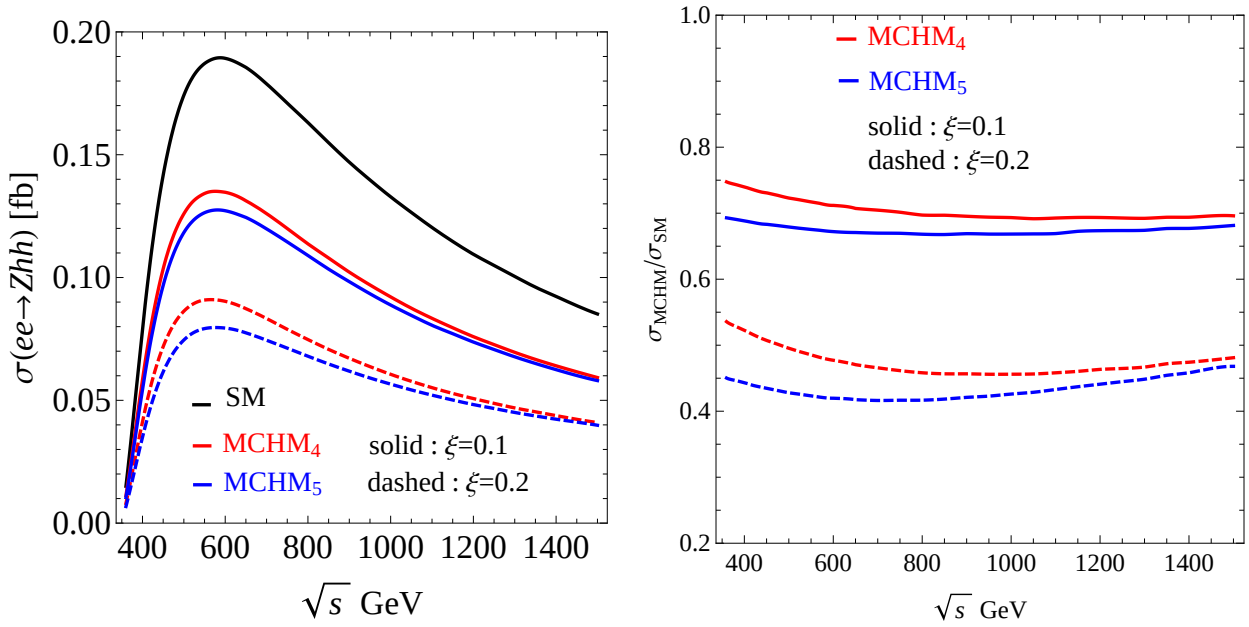

Figure 4.21: The production cross section for $ee \to Zhh$ (left) and its ratios to the SM (right).

The kinetic terms can be decomposed in the polar basis as

$$\mathcal{L}_{\rm kin} = \frac{f^2}{2}\left(D_\mu \Sigma\right)^T \left(D_\mu \Sigma\right) = \frac{1}{2}\left(\partial_\mu \phi\right)^2 + \frac{1}{2}\sin^2\frac{\langle\phi\rangle}{f}\left(\partial_\mu \psi\right)^2 + \frac{g^2 f^2}{4}\sin^2\frac{\langle\phi\rangle}{f}\cos^2\frac{\langle\psi\rangle}{f}\vec{W}^2 + \cdots \tag{4.51}$$

from the third term, the electroweak symmetry breaking vacuum expectation value is defined by

$$v \equiv f \sin\frac{\langle\phi\rangle}{f}\cos\frac{\langle\psi\rangle}{f} \equiv f\sqrt{\xi}\ . \tag{4.52}$$

4.7 $SO(6)/SO(5)$

4.7.1 Z_2 preserving case

Z_2 preserving vacuum

In the Z_2 preserving case, the singlet η does not get vev. Then,

$$h \to \langle h\rangle \neq 0, \quad \eta \to \langle\eta\rangle = 0\ . \tag{4.53}$$

By substituting them to (4.49),

$$\langle h\rangle = \langle\phi\rangle\cos\frac{\langle\psi\rangle}{f}, \qquad 0 = \langle\phi\rangle\sin\frac{\langle\psi\rangle}{f} \quad \to \langle\psi\rangle = 0, \quad \langle\phi\rangle = \langle h\rangle\ . \tag{4.54}$$

Therefore, we obtain

$$v = f \sin \frac{\langle h \rangle}{f} \quad \rightarrow \langle h \rangle = f \sin^{-1} \sqrt{\xi} \ . \tag{4.55}$$

We idetify that

$$h \rightarrow f \sin^{-1} \sqrt{\xi} + h_{car}, \quad \eta \rightarrow \eta_{car}, \tag{4.56}$$
$$\phi \rightarrow f \sin^{-1} \sqrt{\xi} + h_{pol}, \quad \psi \rightarrow \eta_{pol}. \tag{4.57}$$

Next, we normalize the kinetic terms. We extract two derivative terms (h_{car}, η_{car}) and (h_{pol}, η_{pol}).

$$\mathcal{L}_{\rm kin} = \frac{1}{2} \left(\partial_\mu h_{car}\right)^2 + \frac{1}{2} \frac{\xi}{\left(\sin^{-1} \sqrt{\xi}\right)^2} \left(\partial_\mu \eta_{car}\right)^2 + \cdots \ , \tag{4.58}$$
$$= \frac{1}{2} \left(\partial_\mu h_{pol}\right)^2 + \frac{1}{2} \xi \left(\partial_\mu \eta_{pol}\right)^2 + \cdots \ , \tag{4.59}$$

Then, (4.58) and (4.59) are rewritten by

$$h \rightarrow f \sin^{-1} \sqrt{\xi} + h_{car}, \quad \eta \rightarrow \frac{\sin^{-1} \sqrt{\xi}}{\sqrt{\xi}} \eta_{car} \ , \tag{4.60}$$
$$\phi \rightarrow f \sin^{-1} \sqrt{\xi} + h_{pol}, \quad \psi \rightarrow \frac{1}{\sqrt{\xi}} \eta_{pol} \ . \tag{4.61}$$

Kinetic term (Momentum dependent interactions)

From the kinetic terms, the scalar interactions with derivatives are derived.

$$\begin{aligned} \mathcal{L}_{\rm kin} &= \frac{f^2}{2} \left(D_\mu \Sigma\right)^T \left(D_\mu \Sigma\right) \\ &= \frac{1}{2} \left(\partial_\mu h\right)^2 \left(1 + 2\Delta_h \ \frac{h}{v} + \Delta_{hh} \ \frac{h^2}{v^2} + \Delta_{\eta\eta} \ \frac{\eta^2}{v^2} + \cdots \right) \\ &+ \frac{1}{2} \left(\partial_\mu \eta\right)^2 \left(1 + 2\Omega_h \ \frac{h}{v} + \Omega_{hh} \ \frac{h^2}{v^2} + \Omega_{\eta\eta} \ \frac{\eta^2}{v^2} + \cdots \right) \\ &+ \left(\partial_\mu h\right)\left(\partial^\mu \eta\right) \left(\Lambda_\eta \frac{\eta}{v} + \Lambda_{h\eta} \frac{\eta h}{v^2} + \cdots \right) \ , \end{aligned} \tag{4.62}$$

with

	Polar	Cartesian
Δ_h	0	0
Δ_{hh}	0	0
$\Delta_{\eta\eta}$	0	$-1+\frac{\xi}{\left(\sin^{-1}\sqrt{\xi}\right)^2}$
Ω_h	$\sqrt{1-\xi}$	$\sqrt{1-\xi}-\frac{\sqrt{\xi}}{\sin^{-1}\sqrt{\xi}}$
Ω_{hh}	$1-2\xi$	$1-2\xi+\frac{3\xi}{(\sin^{-1}\sqrt{\xi})^2}-\frac{4\sqrt{(1-\xi)\xi}}{\sin^{-1}\sqrt{\xi}}$
$\Omega_{\eta\eta}$	0	$-2+\sqrt{\frac{1-\xi}{\xi}}\sin^{-1}\sqrt{\xi}+\frac{(\sin^{-1}\sqrt{\xi})^2}{\xi}$
Λ_η	0	$\frac{\sin^{-1}\sqrt{\xi}}{\sqrt{\xi}}-\frac{\sqrt{\xi}}{\sin^{-1}\sqrt{\xi}}$
$\Lambda_{h\eta}$	0	$3-\frac{\xi}{(\sin^{-1}\sqrt{\xi})^2}$

Gauge sector

In order to repreduce $U(1)_Y$ hypercharge, $U(1)_X$ symmetry is intoduced. Then, the gauge Lagrangian is

$$\mathcal{L}_{\text{eff}}^{\text{gauge}}=\frac{1}{2}P^{\mu\nu}\left[\Pi_0^X(p)X_\mu X_\nu+\Pi_0(p)\text{Tr}\left[A_\mu A_\nu\right]+\Pi_1(p)\Sigma A_\mu A_\nu\Sigma^T\right] \tag{4.63}$$

The $SU(2)_L$, third component of $SU(2)_R$ and $U(1)_X$ are only gauge. Therefor, the gauge Lagrangian in the cartesian basis is written as

$$\begin{aligned}\mathcal{L}_{\text{eff}}^{\text{gauge}}=\frac{1}{2}P_{\mu\nu}\Bigg[&\left(\Pi_0^X(p)+\Pi_0(p)+\frac{1}{4}\sin^2\frac{\phi}{f}\times\frac{h^2}{\phi^2}\Pi_1(p)\right)B_\mu B_\nu\\&+\left(\Pi_0^X(p)+\frac{1}{4}\sin^2\frac{\phi}{f}\times\frac{h^2}{\phi^2}\Pi_1(p)\right)W_\mu^a W_\nu^a\\&+2\sin^2\frac{\phi}{f_\pi}\times\frac{h^2}{\phi^2}\Pi_1(p)\hat{H}^\dagger T^{a_L}Y\hat{H}W_\mu^{a_L}B_\nu\Bigg].\end{aligned} \tag{4.64}$$

with (Note that T^{a_L} are 2×2 matirces.)

$$\hat{H}=\begin{pmatrix}-h_1+ih_2\\h_3+ih_4\end{pmatrix} \tag{4.65}$$

Then, above equation can be rewritten and we here extract Higgs-gauge interaction terms

$$\mathcal{L}_{\text{eff}}^{\text{gauge}}=P^{\mu\nu}\left[\frac{1}{2}\left(\frac{f^2}{4}\sin^2\frac{\phi}{f}\times\frac{h^2}{\phi^2}\right)(Z_\mu Z_\nu+2W_\mu^+W_\nu^-)\right]\ . \tag{4.66}$$

By expanding ϕ around the electroweak breaking vacuum, the Higgs-gauge coupling constants are obtained.

$$f^2 \sin^2 \frac{\phi}{f} \times \frac{h^2}{\phi^2} \to v^2 + 2v\sqrt{1-\xi}\ h_{car} + (1-2\xi)\ h_{car}^2 + \left(-1 + \sqrt{\frac{1-\xi}{\xi}} \sin^{-1}\sqrt{\xi}\right) \quad \eta_{car}^2 \tag{4.67}$$

Then, we get

$$\mathcal{L}_{\text{eff}}^{\text{gauge}} \simeq P^{\mu\nu}\left[\frac{v^2}{4}V_\mu V_\nu + \frac{v}{2}\sqrt{1-\xi}\ h_{car}V_\mu V_\nu + \frac{1}{4}(1-2\xi)\ h_{car}^2 V_\mu V_\nu + \frac{1}{4}\kappa_{\eta\eta VV}\eta_{car}^2 V_\mu V_\nu\right] . \tag{4.68}$$

with

$$\kappa_{\eta\eta VV} = -1 + \sqrt{\frac{1-\xi}{\xi}} \sin^{-1}\sqrt{\xi}. \tag{4.69}$$

This result is in agreement with [46].

By substituting

$$\frac{h}{\phi} \to \cos\frac{\psi}{f}, \tag{4.70}$$

we also get the polar basis interactions.

$$f^2 \sin^2 \frac{\phi}{f} \cos^2 \frac{\psi}{f} \to v^2 + 2v\sqrt{1-\xi}\ h_{pol} + (1-2\xi)\ h_{pol}^2 + (-1) \quad \eta_{pol}^2 \tag{4.71}$$

Then, we get

$$\mathcal{L}_{\text{eff}}^{\text{gauge}} \simeq P^{\mu\nu}\left[\frac{v^2}{4}V_\mu V_\nu + \frac{v}{2}\sqrt{1-\xi}\ h_{pol}V_\mu V_\nu + \frac{1}{4}(1-2\xi)\ h_{pol}^2 V_\mu V_\nu + \frac{1}{4}\kappa_{\eta\eta VV}\eta_{pol}^2 V_\mu V_\nu\right] . \tag{4.72}$$

with

$$\kappa_{\eta\eta VV} = -1. \tag{4.73}$$

This result is in agreement with [46].

Matter sector

For simplicity, we concentrate on the fermion embedding in the fundamental representation of $SO(6)$, and only introduce the third generation of quark sector. Of course, other quark generatoins and the leptonic sector can be always introduced. Their contributions are negligible since the smallness of contributions to the scalar pontential.

The charge assignment of t_L, b_L, t_R, and b_R is as follows

$$\begin{aligned}(SU(2)_L, SU(2)_R)_{U(1)_X} \quad : \quad & t_L(+,-)_{2/3}, \quad b_L(-,+)_{-1/3}, \\ & t_R(0,0)_{2/3}, \quad b_L(0,0)_{-1/3},\end{aligned} \tag{4.74}$$

The representation is

$$\Psi_{t_L}=\frac{1}{\sqrt{2}}\begin{pmatrix}0\\0\\-it_L\\t_L\\0\\0\end{pmatrix}_{2/3},\quad \Psi_{t_R}=\begin{pmatrix}0\\0\\0\\0\\0\\t_R\end{pmatrix}_{2/3},\quad \Psi_{b_L}=\frac{1}{\sqrt{2}}\begin{pmatrix}0\\0\\ib_L\\b_L\\0\\0\end{pmatrix}_{-1/3},\quad \Psi_{b_R}=\begin{pmatrix}0\\0\\0\\0\\0\\b_R\end{pmatrix}_{-1/3}, \tag{4.75}$$

And we also impose parity,

$$P_\eta=\mathrm{diag}(1,1,1,1,-1,1). \tag{4.76}$$

It ensures the stability of η .

$$\begin{aligned}
\mathcal{L}^{\rm eff}_{\rm Matter}=&\ \overline{\Psi}_{t_L}\not{p}\Pi_0^{t_L}\Psi_{t_L}+(\overline{\Psi}_{t_L}\Sigma^\dagger)\not{p}\Pi_1^{t_L}(\Sigma\Psi_{t_L})\\
&+\overline{\Psi}_{b_L}\not{p}\Pi_0^{b_L}\Psi_{b_L}+(\overline{\Psi}_{b_L}\Sigma^\dagger)\not{p}\Pi_1^{b_L}(\Sigma\Psi_{b_L})\\
&+\overline{\Psi}_{t_R}\not{p}\Pi_0^{t_R}\Psi_{t_R}+(\overline{\Psi}_{t_R}\Sigma^\dagger)\not{p}\Pi_1^{t_R}(\Sigma\Psi_{t_R})\\
&+\overline{\Psi}_{b_R}\not{p}\Pi_0^{b_R}\Psi_{b_R}+(\overline{\Psi}_{b_R}\Sigma^\dagger)\not{p}\Pi_1^{b_R}(\Sigma\Psi_{b_R})\\
&+\overline{\Psi}_{q_L}M_0^t\Psi_{t_R}+(\overline{\Psi}_{q_L}\Sigma^\dagger)M_1^t(\Sigma\Psi_{t_R})\\
&+\overline{\Psi}_{q_L}M_0^b\Psi_{b_R}+(\overline{\Psi}_{q_L}\Sigma^\dagger)M_1^b(\Sigma\Psi_{b_R})+\text{h.c.}\\
=&\bar{t}_L\not{p}\left[\Pi_0^{t_L}+\Pi_1^{t_L}\frac{1}{2}\sin^2\frac{\phi}{f}\times\frac{h^2}{\phi^2}\right]t_L+\bar{b}_L\not{p}\left[\Pi_0^{b_L}+\Pi_1^{b_L}\frac{1}{2}\sin^2\frac{\phi}{f}\times\frac{h^2}{\phi^2}\right]b_L\\
&+\bar{t}_R\not{p}\left[\Pi_0^{t_R}+\Pi_1^{t_R}\times\frac{h^2}{\phi^2}\right]t_R+\bar{b}_R\not{p}\left[\Pi_0^{b_R}+\Pi_1^{b_R}\times\frac{h^2}{\phi^2}\right]b_R\\
&+\bar{t}_L\left[iM_1^t\frac{1}{\sqrt{2}}\cos\frac{\phi}{f}\sin\frac{\phi}{f}\times\frac{h}{\phi}\right]t_R+\bar{b}_L\left[-iM_1^b\frac{1}{\sqrt{2}}\cos\frac{\phi}{f}\sin\frac{\phi}{f}\times\frac{h}{\phi}\right]b_R+\text{h.c.}
\end{aligned} \tag{4.77}$$

The Higgs-fermion interctions are

$$\begin{aligned}
\mathcal{L}^{\rm eff}_{\rm Matter}\ni&\bar{t}_L\left(M_1^t\cos\frac{\phi}{f}\sin\frac{\phi}{f}\times\frac{h}{\phi}\right)t_R+\bar{b}_L\left(M_1^b\cos\frac{\phi}{f}\sin\frac{\phi}{f}\times\frac{h}{\phi}\right)b_R\\
\simeq&M_1^{t,b}\sqrt{1-\xi}\sqrt{\xi}\ \bar{q}_L\left(1+\frac{1-2\xi}{\sqrt{1-\xi}}\ \frac{h_{car}}{v}-2\xi\ \frac{h_{car}^2}{v^2}+\frac{1}{2}\kappa_{\eta\eta ff}\frac{\eta_{car}^2}{v^2}\right)q_R
\end{aligned} \tag{4.78}$$

with

$$\kappa_{\eta\eta ff}=-1+\frac{(1-2\xi)\sin^{-1}\sqrt{\xi}}{\sqrt{(1-\xi)\xi}}\ . \tag{4.79}$$

This result is in agreement with [46].

By substituting

$$\frac{h}{\phi}\to\cos\frac{\psi}{f}, \tag{4.80}$$

we also get the polar basis interactions. The Higgs-fermion interctions are

$$\begin{aligned}\mathcal{L}^{\text{eff}}_{\text{Matter}} \ni & \bar{t}_L \left(M_1^t \cos\frac{\phi}{f} \sin\frac{\phi}{f} \cos\frac{\psi}{f} \right) t_R + \bar{b}_L \left(M_1^b \cos\frac{\phi}{f} \sin\frac{\phi}{f} \cos\frac{\psi}{f} \right) b_R \\ \simeq & M_1^{t,b} \sqrt{1-\xi}\sqrt{\xi}\ \bar{q}_L \left(1 + \frac{1-2\xi}{\sqrt{1-\xi}}\ \frac{h_{pol}}{v} - 2\xi\ \frac{h_{pol}^2}{v^2} + \frac{1}{2}\kappa_{\eta\eta ff} \frac{\eta_{pol}^2}{v^2} \right) q_R \end{aligned} \tag{4.81}$$

with

$$\kappa_{\eta\eta ff} = -1\ . \tag{4.82}$$

This result is in agreement with [46].

Scalar potential

The one-loop effective scalar potential is

$$\begin{aligned} V_{\text{eff}} =& V_{\text{eff}}^{\text{gauge}} + V_{\text{eff}}^{\text{fermion}} \\ =& \frac{9}{2} \int \frac{d^4p}{(2\pi)^4} \ln \Pi_W(p) - (2N_C) \int \frac{d^4p}{(2\pi)^4} \left[\ln \not{p} \Pi^{b_L}(p) + \ln \left(p^2 \Pi^{t_R}(p) \Pi^{t_L}(p) - \left| \Pi^{t_L t_R}(p) \right|^2 \right) \right] \end{aligned} \tag{4.83}$$

where

$$\begin{aligned} \Pi_W(p) &= \Pi_0(p) + \frac{1}{4}\Pi_1(p) \sin^2\frac{\phi}{f} \times \frac{h^2}{\phi^2}\ , \\ \Pi^{t_L}(p) &= \Pi_0^{t_L} + \Pi_1^{t_L} \frac{1}{2} \sin^2\frac{\phi}{f} \times \frac{h^2}{\phi^2}\ , \\ \Pi^{b_L}(p) &= \Pi_0^{b_L} + \Pi_1^{b_L} \frac{1}{2} \sin^2\frac{\phi}{f} \times \frac{h^2}{\phi^2}\ , \\ \Pi^{t_R}(p) &= \Pi_0^{t_R} + \Pi_1^{t_R} \cos^2\frac{\phi}{f}\ , \\ \Pi^{b_R}(p) &= \Pi_0^{b_R} + \Pi_1^{b_R} \cos^2\frac{\phi}{f}\ , \\ \Pi^{t_L t_R}(p) &= +iM_1^t \frac{1}{\sqrt{2}} \sin\frac{\phi}{f} \cos\frac{\phi}{f} \times \frac{h}{\phi}\ , \\ \Pi^{b_L b_R}(p) &= -iM_1^b \frac{1}{\sqrt{2}} \sin\frac{\phi}{f} \cos\frac{\phi}{f} \times \frac{h}{\phi}\ . \end{aligned} \tag{4.84}$$

By expanding logarithmic functions and extracting relevant terms which contain ϕ and h, the scalar potential becomes

$$
\begin{aligned}
V_{\text{eff}} \simeq & \int \frac{d^4p}{(2\pi)^4} \frac{9}{8} \frac{\Pi_1(p)}{\Pi_0(p)} \sin^2 \frac{\phi}{f} \times \frac{h^2}{\phi^2} \\
& -2N_C \int \frac{d^4p}{(2\pi)^4} \log \left[p^2 \left(\Pi_0^{t_L} + \Pi_1^{t_L} \frac{1}{2} \sin^2 \frac{\phi}{f} \times \frac{h^2}{\phi^2} \right) \left(\Pi_0^{t_R} + \Pi_1^{t_R} \cos^2 \frac{\phi}{f} \right) - \left| M_1^t \right|^2 \frac{1}{\sqrt{2}} \sin^2 \frac{\phi}{f} \cos^2 \frac{\phi}{f} \times \right. \qquad (4.85) \\
\simeq & \int \frac{d^4p}{(2\pi)^4} \frac{9}{8} \frac{\Pi_1(p)}{\Pi_0(p)} \sin^2 \frac{\phi}{f} \times \frac{h^2}{\phi^2} \\
& - 2N_C \int \frac{d^4p}{(2\pi)^4} \log \left[1 + \frac{1}{p^2 \Pi_0^{t_L} \Pi_0^{t_R}} \left\{ p^2 \Pi_0^{t_L} \Pi_1^{t_R} \cos^2 \frac{\phi}{f} + \frac{1}{2} p^2 \Pi_1^{t_L} \Pi_0^{t_R} \sin^2 \frac{\phi}{f} \times \frac{h^2}{\phi^2} \right. \right. \\
& \qquad \left. \left. + \left(\frac{1}{2} p^2 \Pi_1^{t_L} \Pi_1^{t_R} - \left| M_1^t \right|^2 \right) \sin \frac{\phi}{f} \cos^2 \frac{\phi}{f} \times \frac{h^2}{\phi^2} \right\} \right] \\
= & \alpha \cos^2 \frac{\phi}{f} + \beta \sin^2 \frac{\phi}{f} \times \frac{h^2}{\phi^2} + \gamma \sin^2 \frac{\phi}{f} \cos^2 \frac{\phi}{f} \times \frac{h^2}{\phi^2} \qquad (4.86)
\end{aligned}
$$

When we expand above equation without introducing vev up to quartic order, we get

$$
\begin{aligned}
V_{\text{eff}} \simeq & \frac{1}{2} \frac{-\alpha + \beta + \gamma}{f^2} h_{pol}^2 + \frac{1}{4} \frac{\alpha - \beta - 4\gamma}{3f^2} h_{pol}^4 - \frac{1}{2} \frac{\beta - \gamma}{f^4 \xi} h_{pol}^2 \eta_{pol}^2 \qquad (4.87) \\
\simeq & \frac{1}{2} \frac{-\alpha + \beta + \gamma}{f^2} h_{car}^2 + \frac{1}{4} \frac{\alpha - \beta - 4\gamma}{3f^2} h_{car}^4 \\
& - \frac{1}{2} \frac{\alpha (\sin^{-1} \sqrt{\xi})^2}{f^2 \xi} \eta_{car}^2 + \frac{1}{4} \frac{\alpha (\sin^{-1} \sqrt{\xi})^4}{3f^4 \xi^2} \eta_{car}^4 + \frac{1}{2} \frac{(2\alpha - \beta - 4\gamma)(\sin^{-1} \sqrt{\xi})^2}{3f^4 \xi} h_{pol}^2 \eta_{pol}^2 \qquad (4.88) \\
& \qquad (4.89)
\end{aligned}
$$

Then, by using statinary conditions and

$$
\begin{aligned}
\frac{\partial^2 V_{\text{eff}}}{\partial h_{phys}^2} &= m_h^2, \\
\frac{\partial^2 V_{\text{eff}}}{\partial h_{phys} \partial \eta_{phys}} &= 0, \\
\frac{\partial^2 V_{\text{eff}}}{\partial \eta_{phys}^2} &= m_\eta^2, \qquad (4.90)
\end{aligned}
$$

scalar triple couplings are

$$\begin{aligned} & & & (\text{Polar}, \quad \text{Cartesian}) \,, \\ hhh & : & & \left(\frac{3m_h^2}{v} \frac{1-2\xi}{\sqrt{1-\xi}}, \quad \frac{3m_h^2}{v} \frac{1-2\xi}{\sqrt{1-\xi}} \right) , \\ hh\eta & : & & 0, \\ h\eta\eta & : & & \left(-\frac{m_h^2 - 4m_\eta^2(1-\xi)}{2v\sqrt{1-\xi}}, \quad \frac{m_h^2}{2v} - \frac{m_h^2 + 8m_\eta^2}{12v}\xi + \mathcal{O}(\xi^2) \right) , \\ \eta\eta\eta & : & & 0. \end{aligned} \tag{4.91}$$

and quartic couplings are

$$\begin{aligned} & & & (\text{Polar}, \quad \text{Cartesian}) \,, \\ hhhh & : & & \left(\frac{m_h^2}{v^2} \frac{3 - 28(1-\xi)\xi}{1-\xi}, \quad \frac{m_h^2}{v^2} \frac{3 - 28(1-\xi)\xi}{1-\xi} \right) , \\ hhh\eta & : & & 0, \\ hh\eta\eta & : & & \left(\frac{-m_h^2(5-6\xi) + 4m_\eta^2(1-\xi)(1-2\xi)}{2v^2(1-\xi)}, \quad \frac{m_h^2}{2v^2} - \frac{17m_h^2 + 4m_\eta^2}{6v^2}\xi + \mathcal{O}(\xi^2) \right) , \\ h\eta\eta\eta & : & & 0, \\ \eta\eta\eta\eta & : & & \left(-\frac{4m_\eta^2}{v^2}, \quad -\frac{m_h^2 + 4m_\eta^2}{v^2}\xi + \mathcal{O}(\xi^2) \right) , \end{aligned} \tag{4.92}$$

The scalar couplings are in agreement with [46] except for η^4 vertex.

4.7.2 Z_2 breaking case : [47]

Next, we consider the Z_2 breaking case. The source of this effect comes from fermion embedding. As discussed in above sections, t_R and b_R are embedded into the eigenvector with $(SU(2)_L, SU(2)_R) \sim (0,0)$.

$$\Psi_{t_R} = \begin{pmatrix} 0 \\ 0 \\ 0 \\ 0 \\ 0 \\ t_R \end{pmatrix}_{2/3} , \quad \Psi_{b_R} = \begin{pmatrix} 0 \\ 0 \\ 0 \\ 0 \\ 0 \\ b_R \end{pmatrix}_{-1/3} \tag{4.93}$$

There is another eigenvector with same quantum number.

$$\Psi'_{t_R} = \begin{pmatrix} 0 \\ 0 \\ 0 \\ 0 \\ t_R \\ 0 \end{pmatrix}_{2/3} , \quad \Psi'_{b_R} = \begin{pmatrix} 0 \\ 0 \\ 0 \\ 0 \\ b_R \\ 0 \end{pmatrix}_{-1/3} \tag{4.94}$$

Then, the RH up-type quark and the RH down-type quark are modified as

$$\Psi_{t_R} \to \Psi_{t_R} + \epsilon_t \Psi'_{t_R} \ , \quad \Psi_{b_R} \to \Psi_{b_R} + \epsilon_b \Psi'_{b_R} \ , \tag{4.95}$$

and normalized multiplets are written explicitly as

$$\Psi^{\theta}_{q_R} = \begin{pmatrix} 0 \\ 0 \\ 0 \\ 0 \\ e^{i\delta_q} \cos\theta_q \ q_R \\ \sin\theta_q \ q_R \end{pmatrix} . \tag{4.96}$$

The scalar potential of η is controlled by $\epsilon_{t,b}$. For simplicity, we set $\delta_q = \pi/2$.

We here also introduce the third generation of the SM leptons and the right-handed neutrinos, N_R. Their charge assignments are

$$\begin{aligned} (SU(2)_L, SU(2)_R)_{U(1)_X} \quad \sim \quad & \tau_L(-,+)_{-1}, \quad \tau_R(0,0)_{-1} \ , \\ & \nu_L(+,-)_0 \ , \quad N_R(0,0)_0 \ . \end{aligned} \tag{4.97}$$

$$\Psi_{\nu_L} = \frac{1}{\sqrt{2}} \begin{pmatrix} 0 \\ 0 \\ -i\nu_L \\ \nu_L \\ 0 \end{pmatrix}_0 , \quad \Psi_{\nu_L} = \frac{1}{\sqrt{2}} \begin{pmatrix} 0 \\ 0 \\ i\tau_L \\ \tau_L \\ 0 \end{pmatrix}_{-1} . \tag{4.98}$$

and

$$\Psi_{\tau_R} = \begin{pmatrix} 0 \\ 0 \\ 0 \\ e^{i\delta_{\tau_R}} \cos\theta_{\tau_R} \ \tau_R \\ \sin\theta_{\tau_R} \ \tau_R \end{pmatrix}_{-1} , \qquad \Psi_{N_R} = \begin{pmatrix} 0 \\ 0 \\ 0 \\ e^{i\delta_{N_R}} \cos\theta_{N_R} \ N_R \\ \sin\theta_{N_R} \ N_R \end{pmatrix}_0 . \tag{4.99}$$

In the following, we assume $\delta_{\tau_R} = \delta_{N_R} = \pi/2$.

Gauge sector

The scalar-gauge boson vertices do not recieve any effects.

Fermion sector

The Z_2 breaking Lagrangian is obtained by substituting $\Psi_{q_R} \to \Psi^{\theta}_{q_R}$. The Lagrangian becomes

$$
\begin{aligned}
\mathcal{L}^{\text{eff}}_{\text{Matter}} = \; & \overline{\Psi}_{t_L} \not{p} \Pi_0^{t_L} \Psi_{t_L} + (\overline{\Psi}_{t_L}\Sigma^\dagger)\not{p}\Pi_1^{t_L}(\Sigma\Psi_{t_L}) \\
& + \overline{\Psi}_{b_L} \not{p} \Pi_0^{b_L} \Psi_{b_L} + (\overline{\Psi}_{b_L}\Sigma^\dagger)\not{p}\Pi_1^{b_L}(\Sigma\Psi_{b_L}) \\
& + \overline{\Psi}_{\nu_L} \not{p} \Pi_0^{\nu_L} \Psi_{\nu_L} + (\overline{\Psi}_{\nu_L}\Sigma^\dagger)\not{p}\Pi_1^{\nu_L}(\Sigma\Psi_{\nu_L}) \\
& + \overline{\Psi}_{\tau_L} \not{p} \Pi_0^{\tau_L} \Psi_{\tau_L} + (\overline{\Psi}_{\tau_L}\Sigma^\dagger)\not{p}\Pi_1^{\tau_L}(\Sigma\Psi_{\tau_L}) \\
& + \overline{\Psi}^{\theta}_{t_R} \not{p} \Pi_0^{t_R} \Psi^{\theta}_{t_R} + (\overline{\Psi}^{\theta}_{t_R}\Sigma^\dagger)\not{p}\Pi_1^{t_R}(\Sigma\Psi^{\theta}_{t_R}) \\
& + \overline{\Psi}^{\theta}_{b_R} \not{p} \Pi_0^{b_R} \Psi^{\theta}_{b_R} + (\overline{\Psi}^{\theta}_{b_R}\Sigma^\dagger)\not{p}\Pi_1^{b_R}(\Sigma\Psi^{\theta}_{b_R}) \\
& + \overline{\Psi}^{\theta}_{N_R} \not{p} \Pi_0^{N_R} \Psi^{\theta}_{N_R} + (\overline{\Psi}^{\theta}_{N_R}\Sigma^\dagger)\not{p}\Pi_1^{N_R}(\Sigma\Psi^{\theta}_{N_R}) \\
& + \overline{\Psi}^{\theta}_{\tau_R} \not{p} \Pi_0^{\tau_R} \Psi^{\theta}_{\tau_R} + (\overline{\Psi}^{\theta}_{\tau_R}\Sigma^\dagger)\not{p}\Pi_1^{\tau_R}(\Sigma\Psi^{\theta}_{\tau_R}) \\
& + \overline{\Psi}_{q_L} M_0^t \Psi^{\theta}_{t_R} + (\overline{\Psi}_{q_L}\Sigma^\dagger) M_1^t (\Sigma\Psi^{\theta}_{t_R}) \\
& + \overline{\Psi}_{q_L} M_0^b \Psi^{\theta}_{b_R} + (\overline{\Psi}_{q_L}\Sigma^\dagger) M_1^b (\Sigma\Psi^{\theta}_{b_R}) \\
& + \overline{\Psi}_{\nu_L} M_0^\nu \Psi^{\theta}_{N_R} + (\overline{\Psi}_{\nu_L}\Sigma^\dagger) M_1^\nu (\Sigma\Psi^{\theta}_{N_R}) \\
& + \overline{\Psi}_{\tau_L} M_0^\tau \Psi^{\theta}_{\tau_R} + (\overline{\Psi}_{\tau_L}\Sigma^\dagger) M_1^\tau (\Sigma\Psi^{\theta}_{\tau_R}) + \text{h.c.} \\
= \; & \bar{t}_L \not{p} \left[\Pi_0^{t_L} + \Pi_1^{t_L} \frac{1}{2} \sin^2\frac{\phi}{f} \cos^2\frac{\psi}{f} \right] t_L \\
& + \bar{b}_L \not{p} \left[\Pi_0^{b_L} + \Pi_1^{b_L} \frac{1}{2} \sin^2\frac{\phi}{f} \cos^2\frac{\psi}{f} \right] b_L \\
& + \bar{\nu}_L \not{p} \left[\Pi_0^{\nu_L} + \Pi_1^{\nu_L} \frac{1}{2} \sin^2\frac{\phi}{f} \cos^2\frac{\psi}{f} \right] \nu_L \\
& + \bar{\tau}_L \not{p} \left[\Pi_0^{\tau_L} + \Pi_1^{\tau_L} \frac{1}{2} \sin^2\frac{\phi}{f} \cos^2\frac{\psi}{f} \right] \tau_L \\
& + \bar{t}_R \not{p} \left[\Pi_0^{t_R} + \Pi_1^{t_R} \cos^2\frac{\phi}{f} \left\{ \sin^2\theta_t + \cos^2\theta_t \tan^2\frac{\phi}{f} \sin^2\frac{\psi}{f} \right\} \right] t_R \\
& + \bar{b}_R \not{p} \left[\Pi_0^{b_R} + \Pi_1^{b_R} \cos^2\frac{\phi}{f} \left\{ \sin^2\theta_b + \cos^2\theta_b \tan^2\frac{\phi}{f} \sin^2\frac{\psi}{f} \right\} \right] b_R \\
& + \overline{N}_R \not{p} \left[\Pi_0^{N_R} + \Pi_1^{N_R} \cos^2\frac{\phi}{f} \left\{ \sin^2\theta_N + \cos^2\theta_N \tan^2\frac{\phi}{f} \sin^2\frac{\psi}{f} \right\} \right] N_R \\
& + \overline{\tau}_R \not{p} \left[\Pi_0^{\tau_R} + \Pi_1^{\tau_R} \cos^2\frac{\phi}{f} \left\{ \sin^2\theta_\tau + \cos^2\theta_\tau \tan^2\frac{\phi}{f} \sin^2\frac{\psi}{f} \right\} \right] \tau_R \\
& + \bar{t}_L \left[+iM_1^t \frac{1}{\sqrt{2}} \sin\frac{\phi}{f} \cos\frac{\phi}{f} \cos\frac{\psi}{f} \left\{ -i\sin\theta_t + \cos\theta_t \tan\frac{\phi}{f} \sin\frac{\psi}{f} \right\} \right] t_R \\
& + \bar{b}_L \left[-iM_1^b \frac{1}{\sqrt{2}} \sin\frac{\phi}{f} \cos\frac{\phi}{f} \cos\frac{\psi}{f} \left\{ -i\sin\theta_b + \cos\theta_b \tan\frac{\phi}{f} \sin\frac{\psi}{f} \right\} \right] b_R \\
& + \overline{\nu}_L \left[-iM_1^\nu \frac{1}{\sqrt{2}} \sin\frac{\phi}{f} \cos\frac{\phi}{f} \cos\frac{\psi}{f} \left\{ -i\sin\theta_N + \cos\theta_N \tan\frac{\phi}{f} \sin\frac{\psi}{f} \right\} \right] N_R \\
& + \overline{\tau}_L \left[-iM_1^\tau \frac{1}{\sqrt{2}} \sin\frac{\phi}{f} \cos\frac{\phi}{f} \cos\frac{\psi}{f} \left\{ -i\sin\theta_\tau + \cos\theta_\tau \tan\frac{\phi}{f} \sin\frac{\psi}{f} \right\} \right] \tau_R + \text{h.c.} \quad (4.100)
\end{aligned}
$$

Scalar potential

The one-loop effective scalar potential is

$$\begin{aligned} V_{\text{eff}} =& V_{\text{eff}}^{\text{gauge}} + V_{\text{eff}}^{\text{fermion}} \\ =& \frac{9}{2}\int \frac{d^4p}{(2\pi)^4} \ln \Pi_W(p) - 2N_C \int \frac{d^4p}{(2\pi)^4} \left[\ln \not{p} \Pi^{b_L}(p) + \ln \left(p^2 \Pi^{t_R}(p) \Pi^{t_L}(p) - \left| \Pi^{t_L t_R}(p) \right|^2 \right) \right] \\ & - 2\int \frac{d^4p}{(2\pi)^4} \left[\ln \not{p} \Pi^{\tau_L}(p) + \ln \left(p^2 \Pi^{N_R}(p) \Pi^{\nu_L}(p) - \left| \Pi^{\nu_L N_R}(p) \right|^2 \right) \right] \end{aligned} \tag{4.101}$$

where

$$\begin{aligned} \Pi_W(p) &= \Pi_0(p) + \frac{1}{4}\Pi_1(p) \sin^2\frac{\phi}{f}\cos^2\frac{\psi}{f} \ , \\ \Pi^{t_L}(p) &= \Pi_0^{t_L} + \Pi_1^{t_L}\frac{1}{2}\sin^2\frac{\phi}{f}\cos^2\frac{\psi}{f} \ , \\ \Pi^{b_L}(p) &= \Pi_0^{b_L} + \Pi_1^{b_L}\frac{1}{2}\sin^2\frac{\phi}{f}\cos^2\frac{\psi}{f} \ , \\ \Pi^{\nu_L}(p) &= \Pi_0^{\nu_L} + \Pi_1^{\nu_L}\frac{1}{2}\sin^2\frac{\phi}{f}\cos^2\frac{\psi}{f} \ , \\ \Pi^{\tau_L}(p) &= \Pi_0^{\tau_L} + \Pi_1^{\tau_L}\frac{1}{2}\sin^2\frac{\phi}{f}\cos^2\frac{\psi}{f} \ , \\ \Pi^{t_R}(p) &= \Pi_0^{t_R} + \Pi_1^{t_R}\cos^2\frac{\phi}{f}\left\{ \sin^2\theta_t + \cos^2\theta_t \tan^2\frac{\phi}{f}\sin^2\frac{\psi}{f} \right\} \ , \\ \Pi^{b_R}(p) &= \Pi_0^{b_R} + \Pi_1^{b_R}\cos^2\frac{\phi}{f}\left\{ \sin^2\theta_b + \cos^2\theta_b \tan^2\frac{\phi}{f}\sin^2\frac{\psi}{f} \right\} \ , \\ \Pi^{N_R}(p) &= \Pi_0^{N_R} + \Pi_1^{N_R}\cos^2\frac{\phi}{f}\left\{ \sin^2\theta_N + \cos^2\theta_N \tan^2\frac{\phi}{f}\sin^2\frac{\psi}{f} \right\} \ , \\ \Pi^{\tau_R}(p) &= \Pi_0^{\tau_R} + \Pi_1^{\tau_R}\cos^2\frac{\phi}{f}\left\{ \sin^2\theta_\tau + \cos^2\theta_\tau \tan^2\frac{\phi}{f}\sin^2\frac{\psi}{f} \right\} \ , \\ \Pi^{t_L t_R}(p) &= +iM_1^t\frac{1}{\sqrt{2}}\sin\frac{\phi}{f}\cos\frac{\phi}{f}\cos\frac{\psi}{f}\left\{ -i\sin\theta + \cos\theta\tan\frac{\phi}{f}\sin\frac{\psi}{f} \right\} \ , \\ \Pi^{b_L b_R}(p) &= -iM_1^b\frac{1}{\sqrt{2}}\sin\frac{\phi}{f}\cos\frac{\phi}{f}\cos\frac{\psi}{f}\left\{ -i\sin\theta + \cos\theta\tan\frac{\phi}{f}\sin\frac{\psi}{f} \right\} \ , \\ \Pi^{\nu_L N_R}(p) &= +iM_1^\nu\frac{1}{\sqrt{2}}\sin\frac{\phi}{f}\cos\frac{\phi}{f}\cos\frac{\psi}{f}\left\{ -i\sin\theta_N + \cos\theta_N\tan\frac{\phi}{f}\sin\frac{\psi}{f} \right\} \ , \\ \Pi^{\tau_L \tau_R}(p) &= -iM_1^\tau\frac{1}{\sqrt{2}}\sin\frac{\phi}{f}\cos\frac{\phi}{f}\cos\frac{\psi}{f}\left\{ -i\sin\theta_\tau + \cos\theta_\tau\tan\frac{\phi}{f}\sin\frac{\psi}{f} \right\} \ . \end{aligned} \tag{4.102}$$

Then,

$$
\begin{aligned}
V_{\text{eff}} \simeq & \int \frac{d^4p}{(2\pi)^4}\frac{9}{8}\frac{\Pi_1(p)}{\Pi_0(p)}\sin^2\frac{\phi}{f}\cos^2\frac{\psi}{f} \\
& -2N_C\int\frac{d^4p}{(2\pi)^4}\log\Bigg[p^2\left(\Pi_0^{t_L}+\Pi_1^{t_L}\frac{1}{2}\sin^2\frac{\phi}{f}\cos^2\frac{\psi}{f}\right)\left(\Pi_0^{t_R}+\Pi_1^{t_R}\cos^2\frac{\phi}{f}\left\{\sin^2\theta+\cos^2\theta\tan^2\frac{\phi}{f}\sin^2\frac{\psi}{f}\right\}\right) \\
& \qquad -\frac{1}{2}\left|M_1^t\right|^2\sin^2\frac{\phi}{f}\cos^2\frac{\phi}{f}\cos^2\frac{\psi}{f}\left\{\sin^2\theta+\cos^2\theta\tan^2\frac{\phi}{f}\sin^2\frac{\psi}{f}\right\}\Bigg]. \qquad (4.103) \\
\simeq & \int\frac{d^4p}{(2\pi)^4}\frac{9}{8}\frac{\Pi_1(p)}{\Pi_0(p)}\sin^2\frac{\phi}{f}\cos^2\frac{\psi}{f} \\
& -2N_C\int\frac{d^4p}{(2\pi)^4}\log\Bigg[1+\frac{1}{p^2\Pi_0^{t_L}\Pi_0^{t_R}} \\
& \qquad\Bigg\{p^2\Pi_0^{t_L}\Pi_1^{t_R}\cos^2\frac{\phi}{f}\left\{\sin^2\theta+\cos^2\theta\tan^2\frac{\phi}{f}\sin^2\frac{\psi}{f}\right\}+\frac{1}{2}p^2\Pi_1^{t_L}\Pi_0^{t_R}\sin^2\frac{\phi}{f}\cos^2\frac{\psi}{f} \\
& \qquad +\left(\frac{1}{2}p^2\Pi_1^{t_L}\Pi_1^{t_R}-\left|M_1^t\right|^2\right)\sin\frac{\phi}{f}\cos^2\frac{\phi}{f}\cos^2\frac{\psi}{f}\left\{\sin^2\theta+\cos^2\theta\tan^2\frac{\phi}{f}\sin^2\frac{\psi}{f}\right\}\Bigg\}\Bigg] \\
= & \ \alpha\cos^2\frac{\phi}{f}\left\{\sin^2\theta+\cos^2\theta\tan^2\frac{\phi}{f}\sin^2\frac{\psi}{f}\right\}+\beta\sin^2\frac{\phi}{f}\cos^2\frac{\psi}{f} \\
& +\gamma\sin^2\frac{\phi}{f}\cos^2\frac{\phi}{f}\cos^2\frac{\psi}{f}\left\{\sin^2\theta+\cos^2\theta\tan^2\frac{\phi}{f}\sin^2\frac{\psi}{f}\right\} \qquad (4.104)
\end{aligned}
$$

In Appendix of [47], the author have discussed that the potential (4.104) have two extrema at $\langle\psi\rangle = 0$ and $\sin(\langle\phi\rangle/f) = 1$. By using

$$
\begin{cases} \dfrac{\partial V_{\text{eff}}}{\partial\phi}=0, \\ \dfrac{\partial V_{\text{eff}}}{\partial\psi}=0, \end{cases} \qquad \rightarrow \qquad V_{\text{eff}}| = -\gamma\cos^2\frac{\langle\phi\rangle}{f}\cos^2\frac{\langle\psi\rangle}{f}\sin^2\frac{\langle\phi\rangle}{f}\ . \qquad (4.105)
$$

Therefore, one can choose the vacuum at $\langle\psi\rangle = 0$ without loss of genelarity. Due to this choise, the scalar-gauge boson couplings does not change. The scalar-charged fermion interactions are modified as

$$
\begin{aligned}
\mathcal{L}_{\text{eff}}^{\text{matter}} \ni & M_1^f\sqrt{1-\xi}\sqrt{\xi}\sin\theta_f(-i)\ \bar{f}_L\left(1+\frac{1-2\xi}{\sqrt{1-\xi}}\frac{h_{pol}}{v}-2\xi\frac{h_{pol}^2}{v^2}\right)f_R \\
& +M_1^f\sqrt{1-\xi}\sqrt{\xi}\sin\theta_f(-i)\ \bar{f}_L\left(0+i\sqrt{\frac{\xi}{1-\xi}}\frac{\eta_{pol}}{v}\cot\theta_f-\frac{1}{2}\frac{\eta_{pol}^2}{v^2}\right)f_R\ , \qquad (4.106)
\end{aligned}
$$

In this case, these fermion masses are

$$
m_f \equiv (-i)M_1^f\sqrt{1-\xi}\sqrt{\xi}\sin\theta_f \qquad (f=t,b,\tau) \qquad (4.107)
$$

For the neutrino sector,

$$\begin{aligned}\mathcal{L}_{\rm eff}^{\rm matter} \ni & M_1^\nu \sqrt{1-\xi}\sqrt{\xi}\sin\theta_N\ \bar{\nu}_L \left(1 + \frac{1-2\xi}{\sqrt{1-\xi}}\frac{h_{pol}}{v} - 2\xi\frac{h_{pol}^2}{v^2}\right) N_R \\ & + M_1^\nu \sqrt{1-\xi}\sqrt{\xi}\sin\theta_N\ \bar{\nu}_L \left(0 + i\sqrt{\frac{\xi}{1-\xi}}\frac{\eta_{pol}}{v}\cot\theta_N - \frac{1}{2}\frac{\eta_{pol}^2}{v^2}\right) N_R\ . \end{aligned} \tag{4.108}$$

We define the dirac neutrino mass as

$$m_D \equiv M_1^\nu \sqrt{1-\xi}\sqrt{\xi}\sin\theta_N\ . \tag{4.109}$$

The scalar-self interactions are

$$\begin{aligned} hhh &: \frac{3m_h^2}{v}\frac{1-2\xi}{\sqrt{1-\xi}}, \\ hh\eta &: 0, \\ h\eta\eta &: -\frac{m_h^2(-1+2\csc^2\theta) - 4m_\eta^2(1-\xi)}{2v\sqrt{1-\xi}}, \\ \eta\eta\eta &: 0. \end{aligned} \tag{4.110}$$

and

$$\begin{aligned} hhhh &: \frac{m_h^2}{v^2}\frac{3-28(1-\xi)\xi}{1-\xi}, \\ hhh\eta &: 0, \\ hh\eta\eta &: \frac{-m_h^2(5-6\xi)(-1+2\csc^2\theta) + 4m_\eta^2(1-\xi)(1-2\xi)}{2v^2(1-\xi)}, \\ h\eta\eta\eta &: 0, \\ \eta\eta\eta\eta &: -\frac{4m_\eta^2}{v^2}\left[\frac{3m_h^2(3-5\csc^2\theta+2\csc^4\theta) + 2m_\eta^2(3-2\csc^2\theta-4\xi\csc^2\theta+3\xi\csc^4\theta)}{2m_\eta^2(1-\xi)(1-2\cot^2\theta)}\right], \end{aligned} \tag{4.111}$$

When we take a lmit $\theta \to \pi/2$, these values becomes Z_2 preserving case.

4.8 Vacuum Structure

The scalar potential without Z_2 symmetry is

$$\begin{aligned} V_{car} = & \ \alpha\cos^2\frac{\phi}{f}\left\{\sin^2\theta + \cos^2\theta\tan^2\frac{\phi}{f}\times\frac{s^2}{\phi^2}\right\} + \beta\sin^2\frac{\phi}{f}\times\frac{h^2}{\phi^2} \\ & + \gamma\sin^2\frac{\phi}{f}\cos^2\frac{\phi}{f}\times\frac{h^2}{\phi^2}\left\{\sin^2\theta + \cos^2\theta\tan^2\frac{\phi}{f}\times\frac{s^2}{\phi^2}\right\} \end{aligned} \tag{4.112}$$

and

$$V_{pol} = \alpha \cos^2\frac{\phi}{f}\left\{\sin^2\theta + \cos^2\theta\tan^2\frac{\phi}{f}\sin^2\frac{\psi}{f}\right\} + \beta\sin^2\frac{\phi}{f}\cos^2\frac{\psi}{f} + \gamma\sin^2\frac{\phi}{f}\cos^2\frac{\phi}{f}\cos^2\frac{\psi}{f}\left\{\sin^2\theta + \cos^2\theta\tan^2\frac{\phi}{f}\sin^2\frac{\psi}{f}\right\} \tag{4.113}$$

where we replace $h_3 \to h$ and $h_5 \to s$. These curvature at the origin $\langle h\rangle = \langle s\rangle = \langle\phi\rangle = \langle\psi\rangle = 0$ are

$$\frac{\partial^2 V_{car}}{\partial\phi_i\partial\phi_j} = \frac{1}{f^2}\begin{pmatrix} -\alpha + 2\beta + \gamma + (\alpha-\gamma)\cos 2\theta & 0 \\ 0 & 2\alpha\cos 2\theta \end{pmatrix}, \tag{4.114}$$

$$\frac{\partial^2 V_{pol}}{\partial\phi_i\partial\phi_j} = \frac{1}{f^2}\begin{pmatrix} -\alpha + 2\beta + \gamma + (\alpha-\gamma)\cos 2\theta & 0 \\ 0 & 0 \end{pmatrix}. \tag{4.115}$$

4.9 Consistency Check

In this section, we check a consistency between two basis, *polar* and *cartesian*. The authors of [46] mentioned that when we compute a physical observable, i.e. unpolarized cross sectoin $\sigma(\eta\eta \to W^+W^-)$, these basis give us the same results.

4.9.1 $\eta\eta \to W^+W^-$ scattering

Let us consider $\eta\eta \to W^+W^-$ scattering. The relevant diagrams are show in Figure 4.27. This amplitude is written as

$$i\mathcal{M} = \left(\frac{i}{s - m_h^2 + i\epsilon}\kappa'_{h\eta\eta}(igm_W)\kappa_{hWW} + i\frac{g^2}{2}\kappa_{\eta\eta WW}\right)\left[\epsilon_+^\mu(p_+,\lambda_+)\epsilon_+^\nu(p_-,\lambda_-)\right]^* g_{\mu\nu} \tag{4.116}$$

where the vertex factor $\kappa'_{h\eta\eta}$ has momentum dependence and can be decomposed as

$$\kappa'_{h\eta\eta} = -iv\ \kappa_{h\eta\eta} + i\ \Omega_h\Big[2\big(-i\ p_{\eta 1}\big)^\mu\big(-i\ p_{\eta 2}\big)_\mu\Big]\frac{1}{v} + i\ \Lambda_\eta\Big[2\big(-i\ p_{\eta 1}\big)^\mu\big(+i\ p_h\big)_\mu\Big]\frac{1}{v} \tag{4.117}$$

with $p_{\eta 1}$ (or $p_{\eta 2}$), p_h are the four-momenta and we write down κ's explicitely following sections.

Very high evergy ($\sqrt{s} \gg m_h^2, m_\eta^2, m_{W,Z}^2$) behaviour at $\xi = 0$

First of all, we calculate the simplest case, $\sqrt{s} \gg m_h^2, m_\eta^2, m_{W,Z}^2$ and $\xi = 0$. We expect that no energy dependence remains. The limiting κ's are

	Polar	Cartesian
$\kappa_{h\eta\eta}$	$-\frac{m_h^2-4m_\eta^2}{2v^2}$	$+\frac{m_h^2}{2v^2}$
Ω_h	1	0
Λ_η	0	0
κ_{hWW}	1	1
$\kappa_{\eta\eta WW}$	-1	0

We only extract the longitudinal contribution,

$$\left[\epsilon_+^\mu(p_+,\lambda_+=0)\epsilon_+^\nu(p_-,\lambda_-=0)\right]^* g_{\mu\nu} = \frac{1}{m_W^2}\left(\frac{s}{2}-m_W^2\right) . \tag{4.118}$$

Therefore, at the very high energy, the cartesian basis amplitude (4.116)is

$$\begin{aligned} i\mathcal{M} &= \left(\frac{i}{s-m_h^2+i\epsilon}\kappa'_{h\eta\eta}(igm_W)\kappa_{hWW}+i\frac{g^2}{2}\kappa_{\eta\eta WW}\right)\left[\epsilon_+^\mu(p_+,\lambda_+=0)\epsilon_+^\nu(p_-,\lambda_-=0)\right]^* g_{\mu\nu} \\ &\sim \left[\frac{i}{s}\,\kappa'_{h\eta\eta}(igm_W)\kappa_{hWW}\left(1+\frac{m_h^2}{s}\right)+i\frac{g^2}{2}\kappa_{\eta\eta WW}\right]\frac{s}{m_W^2} . \end{aligned} \tag{4.119}$$

• Cartesian basis amplitude

$$i\mathcal{M}_{car} = i\frac{\kappa_{h\eta\eta}\kappa_{hWW}}{m_W^2}(igm_W) = \frac{i}{m_W^2}\left(-i\frac{m_h^2}{2v}\right)(igm_W) = +i\frac{m_h^2}{v^2} . \tag{4.120}$$

• Polar basis amplitude

In the centre of mass frame,

$$2(-ip_{\eta 1})^\mu(-ip_{\eta 2})_\mu = -\frac{s}{2}-2|\mathbf{p}_\eta|^2 = -s+2m_\eta^2 . \tag{4.121}$$

Then,

$$\begin{aligned} i\mathcal{M}_{pol} =& i\frac{g^2}{2}\frac{\kappa_{\eta\eta WW}}{m_W^2}s + i(igm_W)\frac{\kappa'_{h\eta\eta}\kappa_{hWW}}{m_W^2}\left(1+\frac{m_h^2}{s}\right) \\ =& \frac{1}{m_W^2}\left(-i\,2\frac{m_W^2}{v^2}\right)s+\frac{i}{m_W^2}\left(i\frac{m_h^2}{2v}-i\frac{2m_\eta^2}{v}-i\frac{s}{v}+i\frac{2m_\eta^2}{v}\right)\left(i\,2\frac{m_W^2}{v}\right)\left(1+\frac{m_h^2}{s}\right) \\ =& -i\frac{m_h^2}{v^2}+i\,2\frac{m_h^2}{v^2} = +i\frac{m_h^2}{v^2} . \end{aligned} \tag{4.122}$$

Therefore,

$$\mathcal{M}_{car} = \mathcal{M}_{pol} . \tag{4.123}$$

Very high evergy ($\sqrt{s} \gg m_h^2, m_\eta^2, m_{W,Z}^2$) behaviour at $\xi \ll 1$

By expanding small ξ, κ's become

	Polar	Cartesian
$\kappa_{h\eta\eta}$	$-\frac{m_h^2 - 4m_\eta^2}{2v^2} - \frac{m_h^2 + 4m_\eta^2}{4v^2}\xi + \mathcal{O}(\xi^2)$	$+\frac{m_h^2}{2v^2} - \frac{m_h^2 + 8m_\eta^2}{12v^2}\xi + \mathcal{O}(\xi^2)$
Ω_h	$1 - \frac{1}{2}\xi + \mathcal{O}(\xi^2)$	$-\frac{\xi}{3} + \mathcal{O}(\xi^2)$
Λ_η	0	$+\frac{\xi}{3} + \mathcal{O}(\xi^2)$
κ_{hWW}	$\left(1 - \frac{1}{2}\xi + \mathcal{O}(\xi^2)\right)$	$\left(1 - \frac{1}{2}\xi + \mathcal{O}(\xi^2)\right)$
$\kappa_{\eta\eta WW}$	-1	$-\left(\frac{\xi}{3} + \mathcal{O}(\xi^2)\right)$

Now, $\kappa'_{h\eta\eta}$ is

$$\kappa'_{h\eta\eta} = -iv\ \kappa_{h\eta\eta} + i\Omega_h \frac{1}{v}(-s + 2m_\eta^2) + i\Lambda_\eta \frac{1}{v} s \tag{4.124}$$

• Cartesian basis amplitude

Then,

$$i\mathcal{M}_{car} \sim +i\frac{m_h^2}{v^2} - i\frac{2m_h^2 + s}{v^2}\xi \tag{4.125}$$

• Polar basis amplitude

$$i\mathcal{M}_{pol} \sim +i\frac{m_h^2}{v^2} - i\frac{2m_h^2 + s}{v^2}\xi \tag{4.126}$$

$\eta\eta \to W_L^+ W_L^-$ above the WW threshold and $\xi = 0$-1

$$i\mathcal{M} = \left(\frac{i}{s - m_h^2 + i\epsilon}\kappa'_{h\eta\eta}(igm_W)\kappa_{hWW} + i\frac{g^2}{2}\kappa_{\eta\eta WW}\right)\frac{1}{m_W^2}\left(\frac{s}{2} - m_W^2\right) \tag{4.127}$$

and $\kappa' s$ are

	Polar	Cartesian
$\kappa_{h\eta\eta}$	$-\dfrac{m_h^2 - 4m_\eta^2(1-\xi)}{2v^2\sqrt{1-\xi}}$	$+\dfrac{m_h^2}{2v^2} - \dfrac{m_h^2 + 8m_\eta^2}{12v^2}\xi + \mathcal{O}(\xi^2)$
Ω_h	$\sqrt{1-\xi}$	$\sqrt{1-\xi} - \dfrac{\sqrt{\xi}}{\sin^{-1}\sqrt{\xi}}$
Λ_η	0	$\dfrac{\sin^{-1}\sqrt{\xi}}{\sqrt{\xi}} - \dfrac{\sqrt{\xi}}{\sin^{-1}\sqrt{\xi}}$
κ_{hWW}	$\sqrt{1-\xi}$	$\sqrt{1-\xi}$
$\kappa_{\eta\eta WW}$	-1	$-1 + \sqrt{\dfrac{1-\xi}{\xi}}\sin^{-1}\sqrt{\xi}$

where explicit form of $\kappa_{h\eta\eta}$ of the cartesian basis do not fit, so that we expand for small ξ.

By using these values, we calculate $|\mathcal{M}_{pol,car}|$ numerically. Input parameters are

$$\begin{aligned} &m_h = 125\text{GeV}, \quad v = 246\text{GeV}, \quad \xi = 0.1, \\ &m_W = 80\text{GeV}, \quad m_\eta = 100\text{GeV}, \quad \sqrt{s} = 3000\text{GeV} \ . \end{aligned} \tag{4.128}$$

The result shown in Figure 4.28. This shows that when we calculate an observable, these basis give us same result.

4.9.2 Unitarity Bound

From this process, we can extract the unitarity bound (almost same case in the MCHM).

$$a_0 = \frac{1}{32\pi}\int_{-1}^{1} d\cos\theta \mathcal{M}(\eta\eta \to W_L^+ W_L^-) = \frac{1}{16\pi}\mathcal{M}(\eta\eta \to W_L^+ W_L^-) \ . \tag{4.129}$$

4.10 Higgs triple coupling

The SM Higgs triple coupling at one-loop level is

$$\lambda_{hhh}^{\text{SM}} = \frac{3m_h^2}{v}\left(1 - \frac{m_t^4}{\pi^2 v^2 m_h^2}\right) \ . \tag{4.130}$$

In the composite Higgs models, this equation is modified as

$$\lambda_{hhh}^{\text{CHM}} = \frac{3m_h^2}{v}\left\{\kappa_{hhh} - \frac{m_t^4}{\pi^2 v^2 m_h^2}\kappa_{htt}^3 + \frac{m_\eta^4}{12\pi^2 v^2 m_h^2}\left(\frac{\kappa'_{h\eta\eta}(\xi \neq 0)}{\kappa'_{h\eta\eta}(\xi = 0)}\right)^3 \ (\leftarrow ?)\right\} \tag{4.131}$$

where $\kappa'_{h\eta\eta}$ is already defined above section,

$$\kappa'_{h\eta\eta} = -iv\ \kappa_{h\eta\eta} + i\ \Omega_h\Big[2\big(-i\ p_{\eta 1}\big)^\mu\big(-i\ p_{\eta 2}\big)_\mu\Big]\frac{1}{v} + i\ \Lambda_\eta\Big[2\big(-i\ p_{\eta 1}\big)^\mu\big(+i\ p_h\big)_\mu\Big]\frac{1}{v} \ . \tag{4.132}$$

When $\xi = 0$, the coefficients of momentum dependent terms Ω_h and Λ_η are 0 in the cartesian basis (see Appendix), shown in Figure 4.29. When $\xi \ll 1$, coefficients are

$$\begin{aligned} &\text{Polar,} \quad \text{Cartesian} \\ \Omega_h =& \begin{pmatrix} 1 - \frac{1}{2}\xi, & -\frac{\xi}{3} \end{pmatrix}, \\ \Lambda_h =& \begin{pmatrix} 0, & +\frac{\xi}{3} \end{pmatrix}, \end{aligned} \tag{4.133}$$

and zero external momentum limit $p_h \to 0$ in (4.132) leads that the third term of (4.132) vanish in the cartesian basis. The result with $\Omega_h = 0$ is shown in Figure. 4.30.

However, in order to get consistent result, we must(?) introduce mometum dependent part. The relevant diagrams are The vertex factors, $\Delta_{\eta\eta}$, Ω_h, Ω_{hh}, Λ_η, Λ_η and $\Lambda_{h\eta}$, are momentum dependent. When we impose zero external momentum limit, $\Omega_{\eta h}$, Λ_η and $\Lambda_{h\eta}$ vanish. ?????????

4.10.1

Diagram (a')

$$i\mathcal{M}_{a'} = \int_0^{\Lambda_{\rm cut}} \frac{d^D k}{(2\pi)^D} \frac{-i}{(k^2 - m_\eta^2)^3} \left(\kappa'_{h\eta\eta}\right)^3 \ . \tag{4.134}$$

where

$$\begin{aligned} \kappa'_{h\eta\eta} &= -iv\kappa_{h\eta\eta} + 2i\frac{k^2}{v}\Omega_h \ , \\ \to \left(\kappa'_{h\eta\eta}\right)^3 &= -i\frac{8k^6}{v^3}\Omega_h^3 + i\frac{12k^4}{v}\Omega_h^2\kappa_{h\eta\eta} - i\ 6k^2 v\ \Omega_h\kappa_{h\eta\eta}^2 + i\ v^3\kappa_{h\eta\eta}^3 \ . \end{aligned} \tag{4.135}$$

Then,

$$\begin{aligned} i\mathcal{M}_{a'} =& \int_0^{\Lambda_{\rm cut}} d^D k \frac{-i}{(k^2 - m_\eta^2)^3} \left(-i\frac{8k^6}{v^3}\Omega_h^3 + i\frac{12k^4}{v}\Omega_h^2\kappa_{h\eta\eta} - i\ 6k^2 v\ \Omega_h\kappa_{h\eta\eta}^2 + i\ v^3\kappa_{h\eta\eta}^3\right) \ . \\ =& (-i)\int_0^{\Lambda_{\rm cut}} d^D k_E \frac{-i}{(k_E^2 + m_\eta^2)^3} \left(+i\frac{8k_E^6}{v^3}\Omega_h^3 + i\frac{12k_E^4}{v}\Omega_h^2\kappa_{h\eta\eta} + i\ 6k_E^2 v\ \Omega_h\kappa_{h\eta\eta}^2 + i\ v^3\kappa_{h\eta\eta}^3\right) \ , \\ =& (-i)\int_0^{\Lambda_{\rm cut}} d^D k_E \frac{1}{(k_E^2 + m_\eta^2)^3} \left(+\frac{8k_E^6}{v^3}\Omega_h^3 + \frac{12k_E^4}{v}\Omega_h^2\kappa_{h\eta\eta} + 6k_E^2 v\ \Omega_h\kappa_{h\eta\eta}^2 + v^3\kappa_{h\eta\eta}^3\right) \ , \\ =& \left(-i\frac{3m_h^2}{v}\right) \frac{1}{12m_h^2\pi^2 v^2} \left[\frac{v^6\kappa_{h\eta\eta}^3}{4m_\eta^2}\frac{\Lambda_{\rm cut}^4}{\left(\Lambda_{\rm cut}^2 + m_\eta^2\right)^2} - 6v^4\kappa_{h\eta\eta}^2\Omega_h \left\{\frac{3\Lambda_{\rm cut}^4 + 2\Lambda_{\rm cut}^2 m_\eta^2}{4\left(\Lambda_{\rm cut}^2 + m_\eta^2\right)^2} - \frac{1}{2}\log\left(1 + \frac{\Lambda_{\rm cut}^2}{m_\eta^2}\right)\right\}\right. \\ &+ 3v^2\kappa_{h\eta\eta}\Omega_h^2 \left\{\frac{2\Lambda_{\rm cut}^6 + 9\Lambda_{\rm cut}^4 m_\eta^2 + 6\Lambda_{\rm cut}^2 m_\eta^4}{\left(\Lambda_{\rm cut} + m_\eta^2\right)^2} - 6m_\eta^2\log\left(1 + \frac{\Lambda_{\rm cut}^2}{m_\eta^2}\right)\right\} \\ &\left. + \Omega_h^3 \left\{\frac{\Lambda_{\rm cut}^2\left(\Lambda_{\rm cut}^2 + 2m_\eta^2\right)\left(\Lambda_{\rm cut}^4 - 6\Lambda_{\rm cut}^2 m_\eta^2 - 6m_\eta^4\right)}{4\left(\Lambda_{\rm cut}^2 + m_\eta^2\right)^2} + 3m_\eta^4\log\left(1 + \frac{\Lambda_{\rm cut}^2}{m_\eta^2}\right)\right\}\right] \end{aligned} \tag{4.136}$$

Diagram (b')

$$
\begin{aligned}
i\mathcal{M}_{b'} =& \int_0^{\Lambda_{\rm cut}} d^D k \frac{-1}{(k^2-m_\eta^2)^2}\left(-iv\kappa_{h\eta\eta}+2i\frac{k^2}{v}\Omega_h\right)\left(i\ \frac{k^2}{2v^2}\Omega_{hh}\right)\\
=& i\int_0^{\Lambda_{\rm cut}} d^D k_E \frac{+i}{(k_E^2+m_\eta^2)^2}\left(\frac{k^4}{v^3}\Omega_h^2+\frac{k^2}{2v}\kappa_{h\eta\eta}\Omega_h\right)\\
=& \left(-i\frac{3m_h^2}{v}\right)\ \frac{1}{12m_h^2\pi^2v^2}\left[\frac{1}{4}\Omega_h\Omega_{hh}\left\{3\Lambda_{\rm cut}^4-6\Lambda_{\rm cut}^2m_\eta^2-\frac{2\Lambda_{\rm cut}^6}{\Lambda_{\rm cut}^2+m_\eta^2}+6\Lambda_{\rm cut}^4\log\left(1+\frac{\Lambda_{\rm cut}^2}{m_\eta^2}\right)\right\}\right.\\
&\left.+\frac{1}{2}v^2\kappa_{h\eta\eta}\Omega_{hh}\left\{\Lambda_{\rm cut}^2-\frac{\Lambda_{\rm cut}^4}{2(\Lambda_{\rm cut}^2+m_\eta^2)^2}-m_\eta^2\log\left(1+\frac{\Lambda_{\rm cut}^2}{m_\eta^2}\right)\right\}\right] \quad (4.137)
\end{aligned}
$$

4.11 Double Higgs production at LHC 14 TeV in $SO(6)/SO(5)$

Let us consider the double Higgs poduction at LHC with 14 TeV. The parton-level differential cross section is

$$\frac{d\hat{\sigma}(gg\to hh)}{d\hat{t}}=\frac{G_F^2\alpha_s^2}{256(2\pi)^3}\left[|C_\Delta F_\Delta+C_\Box F_\Box|^2+|C_\Delta G_\Delta|^2\right] \quad (4.138)$$

where $\hat{t}$ is the momentum transfer squared and F_Δ, $F_\Box$ and $G_\Box$ are the form factors, defined in [43]. The total cross section is calculated by

$$\sigma(pp\to gg\to hh)=\int_{4m_h^2/s}^1 d\tau\frac{d\mathcal{L}_{gg}}{d\tau}\hat{\sigma}(\hat{s}=\tau s) \quad (4.139)$$

In the SM, coefficients C_Δ and $C_\Box$ are

$$
\begin{aligned}
C_\Delta^{\rm SM} =& \frac{3m_h^2}{\hat{s}-m_h^2},\\
C_\Box^{\rm SM} =& 1.
\end{aligned} \quad (4.140)
$$

In the MCHMs, there coefficients are modified as

$$
\begin{aligned}
C_\Delta^{\rm MCHM} =& \frac{3m_h^2}{\hat{s}-m_h^2}\kappa_t\kappa_{hhh}+\frac{m_t}{\sqrt{2}v}c_{hhtt},\\
C_\Box^{\rm MCHM} =& \kappa_t^2.
\end{aligned} \quad (4.141)
$$

Moreover, we introduce one-loop contibutions to the hhh coupling. κ_{hhh} becomes

$$\kappa_{hhh}\to\kappa_{hhh}-\frac{m_t^4}{\pi^2v^2m_h^2}\kappa_t^3+\frac{m_\eta^4}{12\pi^2v^2m_h^2}\kappa_{h\eta\eta}^3. \quad (4.142)$$

In this calculation, we set $\kappa_{h\eta\eta}=1$ since this effect comes from one-loop diagram. The result is shown in Figure 4.32.

4.12 Beyond the Minimal model

The breakdown of global symmetry which is larger than $SO(5)$ generates the extended Higgs sector. For exmaple, the authors in [9] proposed a model whose global symmetry $SU(5)$ is kroken into $SO(5)$. The Higgs sector contains one triplet, one doublet and one singlet. Previous work in [48] lists many composite Higgs models with extended Higgs sector.

4.13 Diphoton execess at 750 GeV

We discuss an extended scalar model which explains the recent results of diphoton excess at 750 GeV at LHC Run II experiments. An additional singlet scalar boson with the mass of 750 GeV, which couples to top quarks via a dimension five operator, is produced via gluon fusion and decays into two photons via loop contributions of a number of (multiply) charged scalar bosons. Origin of such a dimension five operator would be, for example, in the context of composite Higgs models. The excess can be explained without contradicting the data from LHC Run I and also theoretical consistencies such as perturbative unitarity and charge non-breaking. This subsection is based on [3].

4.13.1 Introduction

Since the discovery of the Higgs boson at LHC Run I [49], the main target of high energy collider experiments has turned to detect new direct evidence of physics beyond the standard model (SM). Recently both ATLAS Collaboration and CMS Collaboration reported a new excess in the diphoton data at 750 GeV with the width about 45 GeV at LHC Run II [50, 51], which might be the resonance of a new particle beyond the SM. Many physicists have been trying to understand the new excess based on various ideas, and quite a few papers have already been submitted until now for a short time[52, 53]. In a large number of the proposed models, vector-like fermions are introduced to enhance the diphoton decay of new resonance. Alternatively, there are models in which new charged scalar fields in the extended scalar sector significantly contribute to the diphoton decay [53].

In this paper, we would like to discuss a possibility that an extended Higgs sector would explain this phenomenon in a relatively simple way. Although the Higgs boson was found, the shape of the Higgs sector remains unknown, and there are many possibilities for extended scalar sectors. Such extensions of the Higgs sector are often motivated to understand phenomena which cannot be explained in the SM, such as radiative neutrino mass generation mechanisms, sources of a scalar dark matter and the cause of strongly first order phase transition and CP violation required for electroweak baryogenesis. In addition, new paradigms beyond the SM also require a specific Higgs sector in each model.

We here introduce a simple extension of the SM with an additional real singlet scalar field S and several (multiply) charged scalar bosons. We can assume that the singlet does not have a vacuum expectation value (VEV). The singlet couples to top quarks ($S\bar{t}_L t_R$), whose coupling originally comes form a dimension five operator $St_L\tilde{\Phi}t_R$, and also couples to charged scalars via trilinear scalar couplings with dimensionful parameters. At LHC, the singlet field S can then be produced via the gluon fusion process. The produced S fields mainly decay into $t\bar{t}$ but some do into diphoton. The observed data[50, 51] suggest that the signal at $M_{\gamma\gamma} \simeq 750$ GeV should

satisfy

$$\begin{aligned} \text{ATLAS} &: \sigma(pp \to SX \to \gamma\gamma X) \simeq 5 \pm 4 \text{ fb (95\%CL)} , \\ \text{CMS} &: \sigma(pp \to SX \to \gamma\gamma X) \simeq 9 \pm 7 \text{ fb (95\%CL)} . \end{aligned} \tag{4.143}$$

We show that by our simple setup the observed signal cross section and the observed total width $\Gamma_S \simeq 45$ GeV [50] can be explained without contradicting the data from LHC Run I [54, 55] and also constraints from theoretical consistencies such as perturbative unitarity [56] and charge non-breaking vacuum [57].

4.13.2 Model

We consider the following effective Lagrangian for interactions of the singlet field S as

$$\mathcal{L}_{\text{eff}} = -y\frac{S}{\Lambda}\left(\overline{Q}_L\tilde{\Phi}q_R\right) - \sum_q \sum_{i,j}^{n_q} \mu_q^{ij}\ S\phi_i^{+q}\phi_j^{-q}, \tag{4.144}$$

where Φ is the Higgs doublet field, $\phi_i^{\pm q}$ are scalar bosons with the electric charge of $\pm q$, and n_q is the number of q-charged scalar bosons. We can assume that the singlet S does not have a VEV while the Higgs doublet field Φ does have the VEV $\langle\Phi^0\rangle = v/\sqrt{2}$, where $v \simeq 246$ GeV. Therefore, only v gives the mass to the quarks and leptons.

The origin of the dimension five operator in Eq. (4.144) would be in the context of composite Higgs models [58]. For example, in the $SO(6)/SO(5)$ model where the global symmetry $SO(6)$ is spontaneously broken to $SO(5)$ at the composite scale, there are 5 pseudo Nambu-Goldstone bosons (pNGBs). They become components of one Higgs doublet and one neutral real scalar singlet filed in the Higgs sector [59]. This singlet couples to charged fermions as

$$\mathcal{L}_{\text{int}} = im_f\sqrt{\frac{\xi}{1-\xi}}\cot\theta_f\ S\bar{f}_L f_R\ , \tag{4.145}$$

where m_f is the mass of the fermion, and ξ is the compositeness parameter, and the mixing angle $\cot\theta_f$ is the Z_2 breaking parameter which vanishes at $\theta_f = \pi/2$ where the exact Z_2 symmetry ($S \to -S$) recovers.

The existence of charged singlet scalars would also be realized in the context of composite Higgs models. In the composite Higgs models, the number of light scalar degrees of freedom in the low energy effective theory is determined by the symmetry breaking structure G/H. A part of the list for various G/H and corresponding extended Higgs sectors is presented in Ref. [60]. For example, in the $(SO(6))^2/SO(6)$ model, where the global symmetry $(SO(6))^2$ is spontaneously broken to $SO(6)$, it appear 15 pNGBs which are decomposed as one real singlet, two doublets and two real triplet fields [61]. In such a model, we have the singlet real scalar field S which couples to both $t_L\bar{t}_R$ and a number of (singly) charged scalar bosons.

In the following, however, we do not specify the fundamental model which predicts the Lagrangian in Eq. (4.144). Instead, we consider models with extended scalar sectors with the interaction in Eq. (4.144) in a general framework and try to explain the excess at 750 GeV in the recent LHC data.

For simplicity, we here consider the case where the trilinear scalar couplings μ_q^{ij} in Eq. (4.144) are diagonal and universal, and all charged scalars are degenerate in mass,

$$\mu_q^{ij} = \mu\delta^{ij}, \tag{4.146}$$

$$m_{\phi_i^{\pm q}} = m_\pm, \qquad \forall q, \tag{4.147}$$

so that there are only two coupling parameters y and μ as well as the common mass of charged scalars $m_\pm$.

The basic idea of our scenario is the following. We assume that the excess is the result of the production and decay of S with the mass of 750 GeV. The production cross section $pp \to S + X$ is dominated by gluon fusion of top-quark loop mediation. The main decay mode of S is $t\bar{t}$, so that the production cross section of $\sigma(pp \to SX)$ and the total width Γ_S are correlated and controlled by the coupling y. From the observed value of Γ_S, the magnitude of y is determined. On the other hand, the decay rate of $S \to \gamma\gamma$ is determined by the top-loop contribution and also by the charged-scalar loop effect. If the number of charged scalars is not small, scalar loop contributions dominate the top-loop effect. In such a case, the decay rate is determined by the trilinear scalar coupling μ. In the following, we show that the data of the excess can be explained by tuning these parameters under the constraint from the 8 TeV data.

4.13.3 Numerical Evaluation

The partonic production cross section $gg \to S$ is given by

$$\hat{\sigma}(gg \to S) = \frac{G_F \alpha_S^2(\sqrt{\hat{s}})}{288\sqrt{2}\pi} \left| \frac{3}{4} F_f(\tau_t) \right|^2 \times \frac{yv^2}{\sqrt{2} m_f \Lambda} \ , \tag{4.148}$$

where $\hat{s}$ is the centre-of-mass energy of this subprocess and $\tau_t = 4m_t^2/\hat{s}$. The hadronic cross section is evaluated by

$$\sigma(pp \to SX) = K \int_{\tau_S = m_S^2/s}^1 d\tau \frac{d\mathcal{L}_{gg}}{d\tau} \times \hat{\sigma}(gg \to S) \ , \tag{4.149}$$

where $d\mathcal{L}_{gg}/d\tau$ is the luminosity function. We here use MSTW2008 LO [44], and the K factor is taken to be 2.5 in our calculation [62]. When we take $\Lambda = v$, we obtain

$$\sigma(pp \to S) \simeq 0.3 y^2 \text{ pb} \ . \tag{4.150}$$

for $\sqrt{s} = 13$ TeV. In Fig. 4.33, the production cross section of $pp \to S + X$ is shown at the leading order as a function of y for $\sqrt{s} = 13$ TeV (red) and 8 TeV (blue).

We next consider the decay branching ratios of the produced S. We here assume that $m_S < 2m_\pm$ so that the charged scalars affect the total width Γ_S only via the quantum loop

contributions in $S \to \gamma\gamma$. The decay rates of the singlet S are calculated by

$$\Gamma(S \to t\bar{t}) = \frac{N_c g^2 m_t^2}{32\pi m_W^2} m_S |\kappa_{stt}|^2 \left(1 - \frac{4m_t^2}{m_S^2}\right)^{\frac{3}{2}} , \tag{4.151}$$

$$\Gamma(S \to \gamma\gamma) = \frac{\alpha^2 g^2}{1024\pi^3} \frac{m_S^3}{m_W^2} \times \left| \kappa_{stt} \frac{4}{3} F_t \left(\frac{4m_t^2}{m_S^2}\right) + r\kappa_{s\pm} F_0 \left(\frac{4m_\pm^2}{m_S^2}\right) \right|^2 , \tag{4.152}$$

$$\Gamma(S \to Z\gamma) = \frac{\alpha^2 m_S^3}{128\pi^3 v^2} \left(1 - \frac{m_Z^2}{m_S^2}\right)^3 \times \left| 2\kappa_{stt} J_f + \sum_i \frac{q_i g}{c_W} \left(I_3^i - s_W^2 q_i\right) \frac{\mu}{v} J_S \right|^2 , \tag{4.153}$$

where $r = \sum_q q^2 n_q$, and

$$\kappa_{stt} = \frac{yv}{\sqrt{2} m_t} , \qquad \kappa_{s\pm} = \frac{m_W}{g m_\pm^2} \mu . \tag{4.154}$$

The loop integral functions are defined by [63]

$$F_t(\tau) = -2\tau \left[1 + (1-\tau) f(\tau)\right] , \tag{4.155}$$

$$F_0(\tau) = \tau(1 - \tau f(\tau)), \tag{4.156}$$

and

$$f(\tau) = \begin{cases} \left[\sin^{-1} \frac{1}{\sqrt{\tau}}\right]^2 & \text{for } \tau \geq 1, \\ -\frac{1}{4} \left[\log \left\{ \frac{1+\sqrt{1-\tau}}{1-\sqrt{1-\tau}} \right\} - i\pi \right]^2 , & \text{for } \tau < 1. \end{cases} \tag{4.157}$$

J_f is written by $A_{1/2}^H$ in Ref. [64] as

$$J_f = \frac{v_f}{s_W c_W} A_{1/2}^H . \tag{4.158}$$

The loop contribution J_S is given in Ref. [65]. Our model can be classified by the parameter r, and characterized by the parameters of y, μ and $m_\pm$ with m_S being set to be 750 GeV.

The signal cross section of $pp \to S + X \to \gamma\gamma + X$ is then given by

$$\sigma(pp \to SX \to \gamma\gamma X) = \sigma(pp \to SX) \cdot \mathrm{Br}(S \to \gamma\gamma), \tag{4.159}$$

where we employ the narrow width approximation, because the ratio Γ_S / m_S is smaller than 0.1.

Now we survey the parameter region where the data of the excess at 750 GeV is explained without contradiction with the Run I data for the process $pp \to S + X \to \gamma\gamma + X$ at 8 TeV [54, 55];

$$\begin{aligned} \text{ATLAS} &: \ \sigma(pp \to SX \to \gamma\gamma X) \simeq 1.6 \pm 1.3 \text{ fb (95\%CL)} , \\ \text{CMS} &: \ \sigma(pp \to SX \to \gamma\gamma X) \simeq 0.9 \pm 0.6 \text{ fb (95\%CL)} . \end{aligned} \tag{4.160}$$

If the model contains doubly charged scalar bosons, we have to take into account the constraint on the mass from the LHC data. In particular, if the doubly charged scalars from isospin singlets (triplets) decay into dilepton, the current lower bound is about 430 GeV (550 GeV) [66]. On the other hand, if they are of the complex triplet scalar fields, it can mainly decay into diboson ($W^{\pm}W^{\pm}$) when the VEV for the triplet is larger than 0.1 MeV. In
such a case, the current mass lower limit is about 90 GeV [67], which is much relaxed as compared to the case of dilepton decays. If we consider n_q (> 1) of doubly charged Higgs bosons, these bounds should become stronger. We here do not specify the isospin of charged scalar bosons and also their main decay mode for a while, and we come back to this issue later.

In Fig. 4.34, contour plots of the regions satisfying the data from the 13 TeV Run (red) [50] and those at 8 TeV (grey) [54] are shown (in the 95 % CL) on the y-μ plane for the six models with $r = 1$, 10, 16 25, 50, and 65. The region where the width of S is 40 GeV $< \Gamma_S <$ 50 GeV is indicated by blue shaded regions. We also draw the curve of $\Gamma_S = 5.3$ GeV, the current resolution for the diphoton system [50]. The universal mass of charged scalars is set to be 400 GeV. In each model, there is the region where all data are satisfied. For smaller r, relatively large μ is required to satisfy the data, while for relatively large number of r, μ can be lowered to a few TeV. For instance, for the model with $r = 1$ where only one singly charged scalar filed is introduced, the required value of μ is 100-200 TeV to satisfy the data. On the other hand, for the model with $r = 65$ which corresponds to the models with $(n_1, n_2) = (65, 0)$, $(45, 5)$, $(25, 10)$, $(13, 13)$ etc, the required value of μ is at most a few TeV.

In Fig. 4.35, the similar figures for the results with the mass of the universal charged scalar mass $m_{\pm}$ to be 600 GeV are shown with the same fashion. We see that the required values of μ for each model are larger than the cases with $m_{\pm} = 400$ GeV.

4.13.4 Discussion

We here discuss theoretical constraints which limit parameter regions, and then give some comments on the relation of our model to the new physics phenomena.

First, in order to obtain enough enhancement in the diphoton decay rate of the singlet S, a larger value of μ is required for a smaller values of r. However, taking a too large value of μ compared to m_S and $m_{\pm}$ possibly causes dangerous charge breaking minima. For the case of $m_S = 750$ GeV and $m_{\pm} = 400$–600 GeV, the value of μ larger than about 10 TeV is not favored at all by the similar analysis to the case of large trilinear coupling in the minimal supersymmetric standard model (MSSM)[68].

Second, the perturbative unitarity bound for scattering processes such as $\phi^{+q}\phi^{-q} \to \phi^{+q}\phi^{-q}$ should also be taken into account in the case with a large μ. It is known that in the MSSM, constraints from perturbative unitarity for the trilinear coupling are similar in strength to bounds from color and charge breaking minima[69]. The unitarity bound on μ in our model is also expected to lead to a similar constraint from charge non-breaking vacuum.

Therefore, from these theoretical constraints, the models with a small r and a large $m_{\pm}$ are not favored even though there are regions which satisfy the data of the excess. As seen in Fig. 4.34, for $m_{\pm} = 400$ GeV the cases with $r = 25$, 50 and 65 can be safe from these theoretical bounds, while for $m_{\pm} = 600$ GeV only those with $r = 65$ can be allowed (see Fig. 4.35).

In order to have a relatively large values of r, introduction of a scalar field with a higher isospin representation would be helpful. For example, in the model with an isospin septet scalar field, there are many multiply charged scalar bosons $\phi^{\pm 5}$, $\phi^{\pm 4}$, $\phi^{\pm 3}$, $\phi^{\pm 2}$, $\phi^{\pm}$ and $\overline{\phi}^{\pm}$, which give

$r = 56$. The phenomenology of the septet field is discussed in Ref. [70]. We note that models with a higher representation scalar field than the septet are not realistic from viewpoint of perturbative unitarity [71].

In our analysis, we only have considered the models with only one real singlet field S. However, it would also be possible to consider the cases with more real singlets S_i $(i = 1, \cdots N)$. If they have the common mass and the universal couplings with $t_L\bar{t}_R$ and with charged scalars, then the signal cross section becomes N^2 larger than the case with $N = 1$. In such a case, the magnitude of the trilinear coupling can be smaller so that the constraint from perturbative unitarity and charge non-breaking would be milder. In this case, the excess at 750 GeV can be explained with smaller values of r.

In our scenario, many (multiply) charged scalar fields are introduced. Such introduction of many scalars can also be seen in the models for quantum generation of tiny neutrino masses (so called radiative seesaw scenarios), where neutrino masses are deduced from the extended scalar sectors at one-loop [72, 73], two-loop [74] and three-loop levels [75, 76, 77]. Therefore, the excess at 750 GeV would be indirect evidence for such radiative seesaw scenarios with S which couples to $t_L\bar{t}_R$. In addition, introduction of many scalars can cause strongly first order phase transition at electroweak symmetry breaking [78], which is required for a successful scenario of electroweak baryogenesis [79].

For $m_S = 750$ GeV and the observed value of $\Gamma_S \sim 45$ GeV, the branching ratio of $S \to \gamma\gamma$ is required to take values between about 0.6 % and about 3.5 % to satisfy all the diphoton data for all cases of r and $m_\pm$. The data can be satisfied with similar values of the branching ratio even if the value of the width is smaller than 45 GeV. The main decay mode of S is always tt, whose branching ratio is larger than 95 %. Produced number of $t\bar{t}$ via the S decay is much smaller than the uncertainty in the data of the $t\bar{t}$ production cross section at the 8 TeV [80] and the 13 TeV [81].

In the following, we mention some phenomenological features with speculation. Detailed study is beyond the scope of this letter. If our scenario is true, the second phenomenological signature would be the discovery of charged Higgs bosons with the mass to be 400-600 GeV. In particular, if some of them have double electric charge, the final state would be dilepton or diboson, depending on their isospin charges and the other parameters. If they decay into dilepton, the signature is expected to be observed very soon at LHC Run II, otherwise the model is ruled out. If doubly charged scalars have isospin, the main decay mode can be same sign diboson. In such a case, the current lower limit is about 90 GeV [67]. In order to detect the signal around 400-600 GeV, considerable amount of luminosity has to be accumulated. Finally if the model contains higher order isospin representation scalar fields, their charged scalar components also enhance the $Z\gamma$ decay rate by the loop effect, whose branching ratio can be a few times 1 %. In such a case, the signal of $S \to Z\gamma$ would be discovered in the near future at LHC Run II.

4.14 Conclusion

We have investigated the minimal composite Higgs model and its variation models. In these class of models, the Higgs boson appears as the pNGB associated with the breakwdown of the global symmetry $SO(5)$. The Higgs boson coupling constants are deviated from the SM predictions depending on the matter representation in the global symmetry. These deviation

patters of the MCHM variaion models could be diatinguished by the future collider experiemnts.

The MCHM is an analogy of the realistic QCD theory. Moreover, the Higgs bosons can be identified with the pion, which apeears as the well-known pNGB in Nature. The scatteing amplitude of $\pi\pi \to \pi\pi$ seems to diverge at of order one GeV scale and violate the perturbative unitarirty. However, the phase shift occurs by a nre resonance and the perturbative unitarity is recovered. The new renonance is called the rho menson. In the MCHNs, the energy dependence amplitude for $W_L W_L \to W_L W_l$ does not disappear. There is no such energy dependence in the SM. We assume that a new resonance, like the QCD rho meson, appears and the perturbative unitarity is restored. We can estimate its mass scale by the phase shift imformation beyond the reach of current collider experiments.

We also investigate double Higgs productions at the LHC and the ILC in order to obtain constrains on the compositeness parameter ξ. First, we obtain constraints on ξ from the data of LHC Run-I. Second, we calculate the signal strength of the double Higgs boson cross sections including the Higgs boson decay modes. At the LHC, the signal strength for all decay modes is enhanced in the MCHMs. On the other hand, at the ILC, the signal strength of the MCHMs shows significant energy dependence.

In addition, at the end of 2015, a signal of a new paricle has been found at the LHC. It appears in the Higgs decay mode of diphoton $h \to \gamma\gamma$ around 750 GeV. We want to explain this phenomena in the framework of the composite Higgs models with an extended Higgs sector. A neutral singlet with the mass 750 GeV and a number of *multiply* charger scalars are introduced. We propose this simple model setup and could explain the phenomena. The small number of the charged scalars does not is prefered because of the theoretical constraints. The perturbative unitarity and charge non-breaking minima gives us contrains on the masses and the number of charged scalars.

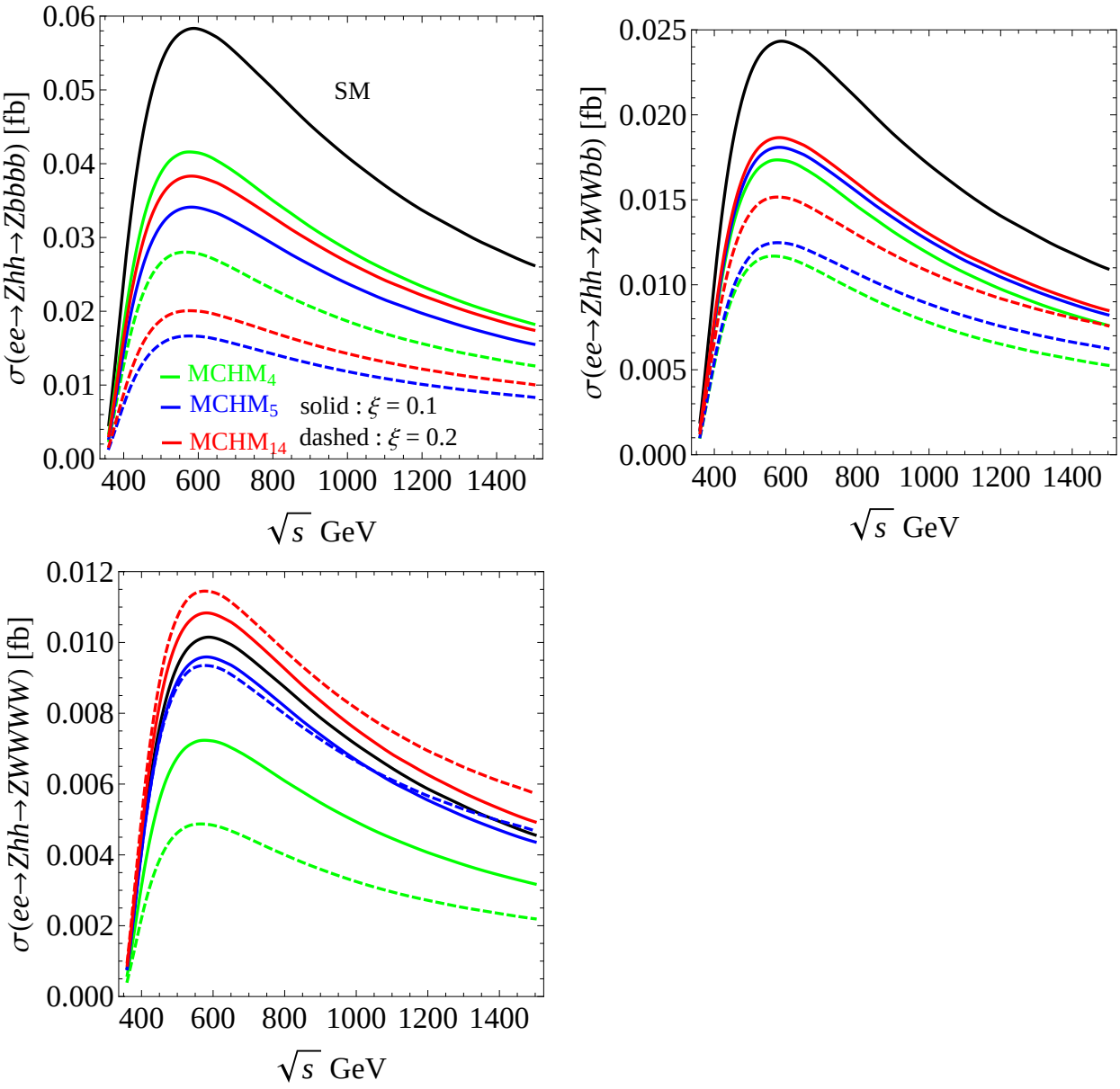

Figure 4.22: The production cross section for $ee \to Zhh \to XXYY$.

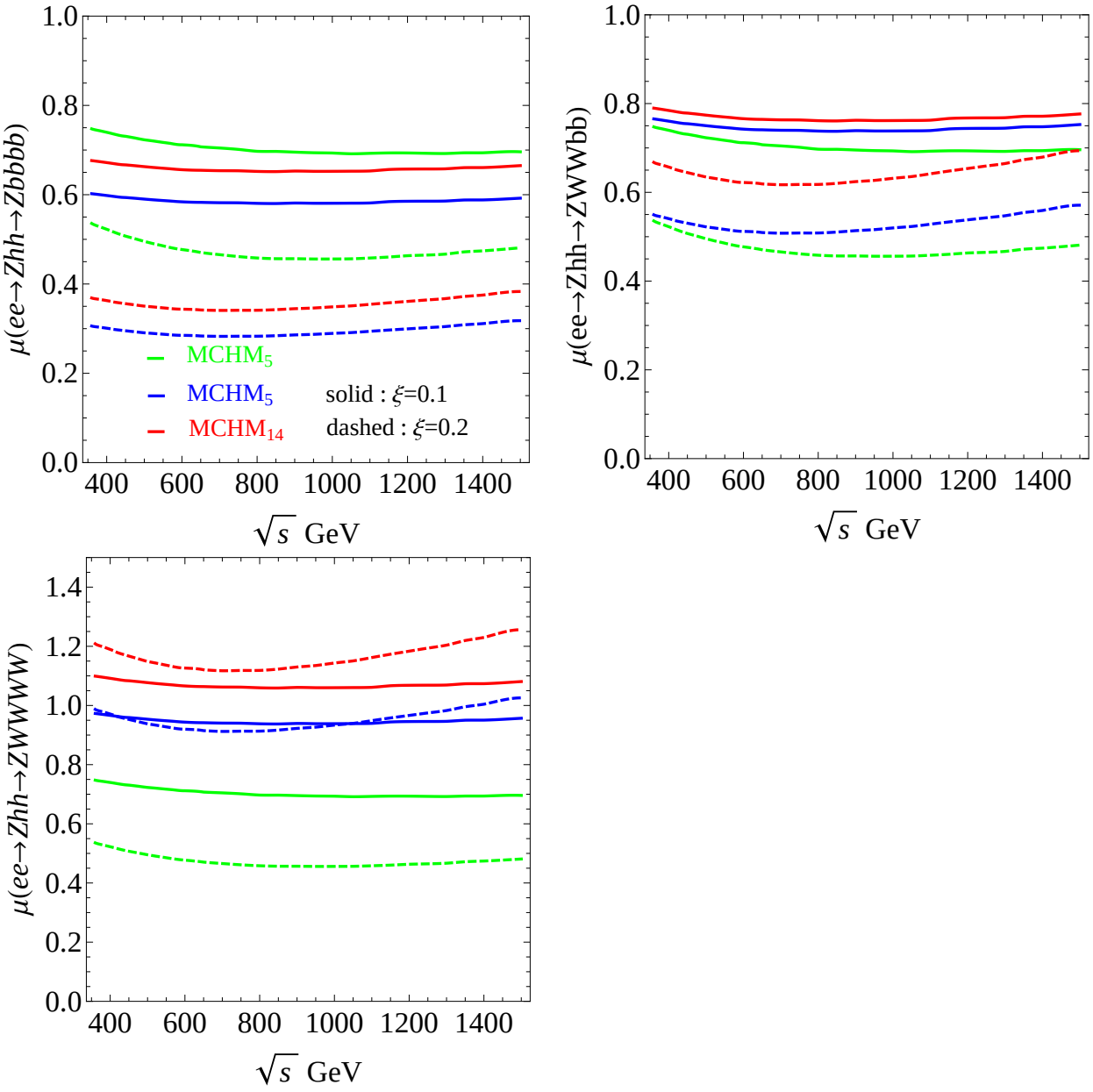

Figure 4.23: The signal strength for $ee \to Zhh \to XXYY$.

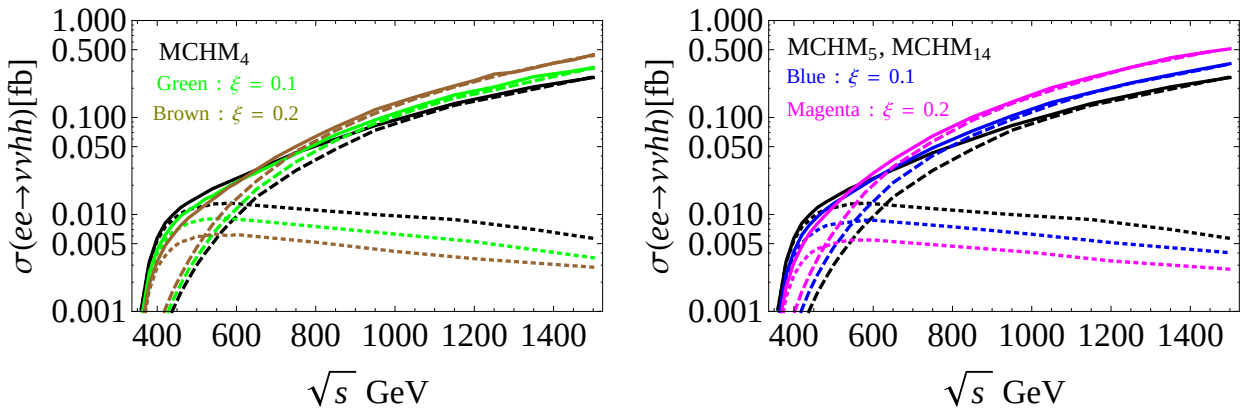

Figure 4.24: The production cross section of $ee \to \nu\nu hh$ for each models with $\xi = 0.1, 0.2$.

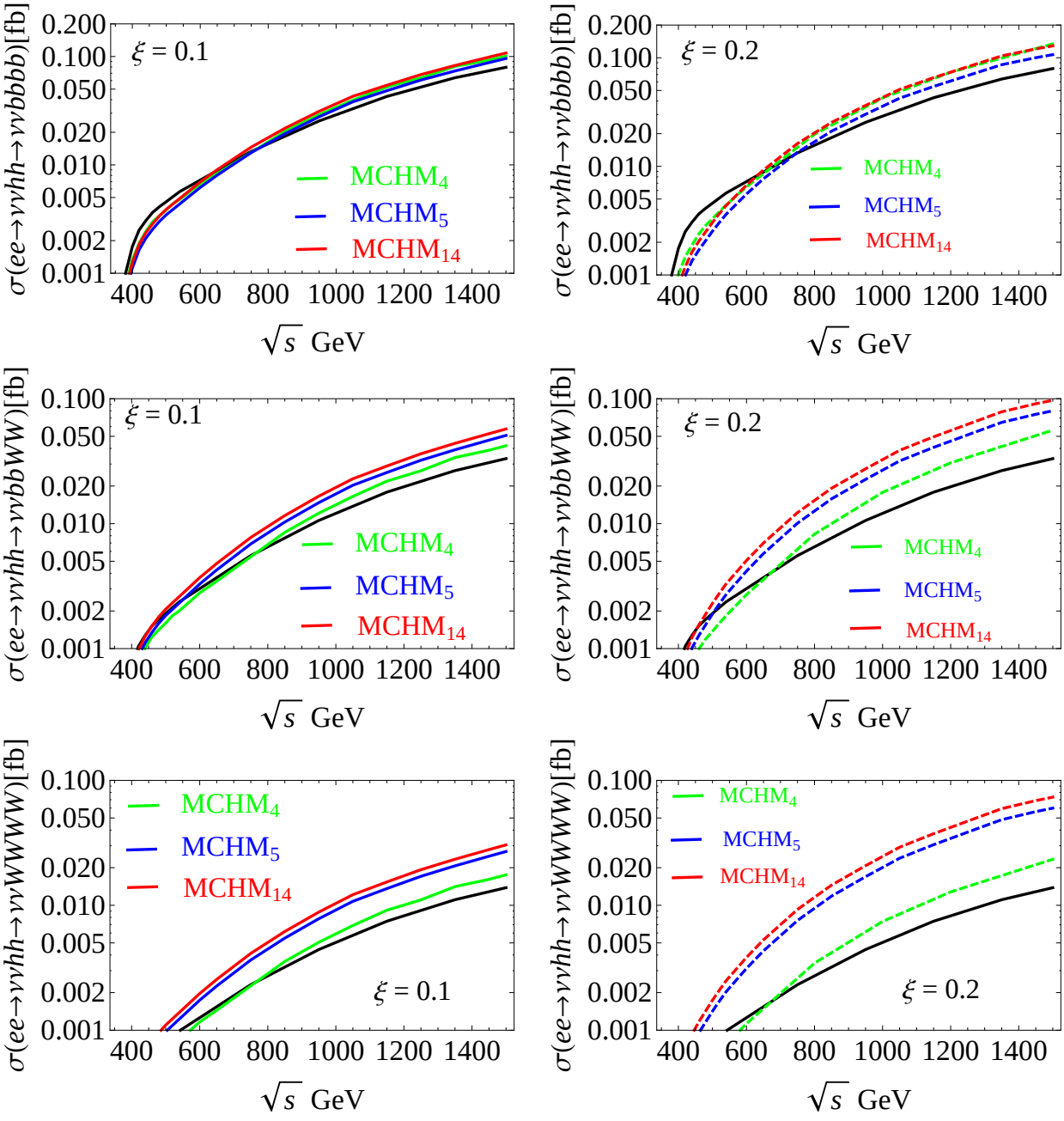

Figure 4.25: The total cross sections including the Higgs decay for each models with $\xi = 0.1$(left column), 0.2(right column).

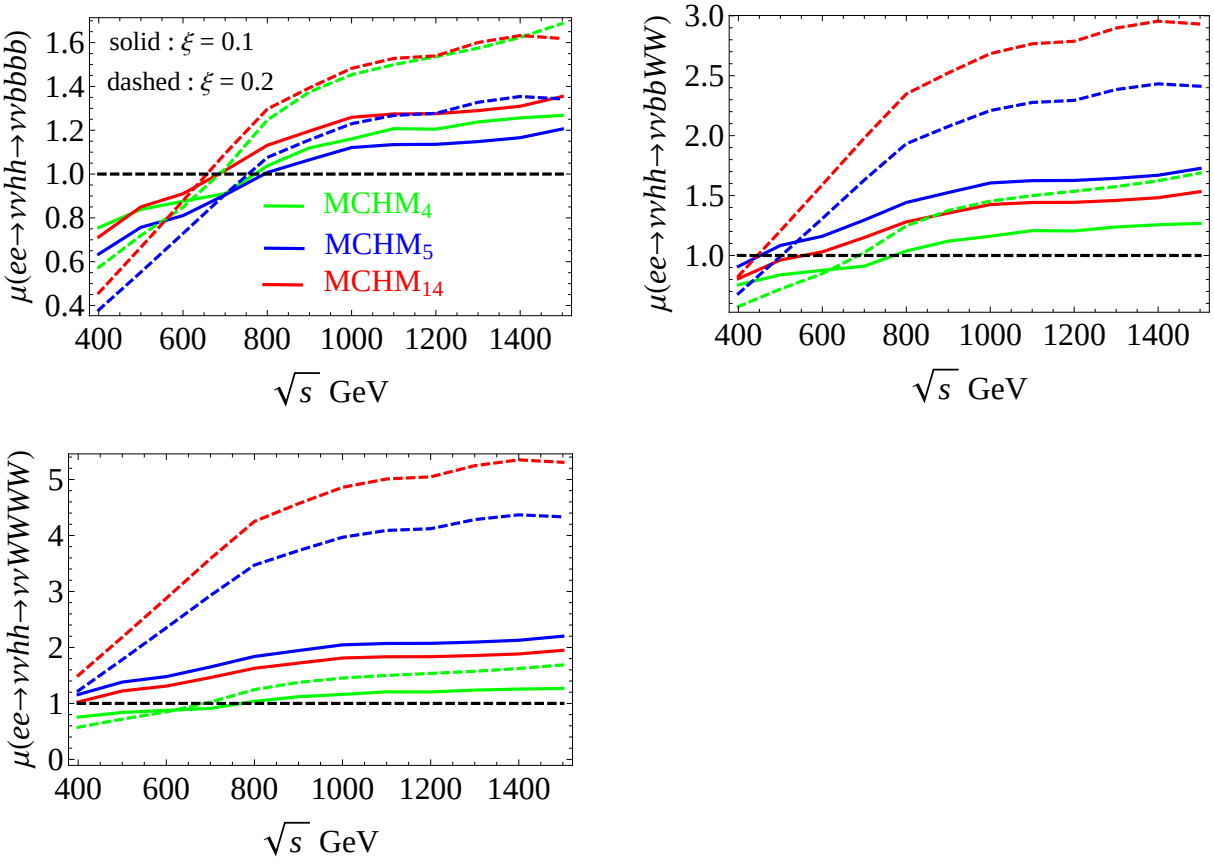

Figure 4.26: The signal strength for $ee \to \nu\nu hh \to \nu\nu XXYY$.

Figure 4.27: $\eta\eta \to W^+W^-$ scattering

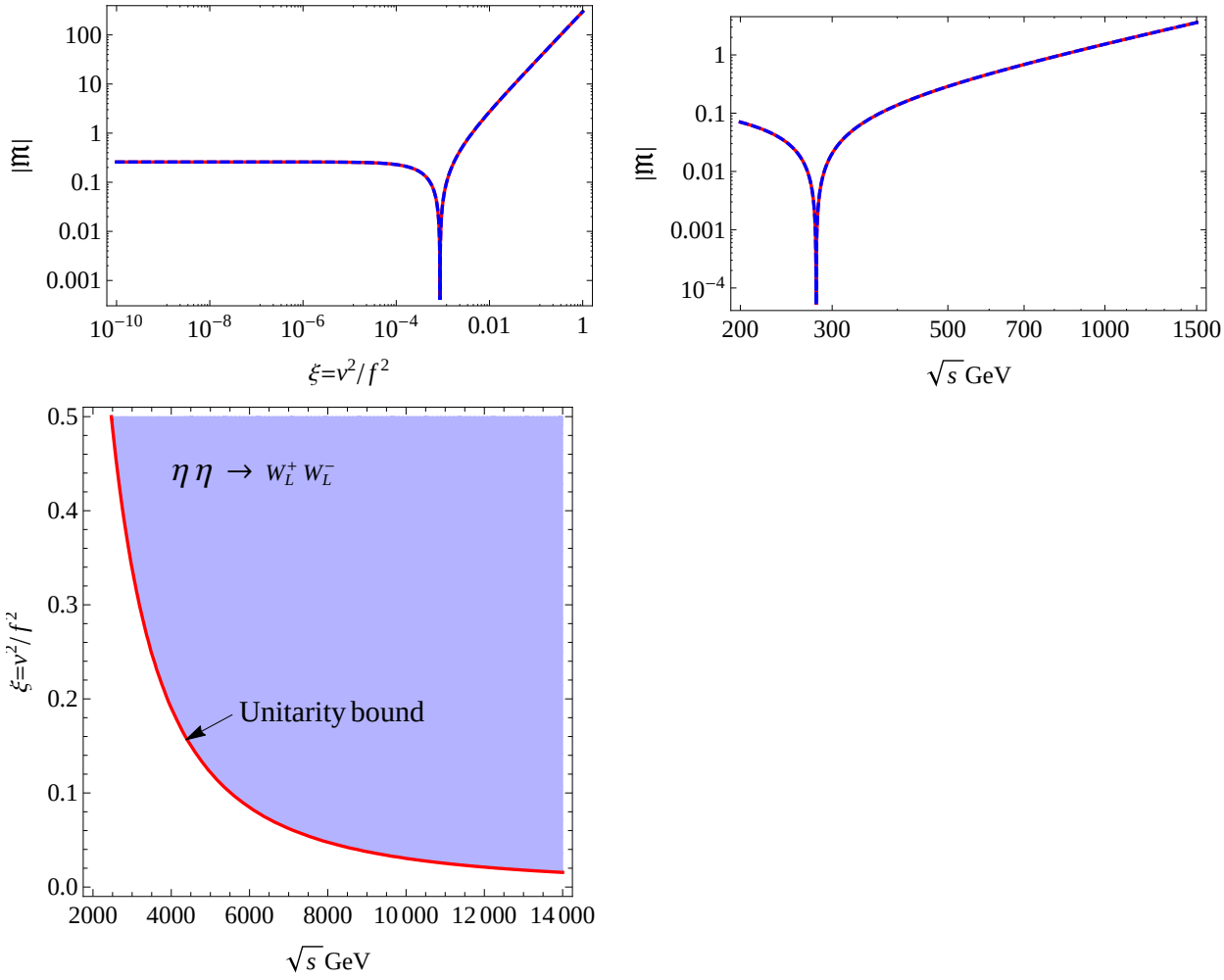

Figure 4.28: (Upper) : Consistency check between the *polar* (dashed blue line) and *cartesian* (solid red line) basis. (Lower) : Unitarity bound from $\eta\eta \to W_L^+ W_L^-$.

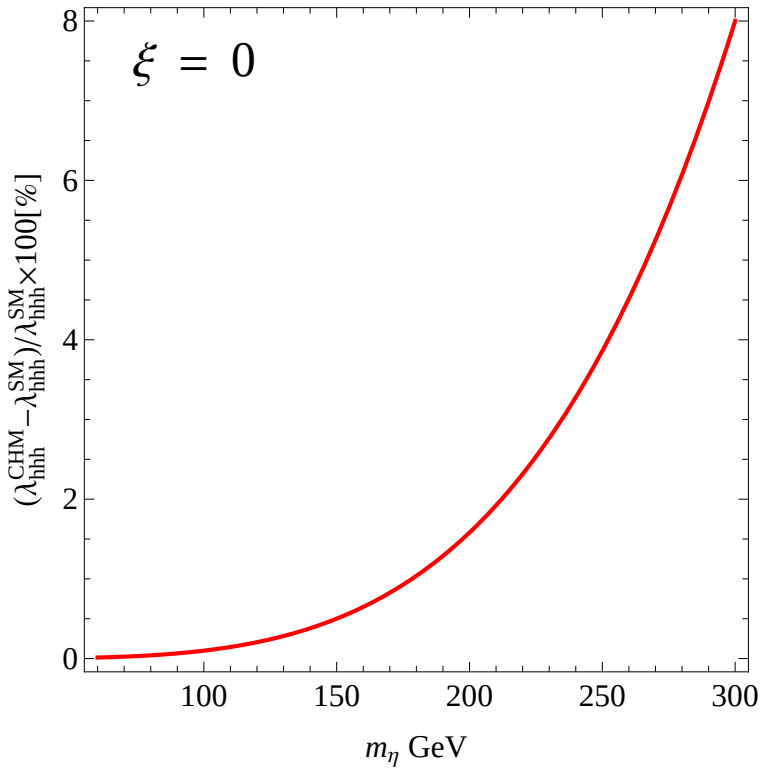

Figure 4.29: The deviation of the Higgs triple couling with $\xi = 0$.

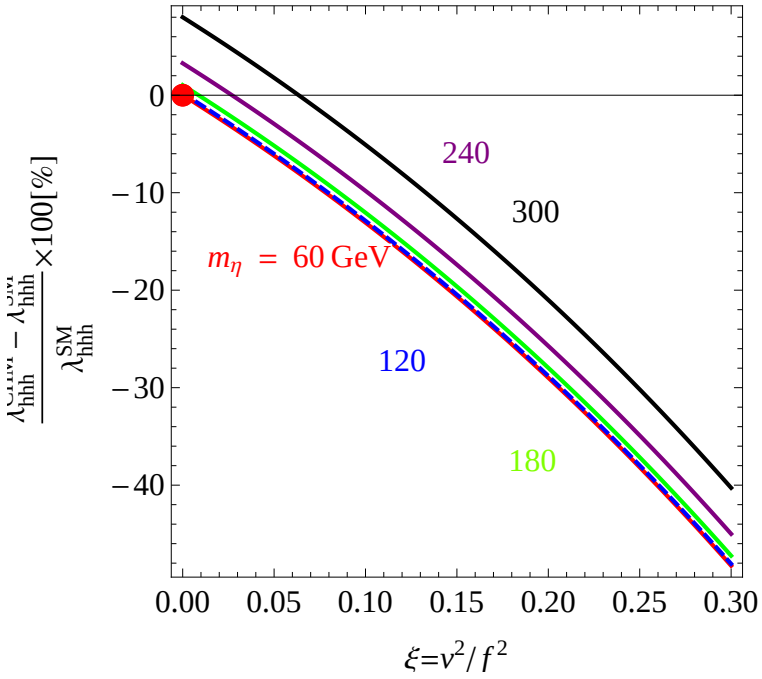

Figure 4.30: The deviation of the Higgs triple couling with $\xi \ll 1$ and negleting loop momentum dependent contributions. Red point shows the SM value.

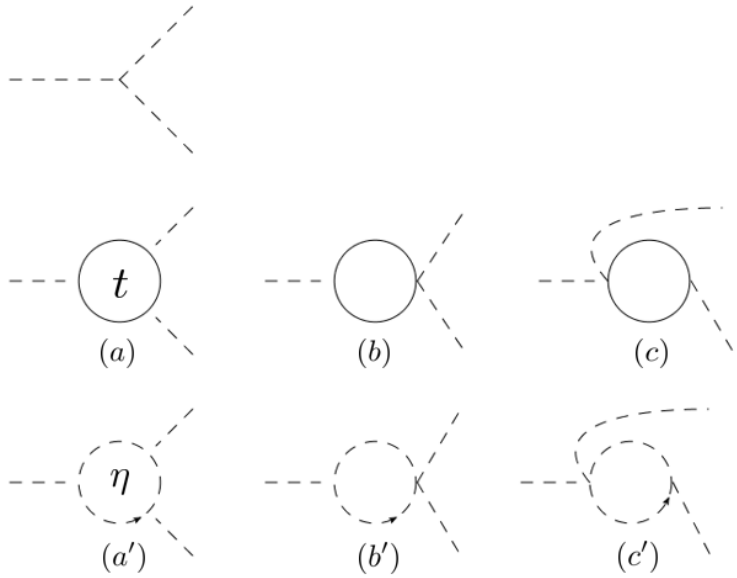

Figure 4.31: hhh diagrams

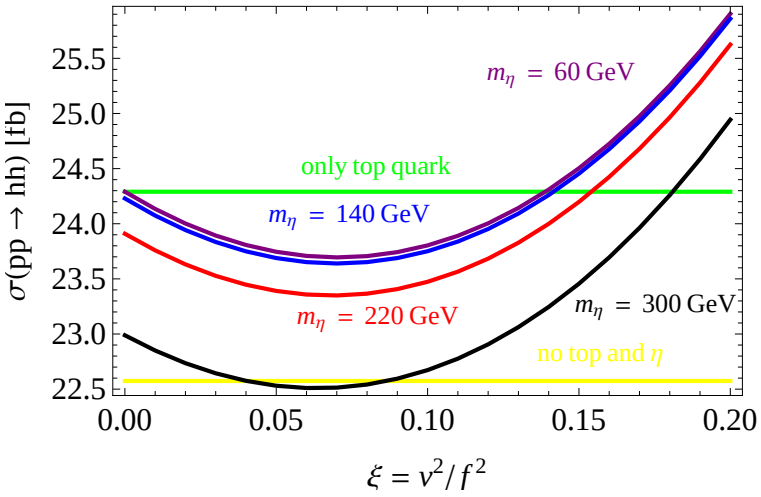

Figure 4.32

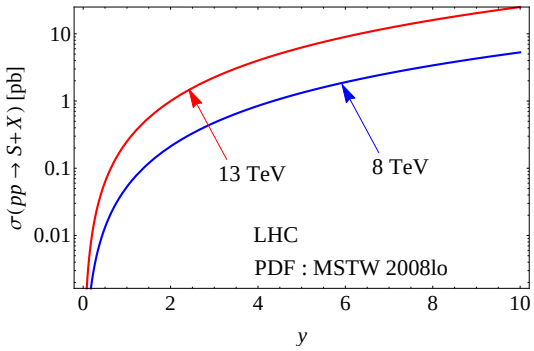

Figure 4.33: The hadronic production cross section $pp \to S + X$ as a function of y at the LHC for the centre-of-mass energy to be 13 TeV (red) and 8 TeV (blue).

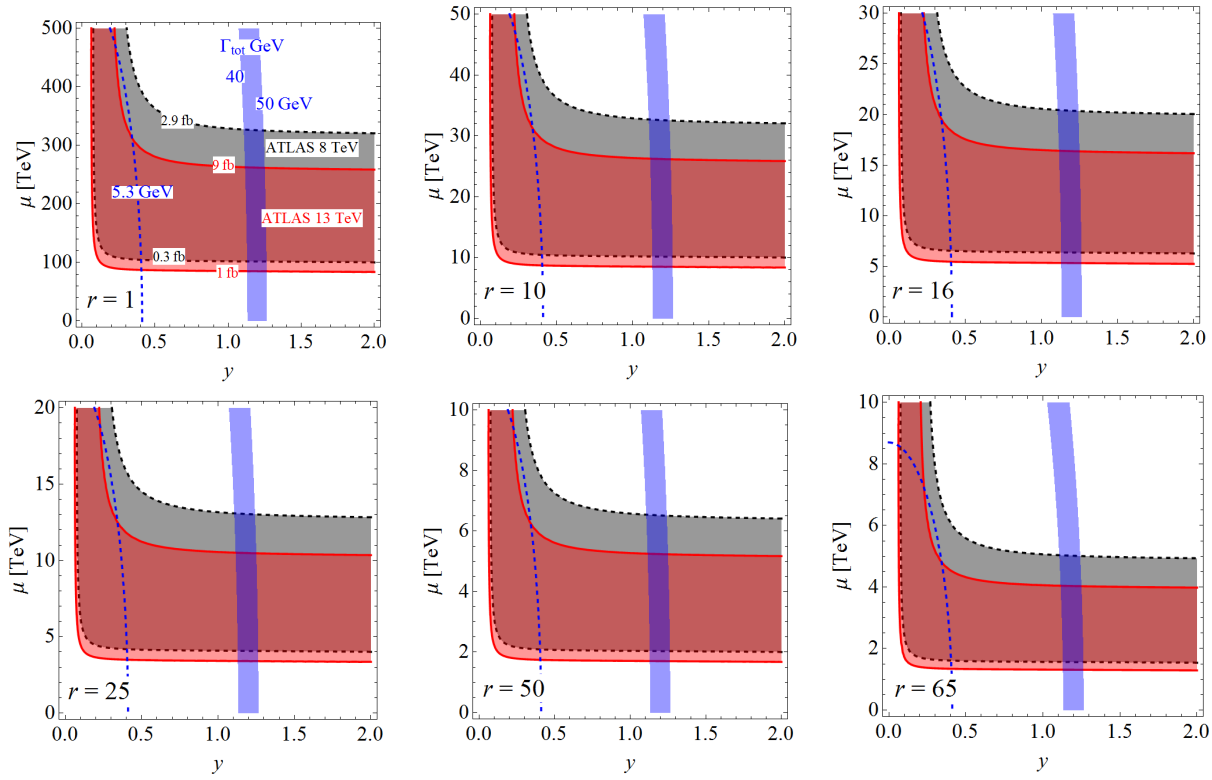

Figure 4.34: Contour plots of the signal cross section $\sigma(pp \to SX) \times \mathrm{Br}(S \to \gamma\gamma)$ [fb] on the y-μ plane for $m_{\pm} = 400$ GeV. The regions which satisfy the 13 TeV data (red) [50] and 8 TeV data (grey) [54] within the 95 % CL are shown. The regions where the total width of S is in 40 GeV $< \Gamma_S <$ 50 GeV (blue band) and the curve of $\Gamma_S = 5.3$ GeV (blue dashed), the energy resolution of the diphoton system, are also indicated. From top-left to bottom-right, the results are shown in the models wish $r = 1$, 10, 16, 25, 50 and 65.

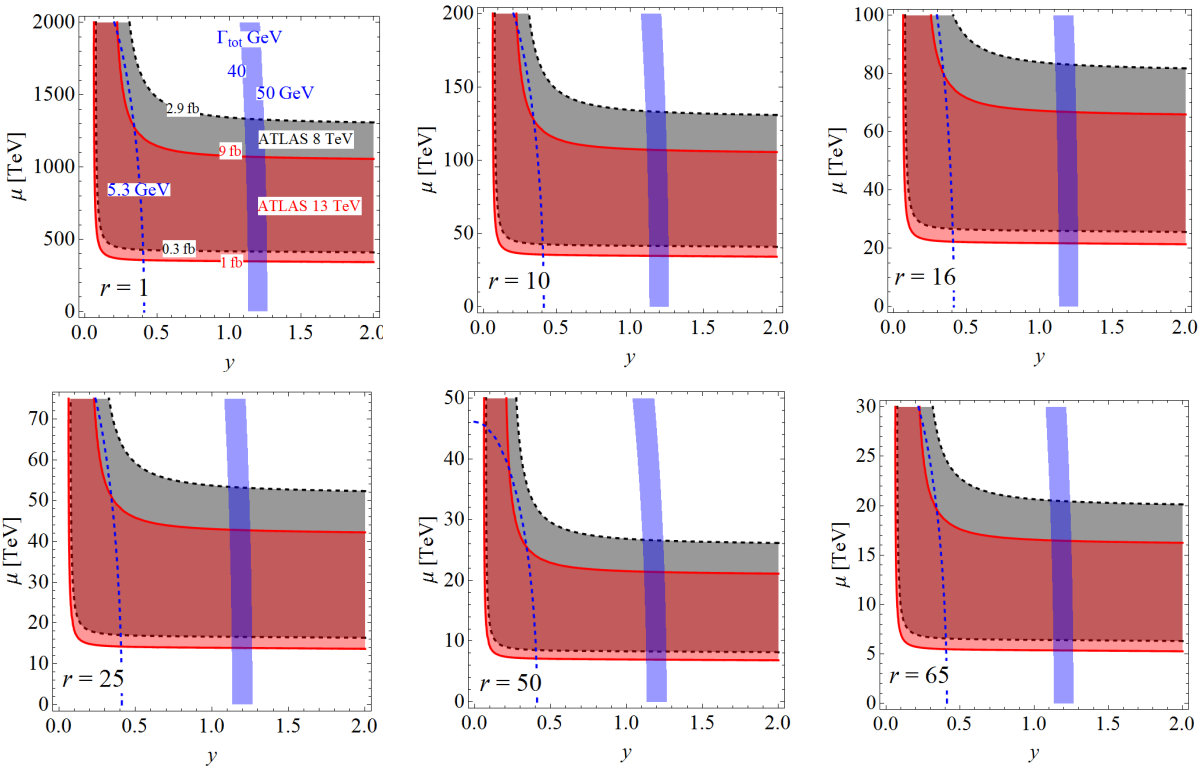

Figure 4.35: Contour plots of the signal cross section $\sigma(pp \to SX) \times \mathrm{Br}(S \to \gamma\gamma)$ [fb] on the y-μ plane for $m_\pm = 600$ GeV. The regions which satisfy the 13 TeV data (red) [50] and 8 TeV data (grey) [54] within the 95 % CL are shown. The regions where the total width of S is in 40 GeV $< \Gamma_S <$ 50 GeV (blue band) and the curve of $\Gamma_S = 5.3$ GeV (blue dashed), the energy resolution of the diphoton system, are also indicated. From top-left to bottom-right, the results are shown in the models wish $r = 1$, 10, 16, 25, 50 and 65.

Chapter 5

Summary of the Thesis

We have discussed two scenarios whose Higgs bosons are composed by the fundametal particle; a scenario based on the supersymmetric QCD and composite Higgs scenario.

In the supersymmetric $SU(2)_H$ QCD scenario, the extended Higgs sector composed by the six fundamental chiral superfields appear at the low-energy effective theory. We introduce an additional unbroken Z_2 symmetry and it ensures the lightest Higgs boson mass could be satisfied 126 GeV because extra scalar bosons does not get the VEV. The stability of the DM cadidates is also ensured by the Z_2 symmetry. The tiny neutrino masses are generated by the loop quantum effects in the framework of the radiative seesaw scenario. The extra scalar bosons which strongly couple to the SM-like Higgs boson enhances the electroweak phase transition to realize the baryon number asymmetry of the Universe. Therefore, this model could explain these three phenomenological problems which cannot be explained in the SM, simultaneously. Fortunately, this scenario could be tested at future coolider experiments because these physics are related to the TeV scale physics.

In the composite Higgs scenario, we focus on the minimal composite Higgs models and their variation models. The breakdown of the global symmetry $SO(5)$ into $SO(4)$ leads 4 NGBs and this corresponds to one Higgs doublet. The Higgs boson couplings deviate from the SM predictions, which is parametrized by one parameter, the copositeness parameter ξ. Their deviation patterns depend on the representaions of the SM particles in $SO(5)$. We make a list these couling deviations. We could distinguish these MCHM variation models at future collider experiments. In addition, we assume the existence of a new particle which is an analogue of the rho meson in QCD. We estimate this mass scale by extracting phase shift imformation beyond the reach of current data. The double Higgs production at the LHC and linear collider experiments are also investigated. At the LHC, all signal strength including the Higgs boson decay are always enhanced. At the ILC, the energy dependence of the productino cross sections show charastaristic behaviour.

We also study the phenomenological application of composite Higgs models to the diphoton excess 750 GeV at the LHC. By using the framework of the extended composite Higgs models, this phenomena could be explained.

Appendix A

Kinematics of $u\bar{d} \to W^+Z \to \ell\nu\ell\ell$

We give the explicit kinematics of the decay product, which is sketched in Ref. [29]. The process considered here is WZ pair production by $u\bar{d}$ scattering, and they decay purely leptonic: $u(p_u)\bar{d}(p_d) \to W^+(p_W)Z(p_Z) \to \nu_l(p_\nu)l^+(p_{l_1})l^-(p_{l_2})l^+(p_{l_3})$. Regarding u and $\bar{d}$ as massless, they only appear as left-handed state in this process. Here we assign their momenta as follows:

$$u: \quad p_u = \sqrt{S}/2\ (1, -\sin\Theta, 0, \cos\Theta), \tag{A.1}$$

$$\bar{d}: \quad p_d = \sqrt{S}/2\ (1, \sin\Theta, 0, -\cos\Theta), \tag{A.2}$$

$$W^+: \quad p_W = (E_W, 0, 0, p_V), \tag{A.3}$$

$$Z: \quad p_Z = (E_Z, 0, 0, -p_V), \tag{A.4}$$

$$\nu_l: \quad p_\nu = \sqrt{E_W^2 - q_V^2}/2\ (1, \sin\theta_1\cos\phi_1, \sin\theta_1\sin\phi_1, \cos\theta_1), \tag{A.5}$$

$$l^+: \quad p_{l_1} = \sqrt{E_W^2 - q_V^2}/2\ (1, -\sin\theta_1\cos\phi_1, -\sin\theta_1\sin\phi_1, -\cos\theta_1), \tag{A.6}$$

$$l^-: \quad p_{l_2} = \sqrt{E_Z^2 - q_V^2}/2\ (1, \sin\theta_2\cos\phi_2, \sin\theta_2\sin\phi_2, \cos\theta_2), \tag{A.7}$$

$$l^+: \quad p_{l_3} = \sqrt{E_Z^2 - q_V^2}/2\ (1, -\sin\theta_2\cos\phi_2, -\sin\theta_2\sin\phi_2, -\cos\theta_2), \tag{A.8}$$

where we define z-axis along to the W-boson momentum direction, and Θ is the angle between $\vec{p}_u$ and $\vec{p}_W$. The phase space of the final state leptons depends on two polar decay angles (θ_1, θ_2) and two azimuthal decay angles (ϕ_1, ϕ_2) from the production plane defined by $\hat{n} \sim \vec{p}_u \times \vec{p}_W$. Therefore, $A_\pm$ defined in Eq. (4.18) represents the asymmetry between the events that the charged lepton goes to "above" or "below" the production plane.

Appendix B

Generators and eigenvectors of Composite Higgs models

In this appendix, we show explicite representations of the $SO(5)$ and $SO(6)$ generators and their eigenvectors.

B.1 $SO(5)$ generators

The $SO(5)$ generators are defined as

$$\begin{aligned}(T^{a_{L,R}})_{ij} &= -\frac{i}{2}\left[\frac{1}{2}\epsilon^{abc}\left(\delta^b_i\delta^c_j - \delta^b_j\delta^c_i\right) \pm \left(\delta^a_i\delta^4_j - \delta^a_j\delta^4_i\right)\right], \\ T^{\hat{a}}_{ij} &= -\frac{i}{\sqrt{2}}\left(\delta^{\hat{a}}_i\delta^5_j - \delta^{\hat{a}}_j\delta^5_i\right). \end{aligned} \tag{B.1}$$

where $T^{a_{L,R}}$ ($a_L,\ a_R = 1,2,3$) are unbroken SO(4) generators, $T^{\hat{a}}$ ($\hat{a} = 1,\cdots,4$) are broken generators. They satisfy these commutators,

$$\left[T^{a_L},\ T^{b_L}\right] = i\epsilon^{abc}\ T^{c_L}, \quad \left[T^{a_R},\ T^{b_R}\right] = i\epsilon^{abc}\ T^{c_R}, \quad \left[T^{a_R},\ T^{b_L}\right] = 0. \tag{B.2}$$

Above commutators are almost the same in $SU(2)$.

B.1.1 5-representation

The generators in 5 dimensional representation are

$$T^{a_{L,R}} = \frac{i}{2}\left\{\begin{pmatrix} & & & \mp 1 & 0 \\ & & -1 & & 0 \\ & 1 & & & 0 \\ \pm 1 & & & & 0 \\ 0 & 0 & 0 & 0 & 0 \end{pmatrix}, \begin{pmatrix} & & 1 & & 0 \\ & & & \mp 1 & 0 \\ -1 & & & & 0 \\ & \pm 1 & & & 0 \\ 0 & 0 & 0 & 0 & 0 \end{pmatrix}, \begin{pmatrix} & -1 & & & 0 \\ 1 & & & & 0 \\ & & & \mp 1 & 0 \\ & & \pm 1 & & 0 \\ 0 & 0 & 0 & 0 & 0 \end{pmatrix}\right\},$$

$$T^{\hat{a}} = \frac{i}{\sqrt{2}}\left\{\begin{pmatrix} & & & & -1 \\ & & & & 0 \\ & & & & 0 \\ & & & & 0 \\ 1 & 0 & 0 & 0 & 0 \end{pmatrix}, \begin{pmatrix} & & & & \\ & & & & -1 \\ & & & & 0 \\ & & & & 0 \\ & 1 & 0 & 0 & 0 \end{pmatrix}, \begin{pmatrix} & & & & \\ & & & & \\ & & & & -1 \\ & & & & 0 \\ & & 1 & 0 & 0 \end{pmatrix}, \begin{pmatrix} & & & & \\ & & & & \\ & & & & \\ & & & & -1 \\ & & & 1 & 0 \end{pmatrix}\right\} \tag{B.3}$$

The Dirac gamma matrices in 5-dimension, denoted by Γ, is

$$\Gamma^{\hat{a}} = \begin{pmatrix} 0 & \sigma^{\hat{a}} \\ \sigma^{\hat{a}\dagger} & 0 \end{pmatrix}, \quad \Gamma^5 = \begin{pmatrix} \mathbf{1}_{2\times 2} & 0 \\ 0 & \mathbf{1}_{2\times 2} \end{pmatrix}, \quad \sigma^{\hat{a}} = \{\vec{\sigma}, -i\mathbf{1}\}\,. \tag{B.4}$$

The eigenvectors of $T_L^3,\ T_R^3$ are,

$$T_L^3 : \frac{1}{\sqrt{2}}\begin{pmatrix} 0 \\ 0 \\ i \\ 1 \\ 0 \end{pmatrix}_{-1/2}, \ \frac{1}{\sqrt{2}}\begin{pmatrix} i \\ 1 \\ 0 \\ 0 \\ 0 \end{pmatrix}_{-1/2}, \ \frac{1}{\sqrt{2}}\begin{pmatrix} 0 \\ 0 \\ -i \\ 1 \\ 0 \end{pmatrix}_{+1/2}, \ \frac{1}{\sqrt{2}}\begin{pmatrix} -i \\ 1 \\ 0 \\ 0 \\ 0 \end{pmatrix}_{+1/2}, \ \begin{pmatrix} 0 \\ 0 \\ 0 \\ 0 \\ 1 \end{pmatrix}_{0}. \tag{B.5}$$

$$T_R^3 : \frac{1}{\sqrt{2}}\begin{pmatrix} 0 \\ 0 \\ -i \\ 1 \\ 0 \end{pmatrix}_{-1/2}, \ \frac{1}{\sqrt{2}}\begin{pmatrix} i \\ 1 \\ 0 \\ 0 \\ 0 \end{pmatrix}_{-1/2}, \ \frac{1}{\sqrt{2}}\begin{pmatrix} 0 \\ 0 \\ i \\ 1 \\ 0 \end{pmatrix}_{+1/2}, \ \frac{1}{\sqrt{2}}\begin{pmatrix} -i \\ 1 \\ 0 \\ 0 \\ 0 \end{pmatrix}_{+1/2}, \ \begin{pmatrix} 0 \\ 0 \\ 0 \\ 0 \\ 1 \end{pmatrix}_{0}. \tag{B.6}$$

where subscripts are eigenvalues under $SU(2)_L$ or $SU(2)_R$. We redefine eigenvectors as follows

$$\begin{aligned} v_{(-,-)} =& \frac{1}{\sqrt{2}}\begin{pmatrix} i \\ 1 \\ 0 \\ 0 \\ 0 \end{pmatrix}, \ v_{(-,+)} = \frac{1}{\sqrt{2}}\begin{pmatrix} 0 \\ 0 \\ i \\ 1 \\ 0 \end{pmatrix}, \\ v_{(+,-)} =& \frac{1}{\sqrt{2}}\begin{pmatrix} 0 \\ 0 \\ -i \\ 1 \\ 0 \end{pmatrix}, \ v_{(+,+)} = \frac{1}{\sqrt{2}}\begin{pmatrix} -i \\ 1 \\ 0 \\ 0 \\ 0 \end{pmatrix}, \ v_{(0,0)} = \begin{pmatrix} 0 \\ 0 \\ 0 \\ 0 \\ 1 \end{pmatrix}. \end{aligned} \tag{B.7}$$

with $\pm \equiv \pm 1/2$.

B.1.2 10-representation

The **10**-representaion is decomposed under $(SU(2)_L, SU(2)_R)$, $\mathbf{10} \sim (\mathbf{3},\mathbf{1}) \oplus (\mathbf{1},\mathbf{3}) \oplus (\mathbf{2},\bar{\mathbf{2}})$. In this case, eigenvectors are defined as

$$\begin{aligned} (\mathbf{3},\mathbf{1}) \ &: \ v_{(\pm 1,0)} = \frac{1}{\sqrt{2}}(T_L^1 \pm iT_L^2), \qquad v_{(0,0)} = T_L^3, \\ (\mathbf{1},\mathbf{3}) \ &: \ v_{(0,\pm 1)} = \frac{1}{\sqrt{2}}(T_R^1 \pm iT_R^2), \qquad v_{(0,0)} = T_R^3, \\ (\mathbf{2},\mathbf{2}) \ &: \ v_{(-1/2,-1/2)} = \frac{1}{\sqrt{2}}(T^{\hat{1}} - iT^{\hat{2}}), \quad v_{(+1/2,+1/2)} = \frac{1}{\sqrt{2}}(T^{\hat{1}} + iT^{\hat{2}}), \\ & \qquad v_{(-1/2,+1/2)} = \frac{1}{\sqrt{2}}(T^{\hat{3}} - iT^{\hat{4}}), \quad v_{(+1/2,-1/2)} = \frac{1}{\sqrt{2}}(T^{\hat{3}} + iT^{\hat{4}}). \end{aligned} \tag{B.8}$$

$$v_{(\pm1,0)} = \frac{1}{2\sqrt{2}} \begin{pmatrix} & & \mp1 & -i & 0 \\ & & -i & \pm1 & 0 \\ \pm1 & +i & & & 0 \\ +i & \mp1 & & & 0 \\ 0 & 0 & 0 & 0 & 0 \end{pmatrix}, \quad v_{(0,0)} = \frac{1}{2} \begin{pmatrix} & -i & & & 0 \\ +i & & & & 0 \\ & & & -i & 0 \\ & & +i & & 0 \\ 0 & 0 & 0 & 0 & 0 \end{pmatrix}, \tag{B.9}$$

$$v_{(0,\pm1)} = \frac{1}{2\sqrt{2}} \begin{pmatrix} & & \mp1 & +i & 0 \\ & & -i & \mp1 & 0 \\ \pm1 & +i & & & 0 \\ -i & \pm1 & & & 0 \\ 0 & 0 & 0 & 0 & 0 \end{pmatrix}, \quad v_{(0,0)} = \frac{1}{2} \begin{pmatrix} & -i & & & 0 \\ +i & & & & 0 \\ & & & +i & 0 \\ & & -i & & 0 \\ 0 & 0 & 0 & 0 & 0 \end{pmatrix}, \tag{B.10}$$

$$v_{(-1/2,-1/2)} = \frac{1}{2} \begin{pmatrix} & & & & -i \\ & & & & -1 \\ & & & & 0 \\ & & & & 0 \\ +i & +1 & 0 & 0 & 0 \end{pmatrix}, \quad v_{(+1/2,+1/2)} = \frac{1}{2} \begin{pmatrix} & & & & -i \\ & & & & +1 \\ & & & & 0 \\ & & & & 0 \\ +i & -1 & 0 & 0 & 0 \end{pmatrix}, \tag{B.11}$$

$$v_{(-1/2,+1/2)} = \frac{1}{2} \begin{pmatrix} & & & & 0 \\ & & & & 0 \\ & & & & -i \\ & & & & -1 \\ 0 & 0 & +i & +1 & 0 \end{pmatrix}, \quad v_{(+1/2,-1/2)} = \frac{1}{2} \begin{pmatrix} & & & & 0 \\ & & & & 0 \\ & & & & -i \\ & & & & +1 \\ 0 & 0 & +i & -1 & 0 \end{pmatrix}. \tag{B.12}$$

B.1.3 14-representation

We can also define the 14-representation generators in $SO(5)$ as

$$
\begin{aligned}
(\mathbf{3},\bar{\mathbf{3}}) \;:\; T^{ab}_{ij} &= \frac{1}{\sqrt{2}}(\delta^a_i\delta^b_j+\delta^a_j\delta^b_i), && a<b,\ a,\ b=1,\cdots,4\\
T^{aa}_{ij} &= \frac{1}{\sqrt{2}}(\delta^a_i\delta^a_j-\delta^{a+1}_i\delta^{a+1}_j), && a=1,2,3\\
(\mathbf{2},\bar{\mathbf{2}}) \;:\; T^{\hat{a}}_{ij} &= \frac{1}{\sqrt{2}}(\delta^a_i\delta^5_j+\delta^a_j\delta^5_i), && a=1,\cdots,4\\
(\mathbf{1},\bar{\mathbf{1}}) \;:\; T^{0}_{ij} &= \frac{1}{2\sqrt{5}}\mathrm{diag}(1,1,1,1,-4). && \text{(B.13)}
\end{aligned}
$$

and eigenvectors as

$$
\begin{aligned}
&(\mathbf{3},\bar{\mathbf{3}}) \;:\\
&v_{(+1,+1)} = \frac{1}{2\sqrt{2}}(2iT^{12}+T^{11}-T^{22}), \qquad v_{(1,0)} = \frac{1}{2}(-T^{13}-iT^{23}-iT^{14}+T^{24}),\\
&v_{(+1,-1)} = \frac{1}{2\sqrt{2}}(2iT^{34}+T^{33}), \qquad v_{(1,0)} = \frac{1}{2}(-T^{13}-iT^{23}+iT^{14}-T^{24}),\\
&v_{(0,0)} = \frac{1}{2\sqrt{2}}(-T^{11}-T^{22}+T^{33}), \qquad v_{(1,0)} = \frac{1}{2}(T^{13}-iT^{23}+iT^{14}+T^{24}),\\
&v_{(-1,+1)} = \frac{1}{2\sqrt{2}}(-2iT^{34}+T^{33}), \qquad v_{(1,0)} = \frac{1}{2}(T^{13}-iT^{23}-iT^{14}-T^{24}),\\
&v_{(-1,-1)} = \frac{1}{2\sqrt{2}}(-2iT^{12}+T^{11}-T^{22}), \qquad \text{(B.14)}\\
&(\mathbf{2},\bar{\mathbf{2}}) \;:\\
&v_{(+1/2,+1/2)} = \frac{1}{\sqrt{2}}(-T^{\hat{1}}-iT^{\hat{2}}), \qquad v_{(+1/2,-1/2)} = \frac{1}{\sqrt{2}}(T^{\hat{3}}+iT^{\hat{4}}),\\
&v_{(-1/2,+1/2)} = \frac{1}{\sqrt{2}}(T^{\hat{3}}-iT^{\hat{4}}), \qquad v_{(-1/2,-1/2)} = \frac{1}{\sqrt{2}}(T^{\hat{1}}-iT^{\hat{2}}), \qquad \text{(B.15)}\\
&(\mathbf{1},\bar{\mathbf{1}}) \;:\\
&v'_{(0,0)} = T^0 \qquad \text{(B.16)}
\end{aligned}
$$

$(\mathbf{3},\bar{\mathbf{3}})$

$$v_{(+1,+1)} = \frac{1}{4}\begin{pmatrix} 1 & 2i & & & 0 \\ 2i & -2 & & & 0 \\ & & 1 & & 0 \\ & & & 0 & 0 \\ 0 & 0 & 0 & 0 & 0 \end{pmatrix},\ v_{(+1,0)} = \frac{1}{2\sqrt{2}}\begin{pmatrix} & & -1 & -i & 0 \\ & & -i & 1 & 0 \\ -1 & -i & & & 0 \\ -i & 1 & & & 0 \\ 0 & 0 & 0 & 0 & 0 \end{pmatrix}, \tag{B.17}$$

$$v_{(+1,-1)} = \frac{1}{4}\begin{pmatrix} 0 & & & & 0 \\ & 0 & & & 0 \\ & & 1 & 2i & 0 \\ & & 2i & -1 & 0 \\ 0 & 0 & 0 & 0 & 0 \end{pmatrix},\ v_{(+1,0)} = \frac{1}{2\sqrt{2}}\begin{pmatrix} & & -1 & +i & 0 \\ & & -i & -1 & 0 \\ -1 & -i & & & 0 \\ i & -1 & & & 0 \\ 0 & 0 & 0 & 0 & 0 \end{pmatrix}, \tag{B.18}$$

$$v_{(0,0)} = \frac{1}{4}\mathrm{diag}(-1,0,2,-1,0), \tag{B.19}$$

$$v_{(0,-1)} = \frac{1}{2\sqrt{2}}\begin{pmatrix} & & 1 & i & 0 \\ & & -i & 1 & 0 \\ 1 & -i & & & 0 \\ i & 1 & & & 0 \\ 0 & 0 & 0 & 0 & 0 \end{pmatrix},\ v_{(-1,+1)} = \frac{1}{4}\begin{pmatrix} 0 & & & & 0 \\ & 0 & & & 0 \\ & & 1 & -2i & 0 \\ & & -2i & -1 & 0 \\ 0 & 0 & 0 & 0 & 0 \end{pmatrix}, \tag{B.20}$$

$$v_{(-1,0)} = \frac{1}{2\sqrt{2}}\begin{pmatrix} & & 1 & -i & 0 \\ & & -i & -1 & 0 \\ 1 & -i & & & 0 \\ -i & -1 & & & 0 \\ 0 & 0 & 0 & 0 & 0 \end{pmatrix},\ v_{(-1,-1)} = \frac{1}{2\sqrt{2}}\begin{pmatrix} 1 & -2i & & & 0 \\ -2i & -2 & & & 0 \\ & & 1 & & 0 \\ & & & 0 & 0 \\ 0 & 0 & 0 & 0 & 0 \end{pmatrix}, \tag{B.21}$$

$(\mathbf{2},\bar{\mathbf{2}})$

$$v_{(+1/2,+1/2)} = \frac{1}{2}\begin{pmatrix} & & & & -1 \\ & & & & -i \\ & & & & 0 \\ & & & & 0 \\ -1 & -i & 0 & 0 & 0 \end{pmatrix},\ v_{(+1/2,-1/2)} = \frac{1}{2}\begin{pmatrix} & & & & 0 \\ & & & & 1 \\ & & & & i \\ & & & & 0 \\ 0 & 0 & 1 & i & 0 \end{pmatrix}, \tag{B.22}$$

$$v_{-1/2,+1/2)} = \frac{1}{2}\begin{pmatrix} & & & & 0 \\ & & & & 1 \\ & & & & -i \\ & & & & 0 \\ 0 & 0 & 1 & -i & 0 \end{pmatrix},\ v_{(+1/2,+1/2)} = \frac{1}{2}\begin{pmatrix} & & & & 1 \\ & & & & -i \\ & & & & 0 \\ & & & & 0 \\ 1 & -i & 0 & 0 & 0 \end{pmatrix}, \tag{B.23}$$

$(\mathbf{1},\bar{\mathbf{1}})$

$$v'_{(0,0)} = \frac{1}{2\sqrt{5}}\mathrm{diag}(1,1,1,1,-4) \tag{B.24}$$

B.1.4 $SO(6)$ generators for $SO(6)/SO(5)$ (Doublet + Singlet)

$$
\begin{aligned}
T^{\hat{a}}_{ij} &= -\frac{i}{\sqrt{2}}\left(\delta^{\hat{a}i}\delta^{6j} - \delta^{\hat{a}j}\delta^{6i}\right), \\
T^{a_{L,R}}_{ij} &= -\frac{i}{2}\left[\frac{1}{2}\epsilon^{abc}\left(\delta^{bi}\delta^{cj} - \delta^{bj}\delta^{ci}\right) \pm \left(\delta^{ai}\delta^{4j} - \delta^{aj}\delta^{4i}\right)\right], \\
T^{\alpha}_{ij} &= -\frac{i}{\sqrt{2}}\left(\delta^{\alpha i}\delta^{5j} - \delta^{\alpha j}\delta^{5i}\right).
\end{aligned} \tag{B.25}
$$

where $T^{\hat{a}}(\hat{a} = 1, \cdots, 5)$ are the broken generators of $SO(6)/SO(5)$, $T^{\alpha}(\alpha = 1, \cdots, 4)$ live in the coset of $SO(6)/SO(5)$ and $T^{a_{L,R}}$ corresponds to $SO(4) \sim SU(2)_L \times SU(2)_R$.

Appendix C

Variation models of the MCHMs

As we mentioned in chapter.3, there are many variation models in the MCHMs. They are listed in [35] except for MCHM_{14}. In this appendix, we show the matter Lagrangian and effective Higgs potential of 13 MCHM variation models since gauge sector does not change. We does not introduce new fermions. The SM fermions are only embedded into $SO(5)$ eigenvectors. The dimensions of representation are 5 (fundamental), 10 (adjoint, anti-symmetric), 14 (symmetric). They can be decomposed as

$$\begin{aligned} \mathbf{5}_X \sim & (\mathbf{2},\mathbf{2})_X \oplus (\mathbf{1},\mathbf{1})_X \ , \\ \mathbf{10}_X \sim & (\mathbf{3},\mathbf{1})_X \oplus (\mathbf{1},\mathbf{3})_X \oplus (\mathbf{2},\mathbf{2})_X \ , \\ \mathbf{14}_X \sim & (\mathbf{3},\bar{\mathbf{3}})_X \oplus (\mathbf{2},\mathbf{2})_X \oplus (\mathbf{1},\mathbf{1})_X \ , \end{aligned} \tag{C.1}$$

where the X is the appropreate $U(1)_X$ charge assignment to reproduce the SM $U(1)_Y$ charge.

We note that untrivial coefficients in the effective Higgs potential (e.g. α and β in (C.4)) are written in terms of form factors. We are not interested in details of these coefficients since we does not discuss the concrete structure at high energy.

C.1 MCHM_5

In this model, all third generation SM quarks are embedded into 5-representation. The first, second generation quarks, and leptons are omitted since their contributions to the Higgs potential is negligible. The quantum charge assignment are

$$\begin{aligned} t_L \ &: \ (1/2,-1/2)_{2/3}, \quad b_L \ : \ (-1/2,-1/2)_{2/3} \ , \\ t_R \ &: \ (0,0)_{2/3}, \qquad\quad\ \ b_R \ : \ (0,0)_{-1/3} \ . \end{aligned} \tag{C.2}$$

The effective matter Lagrangian is

$$\begin{aligned} \mathcal{L}_{\text{eff}}^{\text{matter}} = & \sum_{r=t_L,t_R,b_L,b_R} \overline{\Psi}_r^{(5)} \left[\not{p}\Pi_0^r + \Sigma^\dagger \not{p} \Pi_1^r \Sigma \right] \Psi_r^{(5)} \\ & + \overline{\Psi}_{t_L}^{(5)} \left[M_0^t + \Sigma^\dagger M_1^t \Sigma \right] \Psi_{t_R}^{(5)} + \overline{\Psi}_{b_L}^{(5)} \left[M_0^b + \Sigma^\dagger M_1^b \Sigma \right] \Psi_{b_R}^{(5)} + \text{h.c.} \ . \end{aligned} \tag{C.3}$$

The effective Higgs potential is

$$V_h \simeq \alpha \cos^2(h/f) + \beta \cos^2(h/f) \sin^2(h/f) \ . \tag{C.4}$$

C.2 MCHM$_{10}$

In this model, all third generation SM quarks are embedded into 10-representation. The quantum charge assignment are

$$\begin{aligned} t_L &: (1/2,-1/2)_{2/3}, \quad b_L : (-1/2,-1/2)_{2/3} , \\ t_R &: (0,0)_{2/3}, \qquad\quad b_R : (0,-1)_{2/3} . \end{aligned} \tag{C.5}$$

The effective matter Lagrangian is

$$\begin{aligned} \mathcal{L}_{\text{eff}}^{\text{matter}} = \sum_{r=q_L,t_R,b_R} & \left[\overline{\Psi}_r^{(10)} \not{p} \Pi_0^r \Psi_r^{(10)} + (\Sigma\overline{\Psi}_r^{(10)}) \not{p} \Pi_1^r (\Psi_r^{(10)}\Sigma^\dagger)\right] \\ & + \overline{\Psi}_{q_L}^{(10)} M_0^t \Psi_{t_R}^{(10)} + (\Sigma\overline{\Psi}_{q_L}^{(10)}) M_1^t (\Psi_{t_R}^{(10)}\Sigma^\dagger) \\ & + \overline{\Psi}_{q_L}^{(10)} M_0^b \Psi_{b_R}^{(10)} + (\Sigma\overline{\Psi}_{q_L}^{(10)}) M_1^b (\Psi_{b_R}^{(10)}\Sigma^\dagger) + \text{h.c.} . \end{aligned} \tag{C.6}$$

The effective Higgs potential has the same form in (C.4).

C.3 MCHM$_{14}$

In this model, all third generation SM quarks are embedded into 14-representation. The quantum charge assignment are

$$\begin{aligned} t_L &: (1/2,-1/2)_{2/3}, \quad b_L : (-1/2,-1/2)_{2/3} , \\ t_R &: (0,0)_{2/3}, \qquad\quad b_R : (0,-1)_{2/3} . \end{aligned} \tag{C.7}$$

The effective matter Lagrangian is

$$\begin{aligned} \mathcal{L}_{\text{eff}}^{\text{matter}} = \sum_{r=q_L,t_R,b_R} & \left[\overline{\Psi}_r^{(14)} \not{p} \Pi_0^r \Psi_r^{(14)} + (\Sigma\overline{\Psi}_r^{(14)}) \not{p} \Pi_1^r (\Psi_r^{(14)}\Sigma^\dagger) + (\Sigma\overline{\Psi}_r^{(14)}\Sigma^\dagger) \not{p} \Pi_2^r (\Sigma\Psi_r^{(14)}\Sigma^\dagger)\right] \\ & + \overline{\Psi}_{q_L}^{(14)} M_0^t \Psi_{t_R}^{(14)} + (\Sigma\overline{\Psi}_{q_L}^{(14)}) M_1^t (\Psi_{t_R}^{(14)}\Sigma^\dagger) + (\Sigma\overline{\Psi}_{q_L}^{(14)}\Sigma^\dagger) M_2^t (\Sigma\Psi_{t_R}^{(14)}\Sigma^\dagger) \\ & + \overline{\Psi}_{q_L}^{(14)} M_0^b \Psi_{b_R}^{(14)} + (\Sigma\overline{\Psi}_{q_L}^{(14)}) M_1^b (\Psi_{b_R}^{(14)}\Sigma^\dagger) + (\Sigma\overline{\Psi}_{q_L}^{(14)}\Sigma^\dagger) M_2^b (\Sigma\Psi_{b_R}^{(14)}\Sigma^\dagger) + \text{h.c.} . \end{aligned} \tag{C.8}$$

The effective Higgs potential is

$$V_h \simeq \alpha \sin^2(h/f) + \beta \sin^4(h/f) + \gamma \sin^6(h/f) . \tag{C.9}$$

C.4 MCHM$_{\mathbf{5\text{-}1\text{-}10}}$

In this model, (Q_L, t_R, b_R) are embedded into $(5, 1, 10)$, respectively. The quantum charge assignment are

$$\begin{aligned} t_L &: (1/2,-1/2)_{2/3}, \quad b_L : (-1/2,-1/2)_{2/3} , \\ t_R &: (0,0)_{2/3}, \qquad\quad b_R : (0,-1)_{2/3} . \end{aligned} \tag{C.10}$$

The effective matter Lagrangian is

$$\begin{aligned}\mathcal{L}_{\rm eff}^{\rm matter} =&\overline{\Psi}^{(5)}_{q_L}\not{p}\Pi_0^{q_L}\Psi^{(5)}_{q_L} + (\overline{\Psi}^{(5)}_{q_L}\Sigma^\dagger)\not{p}\Pi_1^{q_L}(\Sigma\Psi^{(5)}_{q_L})\\ &+ \overline{\Psi}^{(1)}_{t_R}\not{p}\Pi_0^{t_R}\Psi^{(1)}_{t_R}\\ &+ \overline{\Psi}^{(10)}_{b_R}\not{p}\Pi_0^{b_R}\Psi^{(10)}_{b_R} + (\Sigma\overline{\Psi}^{(10)}_{b_R})\not{p}\Pi_1^{b_R}(\Psi^{(10)}_{b_R}\Sigma^\dagger)\\ &+ (\overline{\Psi}^{(5)}_{q_L}\Sigma^\dagger)M_1^t\Psi^{(1)}_{t_R} + \overline{\Psi}^{(5)}_{q_L}M_1^b(\Psi^{(10)}_{b_R}\Sigma^\dagger) + \text{h.c.}\ . \end{aligned} \tag{C.11}$$

The effective Higgs potential is

$$V_h \simeq -\beta\sin^2(h/f)\ . \tag{C.12}$$

When we impose the starionary condition, β must be 0. Then, the electroweak symmetry breaking does not ocuur since the Higgs potential is always flat. This is not realistic model.

C.5 $\mathbf{MCHM_{5\text{-}5\text{-}10}}$

In this model, (Q_L, t_R, b_R) are embedded into $(5, 5, 10)$, respectively. The quantum charge assignment are

$$\begin{aligned} t_L &: (1/2,-1/2)_{2/3}, \quad b_L : (-1/2,-1/2)_{2/3}\ ,\\ t_R &: (0,0)_{2/3}, \qquad\quad b_R : (0,-1)_{2/3}\ . \end{aligned} \tag{C.13}$$

The effective matter Lagrangian is

$$\begin{aligned}\mathcal{L}_{\rm eff}^{\rm matter} =&\overline{\Psi}^{(5)}_{q_L}\not{p}\Pi_0^{q_L}\Psi^{(5)}_{q_L} + (\overline{\Psi}^{(5)}_{q_L}\Sigma^\dagger)\not{p}\Pi_1^{q_L}(\Sigma\Psi^{(5)}_{q_L})\\ &+ \overline{\Psi}^{(5)}_{t_R}\not{p}\Pi_0^{t_R}\Psi^{(5)}_{t_R} + (\overline{\Psi}^{(5)}_{t_R}\Sigma^\dagger)\not{p}\Pi_1^{t_R}(\Sigma\Psi^{(5)}_{t_R})\\ &+ \overline{\Psi}^{(10)}_{b_R}\not{p}\Pi_0^{b_R}\Psi^{(10)}_{b_R} + (\Sigma\overline{\Psi}^{(10)}_{b_R})\not{p}\Pi_1^{b_R}(\Psi^{(10)}_{b_R}\Sigma^\dagger)\\ &+ \overline{\Psi}^{(5)}_{q_L}M_0^t\Psi^{(5)}_{t_R} + (\overline{\Psi}^{(5)}_{q_L}\Sigma^\dagger)M_1^t(\Sigma\Psi^{(5)}_{t_R}) + \overline{\Psi}^{(5)}_{q_L}M_1^b(\Psi^{(10)}_{b_R}\Sigma^\dagger) + \text{h.c.}\ . \end{aligned} \tag{C.14}$$

The effective Higgs potential has the same form in (C.4).

C.6 $\mathbf{MCHM_{5\text{-}10\text{-}10}}$

In this model, (Q_L, t_R, b_R) are embedded into $(5, 10, 10)$, respectively. The quantum charge assignment are

$$\begin{aligned} t_L &: (1/2,-1/2)_{2/3}, \quad b_L : (-1/2,-1/2)_{2/3}\ ,\\ t_R &: (0,0)_{2/3}, \qquad\quad b_R : (0,-1)_{2/3}\ . \end{aligned} \tag{C.15}$$

The effective matter Lagrangian is

$$\begin{aligned}\mathcal{L}_{\rm eff}^{\rm matter} =&\overline{\Psi}^{(5)}_{q_L}\not{p}\Pi_0^{q_L}\Psi^{(5)}_{q_L} + (\overline{\Psi}^{(5)}_{q_L}\Sigma^\dagger)\not{p}\Pi_1^{q_L}(\Sigma\Psi^{(5)}_{q_L})\\ &+ \overline{\Psi}^{(10)}_{t_R}\not{p}\Pi_0^{t_R}\Psi^{(10)}_{t_R} + (\Sigma\overline{\Psi}^{(10)}_{t_R})\not{p}\Pi_1^{t_R}(\Psi^{(10)}_{t_R}\Sigma^\dagger)\\ &+ \overline{\Psi}^{(10)}_{b_R}\not{p}\Pi_0^{b_R}\Psi^{(10)}_{b_R} + (\Sigma\overline{\Psi}^{(10)}_{b_R})\not{p}\Pi_1^{b_R}(\Psi^{(10)}_{b_R}\Sigma^\dagger)\\ &+ \overline{\Psi}^{(5)}_{q_L}M_1^t(\Psi^{(10)}_{t_R}\Sigma^\dagger) + \overline{\Psi}^{(5)}_{q_L}M_1^b(\Psi^{(10)}_{b_R}\Sigma^\dagger) + \text{h.c.}\ . \end{aligned} \tag{C.16}$$

The effective Higgs potential has the same in Eq. (C.4).

C.7 MCHM$_{\mathbf{5\text{-}14\text{-}10}}$

In this model, (Q_L, t_R, b_R) are embedded into $(5, 14, 10)$, respectively. The quantum charge assignment are

$$\begin{aligned} t_L &: (1/2, -1/2)_{2/3}, \quad b_L : (-1/2, -1/2)_{2/3} , \\ t_R &: (0, 0)_{2/3}, \qquad\quad b_R : (0, -1)_{2/3} . \end{aligned} \tag{C.17}$$

The effective matter Lagrangian is

$$\begin{aligned} \mathcal{L}_{\text{eff}}^{\text{matter}} =& \overline{\Psi}^{(5)}_{q_L} \not{p} \Pi_0^{q_L} \Psi^{(5)}_{q_L} + (\overline{\Psi}^{(5)}_{q_L} \Sigma^\dagger) \not{p} \Pi_1^{q_L} (\Sigma \Psi^{(5)}_{q_L}) \\ &+ \overline{\Psi}^{(14)}_{t_R} \not{p} \Pi_0^{t_R} \Psi^{(14)}_{t_R} + (\Sigma \overline{\Psi}^{(14)}_{t_R}) \not{p} \Pi_1^{t_R} (\Psi^{(14)}_{t_R} \Sigma^\dagger) + (\Sigma \overline{\Psi}^{(14)}_{t_R} \Sigma^\dagger) \not{p} \Pi_2^{t_R} (\Sigma \Psi^{(14)}_{t_R} \Sigma^\dagger) \\ &+ \overline{\Psi}^{(10)}_{b_R} \not{p} \Pi_0^{b_R} \Psi^{(10)}_{b_R} + (\Sigma \overline{\Psi}^{(10)}_{b_R}) \not{p} \Pi_1^{b_R} (\Psi^{(10)}_{b_R} \Sigma^\dagger) \\ &+ \overline{\Psi}^{(5)}_{q_L} M_1^t (\Psi^{(14)}_{t_R} \Sigma^\dagger) + (\overline{\Psi}^{(5)}_{q_L} \Sigma^\dagger) M_2^t (\Sigma \Psi^{(14)}_{t_R} \Sigma^\dagger) + \overline{\Psi}^{(5)}_{q_L} M_1^b (\Psi^{(10)}_{b_R} \Sigma^\dagger) + \text{h.c.} . \end{aligned} \tag{C.18}$$

The effective Higgs potential takes the same form as one given in Eq. (C.9).

C.8 MCHM$_{\mathbf{10\text{-}5\text{-}10}}$

In this model, (Q_L, t_R, b_R) are embedded into $(10, 5, 10)$, respectively. The quantum charge assignment are

$$\begin{aligned} t_L &: (1/2, -1/2)_{2/3}, \quad b_L : (-1/2, -1/2)_{2/3} , \\ t_R &: (0, 0)_{2/3}, \qquad\quad b_R : (0, -1)_{2/3} . \end{aligned} \tag{C.19}$$

The effective matter Lagrangian is

$$\begin{aligned} \mathcal{L}_{\text{eff}}^{\text{matter}} =& \overline{\Psi}^{(10)}_{q_L} \not{p} \Pi_0^{q_L} \Psi^{(10)}_{q_L} + (\Sigma \overline{\Psi}^{(10)}_{q_L}) \not{p} \Pi_1^{q_L} (\Psi^{(10)}_{q_L} \Sigma^\dagger) \\ &+ \overline{\Psi}^{(5)}_{t_R} \not{p} \Pi_0^{t_R} \Psi^{(5)}_{t_R} + (\overline{\Psi}^{(5)}_{t_R} \Sigma^\dagger) \not{p} \Pi_1^{t_R} (\Sigma \Psi^{(5)}_{t_R}) \\ &+ \overline{\Psi}^{(10)}_{b_R} \not{p} \Pi_0^{b_R} \Psi^{(10)}_{b_R} + (\Sigma \overline{\Psi}^{(10)}_{b_R}) \not{p} \Pi_1^{b_R} (\Psi^{(10)}_{b_R} \Sigma^\dagger) \\ &+ (\Sigma \overline{\Psi}^{(10)}_{q_L}) M_1^t \Psi^{(5)}_{t_R} + \overline{\Psi}^{(10)}_{q_L} M_0^b \Psi^{(10)}_{b_R} + (\Sigma \overline{\Psi}^{(10)}_{q_L}) M_1^b (\Psi^{(10)}_{b_R} \Sigma^\dagger) + \text{h.c.} . \end{aligned} \tag{C.20}$$

The effective Higgs potential has the same form in Eq. (C.4).

C.9 MCHM$_{\mathbf{10\text{-}14\text{-}10}}$

In this model, (Q_L, t_R, b_R) are embedded into $(10, 14, 10)$, respectively. The quantum charge assignment are

$$\begin{aligned} t_L &: (1/2, -1/2)_{2/3}, \quad b_L : (-1/2, -1/2)_{2/3} , \\ t_R &: (0, 0)_{2/3}, \qquad\quad b_R : (0, -1)_{2/3} . \end{aligned} \tag{C.21}$$

The effective matter Lagrangian is

$$\begin{aligned}\mathcal{L}_{\rm eff}^{\rm matter} =&\overline{\Psi}^{(10)}_{q_L}\not{p}\Pi_0^{q_L}\Psi^{(10)}_{q_L} + (\Sigma\overline{\Psi}^{(10)}_{q_L})\not{p}\Pi_1^{q_L}(\Psi^{(10)}_{q_L}\Sigma^\dagger)\\ &+\overline{\Psi}^{(14)}_{t_R}\not{p}\Pi_0^{t_R}\Psi^{(14)}_{t_R} + (\Sigma\overline{\Psi}^{(14)}_{t_R})\not{p}\Pi_1^{t_R}(\Psi^{(14)}_{t_R}\Sigma^\dagger) + (\Sigma\overline{\Psi}^{(14)}_{t_R}\Sigma^\dagger)\not{p}\Pi_2^{t_R}(\Sigma\Psi^{(14)}_{t_R}\Sigma^\dagger)\\ &+\overline{\Psi}^{(10)}_{b_R}\not{p}\Pi_0^{b_R}\Psi^{(10)}_{b_R} + (\Sigma\overline{\Psi}^{(10)}_{b_R})\not{p}\Pi_1^{b_R}(\Psi^{(10)}_{b_R}\Sigma^\dagger)\\ &+(\Sigma\overline{\Psi}^{(10)}_{q_L})M_1^t(\Psi^{(14)}_{t_R}\Sigma^\dagger) + (\Sigma\overline{\Psi}^{(10)}_{q_L})M_1^b(\Psi^{(10)}_{b_R}\Sigma^\dagger) + \text{h.c.}\,. \end{aligned} \tag{C.22}$$

The effective Higgs potential has the same form in Eq. (C.9).

C.10 MCHM$_{14\text{-}1\text{-}10}$

In this model, (Q_L, t_R, b_R) are embedded into $(14, 1, 10)$, respectively. The quantum charge assignment are

$$\begin{aligned} t_L &: (1/2,-1/2)_{2/3}, \quad b_L : (-1/2,-1/2)_{2/3}\,,\\ t_R &: (0,0)_{2/3}, \qquad\quad b_R : (0,-1)_{2/3}\,. \end{aligned} \tag{C.23}$$

The effective matter Lagrangian is

$$\begin{aligned}\mathcal{L}_{\rm eff}^{\rm matter} =&\overline{\Psi}^{(14)}_{q_L}\not{p}\Pi_0^{q_L}\Psi^{(14)}_{q_L} + (\Sigma\overline{\Psi}^{(14)}_{q_L})\not{p}\Pi_1^{q_L}(\Psi^{(14)}_{q_L}\Sigma^\dagger) + (\Sigma\overline{\Psi}^{(14)}_{q_L}\Sigma^\dagger)\not{p}\Pi_2^{q_L}(\Sigma\Psi^{(14)}_{q_L}\Sigma^\dagger)\\ &+\overline{\Psi}^{(1)}_{t_R}\not{p}\Pi_0^{t_R}\Psi^{(1)}_{t_R}\\ &+\overline{\Psi}^{(10)}_{b_R}\not{p}\Pi_0^{b_R}\Psi^{(10)}_{b_R} + (\Sigma\overline{\Psi}^{(10)}_{b_R})\not{p}\Pi_1^{b_R}(\Psi^{(10)}_{b_R}\Sigma^\dagger)\\ &+(\Sigma\overline{\Psi}^{(14)}_{q_L}\Sigma^\dagger)M_2^t\Psi^{(1)}_{t_R} + (\Sigma\overline{\Psi}^{(14)}_{q_L})M_1^b(\Psi^{(10)}_{b_R}\Sigma^\dagger) + \text{h.c.}\,. \end{aligned} \tag{C.24}$$

The effective Higgs potential has the same form in Eq. (C.4).

C.11 MCHM$_{14\text{-}5\text{-}10}$

In this model, (Q_L, t_R, b_R) are embedded into $(14, 5, 10)$, respectively. The quantum charge assignment are

$$\begin{aligned} t_L &: (1/2,-1/2)_{2/3}, \quad b_L : (-1/2,-1/2)_{2/3}\,,\\ t_R &: (0,0)_{2/3}, \qquad\quad b_R : (0,-1)_{2/3}\,. \end{aligned} \tag{C.25}$$

The effective matter Lagrangian is

$$\begin{aligned}\mathcal{L}_{\rm eff}^{\rm matter} =&\overline{\Psi}^{(14)}_{q_L}\not{p}\Pi_0^{q_L}\Psi^{(14)}_{q_L} + (\Sigma\overline{\Psi}^{(14)}_{q_L})\not{p}\Pi_1^{q_L}(\Psi^{(14)}_{q_L}\Sigma^\dagger) + (\Sigma\overline{\Psi}^{(14)}_{q_L}\Sigma^\dagger)\not{p}\Pi_2^{q_L}(\Sigma\Psi^{(14)}_{q_L}\Sigma^\dagger)\\ &+\overline{\Psi}^{(5)}_{t_R}\not{p}\Pi_0^{t_R}\Psi^{(5)}_{t_R} + (\overline{\Psi}^{(5)}_{t_R}\Sigma^\dagger)\not{p}\Pi_1^{t_R}(\Sigma\Psi^{(5)}_{t_R})\\ &+\overline{\Psi}^{(10)}_{b_R}\not{p}\Pi_0^{b_R}\Psi^{(10)}_{b_R} + (\Sigma\overline{\Psi}^{(10)}_{b_R})\not{p}\Pi_1^{b_R}(\Psi^{(10)}_{b_R}\Sigma^\dagger)\\ &+(\Sigma\overline{\Psi}^{(14)}_{q_L})M_1^t\Psi^{(5)}_{t_R} + (\Sigma\overline{\Psi}^{(14)}_{q_L}\Sigma^\dagger)M_2^t(\Sigma\Psi^{(5)}_{t_R}) + (\Sigma\overline{\Psi}^{(14)}_{q_L})M_1^b(\Psi^{(10)}_{b_R}\Sigma^\dagger) + \text{h.c.}\,. \end{aligned} \tag{C.26}$$

The effective Higgs potential has the same form in Eq. (C.9).

C.12 MCHM$_{14\text{-}10\text{-}10}$

In this model, (Q_L, t_R, b_R) are embedded into $(14, 10, 10)$, respectively. The quantum charge assignment are

$$\begin{aligned} t_L &: (1/2, -1/2)_{2/3}, \quad b_L : (-1/2, -1/2)_{2/3} , \\ t_R &: (0, 0)_{2/3}, \qquad\quad b_R : (0, -1)_{2/3} . \end{aligned} \tag{C.27}$$

The effective matter Lagrangian is

$$\begin{aligned} \mathcal{L}_{\text{eff}}^{\text{matter}} =& \overline{\Psi}_{q_L}^{(14)} \not{p} \Pi_0^{q_L} \Psi_{q_L}^{(14)} + (\Sigma \overline{\Psi}_{q_L}^{(14)}) \not{p} \Pi_1^{q_L} (\Psi_{q_L}^{(14)} \Sigma^\dagger) + (\Sigma \overline{\Psi}_{q_L}^{(14)} \Sigma^\dagger) \not{p} \Pi_2^{q_L} (\Sigma \Psi_{q_L}^{(14)} \Sigma^\dagger) \\ &+ \overline{\Psi}_{t_R}^{(10)} \not{p} \Pi_0^{t_R} \Psi_{t_R}^{(10)} + (\Sigma \overline{\Psi}_{t_R}^{(10)}) \not{p} \Pi_1^{t_R} (\Psi_{t_R}^{(10)} \Sigma^\dagger) \\ &+ \overline{\Psi}_{b_R}^{(10)} \not{p} \Pi_0^{b_R} \Psi_{b_R}^{(10)} + (\Sigma \overline{\Psi}_{b_R}^{(10)}) \not{p} \Pi_1^{b_R} (\Psi_{b_R}^{(10)} \Sigma^\dagger) \\ &+ (\Sigma \overline{\Psi}_{q_L}^{(14)}) M_1^t (\Psi_{t_R}^{(10)} \Sigma^\dagger) + (\Sigma \overline{\Psi}_{q_L}^{(14)}) M_1^b (\Psi_{b_R}^{(10)} \Sigma^\dagger) + \text{h.c.} . \end{aligned} \tag{C.28}$$

The effective Higgs potential has the same form in Eq. (C.9).

C.13 MCHM$_{14\text{-}14\text{-}10}$

In this model, (Q_L, t_R, b_R) are embedded into $(14, 14, 10)$, respectively. The quantum charge assignment are

$$\begin{aligned} t_L &: (1/2, -1/2)_{2/3}, \quad b_L : (-1/2, -1/2)_{2/3} , \\ t_R &: (0, 0)_{2/3}, \qquad\quad b_R : (0, -1)_{2/3} . \end{aligned} \tag{C.29}$$

The effective matter Lagrangian is

$$\begin{aligned} \mathcal{L}_{\text{eff}}^{\text{matter}} =& \overline{\Psi}_{q_L}^{(14)} \not{p} \Pi_0^{q_L} \Psi_{q_L}^{(14)} + (\Sigma \overline{\Psi}_{q_L}^{(14)}) \not{p} \Pi_1^{q_L} (\Psi_{q_L}^{(14)} \Sigma^\dagger) + (\Sigma \overline{\Psi}_{q_L}^{(14)} \Sigma^\dagger) \not{p} \Pi_2^{q_L} (\Sigma \Psi_{q_L}^{(14)} \Sigma^\dagger) \\ &+ \overline{\Psi}_{t_R}^{(14)} \not{p} \Pi_0^{t_R} \Psi_{t_R}^{(14)} + (\Sigma \overline{\Psi}_{t_R}^{(14)}) \not{p} \Pi_1^{t_R} (\Psi_{t_R}^{(14)} \Sigma^\dagger) + (\Sigma \overline{\Psi}_{t_R}^{(14)} \Sigma^\dagger) \not{p} \Pi_2^{t_R} (\Sigma \Psi_{t_R}^{(14)} \Sigma^\dagger) \\ &+ \overline{\Psi}_{b_R}^{(10)} \not{p} \Pi_0^{b_R} \Psi_{b_R}^{(10)} + (\Sigma \overline{\Psi}_{b_R}^{(10)}) \not{p} \Pi_1^{b_R} (\Psi_{b_R}^{(10)} \Sigma^\dagger) \\ &+ \overline{\Psi}_{q_L}^{(14)} M_0^t \Psi_{t_R}^{(14)} + (\Sigma \overline{\Psi}_{q_L}^{(14)}) M_1^t (\Psi_{t_R}^{(14)} \Sigma^\dagger) + (\Sigma \overline{\Psi}_{q_L}^{(14)} \Sigma^\dagger) M_2^t (\Sigma \Psi_{t_R}^{(14)} \Sigma^\dagger) \\ &+ (\Sigma \overline{\Psi}_{q_L}^{(14)}) M_1^b (\Psi_{b_R}^{(10)} \Sigma^\dagger) + \text{h.c.} . \end{aligned} \tag{C.30}$$

The effective Higgs potential has the same form in Eq. (C.9).

Appendix D

Decay Rates and Branching Ratios of the SM Higgs boson

In this appendix, we show the calculations of the Sm Higgs boson decay width and branching ratios.

D.1 Input parameters and Notations

Input parameters for numerical calculation are

$$\begin{aligned} G_F &= 1.16637 \times 10^{-5} \ , \\ \alpha_{em}^{-1} &= 137.035999166 \ , \\ m_Z &= 91.1876 \ , \end{aligned} \tag{D.1}$$

and

$$\begin{aligned} m_W &= 80.93875164, \\ m_h &= 125, \\ m_s(1\text{GeV}) &= 0.1, \\ m_c^{pole} &= 1.275, \\ m_b^{pole} &= 4.87, \\ m_t^{pole} &= 173.2, \\ m_\tau^{pole} &= 1.77682, \\ \alpha_s(m_Z) &= 0.1184, \\ \cos\theta_W &= m_W/m_Z, \\ \sin\theta_W &= \sqrt{1 - m_W^2/m_Z^2} \ . \end{aligned} \tag{D.2}$$

where all dimensionful parameters are in GeV unit. In the following, we denote quark pole and running masses as

- the quark pole mass = M_q
- the quark running mass at scale $\mu = m_q(\mu)$

D.2 List of corrections

- $h \to \bar{\tau}\tau$
  - Electroweak correction [82]
  - Higgs-self coupling correction [83]
- $h \to \bar{c}c,\ \bar{b}b$
  - Electroweak correction [82]
  - Higgs-self coupling correction [83]
  - QCD corrections : $\alpha_s(\mu)$[84], $m_q(\mu)$[84] , $\cdots$[85]
- $h \to V^{(*)}V^{(*)}$
  - Vector boson decay : three- and four-body decay [86]
  - Electroweak correction [86]
  - Higgs-self coupling correction [83]
  - Interference effect : $h \to W^+W^-/ZZ \to \ell^+\nu\ell^-\nu$ (Neglected)
- $h \to gg$
  - QCD virtual correction [87] and [88]
  - Electroweak correction [89]
- $h \to \gamma\gamma$
  - QCD virtual correction [88]
  - EW virtual correction [89]
- $h \to Z\gamma$
  - QCD virtual correction [90] and [91] (Neglected)

The interference effect to $h \to VV$ becomes important when the Higgs boson mass is close to the vector boson mass threshold, $m_h \sim 2m_V$. We neglect its effect because the SM Higgs boson mass is 125 GeV. The QCD corrections to $h \to Z\gamma$ is very small about $\sim 0.1\%$. We then omit it.

D.3 Running of Strong coupling constant and Quark masses : RunDec [84]

D.3.1 Strong coupling constant

The strong coupling constant up to four-loop is evaluated by

$$\mu^2 \frac{d}{d\mu^2} \frac{\alpha_s^{(N_f)}(\mu)}{\pi} = -\sum_{i=0}^{3} \beta_i^{(N_f)} \left(\frac{\alpha_s^{(N_f)}(\mu)}{\pi} \right)^{i+2} , \tag{D.3}$$

where N_f is the active flavour number, μ is the scale and

$$\begin{aligned}
\beta_0 &= \frac{1}{4}\left[11 - \frac{2}{3}N_f\right], \\
\beta_1 &= \frac{1}{16}\left[102 - \frac{38}{3}N_f\right], \\
\beta_2 &= \frac{1}{64}\left[\frac{2857}{2} - \frac{5033}{18}N_f + \frac{325}{54}N_f^2\right], \\
\beta_3 &= \frac{1}{256}\left[\frac{149753}{6} + 3564\zeta_3 - \left(\frac{1078361}{162} + \frac{6508}{27}\zeta_3\right)N_f + \left(\frac{50065}{162} + \frac{6472}{81}\zeta_3\right)N_f^2 + \frac{1093}{729}N_f^3\right],
\end{aligned} \tag{D.4}$$

with ζ_i is the Riemann's zeta function, $\zeta_2 = \pi^2/6,\ \zeta_3 \simeq 1.20206$. By solving (D.3) iteratively, we obtain

$$\begin{aligned}
\frac{\alpha_s^{(N_f)}(\mu)}{\pi} = {} & \frac{1}{\beta_0 L} - \frac{1}{(\beta_0 L)^2}\frac{\beta_1}{\beta_0}\log L + \frac{1}{(\beta_0 L)^3}\left[\frac{\beta_1^2}{\beta_0^2}\left(\log^2 L - \log L - 1\right) + \frac{\beta_2}{\beta_0}\right] \\
& + \frac{1}{(\beta_0 L)^4}\left[\frac{\beta_1^3}{\beta_0^3}\left(-\log^3 L + \frac{5}{2}\log^2 L + 2\log L - \frac{1}{2}\right) - 3\frac{\beta_1\beta_2}{\beta_0^2}\log L + \frac{\beta_3}{2\beta_0}\right]
\end{aligned} \tag{D.5}$$

with $L = \log \mu^2/\Lambda^2$. Λ, called the *asymptotic scale parameter*, is determined by $\alpha_s^{(N_f)}(\mu = m_Z)$. For example, by using a certain root-finding method, it can be easily obtained as

$$m_Z = 91.1876 \text{ GeV},\ \alpha_s^{(N_f)}(m_Z) = 0.1184 \text{ and } N_f = 5 \text{ (except for the top quark)}$$

	NLO	NNLO	NNNLO	NNNNLO
Λ [MeV]	89.91	231.35	213.078	213.069

These results are in complete agreement with **RunDec** .

```
<<RunDec.m
LamImpl[asmZ/.NumDef,Mz/.NumDef,5,1]
0.0899122
LamImpl[asmZ/.NumDef,Mz/.NumDef,5,2]
0.231353
```

```
LamImpl[asmZ/.NumDef,Mz/.NumDef,5,3]
0.213078
LamImpl[asmZ/.NumDef,Mz/.NumDef,5,4]
0.213069
```

These results are in GeV unit.

D.3.2 Flavour threshold corrections to strong coupling constant

Next, we introduce flacvour threshold corrections. As I mentioned, contributions from the particles whose masses are lighter than the charm quark can be negligible, since I concentrate on m_h =100-200 GeV. Therefore, I only calculate these corrections at $\mu = m_b^{pole}$, m_t^{pole} .

At the threshold, we demand

- $\alpha_s(\mu = m_Z) = 0.1184$ is fixed.
- $\alpha_s(\mu = M_b \text{ and } M_t)$ is continuous.

The relationship of the strong coupling constant between the effective and the full theory is

$$\alpha_s^{(N_f-1)}(\mu) = \zeta_g^2 \alpha_s^{(N_f)}(\mu) \ . \tag{D.6}$$

$\star$ $\mu = M_b$

We already know the running behavior of $\alpha^{(N_f=5)}(\mu)$. The running of $\alpha^{(4)}(\mu < M_b)$ is calculated by

$$\alpha_s^{(4)}(\mu) = \left(\zeta_g^{\rm OS}(\mu, M_b)\right)^2 \alpha_s^{(5)}(\mu) \tag{D.7}$$

where $\zeta_g^{\rm OS}(\mu, M_b)$ is the threshold correction at $\mu = M_b$;

$$\begin{aligned}\left(\zeta_g^{\rm OS}(\mu, M_b)\right)^2 = 1 &+ \frac{\alpha_s^{(5)}(\mu)}{\pi}\left(-\frac{1}{6}\log\frac{\mu^2}{M_b^2}\right) + \left(\frac{\alpha_s^{(5)}(\mu)}{\pi}\right)^2\left(-\frac{7}{24} - \frac{19}{24}\log\frac{\mu^2}{M_b^2} + \frac{1}{36}\log^2\frac{\mu^2}{M_b^2}\right) \\ &+ \left(\frac{\alpha_s^{(5)}(\mu)}{\pi}\right)^3\left[-\frac{58933}{124416} - \frac{2}{3}\zeta_2\left(1+\frac{1}{3}\log 2\right) - \frac{80507}{27648}\zeta_3 - \frac{8521}{1728}\log\frac{\mu^2}{M_b^2}\right. \\ &\left. - \frac{131}{576}\log^2\frac{\mu^2}{M_b^2} - \frac{1}{216}\log^3\frac{\mu^2}{M_b^2} + 4\left(\frac{2479}{31104} + \frac{\zeta_2}{9} + \frac{409}{1728}\log\frac{\mu^2}{M_b^2}\right)\right] \ . \end{aligned} \tag{D.8}$$

In order to connect continuously at $\mu = M_b$, we must consider a compensating constant, $\delta\zeta_b^{\alpha_s}$:

$$\delta\zeta_b^{\alpha_s} \equiv \left(\zeta_g^{\rm OS}(M_b, M_b)\right)^2 \alpha_s^{(5)}(M_b) - \alpha_s^{(5)}(M_b) \tag{D.9}$$

Then, below $\mu = M_b$, $\alpha_s^{(4)}(\mu)$ is rewritten as the function of $\alpha_s^{(5)}(\mu)$

$$\alpha_s^{(4)}(\mu) \equiv \left(\zeta_g^{\rm OS}(\mu, M_b)\right)^2 \alpha_s^{(5)}(\mu) - \delta\zeta_b^{\alpha_s} \tag{D.10}$$

⋆ $\mu = M_t$

Following same procedure, one can easily obtain a result of $\alpha_s^{(6)}(\mu > M_t)$.

$$\frac{1}{\left(\zeta_g^{\rm OS}(\mu, M_t)\right)^2}\alpha_s^{(5)}(\mu) = \alpha_s^{(6)}(\mu) \tag{D.11}$$

where $\zeta_g^{\rm OS}(\mu, M_t)$ is the threshold correction at $\mu = M_t$;

$$\begin{aligned}\frac{1}{\left(\zeta_g^{\rm OS}(\mu, M_t)\right)^2} = 1 &+ \frac{\alpha_s^{(5)}(\mu)}{\pi}\left(\frac{1}{6}\log\frac{\mu^2}{M_t^2}\right) + \left(\frac{\alpha_s^{(5)}(\mu)}{\pi}\right)^2\left(\frac{7}{24} + \frac{19}{24}\log\frac{\mu^2}{M_t^2} + \frac{1}{36}\log^2\frac{\mu^2}{M_t^2}\right) \\ &+ \left(\frac{\alpha_s^{(5)}(\mu)}{\pi}\right)^3\left[\frac{58933}{124416} + \frac{2}{3}\zeta_2\left(1 + \frac{1}{3}\log 2\right) + \frac{80507}{27648}\zeta_3 + \frac{8941}{1728}\log\frac{\mu^2}{M_t^2}\right. \\ &\left. + \frac{511}{576}\log^2\frac{\mu^2}{M_t^2} + \frac{1}{216}\log^3\frac{\mu^2}{M_t^2} + 5\left(-\frac{2479}{31104} - \frac{\zeta_2}{9} - \frac{409}{1728}\log\frac{\mu^2}{M_t^2}\right)\right] .\end{aligned} \tag{D.12}$$

In order to connect continuously at $\mu = M_b$, we must consider a compensating constant, $\delta\zeta_t^{\alpha_s}$:

$$\delta\zeta_t^{\alpha_s} \equiv \frac{1}{\left(\zeta_g^{\rm OS}(\mu, M_t)\right)^2}\alpha_s^{(5)}(M_t) - \alpha_s^{(5)}(M_t) . \tag{D.13}$$

Then, above $\mu = M_t$, $\alpha_s^{(6)}(\mu)$ is rewritten as the function of $\alpha_s^{(5)}(\mu)$

$$\alpha_s^{(6)}(\mu) \equiv \frac{1}{\left(\zeta_g^{\rm OS}(\mu, M_t)\right)^2}\alpha_s^{(5)}(\mu) - \delta\zeta_t^{\alpha_s} . \tag{D.14}$$

In the following, I omit the superscript (N_f). The running behaviours are shown in Figure D.1. In **RunDec**, the authors numerically calculate the differential equation, (D.3) . The difference is shown in

D.3.3 Qurak running mass : RunDec

The running quark mass at the scale μ is given by

$$\frac{m_q(\mu)}{m_q(\mu_0)} = \frac{c(\alpha_s(\mu)/\pi, N_f)}{c(\alpha_s(\mu_0)/\pi, N_f)} \tag{D.15}$$

with

$$\begin{aligned}c(x, N_f) = x^{\gamma_0/\beta_0}\Bigg\{1 &+ \left(\frac{\gamma_1}{\beta_0} - \frac{\beta_1\gamma_0}{\beta_0^2}\right)x + \frac{1}{2}\left[\left(\frac{\gamma_1}{\beta_0} - \frac{\beta_1\gamma_0}{\beta_0^2}\right)^2 + \frac{\gamma_2}{\beta_0} - \frac{\beta_1\gamma_1}{\beta_0^2} + \frac{\beta_1^2\gamma_0}{\beta_0^3} - \frac{\beta_2\gamma_0}{\beta_0^2}\right]x^2 \\ &+ \left[\frac{1}{6}\left(\frac{\gamma_1}{\beta_0} - \frac{\beta_1\gamma_0}{\beta_0^2}\right)^3 + \frac{1}{2}\left(\frac{\gamma_1}{\beta_0} - \frac{\beta_1\gamma_0}{\beta_0^2}\right)\left(\frac{\gamma_2}{\beta_0} - \frac{\beta_1\gamma_1}{\beta_0^2} + \frac{\beta_1^2\gamma_0}{\beta_0^3} - \frac{\beta_2\gamma_0}{\beta_0^2}\right)\right. \\ &\left. + \frac{1}{3}\left(\frac{\gamma_3}{\beta_0} - \frac{\beta_1\gamma_2}{\beta_0^2} + \frac{\beta_1^2\gamma_1}{\beta_0^3} - \frac{\beta_2\gamma_1}{\beta_0^2} - \frac{\beta_1^3\gamma_0}{\beta_0^4} + 2\frac{\beta_1\beta_2\gamma_0}{\beta_0^3} - \frac{\beta_3\gamma_0}{\beta_0^2}\right)\right]x^3\Bigg\},\end{aligned} \tag{D.16}$$

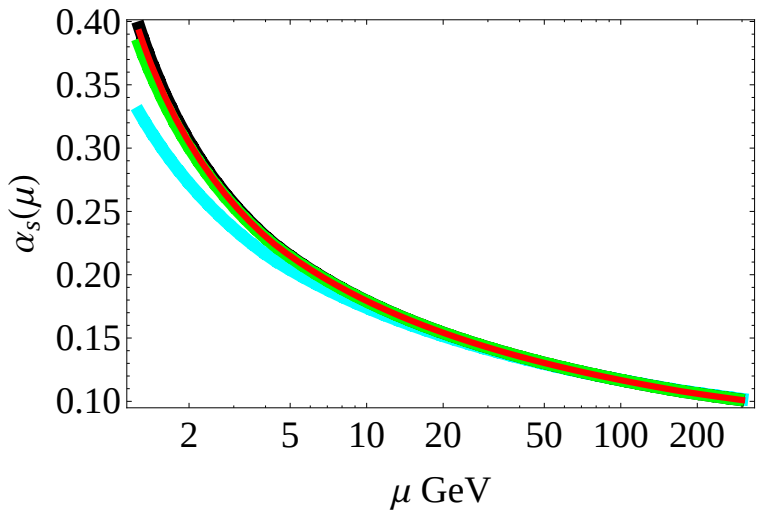

Figure D.1: The scale dependence of the strong coupling constant : $\alpha_s(\mu)$. (NLO, NNLO, NNNLO, NNNNLO) = (cyan, black, green, red)

and

$$
\begin{aligned}
\gamma_0 &= 1, \\
\gamma_1 &= \frac{1}{16}\left[\frac{202}{3} - \frac{20}{9}N_f\right], \\
\gamma_2 &= \frac{1}{64}\left[1249 + \left(-\frac{2216}{27} - \frac{160}{3}\zeta_3\right)N_f - \frac{140}{81}N_f^2\right], \\
\gamma_3 &= \frac{1}{256}\left[\frac{4603055}{162} + \frac{135680}{27}\zeta_3 - 8800\zeta_5 + \left(-\frac{91723}{27} - \frac{34192}{9}\zeta_3 + 880\zeta_4 + \frac{18400}{9}\zeta_5\right)N_f \right. \\
&\quad \left. + \left(\frac{5242}{243} + \frac{800}{9}\zeta_3 - \frac{160}{3}\zeta_4\right)N_f^2 + \left(-\frac{332}{243} + \frac{64}{27}\zeta_3\right)N_f^3\right].
\end{aligned}
\tag{D.17}
$$

with $\zeta_4 \simeq 1.08232,\ \zeta_5 \simeq 1.03693$.
Eqaution (D.15) says that if we know the mass at μ_0, $m_q(\mu_0)$, we can calculate the mass $m_q(\mu)$ at the arbitrary scale μ. We evaluate $m_q(\mu_0)$ as $m_q(M_q)$ by

$$
\begin{aligned}
\frac{m_q(M_q)}{M_q} &= 1 + \frac{\alpha_s(M_q)}{\pi}\left[-\frac{4}{3}\right] \\
&\quad + \left(\frac{\alpha_s(M_q)}{\pi}\right)^2\left[-\frac{3019}{288} - 2\zeta_2 - \frac{2}{3}\zeta_2\log 2 + \frac{1}{6}\zeta_3 + \left(\frac{71}{144} + \frac{1}{3}\zeta_2\right)N_l - \frac{4}{3}\sum_i^{N_l}\Delta\left(\frac{M_i}{M_q}\right)\right] \\
&\quad + \left(\frac{\alpha_s(M_q)}{\pi}\right)^3\left[z_m^{(3)}(M_q)\right]
\end{aligned}
\tag{D.18}
$$

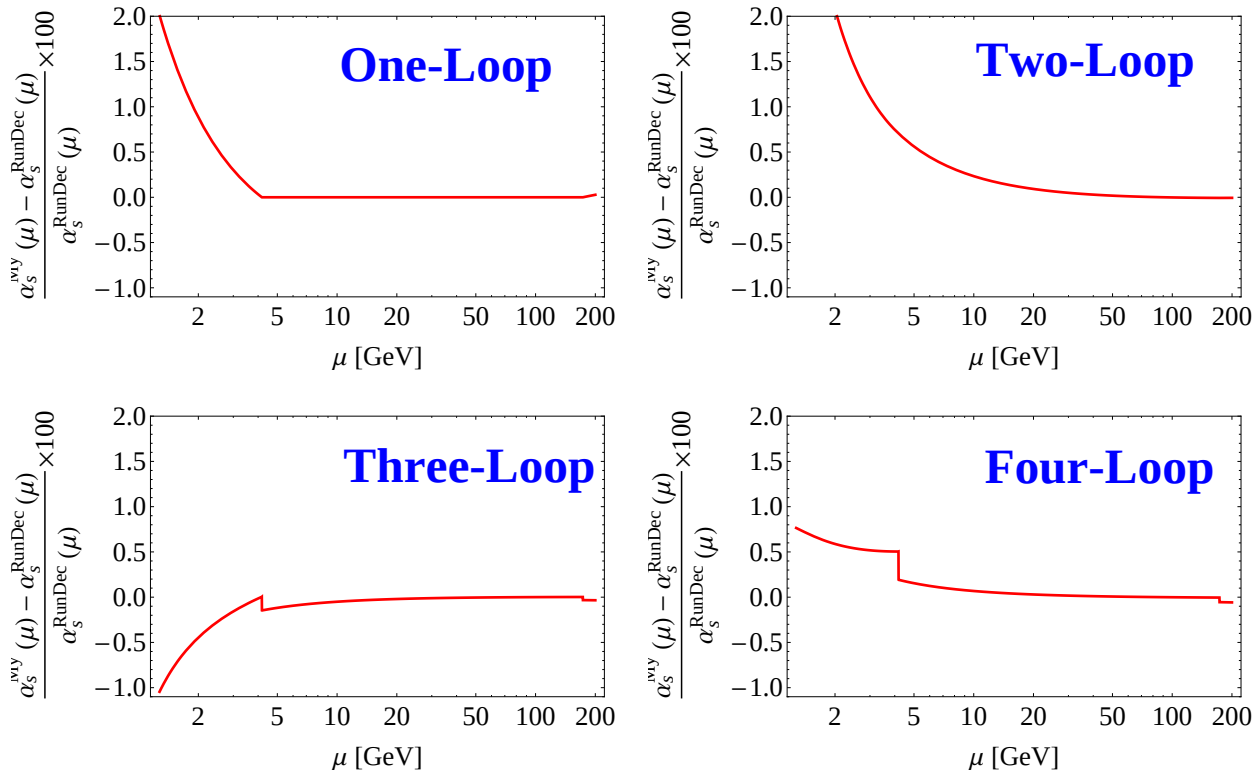

Figure D.2: The scale dependence of the strong coupling constant : $\alpha_s(\mu)$. (NLO, NNLO, NNNLO, NNNNLO) = (cyan, black, green, red)

where M_i are the light flavour masses, a function Δ defined in [92] is approximately written as

$$\Delta(x) = \frac{\pi^2}{8} - 0.597x + 0.230x^3 \tag{D.19}$$

and

$$\begin{aligned} z_m^{(3)}(M) = & -\frac{9478333}{93312} + \frac{55}{162}\ln^4 2 + \left(-\frac{644201}{6480} + \frac{587}{27}\ln 2 + \frac{44}{27}\ln^2 2\right)\zeta_2 - \frac{61}{27}\zeta_3 \\ & + \frac{3475}{432}\zeta_4 + \frac{1439}{72}\zeta_2\zeta_3 - \frac{1975}{216}\zeta_5 + \frac{220}{27}a_4 + N_l\left[\frac{246643}{23328} - \frac{1}{81}\ln^4 2\right. \\ & \left. + \left(\frac{967}{108} + \frac{22}{27}\ln 2 - \frac{4}{27}\ln^2 2\right)\zeta_2 + \frac{241}{72}\zeta_3 - \frac{305}{108}\zeta_4 - \frac{8}{27}a_4\right] \\ & + N_l^2\left[-\frac{2353}{23328} - \frac{13}{54}\zeta_2 - \frac{7}{54}\zeta_3\right]. \end{aligned} \tag{D.20}$$

with $a_4 = \text{Li}_4(1/2)$(see Appendix) . Then, running masses of bottom quark and charm quark (top quark is too heavy) are evaluated as

$$m_{b,c}(\mu) = m_{b,c}(M_{b,c})\frac{c(\alpha_s(\mu)/\pi, N_f)}{c(\alpha_s(M_{b,c})/\pi, N_f)}. \tag{D.21}$$

The threshold corrections to running quark masses are also shown in RunDec [84] .

• m_b **at** $\mu = M_t$

The threshold correction is only introduce at $\mu = M_t$ since I focus on m_h =100-200GeV. The relationship is given by

$$m_b^{(6)}(\mu) = \frac{1}{\zeta_m^{\rm OS}(\mu, M_t)} m_b^{(5)}(\mu) \ . \tag{D.22}$$

$m_b^{(5)}(\mu)$ is expressed as

$$m_b^{(5)}(\mu) = m_b(M_b) \frac{c(\alpha_s(\mu)/\pi, 5)}{c(\alpha_s(M_b)/\pi, 5)}, \quad \mu = M_b\text{-}M_t \ , \tag{D.23}$$

and

$$\begin{aligned} \frac{1}{\zeta_m^{\rm OS}(\mu, M_t)} = \quad & 1 + \left(\frac{\alpha_s(\mu)}{\pi}\right)^2 \left(-\frac{89}{432} + \frac{5}{36}\ln\frac{\mu^2}{M_t^2} - \frac{1}{12}\ln^2\frac{\mu^2}{M_t^2}\right) + \left(\frac{\alpha_s(\mu)}{\pi}\right)^3 \left[-\frac{1871}{2916}\right. \\ & + \frac{407}{864}\zeta_3 - \frac{5}{4}\zeta_4 + \frac{1}{36}B_4 + \left(-\frac{299}{2592} + \frac{5}{6}\zeta_3\right)\ln\frac{\mu^2}{M_t^2} - \frac{299}{432}\ln^2\frac{\mu^2}{M_t^2} \\ & \left. - \frac{35}{216}\ln^3\frac{\mu^2}{M_t^2} + n_l\left(-\frac{1327}{11664} + \frac{2}{27}\zeta_3 + \frac{53}{432}\ln\frac{\mu^2}{M_t^2} + \frac{1}{108}\ln^3\frac{\mu^2}{M_t^2}\right)\right] . \end{aligned} \tag{D.24}$$

with n_l is the light flavour number, $n_l = 5$, and

$$B_4 = 16{\rm Li}_4\left(\frac{1}{2}\right) - \frac{13}{2}\zeta_4 - 4\zeta_2\log^2 2 + \frac{2}{3}\log^4 2 \ . \tag{D.25}$$

A compensating factor is also introduced, $\delta\zeta_{M_t}^{m_b}$.

$$\delta\zeta_{M_t}^{m_b} = \frac{1}{\zeta_m^{\rm OS}(M_t, M_t)} m_b^{(5)}(M_t) - m_b^{(5)}(M_t) \ . \tag{D.26}$$

Threfore, $m_b^{(6)}(\mu > M_t)$ is

$$m_b^{(6)}(\mu) = \frac{1}{\zeta_m^{\rm OS}(\mu, M_t)} m_b^{(5)}(\mu) - \delta\zeta_{M_t}^{m_b} \ . \tag{D.27}$$

• m_c **at** $\mu = M_b$

Following the same procedure,

$$m_c^{(5)}(\mu) = \frac{1}{\zeta_m^{\rm OS}(\mu, M_b)} m_c^{(4)}(\mu) \ . \tag{D.28}$$

$m_c^{(4)}(\mu)$ is expressed as

$$m_c^{(4)}(\mu) = m_c(M_c) \frac{c(\alpha_s(\mu)/\pi, 4)}{c(\alpha_s(M_c)/\pi, 4)}, \quad \mu = M_c\text{-}M_b \ , \tag{D.29}$$

and

$$\frac{1}{\zeta_m^{\rm OS}(\mu, M_b)} = 1 + \left(\frac{\alpha_s(\mu)}{\pi}\right)^2 \left(-\frac{89}{432} + \frac{5}{36}\ln\frac{\mu^2}{M_b^2} - \frac{1}{12}\ln^2\frac{\mu^2}{M_b^2}\right) + \left(\frac{\alpha_s(\mu)}{\pi}\right)^3 \left[-\frac{1871}{2916} + \frac{407}{864}\zeta_3 - \frac{5}{4}\zeta_4 + \frac{1}{36}B_4 + \left(-\frac{299}{2592} + \frac{5}{6}\zeta_3\right)\ln\frac{\mu^2}{M_b^2} - \frac{299}{432}\ln^2\frac{\mu^2}{M_b^2} - \frac{35}{216}\ln^3\frac{\mu^2}{M_b^2} + n_l\left(-\frac{1327}{11664} + \frac{2}{27}\zeta_3 + \frac{53}{432}\ln\frac{\mu^2}{M_b^2} + \frac{1}{108}\ln^3\frac{\mu^2}{M_b^2}\right)\right] . \tag{D.30}$$

with $n_l = 4$. The compensating factor is also introduced, $\delta\zeta_{M_b}^{m_c}$.

$$\delta\zeta_{M_b}^{m_c} = \frac{1}{\zeta_m^{\rm OS}(M_b, M_b)} m_c^{(4)}(M_b) - m_c^{(4)}(M_b) . \tag{D.31}$$

Threfore, $m_c^{(5)}(M_t > \mu > M_b)$ is

$$m_c^{(5)}(\mu) = \frac{1}{\zeta_m^{\rm OS}(\mu, M_b)} m_c^{(4)}(\mu) - \delta\zeta_{M_b}^{m_c} . \tag{D.32}$$

- m_c **at** $\mu = M_t$

$$m_c^{(6)}(\mu) = \frac{1}{\zeta_m^{\rm OS}(\mu, M_t)} m_c^{(5)}(\mu) . \tag{D.33}$$

$m_c^{(5)}(\mu)$ is expressed as

$$m_c^{(5)}(\mu) = \frac{1}{\zeta_m^{\rm OS}(\mu, M_t)} m_c^{(4)}(\mu) - \delta\zeta_{M_b}^{m_c} , \quad \mu = M_b\text{-}M_t \tag{D.34}$$

$$\frac{1}{\zeta_m^{\rm OS}(\mu, M_t)} = 1 + \left(\frac{\alpha_s(\mu)}{\pi}\right)^2 \left(-\frac{89}{432} + \frac{5}{36}\ln\frac{\mu^2}{M_t^2} - \frac{1}{12}\ln^2\frac{\mu^2}{M_t^2}\right) + \left(\frac{\alpha_s(\mu)}{\pi}\right)^3 \left[-\frac{1871}{2916} + \frac{407}{864}\zeta_3 - \frac{5}{4}\zeta_4 + \frac{1}{36}B_4 + \left(-\frac{299}{2592} + \frac{5}{6}\zeta_3\right)\ln\frac{\mu^2}{M_t^2} - \frac{299}{432}\ln^2\frac{\mu^2}{M_t^2} - \frac{35}{216}\ln^3\frac{\mu^2}{M_t^2} + n_l\left(-\frac{1327}{11664} + \frac{2}{27}\zeta_3 + \frac{53}{432}\ln\frac{\mu^2}{M_t^2} + \frac{1}{108}\ln^3\frac{\mu^2}{M_t^2}\right)\right] . \tag{D.35}$$

with $n_l = 5$. The compensating factor is also introduced, $\delta\zeta_{M_t}^{m_c}$.

$$\delta\zeta_{M_t}^{m_c} = \frac{1}{\zeta_m^{\rm OS}(M_t, M_t)} m_c^{(5)}(M_t) - m_c^{(5)}(M_t) . \tag{D.36}$$

Threfore, $m_c^{(6)}(\mu > M_t)$ is

$$m_c^{(6)}(\mu) = \frac{1}{\zeta_m^{\rm OS}(\mu, M_t)} m_c^{(5)}(\mu) - \delta\zeta_{M_t}^{m_c} . \tag{D.37}$$

D.4 Decay Rates of the SM Higgs boson

D.4.1 Leading order formula of $h \to \bar{f}f$

The SM Higgs boson decay rate into fermion pairs with no corrections are

$$\Gamma^{\rm tree}(h \to f\bar{f}) = N_C \frac{G_F m_h}{4\sqrt{2}\pi} M_f^2 \left(1 - \frac{4M_f^2}{m_h^2}\right)^{3/2}, \tag{D.38}$$

where the colour factor N_C is 1 for leptons and 3 for quarks.

D.4.2 Higgs-self coupling correction to $h \to \bar{f}f$

The Higgs-self coupling correction is introduced as [83],

$$\Gamma(h \to f\bar{f}) = \frac{Z_h}{Z_w}\Gamma^{\rm tree}(h \to f\bar{f}) \tag{D.39}$$

with

$$\frac{Z_h}{Z_w} = \frac{1 + a_w\hat{\lambda} + b_w\hat{\lambda}^2}{1 + a_h\hat{\lambda} + b_h\hat{\lambda}^2}, \quad \hat{\lambda} = \frac{\lambda}{16\pi^2}, \quad \lambda = \frac{G_F m_h^2}{\sqrt{2}} \tag{D.40}$$

and

$$\begin{aligned} a_w &= 1, \\ b_w &= \frac{3}{2} + 2\zeta_2 - 6\gamma_E - 3\pi\sqrt{3} + 12{\rm Cl}_2(\pi/3)\sqrt{3}. \end{aligned} \tag{D.41}$$

$$\begin{aligned} a_h &= -12 + 2\pi\sqrt{3}, \\ b_h &= \frac{291}{2} - 96\zeta(2) + 90\zeta_3 - 6\gamma_E - 48\pi{\rm Cl}_2(\pi/3) + 116\pi\sqrt{3} - 216{\rm Cl}_2(\pi/3)\sqrt{3} - 162K_5 \end{aligned} \tag{D.42}$$

where γ_E is the Euler's gamma, Cl_2 is Clausen's function and K_5 is evaluated in [93],

$$\begin{aligned} {\rm Cl}_2(\pi/3) &\simeq 1.01494 \\ K_5 &\simeq 0.923632, \end{aligned} \tag{D.43}$$

and their analytic forms are

$${\rm Cl}_2(z) = \frac{i}{2}\left[{\rm Li}_2(\exp(-iz)) - {\rm Li}_2(\exp(+iz))\right] \tag{D.44}$$

$$K_5 = \int_0^1 dx \int_0^1 dy \frac{1}{xy} \log\left\{1 + \frac{b_x b_y}{2}\left[1 + a_x + a_y - \sqrt{(1 + a_x + a_y)^2 - 4a_x a_y}\right]\right\} \tag{D.45}$$

$$a_z = \frac{1-z}{z}, \quad b_z = \frac{1}{2}\left(1 - \sqrt{1 + \frac{4z}{1-z}}\right) \tag{D.46}$$

where Li_2 is the di-logarithmic function or the Spence's function, see Appendix. Its maginitude at $m_h = 125$ GeV is

$$\frac{Z_h}{Z_w} \simeq 1.00171\ . \tag{D.47}$$

QCD corrections to $h \to \bar{q}q$

For the case of $h \to \bar{q}q$, (D.38) is modified as

$$\Gamma(h \to q\bar{q}) = N_C \frac{G_F m_h}{4\sqrt{2}\pi} m_q^2(m_h) \left\{1 - \frac{4m_q^2(m_h)}{m_h^2}\right\}^{3/2} \left[1 + \Delta_{\rm QCD}(m_h) + \Delta_t(m_h) + \Delta_{\rm mix}(m_h)\right] . \tag{D.48}$$

These corrections can be seen [94], [95], [96], [97] and see also references therein ;

$$\begin{aligned}
\Delta_{\rm QCD} = & \left(\frac{\alpha_S(m_h)}{\pi}\right)\left[\frac{17}{3}\right] \\
& + \left(\frac{\alpha_S(m_h)}{\pi}\right)^2\left[\frac{10801}{141} - \frac{19}{12}\pi^2 - \frac{39}{2}\zeta_3 + \left(-\frac{65}{24} + \frac{1}{18}\pi^2 + \frac{2}{3}\zeta_3\right)N_f\right] \\
& + \left(\frac{\alpha_S(m_h)}{\pi}\right)^3\left[\frac{6163613}{5184} - \frac{3535}{72}\pi^2 - \frac{109735}{216}\zeta_3 + \frac{815}{12}\zeta_5\right. \\
& \qquad + \left(-\frac{46147}{486} + \frac{277}{72}\pi^2 + \frac{262}{9}\zeta_3 - \frac{5}{6}\zeta_4 - \frac{25}{9}\zeta_5\right)N_f \\
& \qquad \left. + \left(\frac{15511}{11664} - \frac{11}{162}\pi^2 - \frac{1}{3}\zeta_3\right)N_f^2\right] \\
& + \left(\frac{\alpha_S(m_h)}{\pi}\right)^4\left[39.34 - 220.9N_f + 9.685N_f^2 - 0.0205N_f^3\right] \\
= & \ 5.6667a_s + 29.147a_s^2 + 41.758a_s^3 - 825.7a_s^4 . \qquad (N_f = 5 \text{ and } a_s = \alpha_S/\pi)
\end{aligned} \tag{D.49}$$

$$\begin{aligned}
\Delta_t(m_h) = & \left(\frac{\alpha_S(m_h)}{\pi}\right)^2\left[3.111 - 0.667\log\frac{m_h^2}{M_t^2} + \frac{m_b^2(m_h)}{m_h^2}\left\{-10 + 4\log\frac{m_h^2}{M_t^2} + \frac{4}{3}\log\left[\frac{m_b^2(m_h)}{m_h^2}\right]\right\}\right] \\
& + \left(\frac{\alpha_S(m_h)}{\pi}\right)^3\left[50.474 - 8.167\log\frac{m_h^2}{M_t^2} - 1.278\log^2\frac{m_h^2}{M_t^2}\right] \\
& + \left(\frac{\alpha_S(m_h)}{\pi}\right)^2\frac{m_h^2}{M_t^2}\left[0.241 - 0.070\log\frac{m_h^2}{M_t^2}\right] \\
& + \left(\frac{G_F m_t^2}{8\pi^2\sqrt{2}}\right)\left[1 - 4.913\left(\frac{\alpha_S(m_h)}{\pi}\right) + \left\{-72.117 - 20.945\log\frac{m_h^2}{M_t^2}\right\}\left(\frac{\alpha_S(m_h)}{\pi}\right)^2\right] ,
\end{aligned} \tag{D.50}$$

$$\Delta_{\rm mix}(m_h) = \left(0.472 - 3.336\frac{m_b^2(m_h)}{m_h^2}\right)\frac{\alpha_{em}(m_h)}{\pi} - 1.455\left(\frac{\alpha_{em}(m_h)}{\pi}\right)^2 + 1.301\frac{\alpha_{em}(m_h)\alpha_S(m_h)}{\pi^2} . \tag{D.51}$$

$\mu = 125$ GeV	LO	NLO	N^{2}LO	N^{3}LO	N^{4}LO
$\Delta_{\rm QCD}$	1	0.203819	0.0377072	0.00194306	-0.00138192

$\mu = 125$ GeV	bottom	charm
Δ_t	0.00968457	0.00969446
$\Delta_{\rm mix}$	0.00119462	0.00119717

D.4.3 EW corrections to $h \to \bar{f}f$

The electroweak corrections to $h \to \bar{f}f$ [82] is given by

$$\begin{aligned}\Gamma_{\rm EW}(h \to \bar{f}f) &= \Gamma_{\rm tree}(h \to \bar{f}f) \times (1 + \delta_{\rm EW}) \\ &= \Gamma_{\rm tree}(h \to \bar{f}f) \times (1 - \Delta r + 2Re(\Delta T_W))\end{aligned} \tag{D.52}$$

These terms can be found in [82]. Its magnitude is shown in Figure D.3.

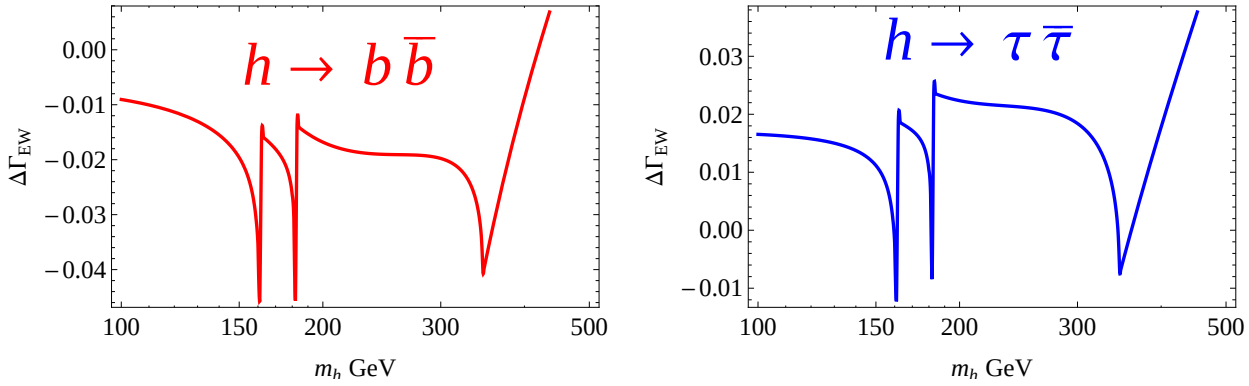

Figure D.3: The electroweak corrections to $h \to b\bar{b}$ and $h \to \tau\bar{\tau}$ as a function of m_h.

$\mu = 125$ GeV	bottom	charm	tau	mu
$\Delta_{\rm EW}$	-0.0121212	0.015023	0.0154297	0.015437

D.4.4 Leading order formulae of $h \to VV$

The decay rate into vector bosons ($V = W, Z$) is

$$\Gamma^{\rm tree}(h \to VV) = \delta \frac{g^2}{128\pi} \frac{m_h^3}{m_V^2} \sqrt{1 - x_V} \left(1 - x_V + \frac{3}{4} x_V^2\right) \tag{D.53}$$

where $x_V = 4m_V^2/m_h^2$ and $\delta = 1$ for Z boson, 2 for W boson. The above equation is only valid above the VV threshold, $m_h > 2m_V$.

D.4.5 Higgs-self coupling correction to $h \to VV$

The Higgs-self coupling correction is

$$\Gamma(h \to VV) = \Gamma^{\rm tree}(h \to VV) \times (1 + \delta_{hVV}) \tag{D.54}$$

with

$$\delta_{hVV} = \lambda' \left(\frac{19}{8} + \frac{5\pi^2}{24} - \frac{3\sqrt{3}\pi}{4}\right) + \lambda'^2 \times 0.97103, \qquad \lambda' = \frac{G_F m_h^2}{2\pi^2\sqrt{2}} \tag{D.55}$$

D.4.6 Off-shell vector boson decay to 4 massless fermions

Below the VV thresholds, virtual gauge boson decay modes become important. The decay width into massless fermion pairs is given by [98]

$$\Gamma(h \to V^*V^*) = \frac{1}{\pi^2}\int_0^{m_h^2} dq_1^2 \frac{m_V\Gamma_V}{(q_1^2 - m_V^2) + m_V^2\Gamma_V^2}\int_0^{(m_h-q_1)^2} dq_2^2 \frac{m_V\Gamma_V}{(q_2^2 - m_V^2) + m_V^2\Gamma_V^2}\Gamma_0^V(q_1^2, q_2^2, m_h^2) \tag{D.56}$$

where q_1^2, q_2^2 are virtual gauge boson masses, Γ_V and m_V are their total decay width and masses, and Γ_0^V is

$$\Gamma_0^V(q_1^2, q_2^2, m_h^2) = \delta_V \frac{G_F m_h^3}{16\sqrt{2}\pi}\sqrt{\lambda(q_1^2, q_2^2, m_h^2)}\left[\lambda(q_1^2, q_2^2, m_h^2) + \frac{12 q_1^2 q_2^2}{m_h^4}\right] \tag{D.57}$$

with

$$\lambda(x, y, z) = \left(1 - \frac{x}{z} - \frac{y}{z}\right)^2 - 4\frac{xy}{z^2}, \tag{D.58}$$

and

$$\begin{aligned} \delta_W &= 2, \\ \delta_Z &= 1. \end{aligned} \tag{D.59}$$

D.4.7 Electroweak corrections to $h \to 4f$

The electroweak corrections and top mass effect are calculated in [86]. The exact evaluation formulae are too complicated because the 5-point one loop function is required. We here use the improved Bron formulae. It can be found in (6.1) of [86].

D.4.8 Leading order formula of $h \to gg$

The dominant contribution is the top quark loop effect. I take into account bottom effect for numerical calculation. The leading order decay width is

$$\Gamma(h \to gg)|_{\rm LO} = \frac{\alpha_s^2 g^2 m_h^3}{128\pi^3 m_W^2}\left|\sum_{i=t,b}\tau_i\left[1 + (1-\tau_i)f(\tau_i)\right]\right|^2 \tag{D.60}$$

where $\tau_i = 4m_i^2/m_h^2$ and

$$f(\tau) = \begin{cases} \left[\sin^{-1}\left(\sqrt{1/\tau}\right)\right]^2, & \tau \geq 1 \\ -\frac{1}{4}\left[\log\left(\frac{1+\sqrt{1-\tau}}{1-\sqrt{1-\tau}}\right) - i\pi\right]^2, & \tau < 1. \end{cases} \tag{D.61}$$

The QCD corrections to this process are calculated in [87]. The above equation is rewritten as

$$\Gamma(h \to gg) = \Gamma(h \to gg)|_{\rm LO}\left[1 + E(\tau_Q)\frac{\alpha_S(m_h)}{\pi}\right] \tag{D.62}$$

with

$$E(\tau_Q) = \frac{95}{4} - \frac{7}{6}N_f + \frac{33-2N_f}{6}\log\frac{\mu^2}{m_h^2} + \Delta E. \tag{D.63}$$

μ is the renormalization scale which is taken to be m_h.

The NLO QCD correction to $h \to gg$ is riginally calculated in [87]. However, the authors in [88] pointed out that the formulae contains some typos. And they show the explicit formulae of this correction as functions of the harmonic polylogarithmic functions, defined in [99].

The EW correction is also calculated in [100] as functions of the *generalized* harmonic polylogarithmic functions.

D.4.9 Leading order formula of $h \to \gamma\gamma$

The dominant contributions comes from WW and $t\bar{t}$ loop effects. We take into account bottom and charm quark and tau lepton for numerical calculation.

$$\Gamma(h \to \gamma\gamma) = \frac{\alpha^2 g^2}{1024\pi^3}\frac{m_h^3}{m_W^2}\left|\sum_{i=t,b,W} N_{ci}e_i^2 F_i\right|^2 \tag{D.64}$$

where e_i is the electric charge in units of e and

$$F_1 = 2 + 3\tau + 3\tau(2-\tau)f(\tau), \tag{D.65}$$
$$F_{1/2} = -2\tau[1 + (1-\tau)f(\tau)], \tag{D.66}$$

where subscripts mean particle spin, f is already defined in $h \to gg$.

D.4.10 Two-Loop : EW and QCD corrections to $h \to \gamma\gamma$ and $h \to gg$

These corrections are calculated in [101] in terms of the Harmonic polylogarithmic funstions.

The QCD and EW corrections are found in [99].

D.4.11 Leading order formula of $h \to Z\gamma$

This channel is dominantly originated from the WW and tt loop effects. We take into account bottom and charm quark and tau lepton effects for numerical calculation.

$$\Gamma(h \to Z\gamma) = \frac{1}{32\pi}\left|\frac{\alpha g}{4\pi m_W}(A_W + A_F)\right|^2 m_h^3\left(1 - \frac{m_Z^2}{m_h^2}\right)^3, \tag{D.67}$$

$$A_W = -\cot\theta_W\Bigg\{4(3-\tan^2\theta_W)I_2(\tau_W,\lambda_W) + \left[\left(1+\frac{2}{\tau_W}\right)\tan^2\theta_W - \left(5+\frac{2}{\tau_W}\right)\right]I_1(\tau_W,\lambda_W)\Bigg\}, \tag{D.68}$$

$$A_F = \sum_{f=t,b} N_c\frac{-2e_f(T_f^3 - 2e_f\sin^2\theta_W)}{\sin\theta_W\cos\theta_W}\left[I_1(\tau_f,\lambda_f) - I_2(\tau_f,\lambda_f)\right] \tag{D.69}$$

where vaiables $\tau_f, \lambda_f, \tau_W, \lambda_W$ are

$$\tau_f = \frac{4m_f^2}{m_h^2}, \quad \lambda_f = \frac{4m_f^2}{m_Z^2}, \quad \tau_W = \frac{4m_W^2}{m_h^2}, \quad \lambda_W = \frac{4m_W^2}{m_Z^2}, \tag{D.70}$$

and functions I_1, I_2 are

$$I_1(a,b) = \frac{ab}{2(a-b)} + \frac{a^2b^2}{2(a-b)^2}\left[f(a)-f(b)\right] + \frac{a^2b}{(a-b)^2}\left[g(a)-g(b)\right], \tag{D.71}$$

$$I_2(a,b) = -\frac{ab}{2(a-b)}\left[f(a)-f(b)\right], \tag{D.72}$$

$$g(\tau) = \begin{cases} \sqrt{1-\tau}\left[\sin^{-1}\left(\sqrt{1/\tau}\right)\right]^2, & \tau \geq 1 \\ \frac{1}{2}\sqrt{\tau-1}\left[\log\left(\frac{1+\sqrt{1-\tau}}{1-\sqrt{1-\tau}}\right) - i\pi\right], & \tau < 1. \end{cases} \tag{D.73}$$

D.5 Scalar boson couplings in $SO(6)/SO(5)$

The Higgs- and singlet-coupling constants are defined as follow.

$$\begin{aligned}
\mathcal{L}_{\text{eff}} &= \frac{1}{2}(\partial_\mu h)^2\left(1 + 2\Delta_h\,\frac{h}{v} + \Delta_{hh}\,\frac{h^2}{v^2} + \Delta_{\eta\eta}\,\frac{\eta^2}{v^2} + \cdots\right) \\
&+ \frac{1}{2}(\partial_\mu \eta)^2\left(1 + 2\Omega_h\,\frac{h}{v} + \Omega_{hh}\,\frac{h^2}{v^2} + \Omega_{\eta\eta}\,\frac{\eta^2}{v^2} + \cdots\right) \\
&+ (\partial_\mu h)(\partial^\mu \eta)\left(\Lambda_\eta \frac{\eta}{v} + \Lambda_{h\eta}\frac{\eta h}{v^2} + \cdots\right) \\
&+ \left[m_W^2 W_\mu^+ W^{-\mu} + \frac{m_Z^2}{2} Z_\mu Z^\mu\right]\left(1 + 2\kappa_{hWW}\frac{h}{v} + \kappa_{hhWW}\frac{h^2}{v^2} + \kappa_{\eta\eta WW}\frac{\eta^2}{v^2} + \cdots\right) \\
&- m_f \overline{\psi}_L^f \psi_R^f\left(1 + \kappa_{hff}\frac{h}{v} + \kappa_{hhff}\frac{h^2}{v^2} + \kappa_{\eta ff}\frac{\eta}{v} + \kappa_{\eta\eta ff}\frac{\eta^2}{v^2} + \cdots\right) \\
&- V_{\text{eff}}(h,\eta)|_{car,pol}\ ,
\end{aligned} \tag{D.74}$$

with

$$V_{\text{eff}}(h,\eta)|_{car} = \alpha\cos^2\frac{\phi}{f} + \beta\sin^2\frac{\phi}{f} \times \frac{h^2}{\phi^2} + \gamma\sin^2\frac{\phi}{f}\cos^2\frac{\phi}{f} \times \frac{h^2}{\phi^2}\ , \tag{D.75}$$

$$V_{\text{eff}}(h,\eta)|_{pol} = \alpha \times \Theta(\theta,\phi,\psi)\cos^2\frac{\phi}{f} + \beta\sin^2\frac{\phi}{f}\cos^2\frac{\psi}{f} + \gamma \times \Theta(\theta,\phi,\psi)\sin^2\frac{\phi}{f}\cos^2\frac{\phi}{f}\cos^2\frac{\psi}{f}\ . \tag{D.76}$$

The scalar-self coupling constants are defined by

$$\frac{\partial^n V_{\text{eff}}}{\partial\phi_1\cdots\partial\phi_n} \equiv \lambda_{\phi_1\cdots\phi_n} \times \kappa_{\phi_1\cdots\phi_n}\ . \tag{D.77}$$

where κ is a dimensionless parameter. Therefore, scalar triple coulings are

$$\frac{\partial^3 V_{\text{eff}}}{\partial h\partial h\partial h} = \frac{3m_h^2}{v}\kappa_{hhh}, \qquad \frac{\partial^3 V_{\text{eff}}}{\partial h\partial\eta\partial\eta} = v\ \kappa_{h\eta\eta}, \qquad \text{the others are 0.} \tag{D.78}$$

and quadruple couplings are

$$\frac{\partial^3 V_{\text{eff}}}{\partial h \partial h \partial h \partial h} = \frac{3m_h^2}{v^2}\kappa_{hhhh}, \qquad \frac{\partial^3 V_{\text{eff}}}{\partial h \partial h \partial \eta \partial \eta} = \kappa_{hh\eta\eta}, \qquad \frac{\partial^3 V_{\text{eff}}}{\partial \eta \partial \eta \partial \eta \partial \eta} = \kappa_{\eta\eta\eta\eta}, \qquad \text{the others are 0.} \tag{D.79}$$

$$\text{eq.1} \quad \kappa_{h\eta\eta} = \frac{m_h^2}{v^2}\left[-\frac{\sqrt{(1-\xi)\xi} - 2(1-\xi)\sin^{-1}\sqrt{\xi}}{2(1-\xi)\sqrt{\xi}}\right] + \frac{2m_\eta^2}{v^2}\left[\sqrt{1-\xi} - \frac{\sqrt{\xi}}{\sin^{-1}\sqrt{\xi}}\right]$$

$$\text{eq.2} \quad \kappa_{hh\eta\eta} = \frac{m_h^2}{v^2}\left[-\frac{(9-10\xi)\sqrt{\xi}\sin^{-1}\sqrt{\xi} - 4\xi\sqrt{1-\xi} - 6\sqrt{1-\xi}(1-2\xi)\left(\sin^{-1}\sqrt{\xi}\right)^2}{2(1-\xi)\sqrt{\xi}\sin^{-1}\sqrt{\xi}}\right] + \frac{2m_\eta^2}{v^2}\left[1 - 2\xi + \frac{3\xi - 4\sqrt{(1-\xi)\xi}\sin^{-1}\sqrt{\xi}}{(\sin^{-1}\sqrt{\xi})^2}\right]$$

$$\text{eq.3} \quad \kappa_{\eta\eta\eta\eta} = \frac{3m_h^2}{v^2}\left[-\frac{\sin^{-1}\sqrt{\xi}\left(\sqrt{(1-\xi)\xi} - (1-\xi)\sin^{-1}\sqrt{\xi}\right)}{(1-\xi)\xi}\right] + \frac{12m_\eta^2}{v^2}\left[-1 + \sqrt{\frac{1-\xi}{\xi}}\sin^{-1}\sqrt{\xi}\right]$$

	Polar	Cartesian
Δ_h	0	0
Δ_{hh}	0	0
$\Delta_{\eta\eta}$	0	$-1+\frac{\xi}{(\sin^{-1}\sqrt{\xi})^2}$
Ω_h	$\sqrt{1-\xi}$	$\sqrt{1-\xi}-\frac{\sqrt{\xi}}{\sin^{-1}\sqrt{\xi}}$
Ω_{hh}	$1-2\xi$	$1-2\xi+\frac{3\xi}{(\sin^{-1}\sqrt{\xi})^2}-\frac{4\sqrt{(1-\xi)\xi}}{\sin^{-1}\sqrt{\xi}}$
$\Omega_{\eta\eta}$	0	$-2+\sqrt{\frac{1-\xi}{\xi}}\sin^{-1}\sqrt{\xi}+\frac{(\sin^{-1}\sqrt{\xi})^2}{\xi}$
Λ_η	0	$\frac{\sin^{-1}\sqrt{\xi}}{\sqrt{\xi}}-\frac{\sqrt{\xi}}{\sin^{-1}\sqrt{\xi}}$
$\Lambda_{h\eta}$	0	$3-\frac{\xi}{(\sin^{-1}\sqrt{\xi})^2}$
κ_{hWW}	$\sqrt{1-\xi}$	$\sqrt{1-\xi}$
κ_{hhWW}	$1-2\xi$	$1-2\xi$
$\kappa_{\eta\eta WW}$	-1	$-1+\sqrt{\frac{1-\xi}{\xi}}\sin^{-1}\sqrt{\xi}$
κ_{hff}	$\frac{1-2\xi}{\sqrt{1-\xi}}$	$\frac{1-2\xi}{\sqrt{1-\xi}}$
κ_{hhff}	-2ξ	-2ξ
$\kappa_{\eta\eta ff}$	$-\frac{1}{2}$	$-\frac{1}{2}\left(1-\frac{(1-2\xi)\sin^{-1}\sqrt{\xi}}{\sqrt{(1-\xi)\xi}}\right)$
κ_{hhh}	$\frac{1-2\xi}{\sqrt{1-\xi}}$	$\frac{1-2\xi}{\sqrt{1-\xi}}$
$\kappa_{h\eta\eta}$	$-\frac{m_h^2-4m_\eta^2(1-\xi)}{2v^2\sqrt{1-\xi}}$	$\frac{m_h^2}{2v^2}-\frac{m_h^2+8m_\eta^2}{12v^2}\xi+\mathcal{O}(\xi^2)$ (see eq.1)
κ_{hhhh}	$\frac{1-\frac{28}{3}(1-\xi)\xi}{1-\xi}$	$\frac{1-\frac{28}{3}(1-\xi)\xi}{1-\xi}$
$\kappa_{hh\eta\eta}$	$-\frac{m_h^2(5-6\xi)-4m_\eta^2(1-\xi)(1-2\xi)}{2v^2(1-\xi)}$	$\frac{m_h^2}{2v^2}-\frac{17m_h^2+4m_\eta^2}{6v^2}\xi+\mathcal{O}(\xi^2)$ (see eq.2)
$\kappa_{\eta\eta\eta\eta}$	$-\frac{4m_\eta^2}{v^2}$	$-\frac{m_h^2+4m_\eta^2}{v^2}\xi+\mathcal{O}(\xi^2)$ (see eq.3)

Table D.1: Couplings to scalar bosons. Red cells are not in agreement with [46] .

$\xi \ll 1$	Polar	Cartesian
Δ_h	0	0
Δ_{hh}	0	0
$\Delta_{\eta\eta}$	0	$-\frac{\xi}{3}$
Ω_h	$1-\frac{1}{2}\xi$	$-\frac{\xi}{3}$
Ω_{hh}	$1-2\xi$	$-\frac{\xi}{3}$
$\Omega_{\eta\eta}$	0	$\frac{2\xi^2}{45}$
Λ_η	0	$\frac{\xi}{3}$
$\Lambda_{h\eta}$	0	$2+\frac{\xi}{3}$
κ_{hWW}	$1-\frac{1}{2}\xi$	$1-\frac{1}{2}\xi$
κ_{hhWW}	$1-2\xi$	$1-2\xi$
$\kappa_{\eta\eta WW}$	-1	$-\frac{\xi}{3}$
κ_{hff}	$1-\frac{3}{2}\xi$	$1-\frac{3}{2}\xi$
κ_{hhff}	-2ξ	-2ξ
$\kappa_{\eta\eta ff}$	$-\frac{1}{2}$	$-\frac{2}{3}\xi$
κ_{hhh}	$1-\frac{3}{2}\xi$	$1-\frac{3}{2}\xi$
$\kappa_{h\eta\eta}$	$-\frac{m_h^2-4m_\eta^2}{2v^2}\left(1+\frac{m_h^2+4m_\eta^2}{2m_h^2-8m_\eta^2}\xi\right)$	$\frac{m_h^2}{2v^2}-\frac{m_h^2+8m_\eta^2}{12v^2}\xi$
κ_{hhhh}	$1-\frac{25}{3}\xi$	$1-\frac{25}{3}\xi$
$\kappa_{hh\eta\eta}$	$-\frac{5m_h^2-4m_\eta^2}{2v^2}\left(1-\frac{m_h^2-8m_\eta^2}{5m_h^2-4m_\eta^2}\xi\right)$	$\frac{m_h^2}{2v^2}-\frac{17m_h^2+4m_\eta^2}{6v^2}\xi$
$\kappa_{\eta\eta\eta\eta}$	$-\frac{4m_\eta^2}{v^2}$	$-\frac{m_h^2+4m_\eta^2}{v^2}\xi$

Table D.2: Couplings to scalar bosons for small ξ. Red cells are not in agreement with [46] .

Bibliography

[1] S. Kanemura, N. Machida, T. Shindou and T. Yamada, Phys. Rev. D **89** (2014) 1, 013005 doi:10.1103/PhysRevD.89.013005 [arXiv:1309.3207 [hep-ph]]. S. Kanemura, N. Machida and T. Shindou, Phys. Lett. B **738** (2014) 178 doi:10.1016/j.physletb.2014.09.013 [arXiv:1405.5834 [hep-ph]].

[2] S. Kanemura, K. Kaneta, N. Machida and T. Shindou, Phys. Rev. D **91** (2015) 115016 doi:10.1103/PhysRevD.91.115016 [arXiv:1410.8413 [hep-ph]].

[3] S. Kanemura, N. Machida, S. Odori and T. Shindou, arXiv:1512.09053 [hep-ph].

[4] R. Barate *et al.* [LEP Working Group for Higgs boson searches and ALEPH and DELPHI and L3 and OPAL Collaborations], Phys. Lett. B **565** (2003) 61 doi:10.1016/S0370-2693(03)00614-2 [hep-ex/0306033].

[5] G. Aad *et al.* [ATLAS Collaboration], Phys. Lett. B **716** (2012) 1 doi:10.1016/j.physletb.2012.08.020 [arXiv:1207.7214 [hep-ex]],

[6] ALTAS collaboration, ATLAS-CONF-2013-040, 16 April 2013

[7] S. Weinberg, Phys. Rev. D **13** (1976) 974. doi:10.1103/PhysRevD.13.974 L. Susskind, Phys. Rev. D **20** (1979) 2619. doi:10.1103/PhysRevD.20.2619 E. Farhi and L. Susskind, Phys. Rept. **74** (1981) 277. doi:10.1016/0370-1573(81)90173-3

[8] M. Schmaltz and D. Tucker-Smith, Ann. Rev. Nucl. Part. Sci. **55** (2005) 229 doi:10.1146/annurev.nucl.55.090704.151502 [hep-ph/0502182].

[9] D. B. Kaplan and H. Georgi, Phys. Lett. B **136** (1984) 183. doi:10.1016/0370-2693(84)91177-8 , D. B. Kaplan, H. Georgi and S. Dimopoulos, Phys. Lett. B **136** (1984) 187. doi:10.1016/0370-2693(84)91178-X , H. Georgi, D. B. Kaplan and P. Galison, Phys. Lett. B **143** (1984) 152. doi:10.1016/0370-2693(84)90823-2 , H. Georgi and D. B. Kaplan, Phys. Lett. B **145** (1984) 216. doi:10.1016/0370-2693(84)90341-1 , M. J. Dugan, H. Georgi and D. B. Kaplan, Nucl. Phys. B **254** (1985) 299. doi:10.1016/0550-3213(85)90221-4

[10] A. Zee, Phys. Lett. B **93** (1980) 389 [Phys. Lett. B **95** (1980) 461]. doi:10.1016/0370-2693(80)90349-4

[11] A. Zee, Nucl. Phys. B **264** (1986) 99. doi:10.1016/0550-3213(86)90475-X K. S. Babu, Phys. Lett. B **203** (1988) 132. doi:10.1016/0370-2693(88)91584-5

[12] E. Ma, Phys. Rev. D **73** (2006) 077301 doi:10.1103/PhysRevD.73.077301 [hep-ph/0601225].

[13] L. M. Krauss, S. Nasri and M. Trodden, Phys. Rev. D **67** (2003) 085002 doi:10.1103/PhysRevD.67.085002 [hep-ph/0210389].

[14] M. Aoki, S. Kanemura and O. Seto, Phys. Rev. Lett. **102** (2009) 051805 doi:10.1103/PhysRevLett.102.051805 [arXiv:0807.0361 [hep-ph]].

[15] M. Aoki, S. Kanemura and O. Seto, Phys. Rev. D **80** (2009) 033007 doi:10.1103/PhysRevD.80.033007 [arXiv:0904.3829 [hep-ph]].

[16] R. Harnik, G. D. Kribs, D. T. Larson and H. Murayama, Phys. Rev. D **70** (2004) 015002 doi:10.1103/PhysRevD.70.015002 [hep-ph/0311349].

[17] K. A. Intriligator and N. Seiberg, Nucl. Phys. Proc. Suppl. **45BC** (1996) 1 doi:10.1016/0920-5632(95)00626-5 [hep-th/9509066].

[18] M. A. Luty, Phys. Rev. D **57** (1998) 1531 doi:10.1103/PhysRevD.57.1531 [hep-ph/9706235].

[19] C. Panagiotakopoulos and K. Tamvakis, Phys. Lett. B **446** (1999) 224; C. Panagiotakopoulos and K. Tamvakis, Phys. Lett. B **469** (1999) 145; C. Panagiotakopoulos and A. Pilaftsis, Phys. Rev. D **63** (2001) 055003; A. Dedes, C. Hugonie, S. Moretti and K. Tamvakis, Phys. Rev. D **63** (2001) 055009.

[20] M. Aoki, M. Duerr, J. Kubo and H. Takano, Phys. Rev. D **86** (2012) 076015 doi:10.1103/PhysRevD.86.076015 [arXiv:1207.3318 [hep-ph]].

[21] S. Kanemura, Y. Okada and E. Senaha, Phys. Lett. B **606** (2005) 361 doi:10.1016/j.physletb.2004.12.004 [hep-ph/0411354].

[22] S. Kanemura, E. Senaha, T. Shindou and T. Yamada, JHEP **1305** (2013) 066 doi:10.1007/JHEP05(2013)066 [arXiv:1211.5883 [hep-ph]].

[23] G. L. Fogli, E. Lisi, A. Marrone, D. Montanino, A. Palazzo and A. M. Rotunno, Phys. Rev. D **86** (2012) 013012; M. C. Gonzalez-Garcia, M. Maltoni, J. Salvado and T. Schwetz, JHEP **1212** (2012) 123.

[24] E. Aprile *et al.* [XENON100 Collaboration], Phys. Rev. Lett. **107** (2011) 131302 doi:10.1103/PhysRevLett.107.131302 [arXiv:1104.2549 [astro-ph.CO]].

[25] D. S. Akerib *et al.* [LUX Collaboration], Phys. Rev. Lett. **112** (2014) 091303 doi:10.1103/PhysRevLett.112.091303 [arXiv:1310.8214 [astro-ph.CO]].

[26] S. Scherer, Adv. Nucl. Phys. **27** (2003) 277 [hep-ph/0210398].

[27] K. Agashe, R. Contino and A. Pomarol, Nucl. Phys. B **719** (2005) 165 doi:10.1016/j.nuclphysb.2005.04.035 [hep-ph/0412089].

[28] A. Dobado, M. J. Herrero and T. N. Truong, Phys. Lett. B **235** (1990) 134. doi:10.1016/0370-2693(90)90109-J

[29] H. Murayama, V. Rentala and J. Shu, arXiv:1401.3761 [hep-ph].

[30] R. Contino, C. Grojean, M. Moretti, F. Piccinini and R. Rattazzi, JHEP **1005** (2010) 089 doi:10.1007/JHEP05(2010)089 [arXiv:1002.1011 [hep-ph]].

[31] W. Y. Keung, I. Low and J. Shu, Phys. Rev. Lett. **101** (2008) 091802 doi:10.1103/PhysRevLett.101.091802 [arXiv:0806.2864 [hep-ph]].

[32] Q. H. Cao, C. B. Jackson, W. Y. Keung, I. Low and J. Shu, Phys. Rev. D **81** (2010) 015010 doi:10.1103/PhysRevD.81.015010 [arXiv:0911.3398 [hep-ph]].

[33] A. D. Martin, W. J. Stirling, R. S. Thorne and G. Watt, Eur. Phys. J. C **63** (2009) 189 doi:10.1140/epjc/s10052-009-1072-5 [arXiv:0901.0002 [hep-ph]].

[34] R. Killick, K. Kumar and H. E. Logan, Phys. Rev. D **88** (2013) 033015 doi:10.1103/PhysRevD.88.033015 [arXiv:1305.7236 [hep-ph]].

[35] M. Carena, L. Da Rold and E. Pontn, JHEP **1406** (2014) 159 doi:10.1007/JHEP06(2014)159 [arXiv:1402.2987 [hep-ph]].

[36] P. P. Giardino, K. Kannike, I. Masina, M. Raidal and A. Strumia, JHEP **1405** (2014) 046 doi:10.1007/JHEP05(2014)046 [arXiv:1303.3570 [hep-ph]].

[37] A. Pomarol and F. Riva, JHEP **1208** (2012) 135 doi:10.1007/JHEP08(2012)135 [arXiv:1205.6434 [hep-ph]].

[38] O. J. P. Eboli, G. C. Marques, S. F. Novaes and A. A. Natale, Phys. Lett. B **197** (1987) 269. doi:10.1016/0370-2693(87)90381-9

[39] J. F. Gunion, H. E. Haber, G. L. Kane and S. Dawson, Front. Phys. **80** (2000) 1; A. Djouadi, Phys. Rept. **457** (2008) 1.

[40] The ATLAS and CMS Collaborations, ATLAS-CONF-2015-044.

[41] https://twiki.cern.ch/twiki/bin/view/LHCPhysics/CERNYellowReportPageAt8TeV.

[42] R. Contino, C. Grojean, M. Moretti, F. Piccinini and R. Rattazzi, JHEP **1005** (2010) 089 doi:10.1007/JHEP05(2010)089 [arXiv:1002.1011 [hep-ph]].

[43] T. Plehn, M. Spira and P. M. Zerwas, Nucl. Phys. B **479** (1996) 46 [Nucl. Phys. B **531** (1998) 655] doi:10.1016/0550-3213(96)00418-X [hep-ph/9603205].

[44] A. D. Martin, W. J. Stirling, R. S. Thorne and G. Watt, Eur. Phys. J. C **63** (2009) 189.

[45] D. de Florian and J. Mazzitelli, Phys. Rev. Lett. **111** (2013) 201801 doi:10.1103/PhysRevLett.111.201801 [arXiv:1309.6594 [hep-ph]].

[46] D. Marzocca and A. Urbano, JHEP **1407** (2014) 107 [arXiv:1404.7419 [hep-ph]].

[47] M. Redi and A. Tesi, JHEP **1210** (2012) 166 [arXiv:1205.0232 [hep-ph]].

[48] B. Bellazzini, C. Cski and J. Serra, Eur. Phys. J. C **74** (2014) 5, 2766 doi:10.1140/epjc/s10052-014-2766-x [arXiv:1401.2457 [hep-ph]].

[49] G. Aad *et al.* [ATLAS Collaboration], Phys. Lett. B **710**, 49 (2012); S. Chatrchyan *et al.* [CMS Collaboration], Phys. Lett. B **710**, 26 (2012).

[50] ATLAS Collaboration [ATLAS Collaboration], ATLAS-CONF-2015-081

[51] CMS Collaboration [CMS Collaboration], CMS-PAS-EXO-15-004

[52] K. Harigaya and Y. Nomura, arXiv:1512.04850 [hep-ph]; Y. Mambrini, G. Arcadi and A. Djouadi, arXiv:1512.04913 [hep-ph]; M. Backovic, A. Mariotti and D. Redigolo, arXiv:1512.04917 [hep-ph]; A. Angelescu, A. Djouadi and G. Moreau, arXiv:1512.04921 [hep-ph]; Y. Nakai, R. Sato and K. Tobioka, arXiv:1512.04924 [hep-ph]; D. Buttazzo, A. Greljo and D. Marzocca, arXiv:1512.04929 [hep-ph]; A. Pilaftsis, arXiv:1512.04931 [hep-ph]; R. Franceschini *et al.*, arXiv:1512.04933 [hep-ph]; S. Di Chiara, L. Marzola and M. Raidal, arXiv:1512.04939 [hep-ph]; T. Higaki, K. S. Jeong, N. Kitajima and F. Takahashi, arXiv:1512.05295 [hep-ph]; S. D. McDermott, P. Meade and H. Ramani, arXiv:1512.05326 [hep-ph]; J. Ellis, S. A. R. Ellis, J. Quevillon, V. Sanz and T. You, arXiv:1512.05327 [hep-ph]; M. Low, A. Tesi and L. T. Wang, arXiv:1512.05328 [hep-ph]; B. Bellazzini, R. Franceschini, F. Sala and J. Serra, arXiv:1512.05330 [hep-ph]; R. S. Gupta, S. Jger, Y. Kats, G. Perez and E. Stamou, arXiv:1512.05332 [hep-ph]; C. Petersson and R. Torre, arXiv:1512.05333 [hep-ph]; E. Molinaro, F. Sannino and N. Vignaroli, arXiv:1512.05334 [hep-ph]; B. Dutta, Y. Gao, T. Ghosh, I. Gogoladze and T. Li, arXiv:1512.05439 [hep-ph]; Q. H. Cao, Y. Liu, K. P. Xie, B. Yan and D. M. Zhang, arXiv:1512.05542 [hep-ph]; S. Matsuzaki and K. Yamawaki, arXiv:1512.05564 [hep-ph]; A. Kobakhidze, F. Wang, L. Wu, J. M. Yang and M. Zhang, arXiv:1512.05585 [hep-ph]; R. Martinez, F. Ochoa and C. F. Sierra, arXiv:1512.05617 [hep-ph]; P. Cox, A. D. Medina, T. S. Ray and A. Spray, arXiv:1512.05618 [hep-ph]. D. Becirevic, E. Bertuzzo, O. Sumensari and R. Z. Funchal, arXiv:1512.05623 [hep-ph]; J. M. No, V. Sanz and J. Setford, arXiv:1512.05700 [hep-ph]; S. V. Demidov and D. S. Gorbunov, arXiv:1512.05723 [hep-ph]; W. Chao, R. Huo and J. H. Yu, arXiv:1512.05738 [hep-ph]; S. Fichet, G. von Gersdorff and C. Royon, arXiv:1512.05751 [hep-ph]; D. Curtin and C. B. Verhaaren, arXiv:1512.05753 [hep-ph]; L. Bian, N. Chen, D. Liu and J. Shu, arXiv:1512.05759 [hep-ph]; J. Chakrabortty, A. Choudhury, P. Ghosh, S. Mondal and T. Srivastava, arXiv:1512.05767 [hep-ph]; A. Ahmed, B. M. Dillon, B. Grzadkowski, J. F. Gunion and Y. Jiang, arXiv:1512.05771 [hep-ph]; P. Agrawal, J. Fan, B. Heidenreich, M. Reece and M. Strassler, arXiv:1512.05775 [hep-ph]; C. Csaki, J. Hubisz and J. Terning, arXiv:1512.05776 [hep-ph]; A. Falkowski, O. Slone and T. Volansky, arXiv:1512.05777 [hep-ph]; D. Aloni, K. Blum, A. Dery, A. Efrati and Y. Nir, arXiv:1512.05778 [hep-ph]; Y. Bai, J. Berger and R. Lu, arXiv:1512.05779 [hep-ph]; S. Ghosh, A. Kundu and S. Ray, arXiv:1512.05786 [hep-ph]; R. Benbrik, C. H. Chen and T. Nomura, arXiv:1512.06028 [hep-ph]; J. S. Kim, J. Reuter, K. Rolbiecki and R. R. de Austri, arXiv:1512.06083 [hep-ph]; A. Alves, A. G. Dias and K. Sinha, arXiv:1512.06091 [hep-ph]; E. Megias, O. Pujolas and M. Quiros, arXiv:1512.06106 [hep-ph]; L. M. Carpenter, R. Colburn and J. Goodman, arXiv:1512.06107 [hep-ph]; J. Bernon and C. Smith, arXiv:1512.06113 [hep-ph]; W. Chao, arXiv:1512.06297 [hep-ph]; M. T. Arun and P. Saha,

arXiv:1512.06335 [hep-ph]; C. Han, H. M. Lee, M. Park and V. Sanz, arXiv:1512.06376 [hep-ph]; S. Chang, arXiv:1512.06426 [hep-ph]; I. Chakraborty and A. Kundu, arXiv:1512.06508 [hep-ph]; R. Ding, L. Huang, T. Li and B. Zhu, arXiv:1512.06560 [hep-ph]; H. Han, S. Wang and S. Zheng, arXiv:1512.06562 [hep-ph]; X. F. Han and L. Wang, arXiv:1512.06587 [hep-ph]; M. x. Luo, K. Wang, T. Xu, L. Zhang and G. Zhu, arXiv:1512.06670 [hep-ph]; J. Chang, K. Cheung and C. T. Lu, arXiv:1512.06671 [hep-ph]; D. Bardhan, D. Bhatia, A. Chakraborty, U. Maitra, S. Raychaudhuri and T. Samui, arXiv:1512.06674 [hep-ph]; T. F. Feng, X. Q. Li, H. B. Zhang and S. M. Zhao, arXiv:1512.06696 [hep-ph]; O. Antipin, M. Mojaza and F. Sannino, arXiv:1512.06708 [hep-ph]; F. Wang, L. Wu, J. M. Yang and M. Zhang, arXiv:1512.06715 [hep-ph]; F. P. Huang, C. S. Li, Z. L. Liu and Y. Wang, arXiv:1512.06732 [hep-ph]; W. Liao and H. q. Zheng, arXiv:1512.06741 [hep-ph]; J. J. Heckman, arXiv:1512.06773 [hep-ph]; M. Dhuria and G. Goswami, arXiv:1512.06782 [hep-ph]; X. J. Bi, Q. F. Xiang, P. F. Yin and Z. H. Yu, arXiv:1512.06787 [hep-ph]. J. S. Kim, K. Rolbiecki and R. R. de Austri, arXiv:1512.06797 [hep-ph]. L. Berthier, J. M. Cline, W. Shepherd and M. Trott, arXiv:1512.06799 [hep-ph]. W. S. Cho, D. Kim, K. Kong, S. H. Lim, K. T. Matchev, J. C. Park and M. Park, arXiv:1512.06824 [hep-ph]; J. M. Cline and Z. Liu, arXiv:1512.06827 [hep-ph]; M. Bauer and M. Neubert, arXiv:1512.06828 [hep-ph]; M. Chala, M. Duerr, F. Kahlhoefer and K. Schmidt-Hoberg, arXiv:1512.06833 [hep-ph]; D. Barducci, A. Goudelis, S. Kulkarni and D. Sengupta, arXiv:1512.06842 [hep-ph]; S. M. Boucenna, S. Morisi and A. Vicente, arXiv:1512.06878 [hep-ph]; C. W. Murphy, arXiv:1512.06976 [hep-ph]; A. E. C. Hernndez and I. Nisandzic, arXiv:1512.07165 [hep-ph]; U. K. Dey, S. Mohanty and G. Tomar, arXiv:1512.07212 [hep-ph]; G. M. Pelaggi, A. Strumia and E. Vigiani, arXiv:1512.07225 [hep-ph]; J. de Blas, J. Santiago and R. Vega-Morales, arXiv:1512.07229 [hep-ph]; A. Belyaev, G. Cacciapaglia, H. Cai, T. Flacke, A. Parolini and H. Serdio, arXiv:1512.07242 [hep-ph]; P. S. B. Dev and D. Teresi, arXiv:1512.07243 [hep-ph]; W. C. Huang, Y. L. S. Tsai and T. C. Yuan, arXiv:1512.07268 [hep-ph]. K. M. Patel and P. Sharma, arXiv:1512.07468 [hep-ph]. M. Badziak, arXiv:1512.07497 [hep-ph]; S. Chakraborty, A. Chakraborty and S. Raychaudhuri, arXiv:1512.07527 [hep-ph]; Q. H. Cao, S. L. Chen and P. H. Gu, arXiv:1512.07541 [hep-ph]; W. Altmannshofer, J. Galloway, S. Gori, A. L. Kagan, A. Martin and J. Zupan, arXiv:1512.07616 [hep-ph]; M. Cveti, J. Halverson and P. Langacker, arXiv:1512.07622 [hep-ph]; J. Gu and Z. Liu, arXiv:1512.07624 [hep-ph]; B. C. Allanach, P. S. B. Dev, S. A. Renner and K. Sakurai, arXiv:1512.07645 [hep-ph]; H. Davoudiasl and C. Zhang, arXiv:1512.07672 [hep-ph]; N. Craig, P. Draper, C. Kilic and S. Thomas, arXiv:1512.07733 [hep-ph]; K. Das and S. K. Rai, arXiv:1512.07789 [hep-ph]; K. Cheung, P. Ko, J. S. Lee, J. Park and P. Y. Tseng, arXiv:1512.07853 [hep-ph]; J. Liu, X. P. Wang and W. Xue, arXiv:1512.07885 [hep-ph]; J. Zhang and S. Zhou, arXiv:1512.07889 [hep-ph]; J. A. Casas, J. R. Espinosa and J. M. Moreno, arXiv:1512.07895 [hep-ph]; L. J. Hall, K. Harigaya and Y. Nomura, arXiv:1512.07904 [hep-ph]; H. Han, S. Wang and S. Zheng, arXiv:1512.07992 [hep-ph]; J. C. Park and S. C. Park, arXiv:1512.08117 [hep-ph]; A. Salvio and A. Mazumdar, arXiv:1512.08184 [hep-ph]; D. Chway, R. Dermek, T. H. Jung and H. D. Kim, arXiv:1512.08221 [hep-ph]; G. Li, Y. n. Mao, Y. L. Tang, C. Zhang, Y. Zhou and S. h. Zhu, arXiv:1512.08255 [hep-ph]; M. Son and A. Urbano, arXiv:1512.08307 [hep-ph]; Y. L. Tang and S. h. Zhu, arXiv:1512.08323 [hep-ph]; H. An, C. Cheung and Y. Zhang, arXiv:1512.08378 [hep-ph]; J. Cao, F. Wang and Y. Zhang, arXiv:1512.08392 [hep-ph];

F. Wang, W. Wang, L. Wu, J. M. Yang and M. Zhang, arXiv:1512.08434 [hep-ph]; C. Cai, Z. H. Yu and H. H. Zhang, arXiv:1512.08440 [hep-ph]; Q. H. Cao, Y. Liu, K. P. Xie, B. Yan and D. M. Zhang, arXiv:1512.08441 [hep-ph]; J. E. Kim, arXiv:1512.08467 [hep-ph]; J. Gao, H. Zhang and H. X. Zhu, arXiv:1512.08478 [hep-ph]; W. Chao, arXiv:1512.08484 [hep-ph]; F. Goertz, J. F. Kamenik, A. Katz and M. Nardecchia, arXiv:1512.08500 [hep-ph]; L. A. Anchordoqui, I. Antoniadis, H. Goldberg, X. Huang, D. Lust and T. R. Taylor, arXiv:1512.08502 [hep-ph]; P. S. B. Dev, R. N. Mohapatra and Y. Zhang, arXiv:1512.08507 [hep-ph]; N. Bizot, S. Davidson, M. Frigerio and J.-L. Kneur, arXiv:1512.08508 [hep-ph].

[53] S. Knapen, T. Melia, M. Papucci and K. Zurek, arXiv:1512.04928 [hep-ph]; E. Gabrielli, K. Kannike, B. Mele, M. Raidal, C. Spethmann and H. Veerme, arXiv:1512.05961 [hep-ph]; J. Cao, C. Han, L. Shang, W. Su, J. M. Yang and Y. Zhang, arXiv:1512.06728 [hep-ph]; S. Moretti and K. Yagyu, arXiv:1512.07462 [hep-ph]; X. J. Bi *et al.*, arXiv:1512.08497 [hep-ph].

[54] G. Aad *et al.* [ATLAS Collaboration], Phys. Rev. D **92** (2015) 3, 032004.

[55] CMS Collaboration [CMS Collaboration], CMS-PAS-HIG-14-006

[56] B. W. Lee, C. Quigg and H. B. Thacker, Phys. Rev. D **16**, 1519 (1977).

[57] J. M. Frere, D. R. T. Jones and S. Raby, Nucl. Phys. B **222**, 11 (1983).

[58] R. Contino, Y. Nomura and A. Pomarol, Nucl. Phys. B **671**, 148 (2003); K. Agashe, R. Contino and A. Pomarol, Nucl. Phys. B **719**, 165 (2005); R. Barbieri, B. Bellazzini, V. S. Rychkov and A. Varagnolo, Phys. Rev. D **76**, 115008 (2007); R. Contino, arXiv:1005.4269 [hep-ph].

[59] B. Gripaios, A. Pomarol, F. Riva and J. Serra, JHEP **0904**, 070 (2009); M. Redi and A. Tesi, JHEP **1210** (2012) 166.

[60] J. Mrazek, A. Pomarol, R. Rattazzi, M. Redi, J. Serra and A. Wulzer, Nucl. Phys. B **853**, 1 (2011); B. Bellazzini, C. Csáki and J. Serra, Eur. Phys. J. C **74**, no. 5, 2766 (2014).

[61] M. Schmaltz, D. Stolarski and J. Thaler, JHEP **1009**, 018 (2010).

[62] C. Anastasiou, C. Duhr, F. Dulat, F. Herzog and B. Mistlberger, Phys. Rev. Lett. **114** (2015) 212001.

[63] M. A. Shifman, A. I. Vainshtein, M. B. Voloshin and V. I. Zakharov, Sov. J. Nucl. Phys. **30** (1979) 711 [Yad. Fiz. **30** (1979) 1368]; L. Bergstrom and G. Hulth, Nucl. Phys. B **259** (1985) 137 [Nucl. Phys. B **276** (1986) 744]; J. F. Gunion, G. L. Kane and J. Wudka, Nucl. Phys. B **299** (1988) 231.

[64] A. Djouadi, Phys. Rept. **457**, 1 (2008).

[65] C. W. Chiang and K. Yagyu, Phys. Rev. D **87**, no. 3, 033003 (2013).

[66] G. Aad *et al.* [ATLAS Collaboration], JHEP **1503**, 041 (2015)

[67] S. Kanemura, K. Yagyu and H. Yokoya, Phys. Lett. B **726** (2013) 316; S. Kanemura, M. Kikuchi, K. Yagyu and H. Yokoya, Phys. Rev. D **90** (2014) 11, 115018; PTEP **2015**, 051B02 (2015).

[68] J. F. Gunion, H. E. Haber and M. Sher, Nucl. Phys. B **306**, 1 (1988); J. A. Casas, A. Lleyda and C. Munoz, Nucl. Phys. B **471**, 3 (1996).

[69] A. Schuessler and D. Zeppenfeld, In *Karlsruhe 2007, SUSY 2007* 236-239 [arXiv:0710.5175 [hep-ph]].

[70] J. Hisano and K. Tsumura, Phys. Rev. D **87** (2013) 053004; S. Kanemura, M. Kikuchi and K. Yagyu, Phys. Rev. D **88** (2013) 015020

[71] K. Hally, H. E. Logan and T. Pilkington, Phys. Rev. D **85** (2012) 095017.

[72] A. Zee, Phys. Lett. B **93** (1980) 389 [Phys. Lett. B **95** (1980) 461].

[73] E. Ma, Phys. Rev. D **73** (2006) 077301.

[74] A. Zee, Nucl. Phys. B **264** (1986) 99; K. S. Babu, Phys. Lett. B **203** (1988) 132.

[75] L. M. Krauss, S. Nasri and M. Trodden, Phys. Rev. D **67** (2003) 085002.

[76] M. Aoki, S. Kanemura and O. Seto, Phys. Rev. Lett. **102** (2009) 051805.

[77] M. Gustafsson, J. M. No and M. A. Rivera, Phys. Rev. Lett. **110** (2013) 21, 211802 [Phys. Rev. Lett. **112** (2014) 25, 259902].

[78] S. Kanemura, Y. Okada and E. Senaha, Phys. Lett. B **606** (2005) 361.

[79] V. A. Kuzmin, V. A. Rubakov and M. E. Shaposhnikov, Phys. Lett. B **155** (1985) 36.

[80] G. Aad *et al.* [ATLAS Collaboration], Eur. Phys. J. C **74** (2014) 10, 3109;
CMS Collaboration CMS-PAS-TOP-13-004.

[81] The ATLAS collaboration, ATLAS-CONF-2015-033;
CMS Collaboration [CMS Collaboration], CMS-PAS-TOP-15-003.

[82] A. Dabelstein and W. Hollik, Z. Phys. C **53** (1992) 507.

[83] L. Durand, B. A. Kniehl and K. Riesselmann, Phys. Rev. D **51** (1995) 5007 [hep-ph/9412311].

[84] K. G. Chetyrkin, J. H. Kuhn and M. Steinhauser, Comput. Phys. Commun. **133** (2000) 43 [hep-ph/0004189].

[85] L. R. Surguladze, Phys. Lett. B **341** (1994) 60 [hep-ph/9405325].

[86] A. Bredenstein, A. Denner, S. Dittmaier and M. M. Weber, Phys. Rev. D **74** (2006) 013004 [hep-ph/0604011].

[87] M. Spira, A. Djouadi, D. Graudenz and P. M. Zerwas, Nucl. Phys. B **453** (1995) 17 [hep-ph/9504378].

[88] R. Harlander and P. Kant, JHEP **0512** (2005) 015 [hep-ph/0509189].

[89] G. Degrassi and F. Maltoni, Nucl. Phys. B **724** (2005) 183 doi:10.1016/j.nuclphysb.2005.06.027 [hep-ph/0504137].

[90] M. Spira, A. Djouadi and P. M. Zerwas, Phys. Lett. B **276** (1992) 350.

[91] R. Bonciani, V. Del Duca, H. Frellesvig, J. M. Henn, F. Moriello and V. A. Smirnov, JHEP **1508** (2015) 108 [arXiv:1505.00567 [hep-ph]].

[92] N. Gray, D. J. Broadhurst, W. Grafe and K. Schilcher, Z. Phys. C **48** (1990) 673. doi:10.1007/BF01614703

[93] P. N. Maher, L. Durand and K. Riesselmann, Phys. Rev. D **48** (1993) 1061 [Phys. Rev. D **52** (1995) 553] [hep-ph/9303233].

[94] M. Drees and K. i. Hikasa, Phys. Rev. D **41** (1990) 1547. doi:10.1103/PhysRevD.41.1547

[95] K. G. Chetyrkin, Phys. Lett. B **390** (1997) 309 doi:10.1016/S0370-2693(96)01368-8 [hep-ph/9608318].

[96] P. A. Baikov, K. G. Chetyrkin and J. H. Kuhn, Phys. Rev. Lett. **96** (2006) 012003 doi:10.1103/PhysRevLett.96.012003 [hep-ph/0511063].

[97] A. L. Kataev and V. T. Kim, arXiv:0804.3992 [hep-ph].

[98] A. Djouadi, In *Barcelona 1997, Quantum effects in the minimal supersymmetric standard model* 197-222 [hep-ph/9712334].

[99] S. Moch and J. A. M. Vermaseren, Nucl. Phys. B **573** (2000) 853 doi:10.1016/S0550-3213(00)00045-6 [hep-ph/9912355],

[100] R. Bonciani, G. Degrassi and A. Vicini, Comput. Phys. Commun. **182** (2011) 1253 doi:10.1016/j.cpc.2011.02.011 [arXiv:1007.1891 [hep-ph]],

[101] S. Actis, G. Passarino, C. Sturm and S. Uccirati, Nucl. Phys. B **811** (2009) 182 doi:10.1016/j.nuclphysb.2008.11.024 [arXiv:0809.3667 [hep-ph]].